Universität Hamburg
DER FORSCHUNG | DER LEHRE | DER BILDUNG

BNITM
Bernhard Nocht Institute for Tropical Medicine

Extracellular vesicles in host-parasite interaction of *Entamoeba histolytica* (Schaudinn, 1903) with primary monocytes

Dissertation

Submitted by

Barbara Irene Honecker

for the attainment of the degree *Doctor rerum naturalium*

Faculty of Mathematics, Informatics, and Natural Sciences

Department of Biology

University of Hamburg

2023

The present work was performed under the guidance of Prof. Dr. Iris Bruchhaus and Prof. Dr. Hanna Lotter at the Bernhard Nocht Institute for Tropical Medicine (BNITM) in Hamburg.

1st Reviewer: Prof. Dr. Iris Bruchhaus
Working group Host-Parasite Interaction
Bernhard Nocht Institute for Tropical Medicine
Bernhard-Nocht-Straße 74, 20359 Hamburg

2nd Reviewer: Prof. Dr. Esther Schnettler
Working group Mosquito-Virus Interaction
Bernhard Nocht Institute for Tropical Medicine
Bernhard-Nocht-Straße 74, 20359 Hamburg

Oral defense: 20.10.2023

Eidesstattliche Erklärung / Declaration on oath

Hiermit erkläre ich an Eides statt, dass ich die vorliegende Dissertationsschrift selbst verfasst und keine anderen als die angegebenen Quellen und Hilfsmittel genutzt habe.

I hereby declare, under oath, that I have written this dissertation on my own and have not used any resources or aids other than those acknowledged.

Hamburg, 19.07.2023

Barbara Honecker

Contents

Summary

Infection with the protozoan parasite *Entamoeba histolytica* (*E. histolytica*) is the cause of amebiasis. While most intestinal infections remain asymptomatic, a minority result in invasive disease. Invasive amebiasis, particularly amebic liver abscess (ALA) formation, occurs predominantly in adult men. An underlying immunopathology, crucially mediated by pro-inflammatory Ly6C^{hi} monocytes, is known to contribute to liver damage in the murine model for the disease and differs between males and females. The mechanisms behind the switch from asymptomatic colonization to parasite invasion are incompletely understood to date. In order to investigate the interaction of the parasite with the host immune system, extracellular vesicles (EVs) as communicators between host and parasite were the focus of this study. EVs are membranous vesicles released by cells into their environment that contain protein, lipids, micro RNAs (miRNAs), and other types of cargo. They are involved in intercellular communication and pathogen-derived EVs have been demonstrated to modulate the host immune response in the context of a variety of infectious diseases. *E. histolytica* EVs and their effects on primary murine monocytes *in vitro* were studied here.

EVs were isolated from amebic clones of differing pathogenicity (low pathogenic A1 and highly pathogenic B2) and characterized with regard to their size, as well as protein and miRNA content. Mass spectrometry and miRNA sequencing revealed differences in the respective cargo between EVs of the two clones that may play a role in pathogenicity. Analysis of the proteome obtained by mass spectrometry showed that *E. histolytica* EVs contained known pathogenicity factors (such as galactose/N-acetylgalactosamine (Gal/GalNac) lectin and the cysteine peptidase (CP) EhCP-A5) and were enriched in transmembrane and signaling proteins. Furthermore, *de novo* miRNA prediction revealed novel mature *E. histolytica* miRNAs that were present in EVs.

Stimulation of male and female primary murine monocytes with EVs *in vitro* resulted in a pro-inflammatory response independent of pathogenicity of the corresponding amebic clone. This was characterized by an increase in the secretion of pro-inflammatory cytokines TNFα, IL-1β, IL-6, and IL-12p40, as well as the chemokines CCL3, CXCL1, and CXCL10, which was partially ablated upon heat inactivation of B2 but not A1 EVs. In addition, EV-stimulated monocytes expressed higher levels of the activation marker CD38 on their surface compared with negative controls. Transcriptome analysis revealed that EV stimulation resulted in activation of key immune pathways, including TLR, TNF, and NF-κB signaling in both male and female monocytes. While the gene expression patterns induced by EV stimulation were similar between male and female monocytes, some sex-specific differences could be detected, for example in the expression of *Lhfpl2*. Stimulation with A1 EVs triggered increased secretion of the granular enzyme myeloperoxidase by monocytes, an effect not observed after B2 EV stimulation. The same was observed in peripheral neutrophils.

In summary, it was shown that A1 and B2 clones of *E. histolytica* release EVs containing immunogenic molecules that activate male and female monocytes, resulting in a pro-inflammatory phenotype.

Zusammenfassung

Die Infektion mit dem protozoischen Parasiten *Entamoeba histolytica* (*E. histolytica*) ist der Auslöser der Amöbiasis. Während die meisten intestinalen Infektionen asymptomatisch verlaufen, führt eine Minderheit zum Ausbruch der Erkrankung nach Invasion des Parasiten. Die invasive Amöbiasis, insbesondere der Amöbenleberabszess (ALA), tritt häufiger bei Männern als bei Frauen auf. Eine maßgeblich durch pro-inflammatorische Ly6C^{hi} Monozyten vermittelte Immunpathologie liegt dem ALA im Mausmodell zugrunde und ist in Männchen und Weibchen unterschiedlich ausgeprägt. Es ist noch nicht gänzlich geklärt, welche Faktoren dazu beitragen, dass aus einer asymptomatischen intestinalen Kolonisierung eine invasive Krankheit entsteht. Um die Interaktion des Parasiten mit dem Immunsystem des Wirts besser zu verstehen, wurden in dieser Arbeit extrazelluläre Vesikel (EV) als Mediatoren der interzellulären Kommunikation untersucht. EV sind von Zellen freigesetzte Membranvesikel, die Proteine, Lipide, Mikro-RNAs (miRNAs) und weitere Moleküle enthalten. Es konnte bereits gezeigt werden, dass EV verschiedener Krankheitserreger die Immunantwort des Wirts zu ihrem Vor- oder Nachteil modulieren können. In dieser Studie wurden die EV von *E. histolytica* und ihre Wirkung auf primäre murine Monozyten *in vitro* untersucht.

Zwei verschiedene *E. histolytica* Klone unterschiedlicher Pathogenität (niedrig pathogener Klon A1 und hoch pathogener Klon B2) wurden zur Isolation von EV genutzt und diese anschließend hinsichtlich ihrer Größe sowie ihres Protein- und miRNA-Gehalts charakterisiert. Durch die Nutzung von Massenspektrometrie und miRNA-Sequenzierung konnten Unterschiede in der Zusammensetzung der EV zwischen den beiden Klonen detektiert werden, die möglicherweise im Kontext der Pathogenität eine Rolle spielen. Die Analyse des Proteoms zeigte, dass die EV von *E. histolytica* bekannte Pathogenitätsfaktoren enthalten (wie zum Beispiel das Galactose/N-Acetylgalactosamin (Gal/GalNac) Lektin und die Cysteinpeptidase (CP) EhCP-A5) und mit Transmembran-, sowie Signalproteinen angereichert sind. Darüber hinaus konnten neue *E. histolytica* miRNAs bioinformatisch identifiziert werden.

Die Stimulation männlicher und weiblicher primärer muriner Monozyten mit EV *in vitro* führte zu einer pro-inflammatorischen Reaktion unabhängig von der Pathogenität des entsprechenden Amöbenklons. Diese war durch einen Anstieg der Sekretion der pro-inflammatorischen Zytokine TNFα, IL-1β, IL-6 und IL-12p40 sowie der Chemokine CCL3, CXCL1 und CXCL10 gekennzeichnet. Die Hitzeinaktivierung von B2 EV führte zum teilweisen Verlust dieses Effekts, nicht aber die Hitzeinaktivierung von A1 EV. Weiterhin waren EV-stimulierte Monozyten im Vergleich zu Negativkontrollen durch eine höhere Oberflächenexpression des Aktivierungsmarkers CD38 gekennzeichnet. Analyse des Transkriptoms ergab, dass die EV-Stimulation zur Aktivierung wichtiger immunologischer Signalwege sowohl in männlichen als auch weiblichen Monozyten führte. Betroffen waren unter anderem die TLR-, TNF- und NF-κB-Signalwege. Obwohl die durch EV-Stimulation in männlichen und weiblichen Monozyten induzierten Genexpressionsmuster große Ähnlichkeiten aufwiesen, konnten geschlechtsspezifische Unterschiede in der Expression einzelner Gene, beispielsweise *Lhfpl2*, festgestellt werden. Des Weiteren löste die Stimulation mit EV des Klons A1 eine erhöhte Freisetzung des granulären Enzyms Myeloperoxidase durch Monozyten aus, welches nach Stimulation mit B2 EV nicht der Fall war. Derselbe Effekt wurde bei peripheren Neutrophilen beobachtet.

Zusammenfassend wurde gezeigt, dass *E. histolytica* Klone A1 und B2 EV freisetzen, welche immunogene Moleküle enthalten und eine aktivierende Wirkung auf männliche und weibliche Monozyten ausüben, die durch einen pro-inflammatorischen Phänotyp charakterisiert ist.

List of figures

List of tables

List of supplementary figures

List of supplementary tables

Abbreviations

AC	Activated charcoal
ACOD1/*Acod1*	Aconitate decarboxylase 1
ADP	Adenosine diphosphate
AF	Alexa Fluor
ALA	Amebic liver abscess
APC	Allophycocyanin
Bhlhe40	*Basic helix-loop-helix family member e40*
BLAST	Basic local alignment search tool
BM	Bone marrow
BNITM	Bernhard Nocht Institute for Tropical Medicine
bp	base pair(s)
BSA	Bovine serum albumin
BV	Brilliant violet
Ca	Calcium
CCL/*Ccl*	CC chemokine ligand
CCR	CC chemokine receptor
CD	Cluster of differentiation
cDNA	Complementary DNA
Clec4e	*C-type lectin domain family 4 member E*
cm^2	square centimeter(s)
CO_2	Carbon dioxide
CP	Cysteine peptidase
CPM	Counts per million
cRPMI	complete RPMI
Ctrl	Control
CXCL/*Cxcl*	CXC motif chemokine ligand
CXCR	CXC motif chemokine receptor
CX_3CR	CX_3C motif chemokine receptor
Cy	Cyanine
DAMP	Damage-associated molecular pattern
DC	Dendritic cell
DE	Differentially expressed
dH_2O	distilled H_2O
DNA	Deoxyribonucleic acid
DPBS	Dulbecco's PBS
E	Efficiency
E.	*Entamoeba*
EDNR/*Ednr*	Endothelin receptor
EDTA	Ethylenediaminetetraacetic acid
ELISA	Enzyme-linked immunosorbent assay
ER	Endoplasmatic reticulum
ESCRT	Endosomal sorting complex required for transport

EV	Extracellular vesicle
FACS	Fluorescence activated cell sorting
FAM20C/*Fam20c*	Family with sequence similarity 20, member C
FBS	Fetal bovine serum
FDR	False discovery rate
FITC	Fluorescein isothiocyanate
FMO	Fluorescence minus one
FSC	Forward scatter
g	gram(s)
G.	*Giardia*
Gal	Galactose
GalNAc	N-acetylgalactosamine
GDP	Guanosine diphosphate
GM-CSF	Granulocyte-macrophage colony-stimulating factor
GO	Gene ontology
GPI	Glycosylphosphatidylinositol
Gpnmb	*Glycoprotein nonmetastatic melanoma protein B*
GTP	Guanosine triphosphate
h	hour(s)
hi	high
h.i.	heat inactivated
HIF	Hypoxia-inducible factor
H_2O	Water
H_2O_2	Hydrogen peroxide
Hpgd	*15-hydroxyprostaglandin dehydrogenase*
HRP	Horseradish peroxidase
HSC70	Heat shock cognate protein 70
H_2SO_4	Hydrogen sulfate (sulfuric acid)
ID	Identifier
Ifi205	*Interferon-activated gene 205*
Ifit	*Interferon induced protein with tetratricopeptide repeats*
IFN	Interferon
Ig	Immunoglobulin
IL-	Interleukin-
ILV	Intraluminal vesicle
iNOS	Inducible nitric oxide synthase
int	intermediate
ISG	Interferon-stimulated gene
Jchain	*Joining chain of multimeric IgA and IgM*
KCl	Potassium Chloride
kDa	kilodalton(s)
KEGG	Kyoto Encyclopedia of Genes and Genomes
K_2HPO_4	di-Potassium hydrogen phosphate
KH_2PO_4	Potassium di-hydrogen phosphate
kV	kilovolt(s)
l	liter(s)

L.	*Leishmania*
LC-MS	Liquid chromatography-mass spectrometry
LFA-1	Lymphocyte function-associated antigen 1
LHFPL2/*Lhfpl2*	Lipoma HMGIC fusion partner-like 2 protein
lo	low
log	logarithm
logfc	log fold change
LPPG	Lipopeptidophosphoglycan
LPS	Lipopolysaccharide
Ly	Lymphocyte (antigen)
MACS	Magnetic-activated cell sorting
MAPK	Mitogen-activated protein kinase
MCP-1	Monocyte chemoattractant protein-1
MET	Monocyte extracellular trap
MFI	Median fluorescence intensity
MHC	Major histocompatibility complex
MIF	Macrophage migration inhibitory factor
min	minute(s)
miRNA	microRNA
MISEV	Minimal information for studies of extracellular vesicles
ml	milliliter(s)
mm	millimeter(s)
MPO/*Mpo*	Myeloperoxidase
mRNA	messenger RNA
MS	Mass spectrometry
MVB	Multivesicular body
N	Normality
NA	Not applicable
NaCl	Sodium chloride
Na_2CO_3	Sodium carbonate
$NaHCO_3$	Sodium hydrogen carbonate
Na_2HPO_4	di-Sodium hydrogen phosphate
NaH_2PO_4	Sodium dihydrogen phosphate
NCBI	National Center for Biotechnology Information
NET	Neutrophil extracellular trap
NF-κB	Nuclear factor kappa-light-chain-enhancer of activated B cells
NGS	Next-generation sequencing
NK	Natural killer
NKT	Natural killer T
NLRP3	NOD-like receptor 3
nm	nanometer(s)
NO	Nitric oxide
NOD	Nucleotide-binding oligomerization domain
ns	not significant
nt	nucleotide(s)
NTA	Nanoparticle tracking analysis

Oasl	*2'-5' oligoadenylate synthetase-like*
PAMP	Pathogen-associated molecular pattern
PBS	Phosphate-buffered saline
PC	Principal component
PCA	Principal component analysis
PCR	Polymerase chain reaction
PE	Phycoerythrin
PerCP	Peridinin-chlorophyll-protein
pg	picogram(s)
PLK/*Plk*	Polo-like kinase
PMA	Phorbol 12-myristate 13-acetate
pmol	picomole(s)
PRR	Patter recognition receptor
Ptges	Prostaglandin E synthase
RasGEF1b/*Rasgef1b*	Ras Guanine Exchange Factor domain family member 1b
RIN	RNA integrity number
RISC	RNA-induced silencing complex
RNA	Ribonucleic acid
RNase	Ribonuclease
RNS	Reactive nitrogen species
ROS	Reactive oxygen species
RPKM	Reads per kilobase per million mapped reads
rpm	revolutions per minute
RPMI	Roswell Park Memorial Institute
Rps9	40S Ribosomal protein S9
RT	Room temperature
RT-qPCR	Real-time quantitative polymerase chain reaction
s	second(s)
SAA/*Saa*	Serum amyloid A
SA-PE	Streptavidin-phycoerythrin
Seq	Sequencing
Sirpb1c	Signal-regulatory protein beta 1C
SLC7A11/*Slc7a11*	*Solute carrier family 7 member 11*
SNARE	Soluble N-ethylmaleimide-sensitive-factor attachment receptor
SOD/*Sod*	Superoxide dismutase
SSC	Sideward scatter
TAN	Tumor-associated neutrophil
TEM	Transmission electron microscopy
TGF	Transforming growth factor
TGM2/*Tgm2*	Transglutaminase 2
Tip-DC	TNF/iNOS-producing dendritic cell
TLR	Toll-like receptor
TM	Transmembrane
TMB	3,3',5,5'-Tetramethylbenzidine
TNF/*Tnf*	Tumor necrosis factor

tRNA	transfer RNA
TSPAN	Tetraspanin
UV	Ultraviolet
Vcam1	*Vascular cell adhesion molecule 1*
VPS	Vacuolar protein sorting
vs.	versus
µg	microgram(s)
µl	microliter(s)
µm	micrometer(s)

1 Introduction

1.1 The innate immune system

The mammalian immune system can be generally divided into two branches: the innate and the adaptive immune system. While innate immune responses are mounted fast in response to an invading pathogen, the adaptive immune response is elicited later but more specific to the pathogen's antigens. Mechanisms of the adaptive immune response include production of antigen-specific antibodies and memory formation, which allows a more rapid and efficient response upon renewed contact with a pathogen after an initial infection. Although many cells are distinctly associated with either innate or adaptive immunity, the two branches do not function completely separately. For example, dendritic cells (DCs), which phagocytose pathogens and present antigens to cells of the adaptive immune system, serve as a bridge between innate and adaptive immunity[1].

Hematopoietic cells of the immune system are macrophages, monocytes, natural killer (NK) cells, natural killer T (NKT) cells, mast cells as well as neutrophilic, eosinophilic and basophilic granulocytes[1,2]. Effector mechanisms of innate immune cells include the phagocytosis of pathogens, the release of cytokines and enzymes with microbicidal activity and degranulation[1].

Release of cytokines and chemokines by cells at the site of infection is an important first step for the recruitment of innate immune cells. Tumor necrosis factor (TNF) α, interleukin (IL-) 1 and IL-6 are some of the first cytokines released during an inflammatory response that contribute to cell recruitment[1]. Innate immune cells recognize pathogen-associated molecular patterns (PAMPs), conserved structures present on the surface of pathogens, via pattern recognition receptors (PRRs), for example toll-like receptors (TLRs), nucleotide-binding oligomerization domain (NOD)-like receptors, or scavenger receptors[2]. In addition, they can recognize damage-associated molecular patterns (DAMPs), molecules released by cells during infection or cell death[2]. Binding to PRRs initiates a signaling cascade, which results in the release of mediators such as cytokines to combat pathogens[3].

This thesis focuses on cells of the innate immune system, which are introduced in further detail below. It should be noted that the innate immune system comprises not only a cellular, but also a humoral component. An important part of this is the complement system, a network of proteins that identify and opsonize invading pathogens, thus aiding with recognition by phagocytic cells and subsequent clearance of the pathogen[1].

1.1.1 Monocytes

Monocytes are mononuclear cells that arise from myeloid precursor cells in the bone marrow and emigrate into the bloodstream, where they constitute 10 % of circulating nucleated immune cells in humans and 4 % in mice[4–7]. In addition, a reservoir of monocytes is present in the spleen, from where they can be rapidly recruited to sites of infection or inflammation[8]. Monocytes have different functions not only in infection and inflammation, but also in homeostasis.

1.1.1.1 Monocyte subsets in mice and humans

In mice, two main types of monocytes are distinguished primarily based on their expression of lymphocyte antigen 6 C (Ly6C) (Figure 1). Classical monocytes expressing high amounts of Ly6C ('Ly6C^{hi}') are recruited to sites of infection, where they release for example pro-inflammatory cytokines and differentiate into M1 macrophages[9]. Ly6C^{hi} monocytes are typically characterized by high expression of the CC chemokine receptor (CCR) 2[4,10,11]. Interaction of CCR2 with CC chemokine ligand (CCL) 2 is required for egress from the bone marrow and recruitment to infected and inflamed tissues[12]. In addition, classical monocytes exhibit high expression of cluster of differentiation (CD) 62L, which is also involved in monocyte migration[4]. Monocytes with low expression of Ly6C ('Ly6C^{lo}'), also called non-classical monocytes, patrol the vasculature, remove cell debris, and repair the endothelium[10]. Ly6C^{lo} monocytes express lower levels of CCR2 than Ly6C^{hi} monocytes but comparatively higher levels of CX_3C motif chemokine receptor (CX_3CR) 1[4,10,11]. They also express the integrin lymphocyte function-associated antigen 1 (LFA-1), which, together with CX_3CR1, is involved in crawling along the endothelium during patrol[7,9,13]. Furthermore, Ly6C^{lo} monocytes do not express CD62L but the glycoprotein CD43[4]. Multiple studies have demonstrated that Ly6C^{lo} monocytes arise from Ly6C^{hi} monocytes, however, evidence also suggests development in the bone marrow without a prior Ly6C^{hi} stage[6,9]. Ly6C^{lo} monocytes are able to differentiate into M2 macrophages[9,13]. Both Ly6C^{hi} and Ly6C^{lo} monocytes express the myeloid marker CD11b. The existence of a Ly6C^{int} monocyte population with intermediate expression of the marker Ly6C, high expression of CX_3CR1 and pro-inflammatory characteristics has also been described in mice[6,10].

In humans, monocytes are distinguished based on their expression of CD14 and CD16. Classical monocytes are CD14^{+}CD16^{-}, intermediate monocytes are CD14^{+}CD16^{+} and non-classical monocytes are CD14^{lo}CD16^{+}[10]. Like murine monocytes, classical human monocytes are characterized by high expression of CCR2 and low expression of CX_3CR1 and vice versa for non-classical monocytes[9]. Human monocyte subsets are phenotypically and functionally equivalent to their murine counterparts.

It should be noted that several studies have identified other monocyte subsets with different functions, particularly through single-cell techniques such as flow cytometry or single-cell RNA sequencing[10,14,15]. For example, a population of classical monocytes with neutrophil-like properties expressing high amounts of granular enzymes has been found in mice[16]. Moreover, monocytes with gene signatures resembling neutrophils have been described in both mouse and human lung tumors and blood[17]. Hence, monocytes are clearly more heterogeneous than illustrated by the categorization into two or three types in mice and humans. Nevertheless, for the purpose of this study, the simple nomenclature of Ly6C^{hi} and Ly6C^{lo} monocytes will be used.

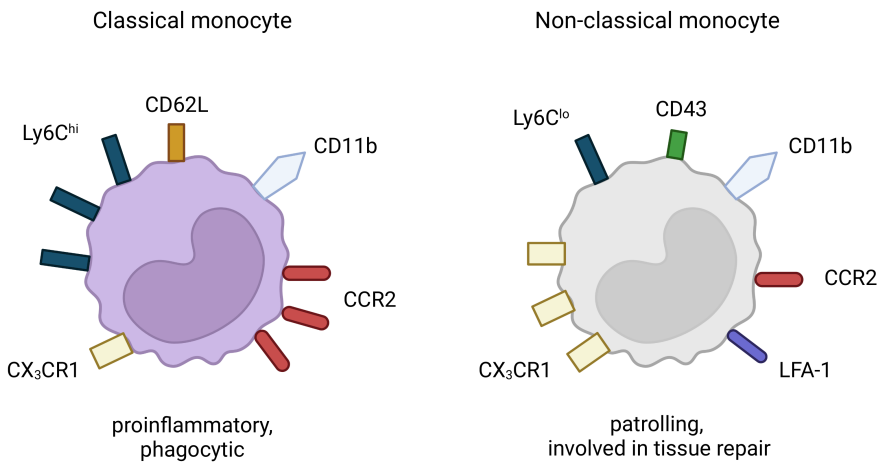

Figure 1: Ly6C^{hi} and Ly6C^{lo} murine monocyte subsets.
Murine monocytes are distinguished into two main subsets based on their expression of Ly6C. Monocytes with high expression of Ly6C ('Ly6C^{hi}') are characterized by high amounts of CCR2, CD62L and low amounts of CX$_3$CR1. In turn, monocytes with low expression of Ly6C ('Ly6C^{lo}') express high amounts of CX$_3$CR1 and low amounts of CCR2. They furthermore express CD43 and LFA-1. Both monocyte subsets are positive for the myeloid marker CD11b. Ly6C^{hi} monocytes are so-called classical monocytes that exhibit pro-inflammatory functions. Non-classical Ly6C^{lo} monocytes are associated more with an anti-inflammatory phenotype and involved in patrol of vasculature and tissue repair. Based on Zimmermann *et al.*[9]. Figure created with BioRender.

1.1.1.2 Monocyte function

Monocytes were long thought to primarily serve the replenishment of the macrophage compartment due to their ability to differentiate into these cells. However, studies have shown that tissue-resident macrophage populations can also be replenished locally and not only by circulating monocytes[5].

The cytokine milieu surrounding monocytes is critically important for their differentiation. While presence of interferon (IFN)-γ, IL-1β, and TNFα promotes the development of M1 macrophages, IL-4, IL-10, IL-13, and transforming growth factor (TGF)-β promote polarization into M2 macrophages[18–22]. M1 macrophages are pro-inflammatory and promote T helper 1 immune responses, whereas M2 macrophages promote T helper 2 responses and contribute to the resolution of inflammation[21,22]. In addition, monocytes can give rise to TNF/inducible nitric oxide synthase (iNOS) producing DCs (Tip-DCs) during infection[23].

Monocytes also possess several effector mechanisms independent of their polarization into another cell type. Ly6C^{hi} monocytes that extravasate into tissues during infection and inflammation contribute to pathogen killing by the release of cytokines and other mediators, as well as phagocytosis[24]. Among the molecules released by activated monocytes to combat an infection are large amounts of reactive oxygen species (ROS), nitric oxide (NO), complement factors, and cytokines like TNFα, CCL3, IL-1β, IL-6, and IL-10[7,24]. Release of chemokines by monocytes also results in chemoattraction of other immune cells to infection and inflammation sites, for example neutrophils. In addition, monocytes have azurophilic granules for the storage of microbicidal mediators such as myeloperoxidase (MPO), which are released during degranulation[25].

As mentioned above, Ly6C^{lo} monocytes are generally described to patrol the vasculature and contribute to tissue repair in steady state. Nevertheless, these monocytes can also egress into infected

tissues. During *Listeria monocytogenes* infection, Ly6C^{lo} monocytes were shown to exhibit a rapid but transient inflammatory response and release TNFα[13].

Although the formation of extracellular DNA traps to capture pathogens is associated mainly with neutrophils (see below, 1.1.2), monocytes are also able to form monocyte extracellular traps (METs) to fight infection[26,27]. Furthermore, monocytes contribute to adaptive immunity through antigen presentation to T cells[4].

1.1.2 Neutrophils

Neutrophils are polymorphonuclear granulocytes, meaning they are characterized by a high amount of protein-containing granules[28]. They are synthesized in the bone marrow in a process called granulopoiesis and their egress into the bloodstream is tightly regulated, particularly by signaling through CXC motif chemokine receptor (CXCR) 2 and CXCR4[28,29]. Neutrophils are the most abundant leukocyte in circulation, constituting approximately 50 – 70 % of all nucleated cells in humans and 10 – 25 % in mice[30]. They are short-lived cells with a rapid turnover and circulate only for around 6 – 8 h[28]. Neutrophils are typically the first cells rapidly recruited to the site of infection and employ several effector mechanisms for the elimination of pathogens, including phagocytosis, neutrophil extracellular trap (NET) formation, and degranulation[31,32]. Degranulation refers to the process of releasing granule cargo either into the phagosome or extracellular space[32]. Neutrophils possess different types of granules, out of which azurophilic granules contain the most toxic and proteolytic cargo, such as MPO or elastase, capable of destroying a vast range of extracellular matrix proteins[32]. During the release of NETs, called NETosis, neutrophils release DNA and granular proteins like MPO to entrap pathogens extracellularly and aid in their killing[32]. NET formation is likely a mechanism employed to combat pathogens that are too big for phagocytosis[33]. Neutrophils also release high amounts of ROS and reactive nitrogen species (RNS) during respiratory burst[28,32]. Through the release of the aforementioned components neutrophils not only contribute to pathogen killing but also inflict damage on host tissue and are involved in a number of acute or chronic inflammatory diseases[28,34].

Furthermore, neutrophils influence tumor development during cancer and influx of neutrophils into tumors has been associated with worse prognosis[28,35]. Studies on tumor-associated neutrophils (TANs) have shown a dual role for these cells and revealed previously unknown diversity and plasticity of neutrophils[29,35]. Similar to the classification of polarized macrophages into M1 and M2 macrophages, N1 and N2 TANs have been described[29,35]. While N2 TANs exert pro-tumor functions through the promotion of cell proliferation, angiogenesis, and metastasis, N1 TANs are associated with anti-tumor activity through direct killing of tumor cells or promotion of T cell-mediated tumor immunity[29,34].

During infection, neutrophils interact with other immune cells such as monocytes or DCs to coordinate pathogen killing. Through the release of chemokines like CCL2 and CCL3, neutrophils lead to the recruitment of monocytes, which, in turn, can also release chemokines for recruitment of more neutrophils[28]. Furthermore, cytokine release by neutrophils can lead to activation and differentiation of T cells[28]. In addition to the role of cytokines in their recruitment or the interaction of neutrophils with other immune cells, neutrophils can also release a number of pro- or anti-inflammatory cytokines that directly act in physiological or inflammatory processes[36].

Murine neutrophils are characterized primarily by their expression of Ly6G, which distinguishes them from Ly6G$^-$ monocytes, together with the myeloid marker CD11b, and Ly6C ($CD11b^+Ly6G^+Ly6C^{int}$)[37–39]. Human neutrophils are characterized by the expression of CD15, CD16 and CD66b and distinguished from monocytes by a lack of CD14 ($CD14^-CD15^+CD16^+CD66b^+$)[39].

1.2 Amebiasis

1.2.1 *Entamoeba histolytica* – life cycle and associated pathophysiology

Entamoeba (E.) histolytica is a unicellular protozoan parasite and the causative agent of the disease amebiasis. *E. histolytica* was first described in 1875 by Fedor Lösch as the cause of dysentery in a patient[40] and given its name by Fritz Schaudinn in 1903 based on the parasite's ability to lyse tissue ('*histolytica*')[41]. Its simple, two-stage life cycle is illustrated in Figure 2.

Infection occurs primarily by ingestion of food or water contaminated with fecal matter, but can also occur through person-to-person contact[40,42]. Sexual transmission has been predominantly, but not exclusively, reported among men who have sex with men[43,44]. The parasite is taken up by the human host as a quadrinucleated cyst that can withstand the gastric acid. Cysts excyst in the small intestine, releasing trophozoites that colonize the intestinal tract and multiply by binary fission. Trophozoites can eventually encyst and be passed with stool again[40,45].

Most infections are asymptomatic, but in an estimated 10 % of cases the parasite becomes invasive, causing disease[40]. Trophozoites can invade the intestinal mucosa, causing amebic dysentery or amebic colitis characterized by inflammation and ulceration of the intestinal tissue. Patients with intestinal amebiasis typically experience pain, weight loss, and bloody or watery diarrhea[42]. The symptoms of amebic colitis mimic those of inflammatory bowel disease, and if misdiagnosed as such and treated with corticosteroids, the risk of developing fulminant amebic colitis, which is associated with high morbidity and mortality, is high[46]. Upon reaching the bloodstream, the parasite can disseminate to other organs, predominantly the liver, causing extraintestinal disease. Parasite invasion into the liver causes the formation of amebic liver abscess (ALA) that is lethal to humans if left untreated. Symptoms of ALA include weight loss, right upper quadrant pain, tenderness, and fever. Onset of symptoms may occur weeks, months, or even years after infection[40]. Hepatic amebiasis occurs in about 1 % of amebiasis cases[45]. Extraintestinal amebiasis in other organs such as brain or skin is rare and occurs almost exclusively in conjunction with ALA[40,45]. Secondary symptoms of ALA rupture may include pleuropulmonary amebiasis[40,45]. Amebic brain abscesses occur almost exclusively in ALA patients, are very rare and exhibit high mortality rates[47,48]. Extraintestinal amebiasis is observed primarily in patients without concurrent intestinal infection[49].

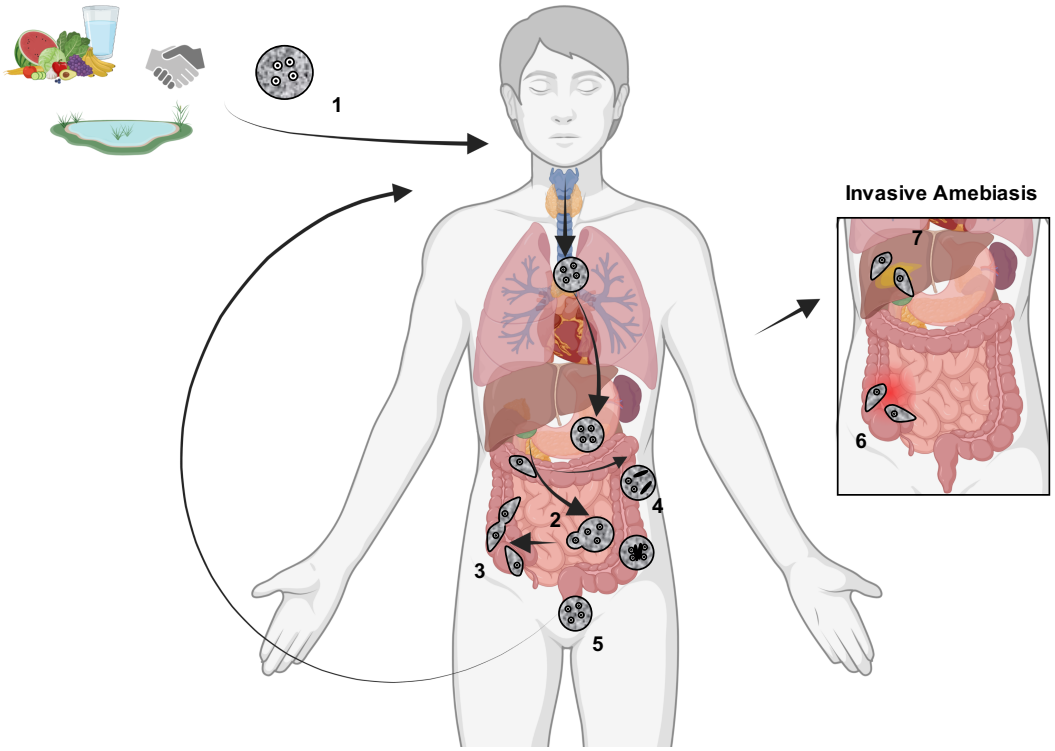

Figure 2: Life cycle of the protozoan parasite *Entamoeba histolytica*.
Infection occurs through the ingestion of cysts present in fecally contaminated food or water or through person-to-person contact (1). Cysts travel through the digestive tract and can withstand the gastric acid. In the small intestine, cysts excyst, releasing trophozoites (2), which can reproduce by binary fission (3) and colonize the intestinal tract. Trophozoites can eventually encyst again (4) and be passed with stool (5). In a minority of infections, the parasite becomes invasive (panel on the right). Invasion of the intestinal mucosa leads to amebic dysentery and amebic colitis (6). Parasites that reach the circulation can disseminate to other organs, predominantly the liver, where they cause amebic liver abscess formation (7).[40,45] Figure created with BioRender.

1.2.2 Epidemiology of *E. histolytica* infection

E. histolytica is endemic to parts of Central and South America, Africa, and Asia and is one of the most common pathogens detected in international travelers returning from endemic countries[42,50]. Several publications report that an estimated 500 million people are infected worldwide. However, many of these are likely colonized by the commensal *E. dispar* and not *E. histolytica,* which also complicates the calculation of the percentage of infections resulting in disease[40]. Infection with *E. histolytica* resulting in amebic colitis is a leading cause of diarrhea worldwide and among the top 15 causes of diarrhea in small children[42,51]. Diarrhea is one of the main causes of death in children under the age of 5[52]. In 2013, 11,300 deaths were reported after infection with *E. histolytica*, a decrease of 39.1 % compared to the death rate in 1990[53,54]. Just three years earlier in 2010, the amount of deaths associated with amebiasis were 55,500[52]. Based on the global burden of disease study 2016 data, it was estimated that more than 26,000 people died of amebiasis in 2016[55]. Nonetheless, current knowledge of the prevalence and disease burden of amebiasis is scarce due to limitations for diagnostics and surveillance in endemic countries as well as heterogeneity of study design[42]. Some reports have shown seroprevalence as high as 42 % in a rural area in Mexico[56], but it should be noted that patients test positive for years after the infection, and it is thus difficult to distinguish current from past infections based on seroprevalence[57,58].

1.2.3 Diagnosis and treatment of amebiasis

Stool microscopy, serological studies, antigen detection (for example via enzyme-linked immunosorbent assay (ELISA)), or polymerase chain reaction (PCR) on stool samples are employed for diagnosis of infection[42]. Morphologically, *E. histolytica* is not distinguishable from three other *Entamoeba* species, *E. moshkovskii, E. dispar,* and *E. bangladeshi*, of which the first is also associated with diarrhea, while the other two are considered non-pathogenic, even though this notion might not be entirely correct for *E. dispar*[41,59]. Furthermore, many ALA patients present without concurrent gastrointestinal infection[42]. Hence, diagnostic methods other than stool microscopy are recommended if available. PCR diagnosis is currently considered the gold standard but may not always be available in resource-limited settings. Computer tomography or magnetic resonance imaging are employed for the diagnosis of ALA[42].

There is currently no vaccine available to prevent infection with *E. histolytica*. Disease prevention relies on provision of access to sanitation and clean drinking water. Patients with symptomatic disease are treated with nitroimidazoles (metronidazole or tinidazole), followed by luminal agents such as paromomycin or iodoquinol for the elimination of remaining trophozoites and cysts in the intestinal lumen[42,60,61]. Asymptomatically infected people are treated with luminal agents to prevent outbreak of invasive disease and further spread of the parasite[40,42]. Significant side effects are associated with the treatment with metronidazole and although resistance has not been detected in *E. histolytica* yet, descriptions of clinical resistance to metronidazole treatment in protozoan parasites of the genera *Giardia* and *Trichomonas* call for the development of alternative treatment options[60].

1.2.4 *E. histolytica* pathogenicity factors and intestinal invasion

During colonization of the host intestine, *E. histolytica* must establish host tolerance in order to survive as a commensal[62]. Symptomatic disease only occurs upon loss of tolerance, resulting in the invasion of the parasite into the intestinal mucosa. To this date, the mechanisms behind onset of invasive disease as opposed to asymptomatic intestinal colonization remain incompletely understood. Changes in the microbiota of symptomatic patients in comparison with asymptomatic carriers have been reported, suggesting a possible involvement of dysbiosis in the onset of disease[63]. Additionally, genetic differences between parasites isolated from asymptomatic carriers, dysenteric patients, and ALA patients were detected in another study, indicating a correlation between parasite genotype and disease outcome[64]. Nevertheless, it has been well studied what happens when the parasite becomes invasive, and several pathogenicity factors have been identified.

The mucus layer of the intestine constitutes the first barrier for the invasion of *E. histolytica*, which the parasite breaks down through the secretion of glycosidases and cysteine peptidases (CPs), particularly EhCP-A5, that can cleave mucin and also contribute to breaking down the extracellular matrix[62,65]. Adherence of amebic trophozoites to host epithelium is essentially mediated by galactose/N-acetylgalactosamine (Gal/GalNac) lectin, which binds to Gal or GalNac on the cell surface, but also involves further proteins such as a 112 kDa adhesin and a metalloprotease[66–68]. The release of the membranolytic amebapore peptides results in the formation of pores in lipid bilayers of host cells, thus conferring cytolytic activity to the parasite[40,69]. Parasites further disrupt tight junctions and induce apoptosis in host cells by activation of caspase 3 to facilitate invasion[70,71]. Dead cells are phagocytosed by amebic trophozoites to evade detection by the immune system and clear the way for invasion[72].

Furthermore, trogocytosis contributes to the destruction of the host epithelium, a process in which trophozoites ingest small pieces of living host cells, thereby killing them and facilitating trophozoite invasion[73]. In addition to the degradation of mucus, CPs are involved in tissue destruction, and overexpression of genes encoding for CPs has been shown to convert non-pathogenic amebae into pathogenic amebae, highlighting the importance of this protein family[74].

The damage induced by *E. histolytica* during invasion elicits a pro-inflammatory response by host cells, leading to chemoattraction of immune cells[62]. Release of prostaglandin E2 by amebae, which is involved in disruption of tight junctions, elicits increased secretion of IL-8 by host epithelial cells, which functions as a chemoattractant for neutrophils and macrophages[67,75,76]. Recognition of Gal/GalNac lectin and lipopeptidophosphoglycan (LPPG) on the surface of amebae through TLRs 2 and 4 on the surface of epithelial cells plays a pivotal role in the activation of Nuclear factor kappa-light-chain-enhancer of activated B cells (NF-κB) signaling leading to the pro-inflammatory response[77]. Antibody-mediated inhibition of LPPG prevents invasive amebiasis, highlighting the importance of this molecule in virulence[78]. Mediators released by recruited immune cells at the site of infection, such as ROS and NETs among others, contribute to tissue damage during inflammation[62,77,79]. In addition, *E. histolytica* can lyse neutrophils, thus contributing to the release of toxic mediators that result in tissue damage[40].

E. histolytica possesses several mechanisms to combat the immune response during invasion. CPs are able to cleave and thus deactivate complement, as well as immunoglobulin A (IgA) and IgG[40,80,81]. Furthermore, the surface of trophozoites is covered by a glycocalyx, of which LPPG is a major component, which functions as a physical barrier for complement[82,83]. In addition, a region within the 170 kDa heavy chain of the Gal/GalNac lectin exhibits antigenic cross-reactivity with human CD59 and thus inhibits the complement membrane attack complex[84]. Surface molecules that have been recognized by the host immune system can be disposed of by the parasite in a process called surface receptor capping[85]. Expression of a superoxide dismutase (SOD) allows the parasite the detoxification of superoxide released during oxidative burst primarily of neutrophils[62,86]. Parasites that enter the circulation to travel to other organs must further survive not only attacks by the host immune system, but also the exposure to oxidative stress, as *E. histolytica* is an anaerobic or microaerophilic organism. In addition to SOD, the parasite therefore possesses several proteins that confer resistance to oxidative stress, such as peroxiredoxin or thioredoxin[77,87,88].

1.2.5 Immune response during hepatic amebiasis

In the liver, *E. histolytica* employs many of the proteins already described in the context of intestinal invasion in order to destroy epithelial cells, hepatocytes and liver-resident macrophages (Kupffer cells), such as glycosidases and CPs[77]. EhCP-A5 is particularly involved in ALA formation[89]. Apart from tissue destructing parasitic pathogenicity factors, the host immune response, elicited in order to control the infection, is also known to contribute to liver damage (Figure 3).

Infection of the liver by amebic trophozoites elicits a rapid influx of neutrophils as the first wave of infiltrating immune cells, which is later followed by monocytes and macrophages[62,90–92]. Control of *E. histolytica* presence is critically mediated by IFN-γ secreting NKT cells activated by LPPG on the surface of trophozoites[93,94]. IFN-γ activates M1 macrophages, which release pro-inflammatory molecules like TNFα, ROS and iNOS[77,95–98]. Nitric oxide (NO) produced by iNOS inhibits amebic pathogenicity factors such as CPs[99]. Liver-resident macrophages (Kupffer cells) also release TNFα[77]. These molecules

contribute to parasite killing but also to tissue damage[77,91]. Parasite-induced tissue damage leads to the secretion of further cytokines by liver cells, including hepatocytes, that recruit immune cells to the site of infection[100,101].

Release of CCL2 by cells at the site of infection, which is amplified by the IL-23/IL-17 immune axis[90,102], leads to recruitment of Ly6C^{hi} monocytes expressing CC chemokine receptor (CCR) 2 from the bone marrow to the site of infection[103]. IL-17 further leads to the recruitment of more neutrophils[104]. The pivotal roles of CCL2 and IL-17 as well as Ly6C^{hi} monocytes recruited by CCL2 in ALA formation have been demonstrated by a reduction in the immunopathology in respective knockout mice[90,91]. Recruited Ly6C^{hi} monocytes produce CXC motif chemokine ligand (CXCL) 1, which binds to CXCR2 on neutrophils but also monocytes and thus increases immune cell infiltration[105–107]. Ly6C^{hi} monocytes can also differentiate into M1 macrophages as the result of the pro-inflammatory environment.

Due to the usually comparatively late diagnosis of ALA in humans, our knowledge of the underlying immune processes stems primarily from animal models, such as mice. Interestingly, in contrast to humans, mice are able to resolve ALAs[90,93]. Ly6C^{lo} monocytes patrolling the endothelium can be recruited to the site of infection via CCR5[90,103]. Release of IL-13 by Ly6C^{lo} monocytes is involved in tissue regeneration[90]. IL-13 and IL-4 lead to the polarization of Ly6C^{lo} monocytes into M2 macrophages, which, in turn, produce arginase 1 and contribute to tissue recovery[90,96,108,109].

In summary, it is well established that the host immune response to *E. histolytica* infection of the liver is critically mediated by monocytes that contribute to liver pathology. The role of neutrophils in this context is comparatively more controversial. Although it is known that mediators released by neutrophils contribute to tissue damage, there is currently no scientific consensus as to whether the general role of neutrophils in hepatic, but also intestinal, amebiasis is a protective or a destructive one, as investigators have found evidence for both in different models[110].

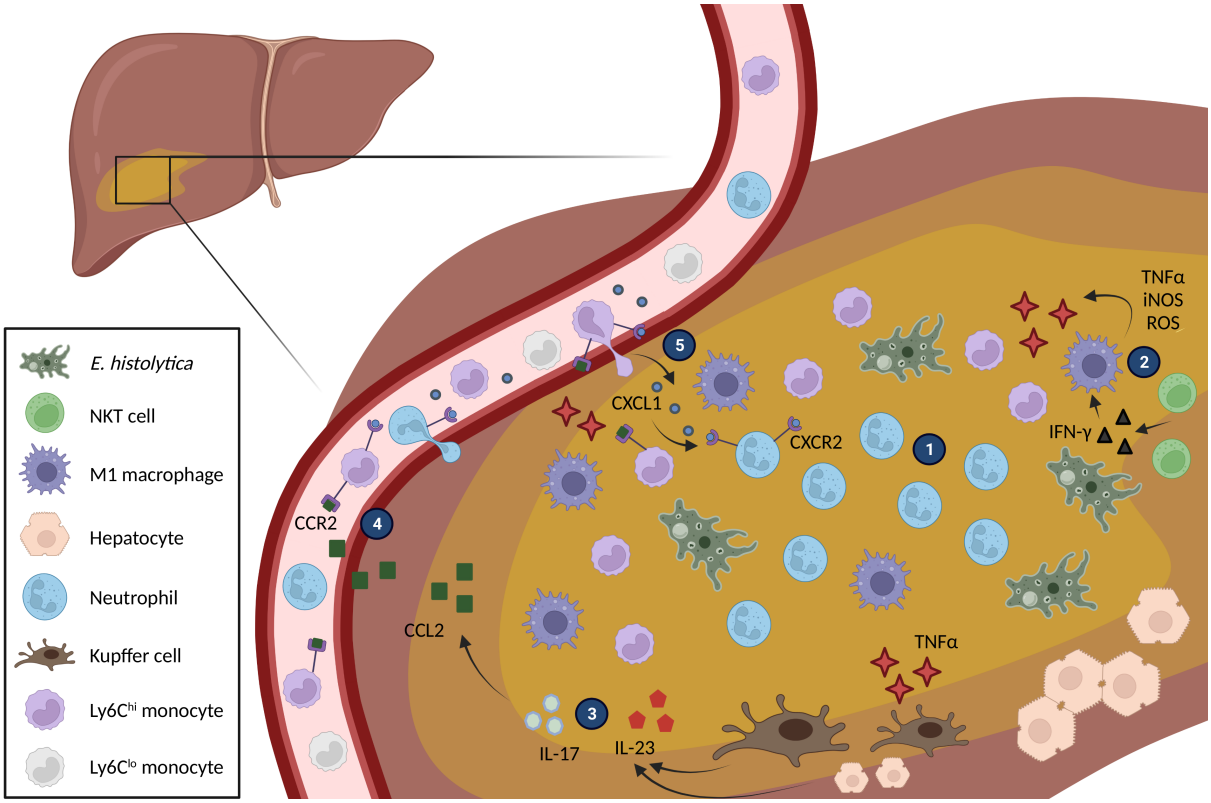

Figure 3: Immunopathology of amebic liver abscess (ALA) formation.
The first wave of infiltrating immune cells upon infection consists primarily of neutrophils, which accumulate at the center of the lesion (1). The presence of *E. histolytica* in the liver triggers IFN-γ release by natural killer T (NKT) cells to combat the infection (2). IFN-γ activates M1 macrophages, which release cytotoxic molecules to kill parasites (TNFα, iNOS, ROS), but also contribute to tissue damage. Liver-resident macrophages (Kupffer cells) and hepatocytes release cytokines in response to tissue damage to attract further immune cells (3). CCL2 release is promoted through the IL-23/IL-17 immune axis and leads to the recruitment of CCR2-expressing pro-inflammatory Ly6C^{hi} monocytes from the bone marrow via the bloodstream (4). Ly6C^{hi} monocytes release CXCL1, which binds to CXCR2 on classical monocytes themselves and on neutrophils, reinforcing the recruitment of more cells (5). Ly6C^{hi} monocytes can also polarize into M1 macrophages. TNFα secreted by Kupffer cells, M1 macrophages and Ly6C^{hi} monocytes is a major contributor to the observed immunopathology. Patrolling Ly6C^{lo} monocytes can also be recruited from the circulation to the site of infection, where they differentiate into M2 macrophages and contribute to tissue regeneration (not shown). Based on Sellau *et al.*[96]. Figure created with BioRender.

1.2.6 Sex difference in hepatic amebiasis

ALA formation is more prevalent in adult men compared with women and very rare in children. In a study in a high-incidence region in Vietnam, a ratio of 7:1 ALA cases in males compared to females ages 30 – 49 years was determined[111]. Other studies have reported a bias towards the male sex also for other manifestations of invasive amebiasis[112]. Although there are some epidemiological studies that have reported higher infection rates in men[57], overall infection rates do not seem to differ between the sexes[112]. In the abovementioned Vietnam study, infection was even higher in females[111]. Consequently, it can be concluded that the observed sex dimorphism in manifestations of invasive amebiasis such as ALA formation is not the result of a bias in infection rates.

Biological sex is known to predispose for susceptibility to infectious and autoimmune diseases. While men generally suffer from higher disease burden caused by infections, autoimmune diseases are more prevalent in women[113]. This effect is caused by a stronger innate and adaptive immune response in women as the result of several genetic and hormonal factors[113]. Multiple studies have reported an

influence of steroid hormones on the outcome of infectious disease, including parasitic infections[114–117].

The use of a mouse model, which exhibits the same sex dimorphism as seen in humans, has allowed the identification of several factors that contribute to differences in ALA formation between the sexes. In this model, abscesses are larger in males and females clear abscesses faster[93]. Although the composition of cellular infiltrates during ALA is similar in males and females, cytokine production during the early phase of abscess formation differs between the sexes. In females, higher concentrations of IFN-γ secreted mainly by NKT cells leads to faster clearance of the parasite, and accordingly, researchers have shown that immunodepletion of IFN-γ in female mice results in larger abscesses[93]. IFN-γ release by NKT cells is known to be enhanced by the female sex hormone estradiol[118]. Furthermore, it was found that testosterone inhibits the release of IFN-γ by NKT cells, and testosterone substitution in females resulted in larger abscesses compared with untreated females in an ALA mouse model[119]. Testosterone also promotes the expression of CXCL1 by Ly6C^{hi} monocytes, which contributes to ALA immunopathology[105]. Relative amounts of Ly6C^{hi} monocytes are higher in male mice at ALA day 3 compared with female mice and Ly6C^{hi} monocytes in males produce more TNFα[105].

The correlation of serum testosterone levels with the incidence of ALA in adult men further underlines the significance of this hormone in parasite-induced liver pathology[114]. In addition, men with asymptomatic *E. histolytica* infection have higher serum levels of CCL2 than women[120] and male Ly6C^{hi} monocytes express higher amounts of CCR2 compared to their female counterparts[105], suggesting a predisposition for CCL2-mediated immunopathologies. Female asymptomatic carriers have higher total IgG and IgG1 serum titers than male carriers[120], indicating a more efficient protective immune response in women. Furthermore, assays with human serum showed that complement-mediated killing of amebic trophozoites is more effective in women compared with men[121].

1.3 Extracellular vesicles

Extracellular vesicles (EVs) are membranous vesicles released by all types of cells, from single-celled microbes to plants or cells in the human body[122]. EVs are typically classified into three main groups based on their biogenesis pathway and size: exosomes, microvesicles, and apoptotic bodies (Figure 4)[123]. While the term exosome denotes small vesicles of typically 30 – 100 nm originating from multivesicular bodies (MVBs), microvesicles are vesicles released by direct budding from the plasma membrane and are typically around 100 – 1000 nm in size[122,124,125]. Apoptotic bodies are vesicles released by membrane blebbing of apoptotic cells that are even larger than microvesicles[123]. However, recent studies have shown that there are many more different types of EVs than can be illustrated by this classification into three types. Furthermore, many researchers have used the terms 'exosomes' and 'microvesicles' to describe EVs of a certain size, without proof of the corresponding biogenesis pathway[125]. Because different EV populations can overlap in their sizes but also in the cargo they contain[122], the International Society for Extracellular Vesicles recommends the use of the general term 'EVs' as opposed to more specific terms in the absence of proof of biogenesis[126], hence, the term 'EVs' will be used in the course of this thesis.

EVs are mediators of intercellular communication in the absence of direct cell-cell contact both during steady state and pathological conditions, for example in infections[125]. They contain proteins, lipids, and nucleic acids, including various species of long and short ribonucleic acids (RNAs), among other types of cargo[122,127]. Apoptotic bodies may even contain entire organelles[123]. Messenger RNA (mRNA) present in EVs can be translated in target cells and transported micro RNA (miRNA) can induce gene silencing, thus, EVs can modulate the genetic profile of their target cells[125,128].

In recent years, EVs have been increasingly investigated with regard to their role in cell-cell communication between pathogens and their host. An overview of the current knowledge of EVs in infectious disease is given in chapter 1.3.2. Furthermore, EVs are studied as promising vehicles for drug delivery or vaccines due to their ability to circulate in bodily fluids, as well as biomarkers for disease due to changes in EV cargo or abundance as the result of disease onset[129–133].

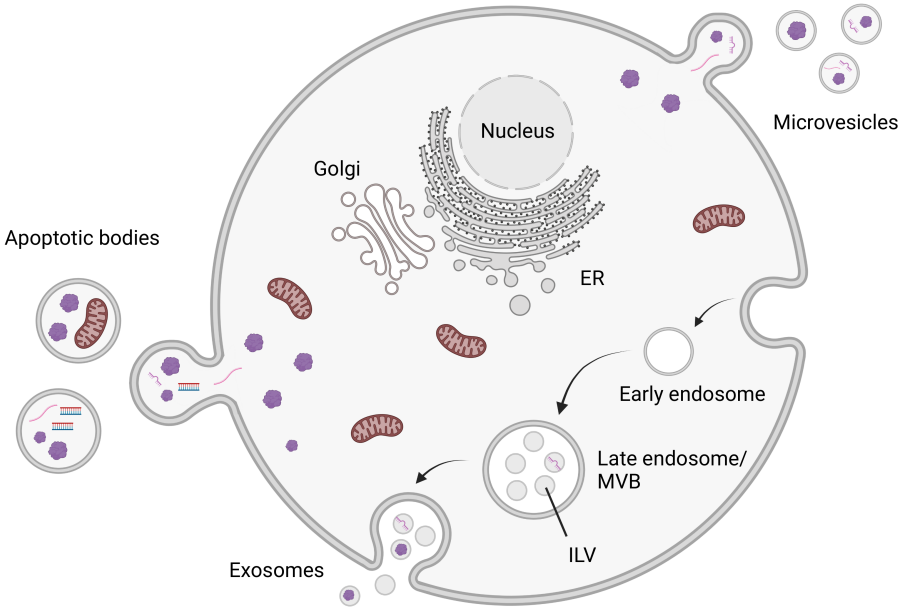

Figure 4: Types of extracellular vesicles.
Three main types of extracellular vesicles (EVs) secreted by cells are distinguished: exosomes, microvesicles, and apoptotic bodies. Exosomes are products of the endosomal pathway, in which invaginations of the endosomal membrane lead to formation of small intraluminal vesicles (ILVs) in multivesicular bodies (MVBs) that are eventually secreted. Microvesicles are released by direct budding from the plasma membrane and are larger than exosomes. Proteins, different species of RNA, DNA, or lipids are among the types of cargo selectively packaged into exosomes and microvesicles. Apoptotic bodies bud off from the plasma membrane of apoptotic cells, are larger than microvesicles and may contain entire organelles and larger amounts of fragmented genetic material compared with microvesicles. This categorization into three types is simplified and non-exhaustive as there are multiple other variations of secreted EVs. ER = Endoplasmatic reticulum. Based on Carrera-Bravo *et al.*[123] and Dang *et al.*[132]. Figure created with BioRender.

1.3.1 Biogenesis of extracellular vesicles

The biogenesis of EVs is complex and although much is already known, many questions remain yet unanswered. In this chapter, the key mechanisms involved in biogenesis of exosomes and microvesicles will be briefly introduced.

Budding of microvesicles from the plasma membrane requires rearrangements in membrane components and alterations in Ca^{2+} levels[122]. Calcium-dependent enzymes catalyze for example the translocation of phosphatidylserine from the inner leaflet to the surface, resulting in bending of the membrane and rearrangement of the actin cytoskeleton, followed by formation of microvesicles[122]. Budding can also occur by mechanisms independent of lipid rearrangement, for example via enzymatic regulation of the cytoskeleton by Rho GTPases[122].

Exosomes are generated as part of the endosomal pathway. During the maturation of the late endosome, invagination of the endosomal membrane results in the formation of intraluminal vesicles (ILVs) (Figure 4). ILV-containing endosomes are called MVBs. In most cases, MVBs are targeted to the lysosome for degradation. However, MVBs can also fuse with the plasma membrane and release their ILV content, then called exosomes[122,125]. It has been suggested by multiple studies that MVBs fated for degradation or exocytosis differ morphologically and also contain different cargo[125].

Cargo is selectively packaged into EVs and depends on cell type, physiological state, and various stimuli. Proteins involved in the recruitment and packaging of EV content are for example syntenin, adenosine diphosphate (ADP)-ribosylation factor 6 or the small GTPase RAS-related protein RAB22A[122]. In order to be packaged into microvesicles, cytosolic cargo needs to bind to the inner leaflet of the plasma membrane[122]. Lipids and membrane-associated proteins cluster in microdomains of either the plasma membrane or the endosomal membrane, depending on the vesicle type[122]. These microdomains are involved in the recruitment of soluble cargo for sorting into EVs[122]. The packaging of short and long RNA species into EVs is not well elucidated yet, but several RNA-binding proteins have been described to play a role in this process[134]. Furthermore, the existence of a specific motif in miRNA packaged into EVs has been determined[135].

There are several mechanisms involved in the formation of ILVs, which may function separately or in concerted efforts. One of the main biogenesis pathways of ILVs is mediated by the endosomal sorting complex required for transport (ESCRT) proteins that cluster in ESCRT-0, -I, -II and -III complexes together with associated proteins, a mechanism highly conserved between different species and also present in protozoa[125,136,137]. ESCRT-0 sequesters ubiquitinated transmembrane proteins into microdomains and recruits ESCRT-I to help with cargo sorting. ESCRT-I subsequently recruits ESCRT-II and ESCRT-III. ESCRT-I and -II are involved in budding of the membrane, while ESCRT-III crucially regulates fission[122,125,136]. Dissociation and recycling of the ESCRT complexes is mediated by interaction with the ATPase vacuolar protein sorting 4 (VPS4)[125]. Sorting of soluble cargo into vesicles is likely aided by chaperones such as heat shock cognate protein 70 (HSC70)[125,138]. In addition to mediating the biogenesis of ILVs, ESCRT complexes are also involved in the budding of microvesicles from the plasma membrane. Here, it is known that ESCRT-I is involved in cargo clustering and ESCRT-III in vesicle fission[122]. ILV formation can also occur via ESCRT-independent mechanisms, as demonstrated by inactivation of all four ESCRT complexes, which did not lead to absence of MVBs[139]. Multiple tetraspanins are involved in ESCRT-independent cargo sorting and biogenesis, particularly CD63, which accumulates in ILVs also in the absence of ESCRTs[139,140]. Clustering of tetraspanins with other transmembrane and membrane-associated proteins leads to the formation of budding microdomains[122]. In addition, the tetraspanins CD9, CD81, and CD82 sort cargo into exosomes[122]. Furthermore, the generation of specific lipids in the endosomal membrane by sphingomyelinase or phospholipase has been shown to induce ILV budding[125]. This was first demonstrated by the finding that ceramide, which results from hydrolyzation of sphingomyelin by sphingomyelinase, creates membrane domains that induce spontaneous negative membrane curvature[122,141,142].

In order to release ILVs into the extracellular space as exosomes, MVBs have to be targeted to the plasma membrane. Interestingly, Rab GTPases are involved in trafficking of MVBs both to the plasma membrane for exocytosis and to the lysosome for degradation[122]. It is still unclear what determines the MVB fate, but changes in their membrane composition might be a reason[122]. Fusion of the MVB membrane with the plasma membrane is likely mediated by soluble N-ethylmaleimide-sensitive-factor attachment receptor (SNARE) proteins[122].

Finally, vesicles released into the extracellular space can bind to target cells through receptor-ligand interaction, involving for example tetraspanins or integrins, or fuse with the plasma membrane, a process that is currently not well understood[122,143]. Bound EVs may be taken up by target cells through endocytosis to deliver their cargo, or remain bound to the cell surface and trigger intracellular signaling cascades or antigen presentation[122].

1.3.2 Extracellular vesicles in host-parasite interaction

Many studies demonstrate the involvement of pathogen-derived, host cell-derived, or infected host cell-derived EVs in the outcome of infectious diseases with bacterial, viral, fungal, or parasitic etiological agents. Key findings for the role of EVs in host-parasite interaction of single-celled parasites are briefly summarized here.

Entamoeba (E.) histolytica-derived EVs have been described in three reports in scientific literature, out of which two were comprehensive studies of the isolated EVs[144–146]. The third study isolated EVs only for the detection of a secreted protein via immunogold labeling and did not characterize them further[146]. Sharma *et al.* investigated the effect of these EVs on encystation of *E. invadens*, an amebic parasite of reptiles that, in contrast to *E. histolytica*, can encyst *in vitro*[144]. Their results suggest a role of amebic EVs in parasite-parasite communication. In addition, they reported an accumulation of transfer RNA (tRNA) halves as stress response in their EVs in a follow-up study[147]. Furthermore, Díaz-Godínez *et al.* found that *E. histolytica* EVs carried ROS to target cells, and reduced NETosis and oxidative burst of human neutrophils *in vitro*[145]. *Giardia intestinalis (G. intestinalis)* is a protozoan parasite with a life cycle that resembles that of *E. histolytica* (described in 1.2.1) and the causative agent of the diarrheal disease giardiasis. *G. intestinalis*-derived EVs have been studied more extensively in the context of host-parasite interaction compared to their *E. histolytica* counterparts. *G. intestinalis* EVs have been found to impact the parasite's capacity to cytoadhere to host cells *in vitro*[148,149] and exert bacteriostatic effects on commensal bacteria[150]. Moreover, Zhao *et al.* showed that *G. intestinalis* EVs could be taken up by murine peritoneal macrophages and triggered pro-inflammatory immune responses via TLR2 and the NOD-like receptor 3 (NLRP3) inflammasome signaling pathway, resulting in increased release of cytokines like TNFα, IL-1β, and IL-6[151].

Studies on malaria parasites have shown that EVs secreted by *Plasmodium falciparum*-infected erythrocytes are implicated in cell-cell communication between parasites and regulate life cycle completion by synchronizing commitment of asexual parasites to the sexual stage[152–154]. They have been found to both activate and suppress innate immune responses, depending on the study context[155]. Furthermore, uptake of miRNA-containing EVs by endothelial cells has been demonstrated to result in parasite sequestration and may be implicated in the breakdown of the blood-brain barrier during cerebral malaria[123,156]. Multiple roles of EVs have also been demonstrated for *Trichomonas vaginalis*, including increase of cytoadhesion to host cells and anti-inflammatory effects, enabling colonization and thus resulting in parasite persistence[157,158].

For *Leishmania (L.)*, EVs secreted *in vitro* as well as *in vivo* in the sandfly midgut harbor virulence factors and possess immunomodulatory properties that are predominantly pro-parasitic[159]. For example, *L. donovani*-derived EVs modulated the cytokine response of human monocytes to IFN-γ by inducing IL-10 and suppressing TNFα release[160,161]. Treatment of mice with *L. donovani* or *L. major*-derived EVs prior to challenge with the corresponding parasite led to disease exacerbation due to immunosuppression[159,161], and, in another study, co-injection of EVs and parasites increased pathology due to increases in pro-inflammatory cytokines[162]. In the context of toxoplasmosis, DC-derived EVs loaded with *Toxoplasma gondii* antigens were used for vaccination of mice, which exhibited increased survival rates upon parasite challenge compared with non-vaccinated mice[163]. In contrast, *Trypanosoma cruzi*-EVs injected into mice prior to challenge severely exacerbated cardiac pathology[164].

In summary, the roles of parasite-derived EVs or EVs secreted by infected host cells in host-parasite interaction are manifold and can be either beneficial to the parasite by suppressing the immune system and promoting persistence or beneficial to the host by accelerating parasite clearance. Understanding the role of EVs in the pathogenesis of parasitic diseases could lead to development of new treatment options.

1.4 Aim of the study

To further elucidate the mechanisms of host-parasite interaction in the context of *E. histolytica* infection, the involvement of EVs was investigated here.

EVs were characterized with regard to their biological properties as well as their immunostimulatory potential. For the investigation of mechanisms involved in amebic virulence, EVs were isolated from two clones of *E. histolytica* differing in their pathogenicity. The two clones, A1 and B2, were previously cloned from amebic cell lines HM-1:IMSS-A and HM-1:IMSS-B at the BNITM[74,165]. While injection of B2 trophozoites into gerbil and mouse livers resulted in ALAs that were still present 7 days after injection, injection of A1 trophozoites resulted in comparatively smaller lesions that were resolved by day 7 after injection. Hence, B2 trophozoites are considered to be pathogenic, while A1 trophozoites are associated with low pathogenicity.

Since a monocyte-mediated immunopathology is known to underlie ALA formation[91,105], interaction of EVs with monocytes was the focus of this study. Monocytes were isolated from male and female mice to determine putative sex-specific differences in the immune response to *E. histolytica* EVs. Furthermore, EV stimulation of neutrophils, another cell type involved in the onset of invasive amebiasis, was characterized as part of a master project[166], whose key findings will be briefly discussed in this thesis.

Taken together, the main aims of this thesis were:

- Isolation of EVs from *E. histolytica* cultured *in vitro* and characterization of EVs using transmission electron microscopy (TEM) and nanoparticle tracking analysis (NTA).
- Analysis of the protein and miRNA cargo of *E. histolytica* EVs using mass spectrometric and sequencing approaches.
- Investigation of the immunostimulatory potential of EVs on male and female murine primary monocytes with regard to:
    - The secretion of cytokines and MPO as determined by ELISA and LEGENDplex™.
    - The expression of surface markers for activation as determined by flow cytometry.
    - The gene expression profile as determined by RNA sequencing (RNA-Seq) and real-time quantitative PCR (RT-qPCR).

2 Material and Methods

2.1 Material

2.1.1 Organisms

Table 1: List of organisms.

Species	Strain / Clone	Origin
Entamoeba histolytica	HM-1:IMSS-A; clone A1	Meyer *et al.* (2016)[165]
Entamoeba histolytica	HM-1:IMSS-B; clone B2	Meyer *et al.* (2016)[165]
Mus musculus	C57BL/6J	BNITM animal facility

2.1.2 Consumables

Table 2: List of consumables.

Consumable	Manufacturer	Catalog number
Anaerocult® A	Merck KGaA	1.13829.0001
Anaerotest® (pH strips)	Merck KGaA	1.15112.0001
Carbon and formvar coated nickel grids for TEM	Plano GmbH	S162N3
Cell strainer, 70 µm, sterile	SARSTEDT AG & Co. KG	83.3945.070
CellTrics™ 30 µm, sterile	Sysmex Partec GmbH	04-004-2326
Disposable hypodermic needle, 0.40 x 20 mm	B. Braun	4657705
Filtropur S 0.2	SARSTEDT AG & Co. KG	83.1826.001
LightCycler® 480 Multiwell Plate 96, white	F. Hoffmann-La Roche AG	04729692001
LS columns	Miltenyi Biotec	130-122-729
Microplate, 96 well, PS, F-bottom, Microlon®, high binding	Greiner Bio-One GmbH	655061
Omnifix®-F Tuberculin 1 ml syringes, Luer Solo	B. Braun Melsungen AG	9161406V
Open-Top Thinwall Polypropylene Tube, 25 x 89mm - 50Pk, 38.5 mL	Beckman Coulter, Inc.	326823
Qubit™ Assay Tubes	Invitrogen™ by Thermo Fisher Scientific Inc.	Q32856
Stericup® Quick Release Millipore Express® PLUS 0.22µm PES, 250 ml	Merck KGaA	S2GPU02RE
Test tubes for haematological analyses	KABE Labortechnik GmbH	078001

Tissue culture flask T25, Standard	SARSTEDT AG & Co. KG	83.3910
Tube, 5 ml, (LxØ): 75 x 12 mm, PS for flow cytometry	SARSTEDT AG & Co. KG	55.1579

2.1.3 Instruments

Table 3: List of instruments.

Instrument	Manufacturer
2100 Bioanalyzer	Agilent Technologies, Inc.
BD Accuri™ C6 Flow Cytometer	BD Biosciences
BD® LSR II Flow Cytometer	BD Biosciences
Cytek® Aurora 5-Laser Spectral Flow Cytometer	Cytek® Biosciences
EasySep™ Magnet	STEMCELL Technologies
LightCycler® 96	F. Hoffmann-La Roche AG
MidiMACS™ Multistand	Miltenyi Biotec
MidiMACS™ Separator	Miltenyi Biotec
MRX^{e} Microplate Reader	DYNEX Technologies, Inc.
NanoDrop™ 2000 Spectrophotometer	Thermo Fisher Scientific Inc.
NanoSight LM10 with LM14C viewing unit	Malvern Panalytical Ltd
NextSeq 550 System	Illumina, Inc.
NovaSeq 6000 System	Illumina, Inc.
Optima XE-90 Ultracentrifuge with SW32 Ti Swinging-Bucket Rotor	Beckman Coulter, Inc.
Qubit™ 4 Fluorometer	Invitrogen™ by Thermo Fisher Scientific Inc.
Sonorex Super ultrasonic bath	Bandelin electronic GmbH & Co. KG
Tecnai™ Spirit TEM	Thermo Fisher Scientific Inc.

2.1.4 Chemicals and reagents

Table 4: List of chemicals and reagents.

Chemical	Manufacturer	Catalog number
Acetic Acid, ROTIPURAN® 100 %, p.a.	Carl Roth GmbH + Co. KG	3738.2
Albumin bovine Fraction V, Protease-free (BSA)	SERVA Electrophoresis GmbH	11926.03
Ammonium chloride (NH_4Cl) ≥99.7 %, p.a.	Merck KGaA	K298.1
Ammonium iron(III) citrate, reagent grade	Sigma-Aldrich, Co.	F5879
Charcoal, Dextran Coated	Sigma-Aldrich, Co.	1003406518
Chlorofom for analysis	Merck KGaA	1.02442.2500

Collagen from calf skin, Bornstein and Traub Type I (Sigma Type III), acid soluble	Sigma-Aldrich, Co.	C3511
D(+)-Glucose, p.a. ACS, anhydrous	Carl Roth GmbH + Co. KG	X997.3
Difco™ Tryptone	Gibco™ by Thermo Fisher Scientific Inc.	211921
di-Potassium hydrogen phosphate (K_2HPO_4), anhydrous for analysis	Merck KGaA	1.05104.1000
di-Sodium hydrogen phosphate dihydrate ($Na_2HPO_4x2H_2O$) ≥99 %, p.a.	Carl Roth GmbH + Co. KG	4984.1
Ethylenediaminetetraacetic acid (EDTA) disodium salt dihydrate	Carl Roth GmbH + Co. KG	8043.2
Ethanol absolute for analysis EMSURE® ACS, ISO, Reag. Ph Eur	Merck KGaA	1.00983.2500
Glutaraldehyde 25 % solution, EM grade distillation purified	Electron Microscopy Sciences	16210
Glycine, BioUltra, for molecular biology ≥99.0% (NT)	Sigma-Aldrich, Co.	50046
L(+)-Ascorbic acid	VWR International, LLC	20150.184
L-Cysteine Hydrochloride Anhydrous	United States Biological	C9005
Lipopolysaccharide (LPS) from Escherichia coli O26:B6, γ-irradiated, BioXtra, suitable for cell culture	Sigma-Aldrich, Co.	L2654
Potassium chloride (KCl) for analysis, EMSURE®	Merck KGaA	1.04936.1000
Potassium dihydrogen phosphate (KH_2PO_4) for analysis, EMSURE® ISO	Merck KGaA	1.04873.0250
2-Propanol ROTIPURAN® ≥99.8 % p.a., ACS, ISO, Reag. Ph Euro	Carl Roth GmbH + Co. KG	6752.4
QIAzol™ Lysis Reagent	QIAGEN	79306
Sodium carbonate (Na_2CO_3), anhydrous for analysis, EMSURE® ISO	Merck KGaA	1.06392.1000
Sodium chloride (NaCl), ≥99.5 %, p.a., ACS, ISO	Carl Roth GmbH + Co. KG	3957.1

Sodium dihydrogen phosphate dihydrate ($NaH_2PO_4x2H_2O$) ≥99 %	Carl Roth GmbH + Co. KG	T879.2
Sodium hydrogen carbonate ($NaHCO_3$)	Sigma-Aldrich, Co.	S5761
Sulfuric acid (H_2SO_4), 95 – 97 %, p.a.	Merck KGaA	100731
TRIS PUFFERAN® ≥99.5 %, p.a.	Carl Roth GmbH + Co. KG	4855.2
Trypan Blue Stain (0.4 %)	Gibco™ by Thermo Fisher Scientific Inc.	15250-061
TWEEN® 20	Sigma-Aldrich, Co.	P1379
2% Uranyl acetate solution	Science Services GmbH	E22400-2
Yeast Extract	Gibco™ by Thermo Fisher Scientific Inc.	211929

2.1.5 Buffers and media supplements

Table 5: Buffers and culture media supplements.

Buffer/Supplement	Manufacturer	Catalog number
Adult Bovine Serum, sterile filtered	Capricorn Scientific GmbH	ABS-1D
Diamond Vitamin Tween 80 Solution, 40x	BioConcept Ltd.	5-78F00-I
DPBS w/o Calcium, Magnesium	PAN-Biotech GmbH	P04-361000
Fc blocking buffer	Kindly provided by the research group Protozoa Immunology (BNITM)	
Fetal Bovine Serum (FBS) Advanced	Capricorn Scientific GmbH	FBS-11A
L-Glutamine (200 mM, sterile filtered)	PAN-Biotech GmbH	P04-80100
Penicillin/Streptomycin Solution (100x) (RPMI supplement)	AppliChem GmbH	A8943,0100
Penicillin/Streptomycin Solution (100x) (for *E. histolytica* culture)	Capricorn Scientific GmbH	PS-B
RPMI 1640 w/o L-Glutamine, w 2.0 g/L $NaHCO_3$	PAN-Biotech GmbH	P04-17500

Table 6: Recipes for buffers and culture media.

Buffer/Medium	Composition
Blocking buffer (TEM)	0.5 % BSA Fraction V in 1x PBS
Coating buffer (ELISA)	8.4 g/l $NaHCO_3$ 3.56 g/l Na_2CO_3 in dH_2O, adjust pH to 9.5
cRPMI	10 % FBS-AC* 1 % 200 mM L-Glutamine 1 % Penicillin/Streptomycin (100x) in RPMI 1640
Erythrocyte lysis buffer	Component I: 0.16 M NH_4Cl (8.5 g/l) in dH_2O Component II: 0.17 M Tris (20.6 g/l) (pH 7.6) in dH_2O combine 9 parts component I with 1 part component II directly before use
Flow cytometry buffer	1 % FBS in 1x PBS
MACS Buffer (10x)	4 % 0.5 M EDTA 50 g/l BSA Fraction V in 1x PBS, adjust pH to 7.2, filter 0.22 µm
NaPBS	1.19 g/l $Na_2HPO_4x2H_2O$ 0.51 g/l $NaH_2PO_4x2H_2O$ 8.18 g/l NaCl in dH_2O, adjust pH to 6.8
PBS (10x)	80 g/l NaCl 2 g/l KCl 2.4 g/l KH_2PO_4 17.8 g/l $Na_2HPO_4x2H_2O$ in dH_2O, adjust pH to 7.4
TY-I-S-33 medium (complete)	10 % Adult Bovine Serum, h.i.** 3 % Diamond Vitamin Tween 80 Solution 1% Penicillin/Streptomycin (100 x) in incomplete TY-I-S-33
TY-I-S-33 medium (incomplete)	11.494 g/l Glucose 0.026 g/l Ammonium iron(III) citrate 1.149 g/l L-Cysteine 0.874 g/l K_2HPO_4 0.690 g/l KH_2PO_4 2.299 g/l NaCl 0.230 g/l L-Ascorbic acid 11.494 g/l Yeast extract 22.989 g/l Tryptone in dH_2O, adjust pH to 6.8, autoclave
Wash buffer (ELISA)	0.5 % Tween-20 in 1x PBS

* Fetal bovine serum (FBS) was heat inactivated (h.i.) at 56°C in a waterbath for 30 min. 0.5 g activated charcoal (AC) were added to 25 ml FBS (h.i.) and incubated over night on a laboratory roller mixer at 4°C. FBS-AC was centrifuged the following day for 15 min at 800 *g,* 0.22 µm sterile filtered and stored at – 20°C.

** Adult bovine serum for *E. histolytica* culture was heat inactivated twice for 30 min each at 56°C in a waterbath prior to use.

2.1.6 Kits

Table 7: List of kits.

Kit	Manufacturer	Catalog number
BD OptEIA™ Mouse IL-6 ELISA Set	BD Biosciences	555240
BD OptEIA™ TMB Substrate Reagent Set	BD Biosciences	555214
EasySep™ Mouse Monocyte Isolation Kit	STEMCELL Technologies	19861
eBioscience™ Foxp3 / Transcription Factor Staining Buffer Set	Invitrogen™ by Thermo Fisher Scientific, Inc.	00-5523-00
ELISA MAX™ Standard Set Mouse MCP-1	BioLegend, Inc.	432701
LEGENDplex™ Mouse M1 Macrophage Panel (8-plex)	BioLegend, Inc.	740848
LEGENDplex™ Mouse Anti-Virus Response Mix and Match Subpanel	BioLegend, Inc.	Detection antibodies: 740625, customized with individual analytes
Maxima First Strand cDNA Synthesis Kit for RT-qPCR	Thermo Fisher Scientific, Inc.	K1642
Maxima SYBR Green/ROX qPCR Master Mix (2X)	Thermo Fisher Scientific, Inc.	K0222
miRNeasy Mini Kit (50)	QIAGEN	217004
Mouse CCL3/MIP-1 alpha DuoSet ELISA	R&D Systems, Inc.	DY450-05
Mouse Myeloperoxidase DuoSet ELISA	R&D Systems, Inc.	DY3667
Neutrophil Isolation Kit, mouse	Miltenyi Biotec	130-097-658
NEXTFLEX® small RNA-Seq kit v3	PerkinElmer Inc.	NOVA-5132-06
NextSeq 500/550 Mid Output Kit v2.5 (150 Cycles)	Illumina, Inc.	20024904
NovaSeq 6000 SP Reagent Kit v1.5 (2x50bp)	Illumina, Inc.	20028401

QIASeq Stranded miRNA Library Kit	QIAGEN	180441
Qubit™ Protein Assay Kit	Invitrogen™ by Thermo Fisher Scientific, Inc.	Q33211
RNA 6000 Pico Kit	Agilent Technologies, Inc.	5067-1513
RNeasy Mini Kit (50)	QIAGEN	74104
UltraComp eBeads™ Plus Compensation Beads	Invitrogen™ by Thermo Fisher Scientific, Inc.	01-3333-42

2.1.7 Antibodies and dyes

Table 8: List of fluorescence-labeled antibodies and dyes for flow cytometry.

Antibody	Host	Clone	Fluorophore	Manufacturer	Catalog number	Dilution used
anti-mouse CD192 (CCR2)	rat	SA203G11	PE-Cy7	BioLegend	150611	1:100
anti-mouse/human CD11b	rat	M1/70	AF488	BD Biosciences	557672	1:400
anti-mouse/human CD11b	rat	M1/70	BV510	BioLegend	101263	1:400
anti-mouse CD38	rat	90	BV421	BioLegend	102732	1:800
anti-mouse CD62L	rat	MEL-14	BV711	BioLegend	104445	1:800
anti-mouse CD69	armenian hamster	H1.2F3	FITC	BD Biosciences	557392	1:200
anti-mouse CD86	rat	GL-1	BV605	BioLegend	105037	1:800
anti-mouse CX_3CR1	mouse	SA011F11	PerCP-Cy5.5	BioLegend	149010	1:200
anti-mouse Ly6C	rat	HK1.4	APC	BioLegend	128016	1:200
anti-mouse Ly6C	rat	HK1.4	PE	BioLegend	128008	1:800
anti-mouse Ly6G	rat	1A8	PE	BioLegend	127608	1:400
anti-mouse Ly6G	rat	1A8	APC	BioLegend	127614	1:400
anti-mouse MHCII	rat	M5/114.15.2	APC-Cy7	BioLegend	107627	1:100
Zombie UV™	-	-	-	BioLegend	423107	1:1000

Table 9: List of primary antibodes for TEM

Antibody	Source
Mouse anti-*E. histolytica* EH5 (designated anti-LPPG here)	Marinets *et al.* (1997)[78] Kindly provided by Prof. Michael Duchene, Medical University of Vienna
Rabbit anti-*E. histolytica* Gal/GalNac lectin (170 kDa heavy subunit)	Previously produced at BNITM

Table 10: List of secondary antibodies for TEM.

Antibody	Manufacturer	Catalog number
Goat anti-mouse colloidal gold-conjugated secondary antibody, 12 nm	Dianova GmbH	115-205-068
Goat anti-rabbit colloidal gold-conjugated secondary antibody, 10 nm	Science Services GmbH	AU25109

2.1.8 Oligonucleotides

Table 11: List of primers for RT-qPCR.

Target	Primer	Sequence (5' → 3')	Amplicon size (bp)
Ccl5	forward	GGACTCTGAGACAGCACATG	90
	reverse	GCAGTGAGGATGATGGTGAG	
Cxcl2	forward	AGTTTGCCTTGACCCTGAAG	78
	reverse	GGTCAGTTAGCCTTGCCTTT	
Ifit1	forward	GACTTTGAAACTGAGGCCCA	127
	reverse	CACGAGGGTCTTGTTGTTCA	
Lhfpl2	forward	ACTCAGGACACAGGAACAGA	107
	reverse	CTGCCAGAGGACTTGCTTAG	
Oasl1	forward	TGACGGTCAGTTTGTAGCCAT	165
	reverse	AAATTCTCCTGCCTCAGGAAC	
Tnf	forward	TCTGTGAAAACGGAGCTGAG	156
	reverse	GGAGCAGAGGTTCAGTGATG	

All primers were manufactured by Eurofins Genomics and stored as 100 pmol/µl stock solutions.

2.1.9 Software

Table 12: List of software.

Software	Manufacturer/Developer
CLC genomics workbench 21	QIAGEN
Excel	Microsoft
FastQC version 0.12.1	Babraham Institute
FlowJo™ version 10.7.1	BD Biosciences
LEGENDplex™ Cloud-based Data Analysis Software	BioLegend
LightCycler® 96 SW 1.1	F. Hoffmann-La Roche AG
MaxQuant version 2.0.3.0	Max Planck Institute of Biochemistry
NTA 3.0	Malvern Panalytical Ltd.
Perseus version 1.6.15.0	Max Planck Institute of Biochemistry
Prism version 9.0.0	GraphPad
SpectroFlo® version 3.1.0	Cytek® Biosciences

2.1.10 Websites and databases

Table 13: List of websites and databases.

Name	Version	URL
AmoebaDB Amoeba Informatics Resources[167]	Release 56+60	https://amoebadb.org/amoeba/app
Cytek® Full Spectrum Viewer	NA	https://spectrum.cytekbio.com/
Galaxy server[168]	NA	https://rna.usegalaxy.eu/
Heatmapper[169]	NA	http://heatmapper.ca/
InteractiVenn[170]	NA	http://www.interactivenn.net/
InterPro[171]	94.0	https://www.ebi.ac.uk/interpro/
Nucleotide BLAST	NA	https://blast.ncbi.nlm.nih.gov/Blast.cgi?PROGRAM=blastn&PAGE_TYPE=BlastSearch&LINK_LOC=blasthome
Nucleotide database[172]	NA	https://www.ncbi.nlm.nih.gov/nuccore
Panther knowledgebase[173]	17.0	http://pantherdb.org/
Primer-BLAST[174]	NA	https://www.ncbi.nlm.nih.gov/tools/primer-blast/
Primer3web[175]	4.1.0	https://primer3.ut.ee/
Protein BLAST	NA	https://blast.ncbi.nlm.nih.gov/Blast.cgi?PAGE=Proteins
Revigo[176]	1.8.1	http://revigo.irb.hr/
ShinyGO[177]	0.77	http://bioinformatics.sdstate.edu/go/
UniProt[178]	2022_04	https://www.uniprot.org/
Vesiclepedia[179]	4.1	http://www.microvesicles.org/

NA = not applicable

2.2 Methods

2.2.1 *E. histolytica* cell culture

E. histolytica trophozoites of clones A1 and B2 were cultured axenically under microaerophilic conditions in TY-I-S-33 medium[180] supplemented with 1 % 100x Penicillin/Streptomycin antibiotic mixture at 37°C. Parasites in the logarithmic growth phase were split every 2 – 3 days and provided with fresh medium. Parasites grown for EV isolations were split no more than 2 days prior to seeding on collagen-coated 6 well plates (2.2.2.1).

2.2.2 Extracellular vesicles

All experiments with EVs were designed in accordance with the guidelines of the International Society for Extracellular Vesicles published as Minimal information for studies of extracellular vesicles (MISEV) 2014[181] and updated in 2018[126].

2.2.2.1 Collagen coating of 6-well plates

For coating of 6-well plates with 5 µg/cm^2 collagen from calf skin (Bornstein & Traub type I), the appropriate amount of collagen was dissolved in 0.2 % acetic acid in 1x PBS at 4°C. The solution was added to the plate so that each well was covered entirely. Plates were incubated at 37°C for 2 h to allow for polymerization of the collagen. The remaining liquid was then removed and the plates dried under a sterile laminar flow hood. Plates were subsequently sterilized under UV light for at least 30 min and stored at 4°C until use.

2.2.2.2 Isolation of extracellular vesicles from *E. histolytica*-conditioned medium

E. histolytica cultured as described in 2.2.1 were washed twice with 1x NaPBS to remove residual culture medium and resuspended in warm EV-depleted TY-I-S-33 medium, which was obtained by ultracentrifugation at 100,000 *g* for 18 h to ensure absence of serum-derived EVs. Cell concentration was determined using a Neubauer chamber. 2x10^5 trophozoites were added to each well of a collagen-coated 6-well plate and EV-depleted medium was added to a final volume of 5 ml. For mock controls, medium was added without adding amebae. Plates were then incubated in an anaerobic chamber with Merck Millipore Anaerocult® at 37°C for 46 h. After incubation, supernatants were harvested and subjected to differential centrifugation to clear the conditioned medium of cells and debris. Differential centrifugation was performed according to a protocol modified from Mantel *et al*[153]. For this, the medium was centrifuged for 15 min each at 600 *g*, 1600 *g*, 3600 *g* and 10,000 *g*, always collecting the supernatant for the following step. Then, EVs were pelleted by ultracentrifugation in Optima XE-90 centrifuge with SW 32 Ti swinging bucket rotor at 100,000 *g* and 4°C for 1 h with maximal acceleration and deceleration set to 5. The supernatant was discarded and the EV pellet washed in 1x PBS with another 1 h 100,000 *g* ultracentrifugation step. Finally, EVs were resuspended in 2x 100 µl 1x PBS (0.22 µm filtered). EVs were aliquoted and stored at – 80°C or used immediately for the determination of protein concentration using Qubit 4™ fluorometer (2.2.5.2). For mock control samples, all steps

were performed the same way. For isolation of total RNA from EVs (2.2.10.1.1), 500 µl QIAzol™ lysis reagent were added to 100 µl of EV sample before storage.

2.2.2.3 EV pools for stimulation experiments

For subsequent stimulation experiments, EVs of four separate EV isolations were combined into EV pools to minimize batch effects on stimulation. EV pools were again aliquoted before storage at – 80°C. EV pool aliquots were only thawed once for use in stimulation experiments and not re-frozen to minimize freeze-thaw cycles as they are known to have an effect on EV integrity[182]. EV pools were tested for their stimulatory capacity on crude bone marrow cells (isolated as described in 2.2.6.3) followed by IL-6 ELISA (2.2.9.1) on the resulting supernatants after 24 h stimulation. Only EV pools eliciting an increase in IL-6 release by bone marrow cells compared with mock control stimulated bone marrow cells were further used for EV stimulation of monocytes (2.2.6.4) or neutrophils (2.2.6.5).

2.2.3 Nanoparticle Tracking Analysis

In order to determine the concentration of EV samples and size distribution of the contained EVs, nanoparticle tracking analysis (NTA) was performed using Malvern Panalytical NanoSight LM14C equipped with a CCD camera with NTA 3.0 software according to the manual. In NTA, particles in suspension are illuminated by a laser beam and the resulting light scattering as well as Brownian motion of the particles are used to obtain size distributions[183]. EV samples were diluted 1:100 or 1:300 in 0.22 µm filtered 1x PBS for measurement and injected into the instrument using 1 ml tuberculin syringes. A total of 900 frames were recorded over five separate 30 s measurements, with the camera level set to 16 and 25°C temperature control. Raw data were processed by the software with the detection threshold set to 6. Obtained particle concentrations for EV pools were then used to calculate the volume of sample needed for EV stimulation experiments (2.2.7).

2.2.4 Immunogold labeling for transmission electron microscopy

Immunogold labeling followed by negative staining for TEM was performed for the antibody-mediated detection of *E. histolytica* antigens on EVs isolated as described in 2.2.2.2. Processing of samples for TEM and imaging were performed by Dr. Katharina Höhn of the BNITM electron microscopy facility.

Glow-discharged, carbon and formvar coated nickel grids were inserted into the EV solution, and EVs were spun down onto the grids via centrifugation at full speed in a table-top centrifuge for 15 min. Grids were washed twice with 1x PBS for 3 min, followed by blotting with Whatman paper. Grids were then washed 4 times with 0.05 % glycine in 1x PBS for 3 min each, again followed by blotting with Whatman paper after the last washing steps. Blocking of unspecific binding was performed by incubation of the grids in blocking buffer (0.5 % BSA in 1x PBS) for 10 min. Subsequently, grids were incubated in primary antibody diluted in blocking buffer for 24 h at 4°C. Antibodies used were rabbit anti-Gal/GalNac lectin (1:200 dilution) and mouse anti-LPPG[78] (1:100 dilution). In order to control for antibody specificity, controls without primary antibody were performed. After incubation, the grids were washed with blocking buffer 6 times for 3 min, followed by incubation in colloidal gold-

conjugated secondary antibody diluted 1:100 in blocking buffer for 24 h at 4°C. Grids were then again washed with blocking buffer 4 times for 3 min, followed by 2 washes with H_2O for 3 min and blotting with Whatman paper. Fixation of the samples was performed using 2 % glutaraldehyde for 5 min, followed by 2 washes with H_2O for 3 min each with blotting after each of the steps. Finally, grids were incubated with 2 % aqueous uranyl acetate for 15 s, washed once with H_2O and dried at RT. Imaging of the stained samples was performed using a Tecnai Spirit electron microscope at 80 kV. Images were recorded with a digital CCD camera.

2.2.5 Mass spectrometry for the analysis of proteomes

2.2.5.1 Sample generation for mass spectrometry

EV samples for proteomic analysis were prepared as described in 2.2.2.2. The supernatant of the first ultracentrifugation step was used as a control for mass spectrometry to determine which proteins might be contaminants and not specific to the EV sample.

For whole cell proteomes, *E. histolytica* trophozoites seeded on collagen-coated 6-well plates and incubated for EV isolation were harvested by resuspension in cold 1x NaPBS, centrifuged at 400 *g* for 4 min, washed once with 1x NaPBS and centrifuged as before, followed by storage of the pellet at – 80°C.

2.2.5.2 Determination of protein concentration using Qubit fluorometer

To determine protein concentration of EV samples with Qubit™ 4 fluorometer, Qubit™ protein assay kit was used according to the manufacturer's instructions. Briefly, protein reagent was diluted 1:200 in protein buffer (both provided with the kit) to obtain the working solution. For each standard, 190 µl working solution were combined with 10 µl of standard. Between 180 µl and 199 µl of working solution were combined with between 20 µl and 1 µl of sample, respectively, depending on whether low or high amounts of protein were expected in the sample. Standards and samples were vortexed and incubated at RT for 15 min prior to measurement at the fluorometer.

2.2.5.3 Liquid chromatography-mass spectrometry

Sample processing and liquid chromatography-mass spectrometry (LC-MS) of EVs and whole amebae as well as raw data analysis were performed at the proteomics core facility at BIOCEV research center, Vestec, Czech Republic under the lead of Karel Harant. 30 µg of protein for each sample were processed according to Hughes *et al.*[184] and Rappsilber *et al.*[185]. Tandem MS was performed with a Thermo Fisher Scientific Orbitrap Fusion (Q-OT-qIT) mass spectrometer.

2.2.5.4 Analysis of mass spectrometry data

Raw MS data were processed using MaxQuant software (version 2.0.3.0)[186]. False discovery rate (FDR)[187] was set to 1 % for proteins and peptides and a minimum peptide length of seven amino acids was specified. Andromeda search engine in MaxQuant was used for spectra search against *E. histolytica* database (annotated proteins, AmoebaDB[167] release 56). The MaxQuant label-free algorithm was used for quantification[188]. Data annotation and statistical analysis of the MaxQuant output were performed with Perseus[189] by MaxQuant. Statistical comparison between two datasets was performed with student's *t* test in Perseus with FDR *p*-value set to 0.05 and s0 = 0.5.

Proteins present in only 1 out of 3 samples of a dataset were excluded from the proteome for downstream analysis. A minimum fold change cutoff of |2| was defined to consider a protein differentially expressed between two datasets. Proteins were further analyzed with AmoebaDB[167] database release 60 (https://amoebadb.org/amoeba/app). Gene ontology (GO) enrichment analysis and metabolic pathways analysis were performed with AmoebaDB[167], and GO term analysis results were visualized with Revigo[176] version 1.8.1 (http://revigo.irb.hr/). In addition, Panther knowledgebase release 17.0[173] (http://pantherdb.org/) was used for functional classification of proteins and visualization in pie charts. Venn diagrams for proteome data were created with InteractiVenn[170] (http://www.interactivenn.net/). Heat maps for proteome data were created with Heatmapper (http://heatmapper.ca/)[169].

In order to compare EV proteomes with whole cell proteomes, statistical overrepresentation test was performed with Panther knowledgebase 17.0[190] using Fisher's exact test with FDR-adjusted *p* value < 0.05 in accordance with Sharma *et al*.[144]

2.2.6 Isolation of primary murine immune cells

All mice used were bred in the animal facility of the BNITM and kept in individually ventilated cages under pathogen-free conditions. For harvesting of organs, C57BL/6J mice aged 9 – 13 weeks were euthanized by carbon dioxide (CO_2) overdose followed by cervical dislocation or cardiac puncture and blood withdrawal in accordance with German animal protection laws. Organ harvest was approved by the Authority for Justice and Consumer Protection, Veterinary Affairs, Hamburg, Germany under the permission file number T-008.

2.2.6.1 Splenocyte isolation

Spleens were harvested from euthanized mice and placed in tubes containing 1x PBS. 70 µm cell strainers were placed on 50 ml tubes and washed twice with 2 ml 1x DPBS each. Spleens were strained through the cell strainer using the rough end of the plunger of a 5 ml syringe. 2 washes with 5 ml 1x DPBS each were performed to rinse all remaining cells from the cell strainer. Samples were centrifuged at 290 *g* and 4°C for 5 min. The supernatant was discarded and replaced with 5 ml erythrocyte lysis buffer. The pellet was resuspended and incubated at RT for 5 min to lyse erythrocytes. The reaction was then quenched with 45 ml 1x DPBS. Centrifugation was performed as before, the supernatant discarded and replaced with 5 ml 1x DPBS. If the pellet exhibited red color at this step, indicating incomplete erythrolysis, incubation in erythrocyte lysis buffer was repeated as before. If

clumping of cells was observed, the sample was passed through a 30 µm falcon-top filter. Cell concentration was determined with a Neubauer chamber using a 1:100 dilution in 0.04 % trypan blue solution (0.4 % trypan blue diluted 1:10 in 1x DPBS). Obtained splenocytes were then pooled with immune cells obtained from blood (2.2.6.2) for the isolation of neutrophils (2.2.6.5).

2.2.6.2 Isolation of immune cells from blood

Blood was obtained from mice by cardiac puncture and transferred to test tubes for hematological analyses containing ethylenediaminetetraacetic acid (EDTA) to prevent coagulation. Blood samples were centrifuged at 290 *g* and 4°C for 5 min. The supernatant was discarded and replaced with 5 ml erythrocyte lysis buffer, followed by 5 min incubation at RT to lyse erythrocytes. The reaction was then quenched with 45 ml 1x DPBS, followed by centrifugation as before. Erythrolysis was performed twice for blood samples. After the second step, cells were resuspended in 1 ml complete Roswell Park Memorial Institute medium (cRPMI) and combined with isolated splenocytes (2.2.6.1) for subsequent isolation of peripheral neutrophils. Combined cells were passed through a 30 µm filter, and cell concentration was determined with a Neubauer chamber using a 1:100 dilution in 0.04 % trypan blue. Isolation of neutrophils was then performed as described in 2.2.6.5.

2.2.6.3 Isolation of murine bone marrow cells

Front and hind legs of euthanized mice were used for the isolation of bone marrow (BM) cells. Muscle and residual tissue were cleaned from the bones, which were then sterilized by incubation in 70 % isopropanol for 2 minutes. Once all isopropanol was evaporated from the bones, sterile scissors were used to cut open the ends. Bone marrow was flushed out with 1x DPBS using 5 ml syringes with 0.4 mm hypodermic needles. The resulting cell suspension was passed through a 70 µm cell strainer into a 50 ml centrifuge tube and centrifuged at 290 *g* and 4°C for 5 min. The supernatant was discarded and the cell pellet resuspended in 1 ml of 2% FBS/DPBS + 1 mM EDTA. Cell concentration was determined with a Neubauer chamber using a 1:100 dilution in 0.04 % trypan blue solution. Cells were then either used directly for EV stimulation experiments (2.2.7), stained for fluorescence minus one (FMO) controls for flow cytometry (2.2.8.2), or processed further for monocyte (2.2.6.4) or neutrophil isolation (2.2.6.5).

2.2.6.4 Isolation of monocytes from murine bone marrow cells

Monocytes were isolated from murine BM (2.2.6.3) by antibody-mediated negative selection using the EasySep™ Mouse Monocyte Isolation Kit from StemCell Technologies according to the manufacturer's instructions. In order to control isolation efficacy, $2x10^5$ of the previously isolated BM cells were set aside each for 'before isolation' and 'unstained' controls.

For further processing, cell concentration was adjusted to $1x10^8$ cells/ml. Selection cocktail containing antibodies for non-monocyte cells was prepared by combining components A and B according to the manufacturer's instructions. Cells were transferred to a sterile flow cytometry tube. Per $1x10^8$ cells, 50 µl rat serum (provided with the kit) and 100 µl selection cocktail were added. After 5 min incubation at 4°C, 75 µl RapidSpheres were added, followed by 3 min incubation at 4°C. 2% FBS/DPBS + 1mM

EDTA was added to a final volume of 2.5 ml. The tube was then inserted into the EasySep™ magnet. After 3 min incubation at RT, the magnet with the tube was tilted, allowing the cell suspension to flow into a new tube. This was then again inserted into the magnet and incubated for another 3 min at RT, before the cell suspension containing isolated monocytes was again poured off into another tube. The suspension was centrifuged at 290 *g* and 4°C for 5 min, the supernatant discarded and the cell pellet resuspended in 1 ml cRPMI. Cell concentration was determined with a Neubauer chamber as before, using an appropriate dilution in trypan blue solution. $2x10^5$ cells of the isolated monocytes were set aside for 'after isolation' efficacy control. Efficacy was controlled as described in 2.2.8.1. Isolated monocytes were used immediately for stimulation experiments (2.2.7). For isolation of RNA from unstimulated monocytes, 350 µl or 600 µl of RLT buffer, depending on the cell number according to the RNeasy handbook, were added to freshly isolated cells before storage at – 80°C and RNA isolation as described in 2.2.10.1.

2.2.6.5 Isolation of neutrophils from murine bone marrow and peripheral cells

Neutrophils were isolated from murine BM (2.2.6.3) or peripheral cells (2.2.6.1, 2.2.6.2) by antibody-mediated negative selection using Miltenyi Neutrophil Isolation Kit according to the manufacturer's instructions with minor changes. In order to control efficacy (2.2.8.1), $2x10^5$ of the previously isolated crude cells were set aside each for 'before isolation' and 'unstained' controls.

BM cells or peripheral cells were centrifuged at 290 *g* and 4°C for 7 min, the supernatant was discarded and replaced with 200 µl 1x MACS buffer (10x MACS buffer diluted 1:10 in PBS) per $5x10^7$ cells. 50 µl Biotin Antibody Cocktail was then added per $5x10^7$ cells, followed by 12 min incubation at 4°C to allow for labeling of all non-neutrophil cells. 7 ml 1x MACS buffer were added and the sample was centrifuged as before. The supernatant was discarded and the cell pellet resuspended in 400 µl 1x MACS buffer per $5x10^7$ cells. 100 µl Anti-Biotin MicroBeads were then added per $5x10^7$ cells, followed by 15 min incubation at 4°C. Again, 7 ml 1x MACS buffer were added and the sample centrifuged as before. Up to $1x10^8$ cells were then resuspended in 500 µl 1x MACS buffer and loaded onto a LS column that was previously prepared with a rinse of 3 ml 1x MACS buffer. Upon loading of the cell suspension, the flow-through containing neutrophils was collected on ice. The column was rinsed 3 times with 3 ml buffer each and the flow-through was collected. The neutrophil cell suspension was then centrifuged as before, the supernatant was discarded and the pellet resuspended in 1 ml cRPMI. Cell concentration was determined using a 1:10 dilution of the cell suspension in 0.04 % trypan blue solution. $2x10^5$ cells were set aside for 'after isolation' sample, and the remaining isolated neutrophils were used immediately for stimulation experiments as described in 2.2.7. Neutrophil experiments were performed within the framework of Valentin Bärreiter's master thesis[166], supervised as part of this doctoral thesis.

2.2.7 EV stimulation of immune cells

Crude BM cells (2.2.6.3), isolated monocytes (2.2.6.4) or isolated neutrophils (2.2.6.5) were stimulated with *E. histolytica* EV pools (2.2.2.3) in round-bottom 96 well plates. $1x10^5$ monocytes/peripheral neutrophils or $5x10^5$ BM neutrophils were added to each well. For stimulation, 1000 EVs/cell were added (concentration determined as described in 2.2.3). For heat inactivated controls, EV samples

were incubated in a heating block at 95°C for 10 min prior to use. For positive controls, 5 µg/ml LPS was added, while for negative controls, mock control sample was added in the same volume as EV samples. The final volume was made up to 200 µl with cRPMI. For stimulation periods of 12 h and longer, 1x DPBS was added to surrounding wells to prevent evaporation. Cells were then incubated at 37°C and 5 % CO_2 for the required period of time. After stimulation, plates were centrifuged at 4°C and 450 *g* for 5 min. Supernatants were then harvested for subsequent ELISA or LEGENDplex™ (2.2.9) and stored at – 80°C. Cells were either processed immediately for antibody staining (2.2.8.2) or resuspended in RLT buffer and stored at – 80°C for future RNA isolation (2.2.10.2.1).

2.2.8 Flow cytometry

2.2.8.1 Control of monocyte/neutrophil isolation efficacy

Cells previously set aside before and after monocyte or neutrophil isolation (2.2.6.4, 2.2.6.5) were used to control isolation efficacy of the desired cell type via flow cytometry. 1 ml flow cytometry buffer (1 % FBS in 1x PBS) was added to each tube and the suspension was centrifuged at 290 *g* and 4°C for 5 min. Antibody master mix was prepared in Fc blocking buffer. Alexa Fluor (AF) 488-conjugated anti-CD11b (1:400), allophycocyanin (APC)-conjugated anti-Ly6C (1:200) and phycoerythrin (PE)-conjugated anti-Ly6G (1:400) antibodies were used. After centrifugation, supernatant was discarded and 50 µl master mix were added to each sample. 50 µl Fc blocking buffer without antibodies were added to unstained controls. Samples were incubated with the antibodies at 4°C in the dark for 30 min. The cells were then washed twice with 1 ml 1x PBS and centrifuged as before. After the second centrifugation step, cells were resuspended in 150 µl 1x PBS and measured at accuri C6 flow cytometer immediately.

2.2.8.2 Antibody staining of EV-stimulated cells for flow cytometry

In order to determine the presence of certain markers on the surface of EV-stimulated cells (2.2.7) and thus assess the activation state, flow cytometry was performed. Stimulated cells in 96-well plates were centrifuged at 450 *g* and 4°C for 5 min. For labeling of dead cells, the pellet was resuspended in 100 µl 1:1000 Zombie UV™ in 1x PBS, transferred to flow cytometry tubes and incubated at 4°C for 30 min in the dark. After incubation, 200 µl flow cytometry buffer were added and samples were centrifuged at 290 *g* and 4°C for 5 min. The supernatant was discarded, 200 µl flow cytometry buffer were added and centrifugation was repeated as before. The supernatant was discarded again and the cells resuspended in 50 µl antibody master mix in Fc blocking buffer. After 30 min incubation at 4°C in the dark, 200 µl flow cytometry buffer were added and the samples centrifuged as before. Supernatants were discarded. Cells of stained samples as well as unstained controls were then fixed using Invitrogen™ eBioscience™ Foxp3 / Transcription Factor Staining Buffer Set. For fixation, 100 µl of Fix/Perm were added to each sample, followed by incubation at 4°C for 30 min in the dark. 100 µl of Perm/Wash solution were then added to each sample, and centrifugation was performed as before. This washing step was repeated once and the cells finally resuspended in 150 µl Perm/Wash. Samples were stored at 4°C until measurement at Cytek® Aurora flow cytometer. Samples were measured no later than 72 h after staining. Data analysis was performed using FlowJo™ software.

To differentiate between positive and negative populations for each marker, an unstained control was performed for each staining. In addition, fluorescence minus one (FMO) controls were performed on crude bone marrow cells ($2x10^6$ per control) at the establishment of the panel for all markers but CD11b, Ly6C and Ly6G. FMO controls contain all fluorescence-labelled antibodies of the panel except for one and are thus used for setting the gate between positive and negative populations. In contrast to unstained controls, the presence of all other antibodies in FMO controls aids in accounting for fluorescence spillover between different fluorophores.

2.2.8.3 Spectral unmixing for flow cytometry

Spectral unmixing at Cytek® Aurora flow cytometer was performed to distinguish fluorophore signatures and correct for fluorescence spillover. For this, single stained samples were performed for each fluorophore in the antibody panel by adding the respective antibody diluted in Fc blocking buffer to UltraComp eBeads™ Plus compensation beads. Beads were stained and subsequently washed and fixed as described in 2.2.8.2. For Zombie UV™ single stained samples, $4x10^6$ bone marrow cells (2.2.6.3) were killed by resuspension in 5 ml ice-cold 70 % ethanol and incubation at RT for 10 min. 10 ml 1x PBS were then added to the sample, and centrifugation was performed at 290 *g* and 4°C for 5 min. Cells were stained with Zombie UV™ and fixed as described in 2.2.8.2. Unstained but fixed cells were added to Zombie UV™ controls to include both Zombie UV™-positive and negative cells in the sample, which is needed for spectral unmixing. Unmixing was performed in SpectroFlo® software with autofluorescence correction at Cytek® 5-laser Aurora according to the manufacturer's instructions.

2.2.9 Immunoassays

2.2.9.1 IL-6 ELISA

For detection of IL-6 in supernatants of EV-stimulated cells, BD OptEIA™ Mouse IL-6 ELISA Set was used according to the manufacturer's instructions with minor adjustments. On the day before the assay, a 96-well high binding plate was coated with 50 µl of capture antibody diluted 1:250 in coating buffer. The plate was sealed and incubated overnight at 4° C. The next day, supernatants were discarded and the plate was washed 3 times with wash buffer (0.05 % Tween-20/PBS). After the last wash, the plate was inverted and blotted on absorbent paper to remove any residual buffer. Blocking of unspecific binding was performed by the addition of 100 µl 10 % FBS in 1x PBS and incubation at RT for 1 h. Washing was then performed as before. Standard dilutions were prepared in 10 % FBS/PBS by diluting the stock standard to a top concentration of 1000 pg/ml with subsequent two-fold dilutions. Standards were prepared in duplicates. 50 µl of standard dilutions and samples were added to the appropriate wells. Supernatants of LPS stimulated cells were diluted 1:2 in 10 % FBS/PBS. All other samples were used without further dilution. 10 % FBS/PBS was used as blank. The plate was sealed and incubated at RT for 2 h, followed by washing as before but with 5 total washes. Working detector was prepared by diluting Streptavidin-HRP reagent 1:250 and detection antibody 1:500 in 10 % FBS/PBS. 50 µl of this solution were added to each well and the sealed plate incubated at RT for 1 h. Washing was performed as before but this time with 7 total washes and 30 s to 1 min soaking for each wash to minimize background. 50 µl 3,3',5,5'-Tetramethylbenzidine (TMB) substrate solution were then added to each well. TMB is a substrate for horseradish peroxidase (HRP) and its oxidation in the presence of hydrogen

peroxide (H_2O_2) leads to the formation of a blue-colored product[191]. The plate was incubated in the dark for 30 min at RT, and the color reaction was stopped by addition of 25 µl stop solution (2 N H_2SO_4) to each well, resulting in a colorimetric change from blue to yellow. Absorbance at 450 nm was measured within 30 min using MRX^e plate reader.

2.2.9.2 CCL3 ELISA

For detection of CCL3 in supernatants of EV-stimulated cells, Mouse CCL3/MIP-1 alpha DuoSet ELISA was used according to the manufacturer's instructions with minor adjustments. On the day before the assay, capture antibody was diluted 1:250 in 1x PBS. 50 µl of this capture antibody solution were added to the wells of a 96-well high binding plate and incubated overnight at RT. The next day, the plate was washed 3 times with wash buffer (0.05 % Tween-20/PBS), after which residual buffer was blotted off by firmly tapping the plate upside down on absorbent paper. 150 µl 1 % BSA/PBS were added to each well to block non-specific binding. The plate was sealed and incubated at RT for 1 h. After incubation, washing was performed as before. Standard dilutions were prepared in 1 % BSA/PBS by diluting the stock standard to a top concentration of 500 pg/ml with subsequent two-fold dilutions. Standards were prepared in duplicates. 50 µl of standard dilutions and samples were added to the appropriate wells. Supernatants of LPS stimulated cells were diluted 1:4 in 1 % BSA/PBS. All other samples were used without further dilution. The plate was sealed and incubated at RT for 2 h, after which washing was performed as before. 50 µl of detection antibody (6 µg/ml stock concentration) diluted 1:60 in 1 % BSA/PBS were then added to each well. The sealed plate was incubated at RT for 2 h, followed by washing as before. 50 µl of Streptavidin-HRP diluted 1:40 in 1 % BSA/PBS were added to each well and the sealed plate incubated at RT for 20 min in the dark. Washing was performed as before. Next, 50 µl of TMB substrate solution were added to each well and the plate was incubated in the dark for 20 min. The color reaction was stopped by addition of 25 µl stop solution (2 N H_2SO_4) to each well, resulting in a colorimetric change from blue to yellow. Absorbance was measured at 450 nm with wavelength correction at 570 nm using MRX^e plate reader within 15 min.

2.2.9.3 CCL2 ELISA

For detection of CCL2 (also named monocyte chemoattractant protein-1 (MCP-1)) in supernatants of EV-stimulated cells, mouse MCP-1 ELISA MAX^{TM} Standard set by BioLegend was used according to the manufacturer's instructions with minor adjustments. One day prior to running the ELISA, capture antibody was diluted 1:200 in coating buffer. 50 µl of this capture antibody solution were added to the wells of a 96-well high binding plate and incubated overnight at 4°C. The next day, the plate was washed 4 times with at least 300 µl wash buffer (0.05 % Tween-20/PBS) per well, after which residual buffer was blotted off by firmly tapping the plate upside down on absorbent paper. 100 µl 1 % BSA/PBS were added to each well to block non-specific binding. The plate was sealed and incubated at RT for 1 h on a plate shaker. After incubation, washing was performed as before. Standard dilutions were prepared by diluting the stock standard in 1 % BSA/PBS to a top concentration of 4000 pg/ml and subsequently performing two-fold dilutions. Standards were prepared in duplicates. 50 µl of standard dilutions and samples were added to the appropriate wells. Supernatants of LPS stimulated cells were diluted 1:4 in 1 % BSA/PBS. All other samples were used without further dilution. The plate was sealed and incubated at RT for 2 h with shaking. Washing was performed as before. 50 µl of detection

antibody diluted 1:200 in 1 % BSA/PBS were then added to each well. The sealed plate was incubated at RT for 1 h with shaking, followed by washing as before. 50 µl of Avidin-HRP diluted 1:1000 in 1 % BSA/PBS were added to each well and the sealed plate incubated at RT for 30 min with shaking. The plate was then washed 5 times with 30 s to 1 min soaking in wash buffer for each wash step to minimize background. 50 µl of TMB substrate solution were added to each well and the plate then incubated in the dark for 15-30 min. The color reaction was stopped by addition of 50 µl stop solution (2 N H_2SO_4) to each well, resulting in a colorimetric change from blue to yellow. Absorbance was measured at 450 nm using MRX^e plate reader within 15 min.

2.2.9.4 Myeloperoxidase ELISA

To detect myeloperoxidase (MPO) released during degranulation in the supernatants of stimulated cells, R&D Systems Mouse Myeloperoxidase DuoSet ELISA was used according to the manufacturer's instructions with minor adjustments. One day before the assay, the capture antibody was diluted 1:180 in 1x PBS. A 96-well high binding plate was coated with 50 µl per well of the diluted capture antibody. The plate was sealed and incubated overnight at RT. The next day, the plate was washed 3 times with wash buffer as described in 2.2.9.3. Unspecific binding was then blocked by addition of 150 µl 1 % BSA in 1x PBS to each well and incubation at RT for 1 h. The plate was then washed as before. Standard dilutions were prepared in 1 % BSA/PBS by diluting the stock standard to a top concentration of 16,000 pg/ml and subsequently performing two-fold serial dilutions. Standards were prepared in duplicates. 50 µl of standard dilutions and samples were added to the appropriate wells. Supernatants of LPS stimulated cells were diluted 1:4 in 1 % BSA/PBS. All other samples were used without further dilution. The plate was sealed and incubated at RT for 2 h, followed by washing as before. 50 µl of detection antibody diluted 1:180 in 1 % BSA/PBS were added to each well and the sealed plate was incubated at RT for another 2 h, again followed by washing as before. Streptavidin-HRP was diluted 1:200 in 1 % BSA/PBS and 50 µl of this solution were then added to each well. The plate was incubated in the dark at RT for 20 min. The plate was then washed as before. 50 µl of TMB substrate solution were added to each well and the plate incubated for 20 min at RT in the dark again. The color reaction was stopped by adding 25 µl stop solution (2 N H_2SO_4), resulting in a colorimetric change from blue to yellow. Finally, absorbance was measured at 450 nm with 570 nm wavelength correction at MRX^e plate reader.

2.2.9.5 LEGENDplex™ multiplex cytokine assay

BioLegend's LEGENDplex™ is a multiplex cytokine assay that allows for the simultaneous detection of several analytes in samples and was used to investigate cytokine profiles in cell culture supernatants of stimulated monocytes. LEGENDplex™ uses the same principle of analyte capture between two antibodies as other sandwich immunoassays and makes use of beads of different sizes and fluorescence intensities. Bead populations with bound target analytes can thus be distinguished using a flow cytometer.

In preparation for the assay, provided beads were sonicated in an ultrasonic bath for 1 min, followed by 30 s vortexing to break up potential bead aggregates. If beads for individual cytokines were provided separately, a bead master mix was prepared out of 13x beads, which were diluted to 1x in assay buffer.

Standard series was prepared by performing 1:4 serial dilutions in assay buffer, starting from the top standard C7. Assay buffer was used as C0 (blank).

In a V-bottom 96-well plate, 10 µl sample or standard were combined with 10 µl beads and 10 µl assay buffer per well. All standards and samples were prepared in duplicates. The plate was sealed, wrapped in tinfoil and incubated at 4°C overnight with shaking at 800 rpm. The next day, the plate was centrifuged at 250 *g* for 5 min. The supernatant was discarded with a quick shaking motion and 200 µl 1x wash buffer were added to each well. After 1 min incubation, the plate was centrifuged as before and the supernatant discarded again. 10 µl detection antibody were then added into each well containing sample or standard, the plate was sealed and wrapped in tinfoil again, and incubated at RT and 800 rpm on a shaker for 1 h. Next, 10 µl SA-PE were added to each well, followed by incubation for 30 min as before. The plate was centrifuged as before, the supernatant discarded and the pellet containing the beads with bound analytes resuspended in 150 µl 1x wash buffer. Samples were transferred into flow cytometry tubes and measured at BD® LSR II flow cytometer on the same day. Approximately 300 beads were recorded per analyte. Data analysis was performed with LEGENDplex™ Cloud-based Data Analysis Software.

2.2.10 RNA analysis

2.2.10.1 Analysis of the miRNA content of EVs

2.2.10.1.1 Isolation of total RNA from *E. histolytica* EVs

For purification of total RNA, including small RNAs such as miRNAs, QIAGEN miRNeasy Mini Kit was used according to the manufacturer's instructions. EVs previously isolated from culture supernatant and stored in QIAzol™ lysis reagent (2.2.2.2) were thawed on ice and then incubated at RT for 5 min. 140 µl chloroform were added to the sample, followed by vigorous shaking for 15 s and another 3 min incubation at RT. For phase separation, samples were centrifuged at 12,000 *g* and 4°C for 15 min. The upper aqueous phase containing RNA was transferred to a new RNase-free tube. 1.5 volumes of 100 % ethanol were added to the sample and mixed by pipetting. Up to 700 µl were then added onto a RNeasy Mini spin column, followed by centrifugation at over 8,000 *g* and RT for 15 s. The flow-through was discarded, and, in case of higher volumes of sample, the step was repeated. 700 µl buffer RWT were added to the column, followed by centrifugation as before and discarding of the flow-through. 2 washing steps with 500 µl buffer RPE ensued with centrifugation as above, but for the second step the centrifugation time was increased to 2 min. The flow-through was discarded after each step. The column was then placed in a new collection tube and centrifuged for 1 min to dry the membrane. Finally, 25 µl RNase-free H_2O were added to the column to elute the RNA in a 1 min centrifugation step. This step was performed twice to result in a final elution volume of 50 µl. RNA concentration was determined using NanoDrop™ 2000. Samples were then stored at – 80°C until further use. For later analysis of RNA integrity with Agilent 2100 Bioanalyzer (2.2.10.3), small aliquots (2 µl) of each sample were stored separately to avoid freezing and thawing of RNA samples. Ultimately, isolated samples were sequenced as described in 2.2.10.1.2 to characterize the miRNA content of *E. histolytica* EVs.

2.2.10.1.2 miRNA sequencing

Sample processing and miRNA sequencing of isolated total RNA were performed at the Institute of Clinical Molecular Biology of Kiel University. Libraries were constructed using NEXTFLEX® small RNA-Seq Kit (PerkinElmer Inc.). Samples were sequenced at a depth of around 50 million paired-end reads per sample (with read depth varying between 27 and 132 million reads per sample) with 50 bp read length using Illumina NovaSeq 6000 System with NovaSeq SP flow cell. Quality control of generated reads was performed in the sequencing facility using FastQC.

2.2.10.1.3 Analysis of miRNA sequencing data

Analysis of raw miRNA sequencing data was performed with CLC genomics workbench 21 in cooperation with Dr. Nahla Metwally. For annotation of miRNAs, a custom reference sequence list was created based on *E. histolytica* miRNAs published by Mar-Aguilar *et al*.[192]. Raw reads were trimmed and mapped to the custom reference. 'Quantify miRNA' function in CLC was used for quantification of the annotated miRNAs in the sequence data. Sequence length for seed counting was set to 18 – 25 nt. Differential expression between two sample sets was analyzed using 'differential expression in two groups' function for small RNA with TMM normalization.

De novo miRNA prediction from sequencing data was performed by Balázs Horváth using BrumiR algorithm (version 3.0)[193] (accessed from https://github.com/camoragaq/BrumiR). Out of the three sequenced samples per clone, the largest dataset each was chosen for miRNA discovery. Validation of the mature miRNAs predicted by BrumiR was done by mapping to the *E. histolytica* genome with BrumiR2reference and predicting miRNA precursors based on possible hairpin structures in the genome. Precursor clustering was performed at 98 % identity to reduce redundancy since around 20 % of the *E. histolytica* genome consists of repeat elements[194]. Quantification and annotation of the BrumiR output was performed using CLC genomics as described above. Differential expression between two sample sets was analyzed using the tool for empirical analysis of differential expression with tagwise dispersions. For further analysis, a total count cutoff of 5 read counts was set. All miRNAs that were not present in at least 2 out of 3 samples of either A1 or B2 EVs with a minimum of 5 counts were excluded.

FDR p value < 0.05 and fold change ≥ |2| were set to define a miRNA as significantly differentially expressed. Volcano plots for miRNA sequencing data were created with the European Galaxy Server[168] (https://rna.usegalaxy.eu/).

2.2.10.2 Transcriptome analysis of stimulated monocytes

2.2.10.2.1 RNA isolation

For isolation of RNA from cells previously fixed in RLT buffer (2.2.7), QIAGEN RNeasy Mini Kit was used according to the manufacturer's instructions. Briefly, thawed samples were vortexed and 70 % ethanol was added to the samples in equal volume to the previously added RLT buffer and mixed by pipetting. Up to 700 µl of the solution were added onto a RNeasy Mini spin column, followed by centrifugation for 15 s at > 8000 *g*. The flow-through was discarded and if required, remaining sample was added

onto the column, followed by centrifugation as before. 700 µl of wash buffer RW1 were then added to the column, centrifugation was performed as before and the flow-through discarded. 2 washing steps with 500 µl buffer RPE each were then performed as for buffer RW1 before, with centrifugation at the second step for 2 min. Subsequently, the column was transferred into an empty 2 ml collection tube and centrifuged at full speed in a table-top centrifuge for 1 min to dry the membrane. The column was then placed into a new 1.5 ml collection tube, 25 µl RNase-free H_2O were added directly to the membrane, followed by centrifugation for 1 min at > 8000 *g* to elute the RNA. This step was repeated with 25 µl RNase-free H_2O, resulting in a total elution volume of 50 µl. RNA concentration was then measured at NanoDrop™ 2000. Samples were stored at – 80°C until further use for RNA-Seq using next-generation sequencing (NGS) (2.2.10.2.2) or RT-qPCR (2.2.10.4). For later analysis of RNA integrity with Agilent 2100 Bioanalyzer (2.2.10.3), small aliquots (1-2 µl) of RNA were stored separately to avoid freezing and thawing of RNA samples.

2.2.10.2.2 RNA sequencing

RNA isolated from stimulated murine monocytes that passed integrity control with the Bioanalyzer (2.2.10.3) was processed and sequenced using NGS at the BNITM sequencing facility under the lead of Dr. Dániel Cadar. Library preparation for bulk RNA-Seq was performed using the QIASeq Stranded mRNA Library Kit according to the manufacturer's instructions. Libraries were then pooled and sequenced on an Illumina NextSeq 550 system with NextSeq 500/550 Mid Output Kit v2.5 (150 cycles). 75 bp paired-end reads were generated at a sequencing depth of 5-6 million (first NGS run) or 17-22 million (second NGS run) reads per sample. Raw data were processed as described in 2.2.10.2.3.

2.2.10.2.3 Analysis of RNA sequencing data

Quality control of raw sequencing data was performed with FastQC version 0.12.1. Data were then processed using CLC genomics Workbench 21 software. RNA-Seq analysis tool was used to map reads to the murine genome (GenBank assembly GCA_003774525.2). Differential expression in two groups function was used to calculate gene expression of a sample set relative to a control set. For further analysis of gene expression data, fold change ≥ |2| and FDR *p*-value < 0.05 were set to define a gene as differentially expressed between two sample sets. In addition, a total count cutoff of 30 reads was set, meaning that all genes with less than 30 reads per sample in both conditions to be compared were excluded. If a gene was present in one condition with less than 30 counts but in the other with more than 30 counts in all of the samples, the gene was not excluded. For analysis of differentially expressed genes between samples from male and female cells, X and Y chromosomal genes were excluded.

Volcano plots for NGS data were created with the European Galaxy Server[168] (https://rna.usegalaxy.eu/) using all genes detected without applying a total count cutoff. Heatmaps were created with Heatmapper[169] (http://heatmapper.ca/) using Reads per kilobase per million mapped reads (RPKM) normalized sample data. Venn diagrams were created using InteractiVenn[170] (http://www.interactivenn.net/). GO term enrichment analysis and Kyoto Encyclopedia of Genes and Genomes (KEGG) pathways analysis of differentially expressed genes that passed the total count cutoff was performed using shinyGO[177] version 0.77 (http://bioinformatics.sdstate.edu/go/) with default settings and all detected genes of the transcriptome as background.

2.2.10.3 RNA integrity control using Agilent 2100 Bioanalyzer

For integrity control of RNA samples prior to whole transcriptome sequencing (2.2.10.2.2) or miRNA sequencing (2.2.10.1.2) and precise sample quantitation, on-chip automated electrophoresis was performed using Agilent 2100 Bioanalyzer with Agilent RNA 6000 Pico Kit and 2100 Expert Software. For this, samples were diluted to a maximum concentration of 5 ng/µl with RNase-free H_2O based on concentrations measured using the NanoDrop™ 2000. Diluted samples and reconstituted RNA ladder were denatured at 70°C for 2 min. Preparation of gel-dye mix and loading of reagents and samples onto the chip were performed according to the manufacturer's instructions. 1 µl of diluted sample was used. Assessment of RNA integrity was performed according to the RNA integrity number (RIN) calculated by the built-in software, which assesses various features of the resulting electropherograms for each sample, among them peaks for 18S and 28S ribosomal RNA[195]. RIN values are given on a range from 1 to 10, where 10 marks the highest possible RNA integrity. Samples with RIN between 8 and 10 were considered to be of high integrity and samples processed for whole transcriptome sequencing (2.2.10.2.2) were required to have a RIN of at least 6. For EV samples sent for miRNA sequencing (2.2.10.1), electropherograms resulting from Bioanalyzer runs were used to judge the presence of small RNAs in the sample, appearing as a peak at over 25 nt.

2.2.10.4 RT-qPCR

2.2.10.4.1 Primer design for RT-qPCR

For amplification of genes of interest via real-time quantitative polymerase chain reaction (RT-qPCR), gene-specific primers were designed using Primer3web version 4.1.0[175] (https://primer3.ut.ee/) and Primer-BLAST[174] (https://www.ncbi.nlm.nih.gov/tools/primer-blast/). Nucleotide sequences used for the design of primers were accessed from NCBI Nucleotide Database[172] (https://www.ncbi.nlm.nih.gov/nuccore). In case of multiple transcript variants of a target gene, the variant with the longest sequence was chosen. Primers were designed to yield an amplicon of between 75 and 200 bp in size. All primers designed were around 20 nt in length with an optimal annealing temperature of 58°C and 50 – 60 % GC content. Primers were manufactured by Eurofins Genomics GmbH.

2.2.10.4.2 cDNA synthesis

cDNA synthesis for RT-qPCR was performed using Thermo Fisher Maxima First Strand cDNA Synthesis Kit according to the manufacturer's instructions. Briefly, 4 µl 5x Reaction Mix and 2 µl Maxima Enzyme Mix, both components provided with the kit, were combined in a RNase-free tube with 200 ng template RNA (isolated as described in 2.2.10.1). RNase-free H_2O was added to a final volume of 20 µl. The reaction was first incubated at 25°C for 10 min, followed by 15 min incubation at 50°C in a heating block. The reaction was finally stopped by 5 min incubation at 85°C. Synthesized cDNA was further used for RT-qPCR as described below.

2.2.10.4.3 Gradient RT-qPCR

Gradient RT-qPCR was performed with newly designed primer pairs to assess optimal annealing temperature of the primers. 2 primer pairs per target gene were investigated. 100 pmol/µl primers were diluted 1:10 with RNase-free H_2O for further use. Thermo Fisher Maxima SYBR Green/ROX qPCR Master Mix (2X) was used according to the manufacturer's instructions with adjustments to the volumes used per reaction. In a RNase-free tube, 5 µl SYBR Green Master Mix (2X) were combined with 0.3 µl each of the 1:10 dilutions of forward and reverse primers and 3.4 µl RNase-free H_2O per reaction. In a LightCycler Multiwell 96-well plate, 9 µl of this master mix were combined with 1 µl cDNA (2.2.10.4.2) or RNase-free H_2O (control) per well. cDNA of LPS stimulated male monocytes was used for gradient RT-qPCR. Reactions were performed in duplicates. The plate was sealed with an adhesive plate sealer and subjected to short centrifugation. RT-qPCR was performed using LightCycler® 96 with the following program:

Table 14: Cycler program for gradient RT-qPCR.

Step	Temperature	Time	Repetition
Preincubation	95°C	300s	
3-step amplification	95°C	10 s	45 x
	52 - 62°C	10 s	
	72°C	10 s	
Melting	95°C	10 s	
	65°C	60 s	
	97°C	1 s	
Cooling	37°C		

Obtained data were processed using LightCycler® 96 SW 1.1 software. Melting curves were analyzed to assess specificity of the amplification by the investigated primer pairs. Melting curves with a single peak indicated the synthesis of a single, specific amplicon. Based on the appearance of amplification curve and melting curve as well as the absence of an amplicon detected in the H_2O control, one primer pair per target gene out of the two tested pairs was chosen for further use.

2.2.10.4.4 Determination of primer efficiency

Following gradient RT-qPCR (2.2.10.4.3), primer efficiency was assessed for one chosen primer pair per target gene. For this, RT-qPCR was performed on 1:10 serial dilutions of cDNA of LPS stimulated male monocytes. 4 dilutions of cDNA were used. Reactions were performed in duplicates. The reaction mix was pipetted as described in 2.2.10.4.3. The following cycler program was used for amplification of the target gene:

Table 15: Cycler program for primer efficiency RT-qPCR.

Step	Temperature	Time	Repetition
Preincubation	95°C	300s	
3-step amplification	95°C	10 s	60 x
	58°C	10 s	
	72°C	10 s	
Melting	95°C	10 s	
	65°C	60 s	
	97°C	1 s	
Cooling	37°C		

Obtained data were processed using LightCycler® 96 SW 1.1 software. Means of Cq values from duplicates were calculated and plotted against corresponding concentrations on a logarithmic scale using Microsoft Excel. A linear trend line of the data points was generated and the slope calculated. Primer efficiency (*E*) was then calculated using the following equation[196]:

$$E = 10^{(-\frac{1}{slope})}$$

A primer efficiency of 2 indicates perfect duplication of the template in every cycle. Thus, calculated primer efficiency close to the value 2 were aimed for.

2.2.10.4.5 Quantification of target mRNA using RT-qPCR

For quantification of target mRNA from monocytes stimulated as described in 2.2.7, RNA was isolated (2.2.10.1) and cDNA synthesized (2.2.10.4.2). Reactions for RT-qPCR were pipetted as described in 2.2.10.4.3 and the program described in 2.2.10.4.4 was used for amplification with LightCycler 96®, with a decrease in the number of cycles to 55. Reactions were performed in duplicates. cDNA was used undiluted or in 1:2 dilution, depending on the expected abundance of the gene of interest. For each sample and primer pair combination, a fragment of the gene encoding 40S ribosomal protein S9 (*Rps9*) was amplified as housekeeping control. For each primer pair, a negative control with H_2O instead of cDNA was used. RT-qPCR data were processed using LightCycler® 96 SW 1.1 software, analyzed using Microsoft Excel and plotted using GraphPad Prism 9. Mean Cq values of duplicates were calculated, and fold changes in the expression of the gene of interest in stimulated samples compared with means of the control group were calculated according to the following equation[196]:

$$fold\ change = \frac{(Etarget)^{\Delta Cqtarget(control-sample)}}{(Ereference)^{\Delta Cqreference(control-sample)}}$$

With E_{target} = primer efficiency of the gene of interest

$E_{reference}$ = primer efficiency of the housekeeping gene (*Rps9*)

ΔCq_{target} = Cq control condition – Cq stimulation condition (gene of interest)

$\Delta Cq_{reference}$ = Cq control condition – Cq stimulation condition (housekeeping gene)

2.2.11 Statistics

Statistical analysis between two datasets was performed using Mann-Whitney U test in GraphPad Prism 9 for all but sequencing and MS data. Significance levels were defined as follows:

* = $p < 0.05$
** = $p < 0.01$
*** = $p < 0.001$
**** = $p < 0.0001$

For comparisons with $p < 0.1$ that were not significant (ns), p values are shown in this thesis to describe trends. p values for all other non-significant comparisons are not shown.

3 Results

3.1 Workflow for the investigation of *E. histolytica*-derived EVs and their properties

In this project, the biological and immunostimulatory properties of *E. histolytica*-derived EVs were investigated to gain further insight into host-parasite interaction. To this end, an ultracentrifugation-based EV isolation protocol was established (Figure 5 A). Culture medium conditioned by *E. histolytica* trophozoites was subjected to differential centrifugation to remove cells and debris and EVs were pelleted by ultracentrifugation. EVs were isolated from two *E. histolytica* clones differing in their pathogenicity (low pathogenic A1 and highly pathogenic B2) to investigate putative mechanisms involved in amebic virulence. The isolated EVs were then further characterized with different methods (Figure 5 B). NTA was employed to determine particle size and concentration (3.2.1), and TEM was used for visualization of EVs as well as the detection of antigens on EVs through immunogold labeling (3.2.2). Mass spectrometry and miRNA sequencing were performed in order to better characterize the protein (3.2.3) and miRNA content (3.2.4) of the EVs. Finally, immune cell stimulations were performed with isolated murine monocytes and neutrophils in order to gain an understanding of the immunostimulatory capacities of the isolated EVs and the host cell response (3.3). Both male and female cells were studied to determine whether the putative immune response was dependent on the biological sex of the host. Monocytes and neutrophils were studied due to their known involvement in immune response to *E. histolytica* infection. The response of neutrophils to EV stimulation was studied in detail in the framework of a master thesis supervised as part of this doctoral project[166]. Therefore, this thesis will focus on the interaction of *E. histolytica* EVs with monocytes.

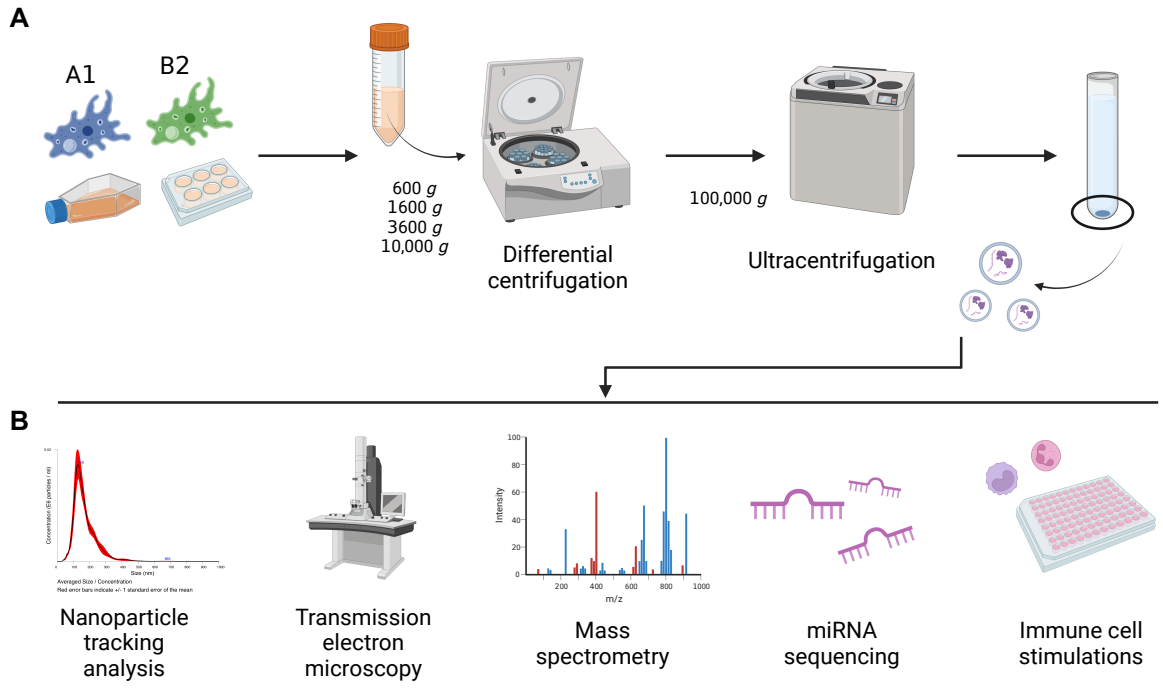

Figure 5: Schematic depiction of the workflow of EV isolation and downstream applications.
(A) Culture supernatant of A1 and B2 *E. histolytica* was subjected to differential centrifugation at increasing speeds, with the pellet discarded at each step, to remove cells and debris. EVs were then pelleted by ultracentrifugation at 100,000 *g*. The resulting EV samples were then used for a variety of downstream applications (B), namely NTA, TEM, mass spectrometry, miRNA sequencing and immune cell stimulations. Figure created with BioRender.

3.2 Characterization of *E. histolytica* EVs

3.2.1 Determination of EV size and concentration using nanoparticle tracking analysis

EVs isolated from culture supernatants of A1 or B2 *E. histolytica* trophozoites via differential ultracentrifugation were quantified using nanoparticle tracking analysis (NTA) to determine particle size distribution and concentration. Particles in the isolated EV samples were heterogeneous in size, with some particles smaller than 100 nm and others larger than 400 nm (Figure 6 A, B). It should be noted that NTA has a resolution limit of around 50 nm for EVs and can thus not detect particles that may be even smaller[197]. There were no significant differences in the size and number of particles released by the two clones (Figure 6 C, D). Particle concentration of EV samples as determined by NTA was used to calculate sample amounts needed for later immune cell stimulations (3.3).

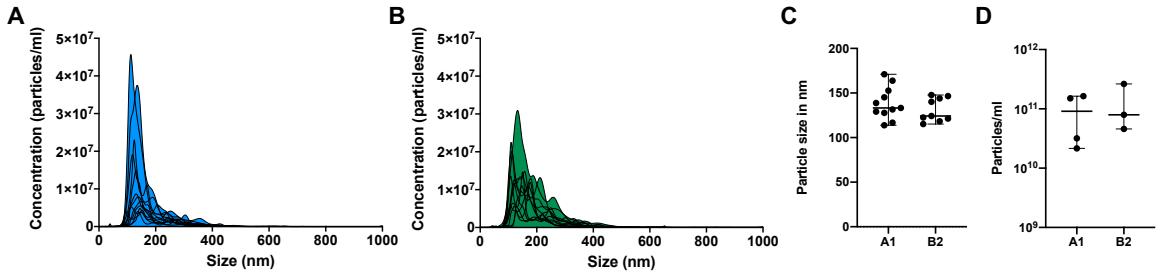

Figure 6: Nanoparticle tracking analysis (NTA) for the determination of particle size and concentration.
(A, B) Overlay of NTA data from multiple independent measurements of A1 EVs (A, n = 13) and B2 EVs (B, n = 12). Depicted are averaged data from 5 videos per sample. (C) Comparison of the modal particle size of A1 and B2 EVs as determined by NTA (n = 9-11). (D) Comparison of the particle concentration of A1 and B2 EV samples in a set of standardized experiments (n = 3-4). Calculation of *p* values for statistical significance was performed using Mann-Whitney U test.

3.2.2 Visualization of EVs by transmission electron microscopy

Immunogold labeling followed by negative staining for TEM was performed to visualize isolated *E. histolytica* EVs. Detection of the prominent membrane-associated *E. histolytica* molecules Gal/GalNac lectin (Figure 7) and LPPG (Figure 8) on the EV surface was performed to verify their amebic origin. Secondary antibodies for immunogold labeling are conjugated to gold particles that appear as black dots in TEM images.

TEM showed that EV samples were heterogeneous with regard to vesicle size, with some smaller than 100 nm and others as big as 500 nm (Figure 7, Figure 8), which corresponds to the findings obtained by NTA (Figure 6). EVs secreted by both A1 and B2 amebae contained Gal/GalNac lectin (Figure 7), but it was not present on all particles. 'Background' labeling could be seen in samples of both clones that was absent in secondary antibody controls, indicating that the lectin was present in the samples but not bound to EVs. This effect could be the result of EV disintegration during storage or sample processing. A similar picture could be observed for LPPG (Figure 8), which was also detected on EVs from A1 and B2 amebae. Labeling was performed twice for A1 and B2 EVs with each antibody to ensure reproducibility of the result.

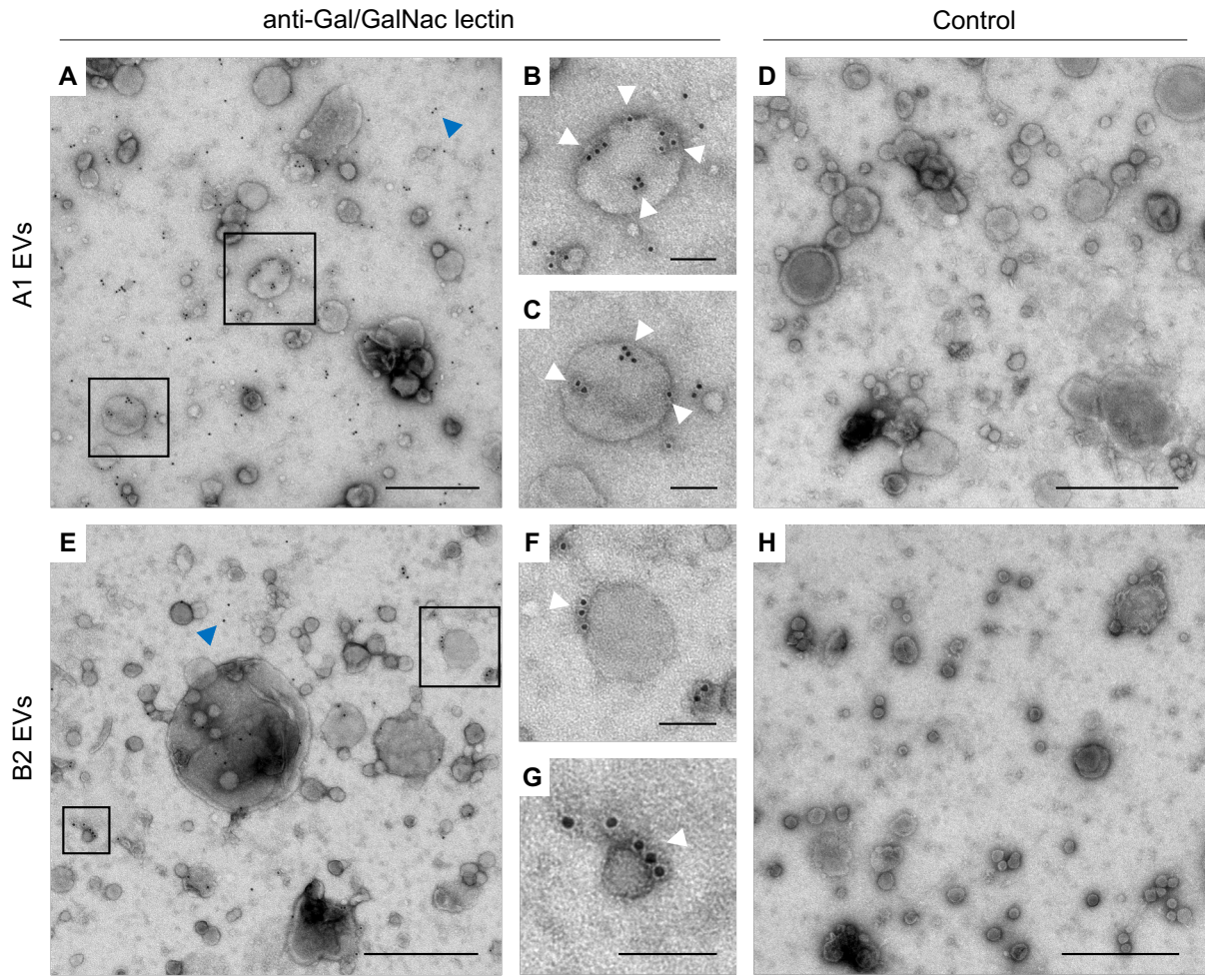

Figure 7: Detection of Gal/GalNac lectin on *E. histolytica* EVs by immunogold labeling.
EVs isolated from A1 (A-D) and B2 (E-H) *E. histolytica* were labeled with anti-Gal/GalNac lectin primary and goat anti-rabbit gold-conjugated secondary antibodies, followed by negative staining and detection by TEM. (A, E) Overview of labeled EV samples from A1 (A) and B2 (E) amebae. Blue arrowheads indicate examples of background labeling (black dots). (B, C, F, G) Close-up images of individual labeled A1 (B, C) or B2 (F, G) EVs. Every black dot corresponds to a bound gold-conjugated secondary antibody (indicated by white arrowheads). (D, H) Secondary antibody only controls of A1 (D) and B2 (H) EVs, in which the primary antibody was omitted. Shown are representative images from two separate labelings for A1 and B2 EVs. Scale bars correspond to 500 nm in overview images (A, D, E, H) and 100 nm in close-ups (B, C, F, G).

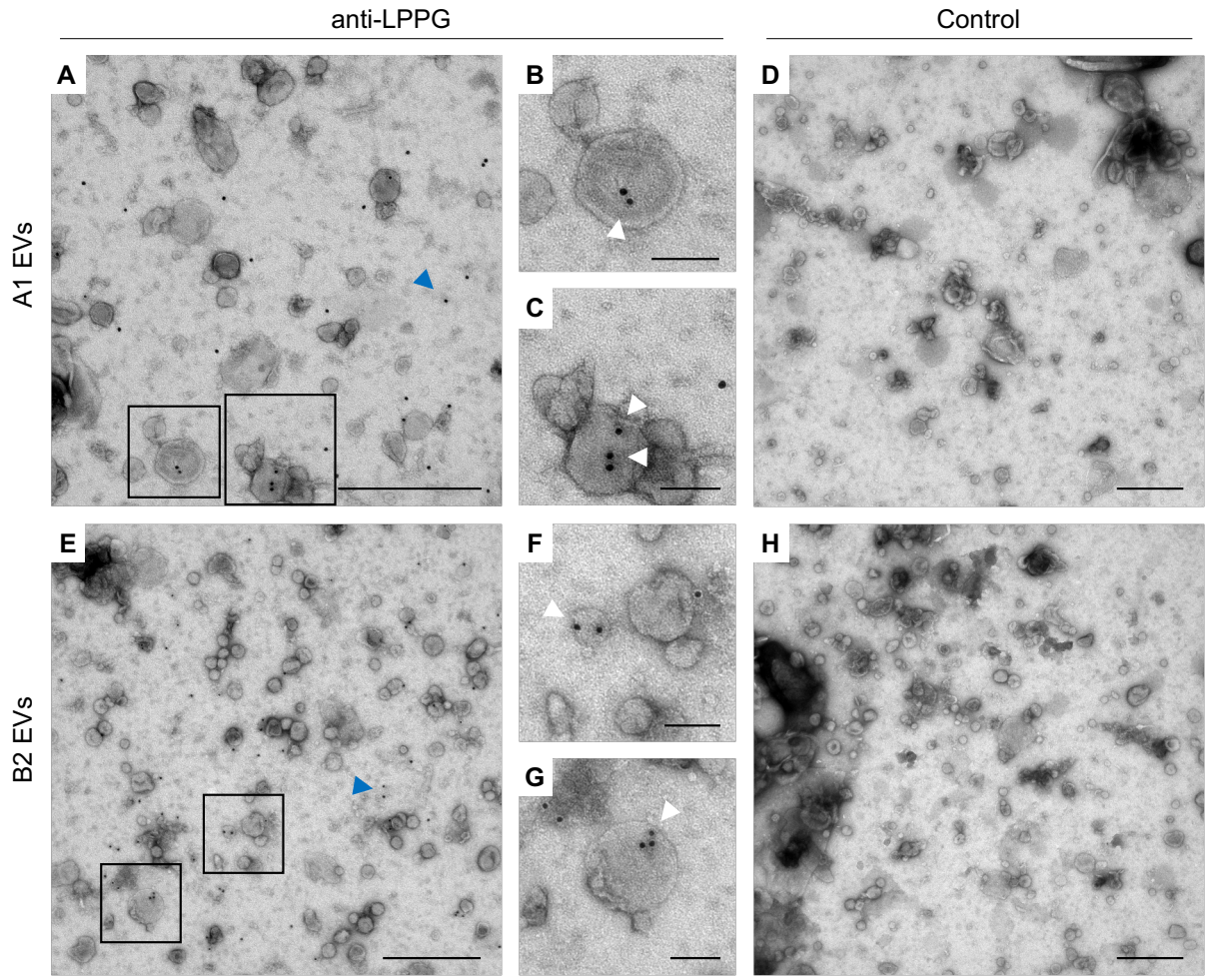

Figure 8: Detection of LPPG on *E. histolytica* EVs by immunogold labeling.
EVs isolated from A1 (A-D) and B2 (E-H) *E. histolytica* were labeled with anti-LPPG primary and goat anti-mouse gold-conjugated secondary antibodies, followed by negative staining and detection by TEM. (A, E) Overview of labeled EV samples from A1 (A) and B2 (E) amebae. Blue arrowheads indicate examples of background labeling (black dots). (B, C, F, G) Close-up images of individual labeled A1 (B, C) or B2 (F, G) EVs. Every black dot corresponds to a bound gold-conjugated secondary antibody (indicated by white arrowheads). (D, H) Secondary antibody only controls of A1 (D) and B2 (H) EVs, in which the primary antibody was omitted. Shown are representative images from one labeling. Scale bars correspond to 500 nm in overview images (A, D, E, H) and 100 nm in close-ups (B, C, F, G).

3.2.3 The *E. histolytica* EV proteome

3.2.3.1 Analysis of the protein content of *E. histolytica* EVs and comparison to other organisms

Mass spectrometry was performed to analyze the protein composition of A1 and B2 *E. histolytica*-derived EVs. Principal component analysis (PCA) revealed that A1 and B2 EV proteomes were similar to each other with regard to principal component (PC) 1 and distinct from negative controls (Figure 9 A; n = 3). Functional classification of proteins in A1 EVs (Figure 9 B, C) and B2 EVs (Supplementary figure 1) with Panther knowledgebase[173] showed that most proteins were associated with the cellular component gene ontology (GO) terms membrane, endomembrane system, intracellular anatomical structures, organelle, cytoplasm, and cell periphery, and out of proteins with the assigned molecular function 'catalytic activity', about half possessed hydrolase activity.

A total of 863 proteins were detected in at least 2 out of 3 A1 EV samples and 711 proteins in 2 out of 3 B2 EV samples, 674 of which were common proteins (Figure 9 D, Figure 11 A). 78 proteins were detected uniquely in the A1 EV proteome and not the B2 EVs, whereas 7 proteins were detected only in the B2 EV proteome (Figure 9 D, Supplementary table 1). GO term enrichment analysis for the proteins unique to A1 EVs revealed molecular functions in organic substance transport, localization, guanosine triphosphate (GTP) binding, and GTPase activity (Figure 9 F, Supplementary table 2). Glycosylphosphatidylinositol (GPI)-anchor biosynthesis was the most significantly associated KEGG pathway (pathway ID ec00563, data not shown). Out of the 7 proteins present only in B2 EVs, 4 were hypothetical proteins (EHI_072010, EHI_023070, EHI_130950 and EHI_095850; Supplementary table 1). EHI_072010 is annotated in UniProt[178] as autophagy-related protein 9 and involved in phagophore assembly (entry C4M606). The three annotated proteins were one putative mannosyltransferase (EHI_029580), putative syntaxin (EHI_181290) and the alpha subunit of beta-N-acetylhexosaminidase (EHI_148130) (Supplementary table 1). Reliable GO term enrichment or pathway analysis could not be performed for this short list of proteins.

The only protein present in both A1 and B2 EV proteomes and significantly regulated with a fold change ≥ |2| was the hypothetical protein EHI_161930, which was present at higher levels in B2 EVs compared with A1 EVs (Figure 9 E; Supplementary table 1). For further analysis, the sequence of this protein was accessed from AmoebaDB[167] and subjected to InterProScan using InterPro database[171] 94.0. Four transmembrane domains, three cytoplasmic domains and two non-cytoplasmic domains were detected in the EHI_161930 sequence (data not shown). No orthologs for this protein in other organisms outside of the genus *Entamoeba* were identified by protein BLAST (blastp, National Center for Biotechnology Information (NCBI)).

Both EV proteomes were controlled for the presence of proteins typically identified in EV proteomes, such as heat shock proteins, 14-3-3 proteins, ADP-ribosylation factor, and metabolic enzymes like peroxiredoxin[198], which were all present (Supplementary table 3). In order to assess how similar the *E. histolytica* EV proteomes were to EV proteomes of other organisms, comparison to the top 100 most commonly detected mammalian EV proteins according to Vesiclepedia[179] was performed. To this end, protein sequences of these 100 proteins were retrieved from UniProt (release 2022_04)[178] and protein BLAST against *E. histolytica* was performed (blastp, NCBI). Orthologs were found in *E. histolytica* for 67 out of 100 proteins. Of these, 42 were present in at least 1 of 3 A1 EV proteome samples and 41 in at least 1 of 3 B2 EV samples (Supplementary table 16), showing that the *E. histolytica* EV protein cargo is similar to that of other organisms.

Furthermore, the supernatant of the first ultracentrifugation step was included as a negative control to determine which proteins were present in samples but not specific to EVs. A total of 30 proteins was detected in at least 1 of 3 control samples (Supplementary table 6). This included five of the top EV protein orthologs (Supplementary table 16).

Another class of proteins typically present in EVs due to the involvement in their biogenesis are tetraspanins (TSPANs)[198]. Of the 17 known and putative *E. histolytica* tetraspanins, as described by Tomii *et al.*[199], 4 were detected in a minimum of 1 of the A1 or B2 EV proteome samples (Supplementary table 4). EHI_022890 (TSPAN1) and EHI_091490 (TSPAN12) were detected in both EV proteomes in all samples. EHI_075690 (TSPAN4) was present in 2 of 3 A1 EV samples but only 1 of 3 B2 EV samples. EHI_107790 (TSPAN13) was absent from B2 EVs but present in 1 of 3 A1 EV samples. The other tetraspanins were not detected. It should be noted that also in proteomes of *E. histolytica* trophozoites (see below, 3.2.3.2), only 6 of the known and potential tetraspanins were detected, namely TSPAN1, TSPAN2, TSPAN4, TSPAN7, TSPAN12, and TSPAN15 (Supplementary table 4). Interestingly, TSPAN13 was not detected in trophozoite proteomes although it was detected in one EV sample. Additionally, the presence of ESCRT proteins described by López-Reyes *et al.*[200] in *E. histolytica* EV proteomes was investigated, since these proteins are also associated with EV biogenesis. Four proteins that were predicted to be components of either ESCRT complex 0, I or II (EHI_091530, EHI_135460, EHI_137860, and EHI_045320) were detected in at least 1 out of 3 EV samples for A1 and B2 EVs (Supplementary table 5).

Taken together, it was shown that the *E. histolytica* EV proteomes are comparable to EV proteomes of other organisms and contain typical EV markers. A1 and B2 EV proteomes exhibited some differences, but many of the differentially expressed proteins were hypothetical proteins and further investigation will be needed to elucidate their functions.

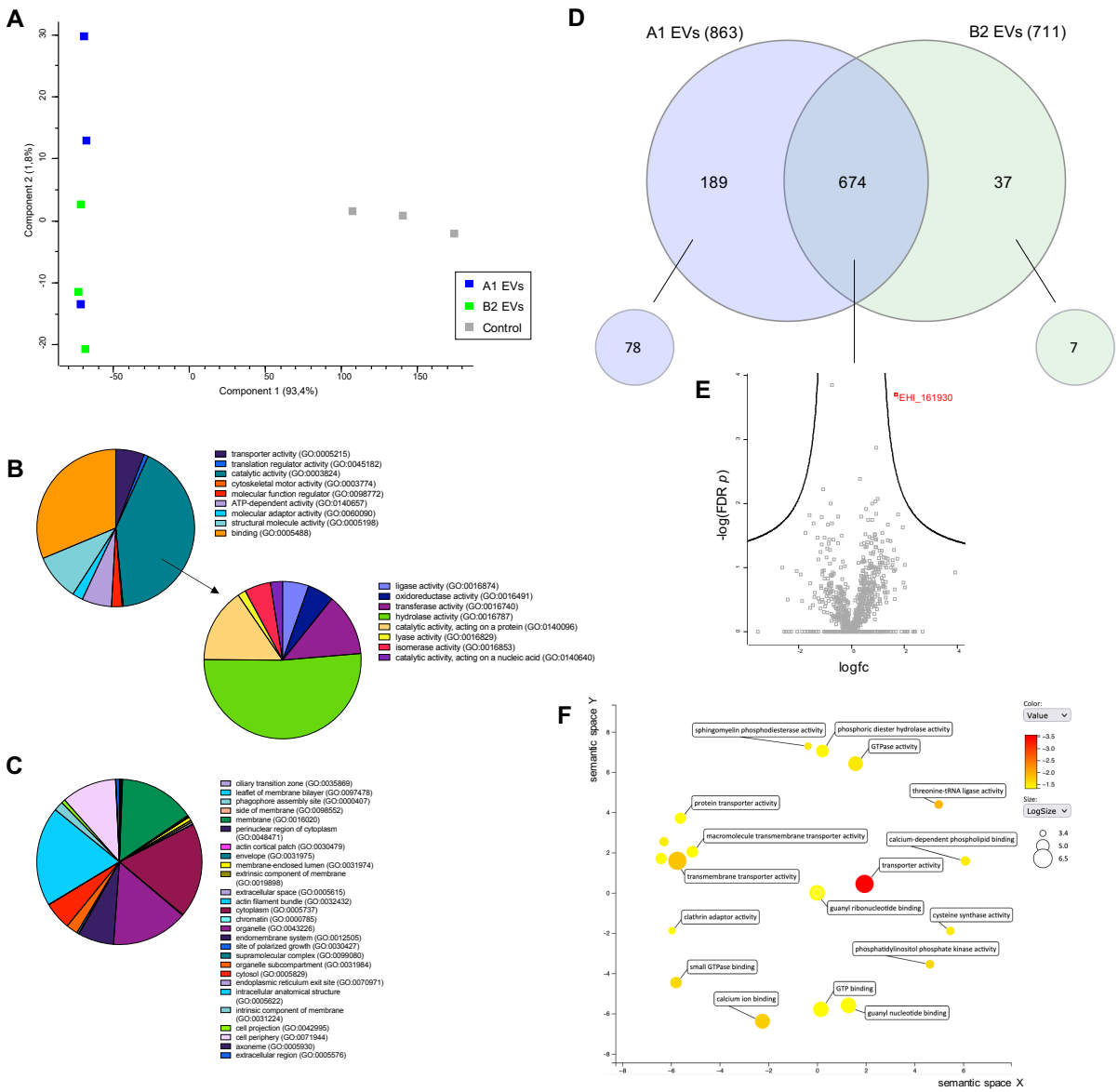

Figure 9: The proteomes of A1 and B2 *E. histolytica* EVs.

(A) Principal component analysis of EV proteome samples, generated using Perseus software[189] (n = 3). Controls are supernatants of the first ultracentrifugation step. (B, C) Pie charts depicting the relative amount of proteins in the A1 EV proteome with GO terms for (B) molecular function (left) and molecular function sublevel 1 catalytic activity (right) and (C) cellular component, sublevel 1 cellular anatomical entity. Pie charts were created with Panther knowledgebase[173]. (D) Venn diagram depicting the number of proteins present in A1 and B2 EV proteomes (at least 2/3 samples) and the number of proteins shared between the two proteomes. Diagram was created with InteractiVenn[170]. Small bubble diagrams on the bottom of the Venn diagram depict the number of proteins uniquely present in the corresponding proteome (0/3 in the other proteome). (E) Volcano plot depicting relative presence of proteins between A1 and B2 EV proteomes according to statistical significance (-log10 of the FDR-adjusted *p* value) versus magnitude of change (logfc = log fold change). Marked in red is a significantly regulated protein (downregulated in A1 EVs compared with B2 EVs). Volcano plot was created with Perseus software[189]. (F) Molecular function GO terms associated with the 78 proteins unique to A1 EVs. GO term analysis was performed with AmoebaDB[167] and visualized with Revigo[176].

3.2.3.2 Comparison of the EV proteome to *E. histolytica* whole cell proteomes

To investigate whether selective enrichment or depletion of certain protein groups could be detected in EVs, mass spectrometry on whole amebae from the same clones was performed (Figure 10). PCA showed that A1 and B2 amebae proteomes were distinct from one another with regard to PC 1, and samples for the same clone clustered together (Figure 10 A; n = 3). A total of 2711 proteins were detected in at least 2 out of 3 A1 *E. histolytica* and 2496 proteins were detected in at least 2 out of 3 B2 *E. histolytica* (Figure 10 B, Figure 11 A). 2374 of these proteins were common between the clones (Figure 10 B). 214 proteins were detected only in A1 and not B2 amebae, whereas 53 proteins were detected uniquely in the B2 amebae proteome (Figure 10 B, Supplementary table 8, Supplementary table 9). A total of 312 proteins that were present in both A1 and B2 proteomes were present in significantly different amounts (FDR $p < 0.05$, fold change $\geq |2|$) (Figure 10 C). Such proteins will henceforth be defined as 'differentially expressed' for the purpose of clarity, although it should be noted that proteins are synthesized and not expressed. A heatmap of the top 50 differentially expressed proteins between A1 and B2 amebae is depicted in Figure 10 D (highest fold changes; refer also to Supplementary table 7). Molecular function GO term enrichment analysis showed that proteins significantly more present in A1 amebae (unique proteins + upregulated proteins) have roles in nucleic acid binding, actin binding, protein binding, and ligase activity, among others (Figure 10 E, Supplementary table 10). Proteins significantly more present in B2 amebae are involved in oxidoreductase, lyase and amylase activity, phospholipid binding, or antioxidant activity, among other functions (Figure 10 E, Supplementary table 11).

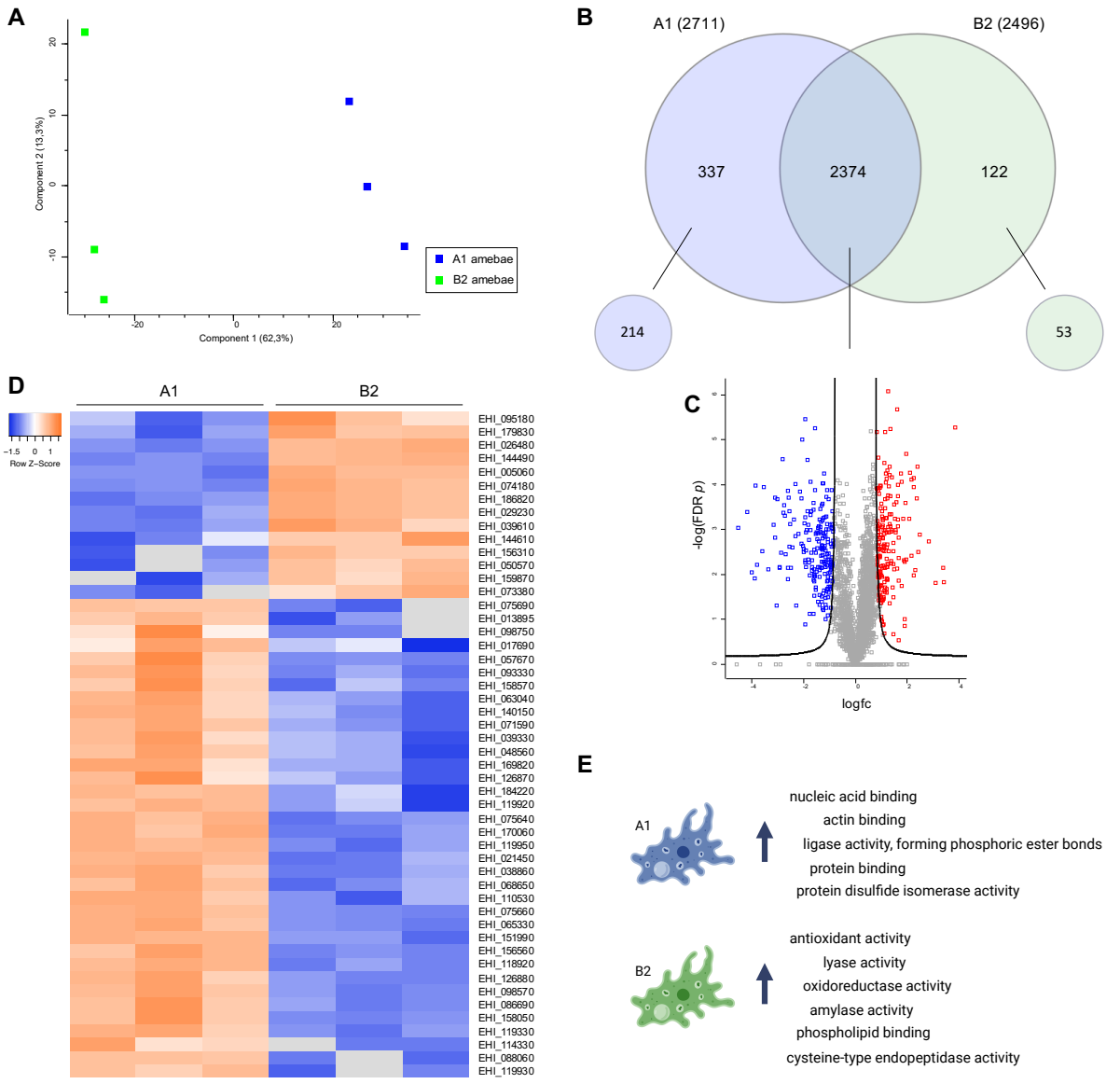

Figure 10: The proteomes of A1 and B2 *E. histolytica* trophozoites.
(A) Principal component analysis of A1 and B2 amebae proteome samples, generated using Perseus software[189] (n = 3). (B) Venn diagram depicting the number of proteins present in A1 and B2 amebae (at least 2/3 samples) and the number of proteins shared between the two proteomes. Diagram was created with InteractiVenn[170]. Small bubble diagrams on the bottom of the Venn diagram depict the number of proteins uniquely present in the corresponding proteome (0/3 in the other proteome). (C) Volcano plot depicting relative presence of proteins between A1 and B2 EV proteomes according to statistical significance (-log10 of the FDR-adjusted *p* value) versus magnitude of change (logfc = log fold change). Marked in blue are proteins significantly more highly present in A1 amebae and in red are those proteins more highly present in B2 amebae. Volcano plot was created with Perseus software[189]. (D) Heatmap depicting the z-score of the top differentially expressed proteins between A1 and B2 amebae. Shown are the top 50 significantly (FDR $p < 0.05$) differentially expressed proteins according to fold change. Sample data binary logarithm was used for mapping. Orange indicates high levels of protein, while blue indicates low levels. Grey color was used for missing data. Heatmap was created with Heatmapper[169]. (E) Selected molecular function GO terms associated with proteins more highly expressed in A1 or B2 amebae (proteins present in both but differentially expressed + unique proteins) based on analysis with AmoebaDB[167] (created with BioRender).

Comparison of EV and amebae proteomes based on AmoebaDB[167] results showed that between 37 – 40 % of proteins in all four proteomes were hypothetical proteins (Figure 11 A). While around 13 % of proteins in whole amebae had a transmembrane (TM) domain, around 30 % of EV proteins were TM proteins (Figure 11 A). Additionally, an enrichment of proteins with a signal peptide to the EV proteomes could be observed (more than 26 % proteins with signal peptide in EVs compared with

9 – 10 % in whole amebae, Figure 11 A). Interestingly, 71 proteins detected in EV proteomes were not present in whole cell proteomes, 35 of which were shared between A1 and B2 EV proteomes with presence of the protein in at least 2/3 samples (Figure 11 B, Supplementary table 12). This indicates that these proteins may be specifically enriched in EVs. Many of these 71 proteins are hypothetical proteins (Supplementary table 12). When comparing the 579 differentially expressed proteins in whole cells to the 86 differentially expressed between the two EV proteomes, only 15 were common (Figure 11 C; Supplementary table 1).

For further comparison of EV proteomes to the corresponding whole cell proteome, statistical overrepresentation test was performed in Panther knowledgebase for GO terms biological process, molecular function, and cellular component[190]. Regarding cellular components, membrane-associated and endoplasmatic reticulum (ER) proteins were enriched in EV proteomes, whereas nucleic proteins were depleted (Supplementary table 15). Biological process GO terms associated with transmembrane transport, lipid metabolism, and localization were significantly enriched, while RNA and DNA metabolic processes were depleted (Figure 11 D, Supplementary table 13). With regard to molecular function GO terms, proteins involved in GTPase, phosphatase, or hydrolase activity were enriched in EVs (Figure 11 D, Supplementary table 14). Proteins involved in binding of nucleic acids or catalytic activity acting on nucleic acids were depleted (Figure 11 D, Supplementary table 14).

A

Proteome	Total proteins	Hypothetical proteins	% Hypothetical proteins	TM domain	% TM domain	Signal peptide	% Signal peptide
A1 EVs	863	320	37,08	265	30,71	231	26,77
B2 EVs	711	281	39,52	238	33,47	205	28,83
A1 amebae	2711	1046	38,58	361	13,32	248	9,15
B2 amebae	2496	926	37,1	332	13,3	252	10,1

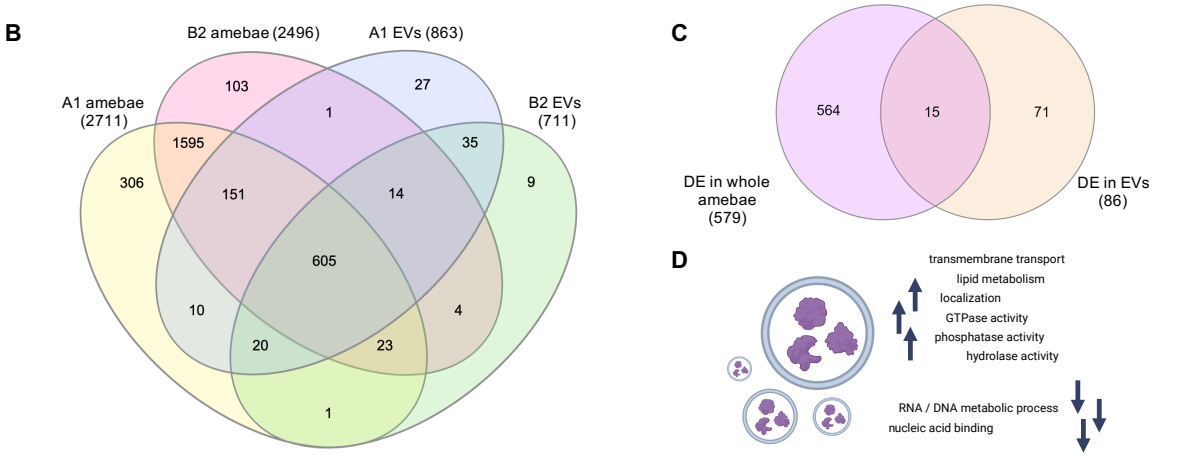

Figure 11: Comparison of *E. histolytica* EV and trophozoites proteomes.
(A) Table listing the number of total proteins, hypothetical proteins and proteins with a transmembrane (TM) domain or a signal peptide detected in A1 and B2 EV and whole amebae proteomes. Data on hypothetical proteins, TM domains and signal peptides are based on annotations in AmoebaDB[167] (release 60). (B) Venn diagram depicting the number of proteins present in and shared between A1 and B2 EV and whole cell proteomes. (C) Venn diagram depicting the number of proteins differentially expressed (DE) between A1 and B2 amebae or EVs or both. Diagrams were created with InteractiVenn[170]. (D) Selected GO terms associated with proteins enriched in EVs compared with whole cell proteomes (upward arrows) or depleted in EVs (downward arrows), based on statistical overrepresentation test performed with Panther knowledgebase[190] (created with BioRender).

In summary, EV proteomes were enriched in membrane and ER proteins as well as proteins with a signal peptide in comparison to the whole cell proteome. EVs were furthermore enriched in proteins with various enzymatic activities, such as GTPase activity, and proteins involved in transmembrane transport. Several proteins were differentially expressed between A1 and B2 EVs but not between the corresponding whole cell proteomes, indicating selective enrichment to EVs that differs between the *E. histolytica* clones and may play a role in EV-mediated communication with the host immune system in the context of pathogenicity.

3.2.4 The miRNA cargo of *E. histolytica* EVs

Analysis of the miRNA content of EVs was performed in order to gain insight into involvement of EVs in the regulation of gene expression in EV target cells. miRNAs are small, single-stranded, non-coding RNAs. When incorporated into the RNA-induced silencing complex (RISC), miRNAs mediate gene silencing by binding to target mRNAs, which results in inhibition of translation and cleavage of mRNA[201].

For this purpose, total RNA was isolated and subjected to miRNA sequencing. RNA integrity control with Agilent Bioanalyzer prior to sequencing revealed the presence of a population of short RNAs larger than 25 nt in the EVs (Figure 12 A), which corresponds to the knowledge that *E. histolytica* has an abundant population of 27 nt small RNAs[202,203]. Notably, no peaks for ribosomal RNA were detected in EV samples (Figure 12 A).

Out of all sequenced reads, between 5,848,946 and 20,900,954 unique sequences could be detected per sample (data not shown). PCA showed that samples from A1 and B2 EVs did not cluster distinctly apart, indicating similar miRNA content in EVs of both clones (Figure 12 B; n = 3). For the detection of mature miRNAs in the sequence data, a custom reference sequence list was created based on previously published mature miRNAs[192]. Interestingly, none of the reported mature miRNAs were found in the EV samples, with the exception of Ehi-miR-4, which was detected in low quantities in some samples, and one count of Ehi-miR-3 present in one sample (data not shown). Therefore, we investigated whether isomiRs of the described mature miRNAs were present in the samples. IsomiRs are variants of mature miRNAs, and isomiRs with modifications at the 3' end (3' isomiRs) share the same seed sequence[204], which is the sequence of nucleotides in position 2 – 8 at the 5' end of the miRNA that essentially mediates binding to target mRNA and thus gene silencing[205]. For this, we analyzed the 'grouped on seed' output of the miRNA quantification. 191 different seed sequences were detected in the 199 previously described mature miRNAs due to some redundant miRNA sequences in the annotation (Supplementary table 17). In addition to miRNAs with identical sequences, it was apparent that Ehi-miR-60 and Ehi-miR-117 as well as Ehi-miR-143 and Ehi-miR-193 had the same respective seed sequence, even though they otherwise differed in their sequences (data not shown; Mar-Aguilar *et al.*[192]). Analysis of differential expression between A1 and B2 EVs revealed that 3' isomiRs of Ehi-miR-35 and Ehi-miR-55 were significantly more expressed in A1 EVs (fold changes 3.77 and 5.00, respectively) (Figure 12 C, Supplementary table 17). To determine targets of these isomiRs in the *E. histolytica* and human genome, nucleotide BLAST was performed with the seed sequences against the corresponding genome (blastn and megablast, NCBI). No significant similarity could be identified in either species.

Furthermore, we performed *de novo* miRNA prediction based on our sequencing data using BrumiR algorithm[193] to identify other mature *E. histolytica* miRNAs that were not previously described in literature. A total of 1016 novel mature miRNAs were predicted by BrumiR based on A1 and B2 EV samples (data not shown). Of these, 167 miRNA sequences were present with a minimum of 5 total counts in at least 2 out of 3 samples of either the A1 or B2 EVs (Supplementary table 18). Differential expression analysis showed that only one miRNA was significantly regulated (FDR $p < 0.05$, fold change ≥ |2|) between A1 and B2 EVs (Figure 12 D; Supplementary table 18). Again, nucleotide BLAST was performed with the sequence of this miRNA against the *E. histolytica* and human genomes. Since the seed sequence of a mature miRNA is essential for binding to target mRNA, hits were considered of interest if alignment of the miRNA sequence to the target genome was detected from nucleotide 1 or 2 of the query sequence onwards. In the *E. histolytica* genome, alignment with mostly hypothetical or uncharacterized proteins (for example EHI_012280, EHI_035770, EHI_040950, EHI_057700, EHI_117860, EHI_122710) was detected (data not shown). It is therefore difficult to conclude which processes in the parasite are regulated by this miRNA. Interestingly, several targets of this miRNA were detected in the human genome, including *SEPTIN9* and multiple transcript variants of *CCL25*, which are both involved in T cell development[206,207] (data not shown). Additional hits included genes encoding for RAP1 GTPase activating protein 2, Rho GTPase activating protein 26, and LysM domain containing 4 (data not shown). These results indicate that miRNAs packaged into *E. histolytica* EVs have the potential to regulate, among others, GTPase activity and immunological processes in target cells in the human host. A more comprehensive target gene analysis of the miRNA content of *E. histolytica* A1 and B2 EVs could not be performed with currently available tools due to the lack of annotation for *E. histolytica* miRNAs.

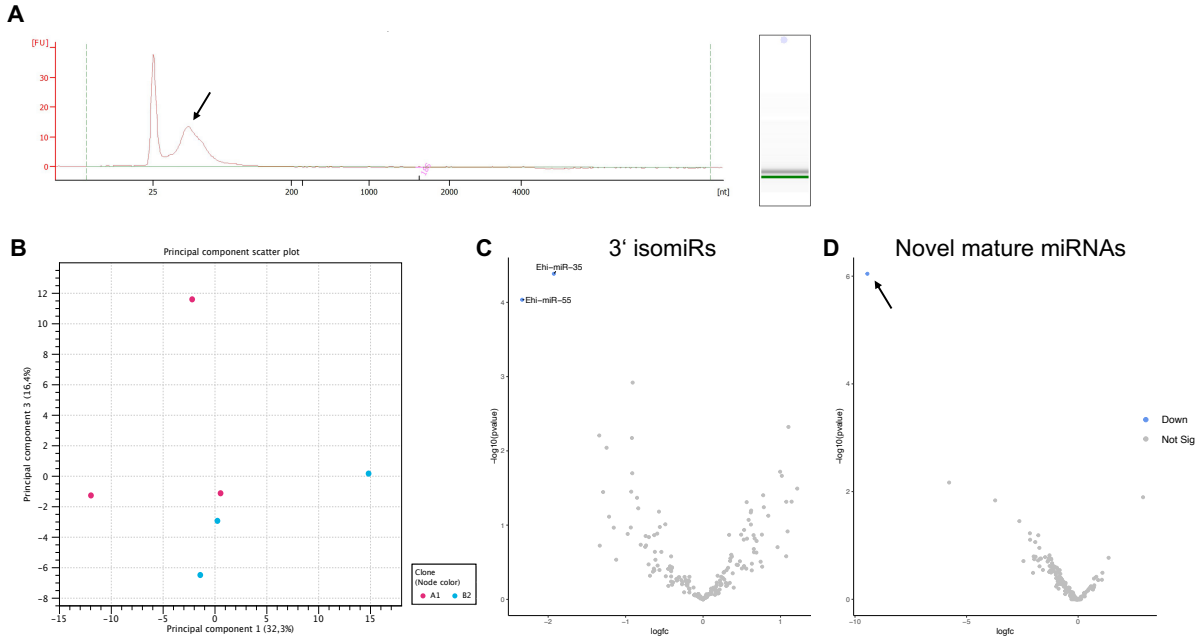

Figure 12: The miRNA content of *E. histolytica* EVs.
(A) Electropherogram (left) and gel image (right) of total RNA isolated from EVs during integrity control with Agilent Bioanalyzer. Peak at 25 nt corresponds to the marker. Arrow indicates the presence of a population of short RNAs. Shown is a representative sample. (B) PCA of miRNA sequencing data according to *E. histolytica* clone (node color). PCA was generated using CLC genomics (n = 3). (C, D) Volcano plots depicting relative miRNA expression between two sample sets according to statistical significance (-log10 of the FDR-adjusted *p* value) versus magnitude of change (logfc = log fold change). miRNAs significantly regulated between the two conditions with a fold change ≥ |2| (logfc = 1) and FDR *p* value < 0.05 are colored in blue (downregulated in B2 compared to A1) or red (upregulated, not applicable). miRNAs not significantly regulated are colored in grey (not sig). Shown are (C) 3' isomiRs of annotated mature miRNAs[192] and (D) *de novo* predicted mature miRNAs. Arrow in (D) indicates a significantly differentially expressed miRNA. Volcano plots were created with Galaxy server[168].

In summary, we found almost no expression of the previously described *E. histolytica* miRNAs in our samples, but found 3' isomiRs of them. Moreover, we were able to predict novel miRNAs using BrumiR algorithm based on the sequence data. Differential expression analysis revealed only very few significant differences between the EVs of the different clones. 3' isomiRs of Ehi-miR-35 and Ehi-miR-55 as well as one novel mature miRNA were significantly more highly expressed in A1 EVs compared with B2 EVs. BLAST analysis revealed initial insight into possible target genes of one miRNA in the human host, but a more comprehensive target gene analysis of the detected miRNAs using bioinformatics approaches is needed in the future.

3.3 Immunostimulatory properties of *E. histolytica* EVs

3.3.1 EV stimulation of primary murine monocytes

In order to characterize the immune response of monocytes to *E. histolytica* EVs, monocytes were isolated from murine bone marrow (BM) cells through antibody-mediated immunomagnetic negative selection and stimulated with EVs. Subsequently, stimulated monocytes were processed for RNA-Seq using NGS or analysis of surface markers via flow cytometry. Supernatants of stimulated monocytes were used for detection of cytokines and MPO (Figure 13). Stimulation with LPS served as a positive control and stimulation with a mock control as a negative control. Mock controls were obtained by processing culture medium for differential ultracentrifugation in the same way as supernatants of *E. histolytica* cultures (2.2.2.2). The amount of EVs used for stimulation as well as stimulation period were established in previous experiments on splenocytes and BM cells derived from male mice. Flow cytometry and RT-qPCR were used to control for the upregulation of activation markers and IL-6 ELISA on supernatants in those experiments (data not shown). Experiments on BM cells showed that most isolated *E. histolytica* EVs elicited increased IL-6 release by the stimulated cells, while some did not (data not shown). Therefore, induction of IL-6 release was determined as a functionality criterion for EV pools used for further immune cell stimulations.

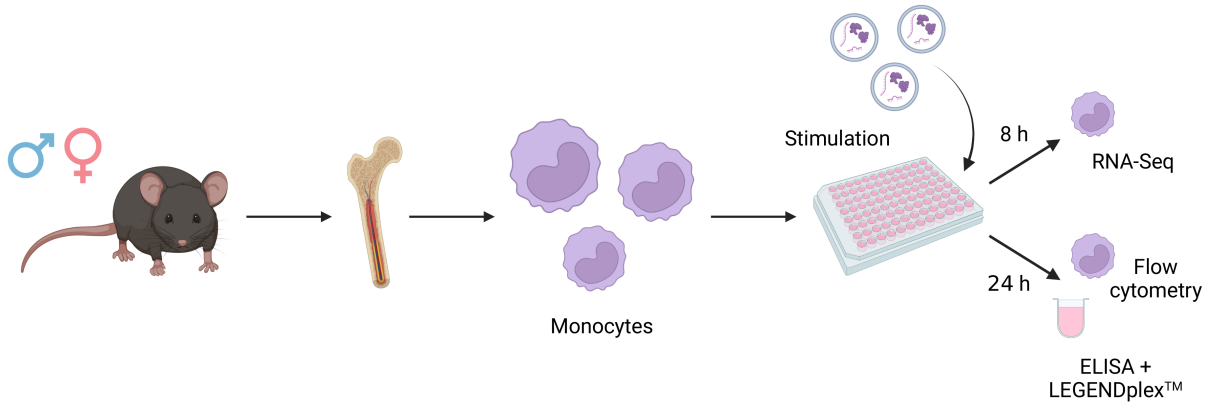

Figure 13: Schematic depiction of the workflow of stimulation experiments on monocytes.
The bones of male and female C57BL/6J mice were harvested and monocytes isolated out of bone marrow cells via immunomagnetic negative selection. Isolated monocytes were then stimulated with 1000 EVs/cell, together with positive and negative controls, for 8 h or 24 h. Cells stimulated for 8 h were processed for RNA sequencing (RNA-Seq), while cells stimulated for 24 h were analyzed using flow cytometry and their supernatants were used for ELISA and LEGENDplex™ to assess cytokine profiles and MPO concentration. Figure created with BioRender.

Efficacy of monocyte isolation was controlled using flow cytometry as shown in Figure 14 A. Only isolations with at least 85 % total Ly6C$^+$ (Ly6C^{hi} + Ly6C^{lo}) cells out of CD11b$^+$ cells were used for experiments. The same gating strategy was applied for control of neutrophil isolation (Supplementary figure 2). Analysis of 'before isolation' samples revealed that around 20 – 40 % of murine bone marrow cells are positive for the myeloid marker CD11b and the proportion is significantly higher in male compared with female mice (Figure 14 B, * $p < 0.05$). Within the CD11b$^+$ compartment, no significant differences in the proportion of Ly6C^{hi} classical monocytes (Figure 14 C), Ly6C^{lo} non-classical monocytes (Figure 14 D) or Ly6G$^+$ neutrophils (Supplementary figure 2 C) between males and females could be detected.

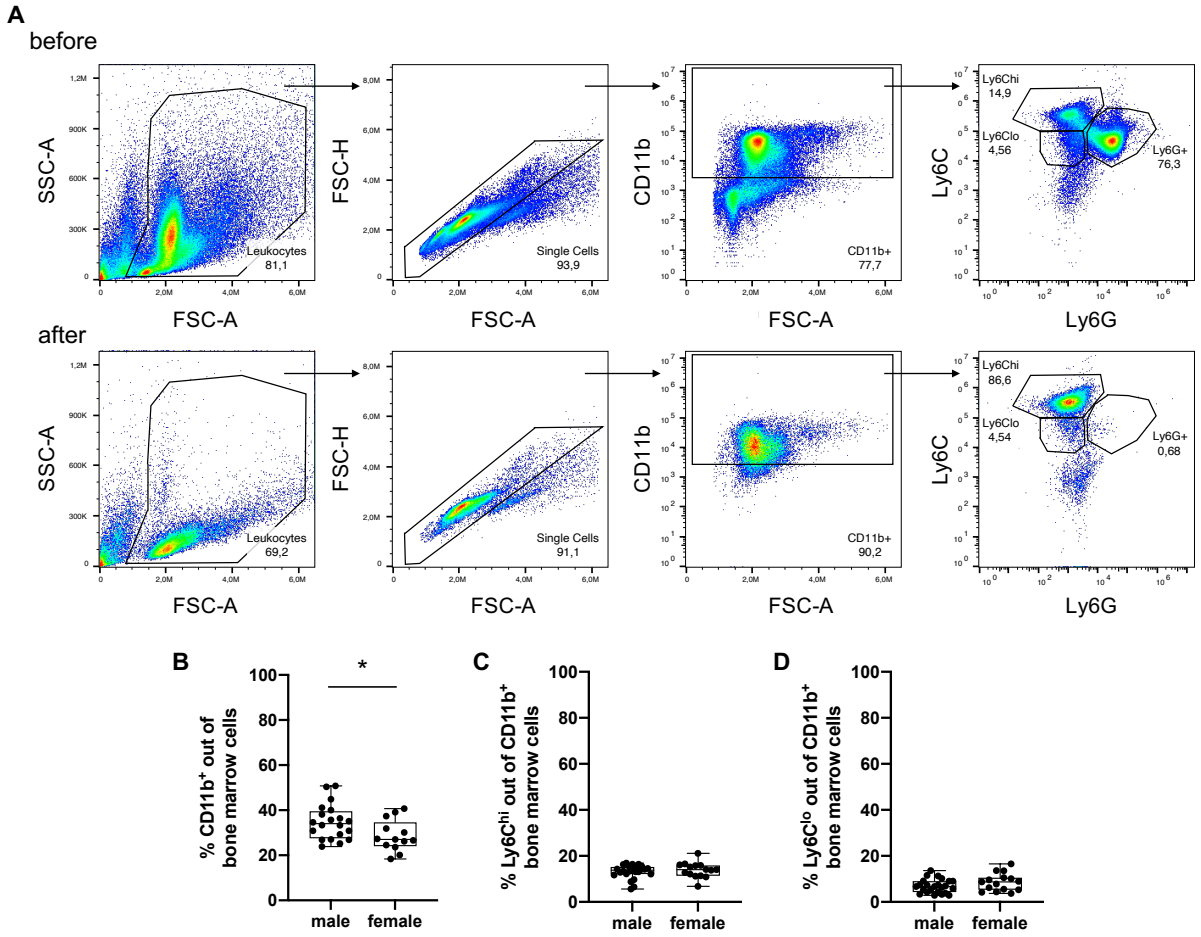

Figure 14: Monocyte isolation control and comparison of cell population frequencies between male and female mice.
(A) Efficacy control of monocyte isolation using flow cytometry. Cells before and after isolation were stained with anti-CD11b, anti-Ly6C and anti-Ly6G antibodies to identify CD11b$^+$Ly6C$^+$ monocytes. Intensity of Ly6C was used to distinguish between Ly6C^{hi} classical monocytes and Ly6C^{lo} non-classical monocytes. Shown is one representative experiment. (B-E) Quantification of the relative amount of CD11b$^+$ cells (B), Ly6C^{hi} monocytes (C) and Ly6C^{lo} monocytes (D) in male and female mice (n = 13-20). Percentage of cells was determined based on 'before enrichment' samples (A). Testing for statistical significance was performed with Mann-Whitney U test (* $p < 0.05$).

3.3.2 The cytokine profile of EV stimulated murine monocytes

Supernatants of monocytes stimulated with EVs were subjected to cytokine profiling with LEGENDplex™ anti-virus response panel containing antibodies against TNFα, IL-1β, IL-10, IFN-β, CXCL10, and granulocyte-macrophage colony-stimulating factor (GM-CSF) (Figure 15, Supplementary figure 3) to analyze whether EV stimulation had an effect on cytokine release. Several of the analytes detected with this panel have been implicated in the immune response to *E. histolytica* by monocytes or macrophages in previous studies, particularly TNFα[91], IL-10[208], IL-1β[209,210], and CXCL10[209], thus making them interesting candidates to investigate in the context of EV-monocyte interaction. GM-CSF was the only cytokine below the detection threshold in all samples (data not shown). Results for all other cytokines are presented in the following paragraph.

No significant effect of EV stimulation on the concentration of IFN-β in comparison with mock controls was observed in supernatants of female monocytes or upon A1 EV stimulation of male monocytes (Figure 15 A). Stimulation of male monocytes with B2 EVs led to a significant decrease in the concentration of IFN-β compared with mock controls (* $p < 0.05$). However, it should be noted that overall concentration of IFN-β in all samples was very low. No significant impact of EV stimulation on IL-10 concentration could be detected either, in fact, IL-10 could not be detected in these samples at all but was present in the positive control (Figure 15 B). In contrast, both male and female monocytes secreted significantly more TNFα upon A1 and B2 EV stimulation compared with mock controls (Figure 15 C, * $p < 0.05$, ** $p < 0.01$). CXCL10 release was significantly increased by A1 EV stimulation of male monocytes (* $p < 0.05$) and a similar tendency could be observed for B2 EV stimulation of male monocytes and both EV stimulations of female monocytes but was not statistically significant (Figure 15 D). IL-1β concentration was higher in A1 and B2 EV stimulated male and female monocytes in comparison with mock control stimulated monocytes (Figure 15 E), but since the concentration was below the lower detection limit in some samples, this effect was not statistically significant. Nevertheless, analysis of the median fluorescence intensity (MFI) for this marker revealed that the increase in IL-1β was statistically significant after A1 EV stimulation of male monocytes (Supplementary figure 3 E).

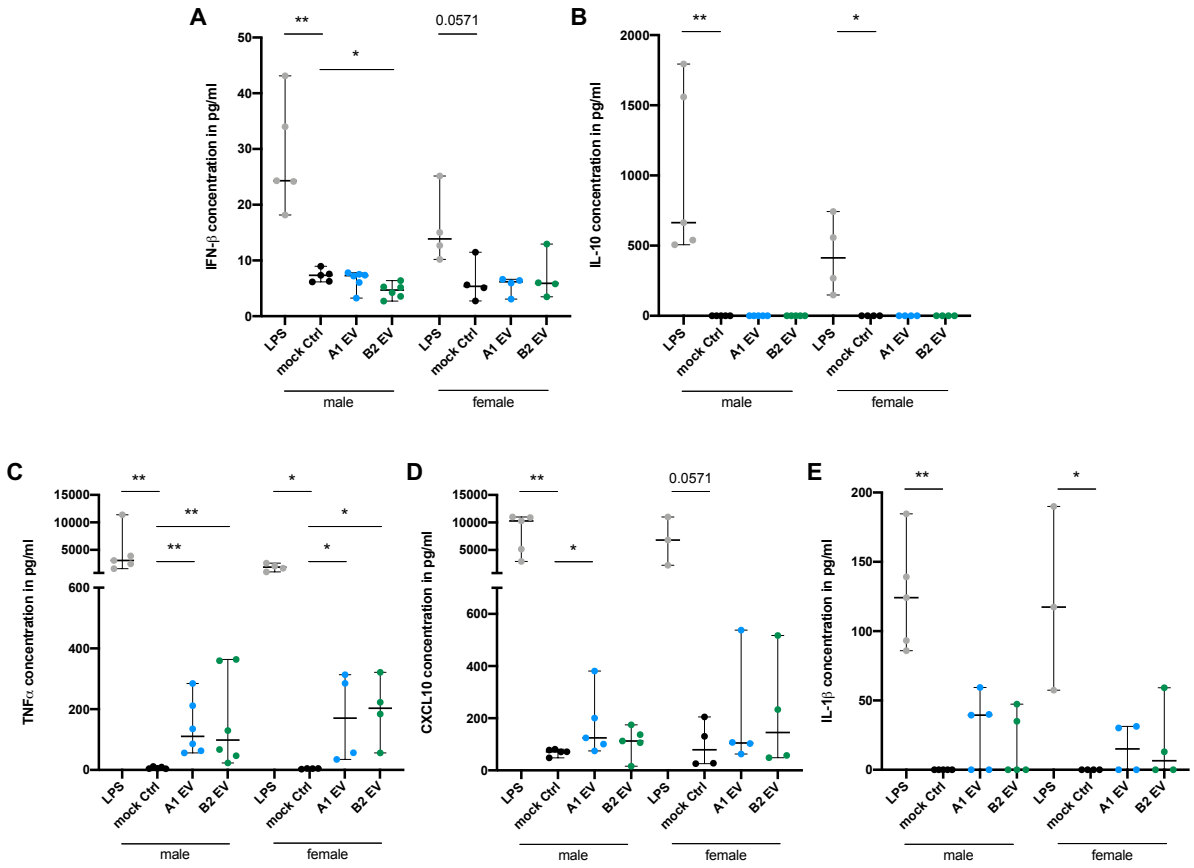

Figure 15: Cytokine profiling of EV-stimulated monocyte culture supernatants with LEGENDplex™ anti-virus response panel.
Male and female bone marrow-derived monocytes were stimulated for 24 h with LPS (positive control), mock control or 1000 EVs/cell of A1 or B2 EVs. IFN-β (A), IL-10 (B), TNFα (C), CXCL10 (D), and IL-1β (E) were detected in supernatants after stimulation by LEGENDplex™. Depicted is the median with range (n = 3-6). Testing for significance was performed using Mann-Whitney U test (* $p < 0.05$, ** $p < 0.01$).

The cytokine profile of monocytes after EV stimulation was then further investigated with ELISA for the cytokines CCL2, CCL3, and IL-6 (Figure 16). Additionally, M1 macrophage LEGENDplex™ panel was used to assess IL-12p40, IL-12p70, IL-18, IL-23, and CXCL1 levels in response to EV stimulation together with the already previously analyzed cytokines TNFα, IL-1β, and IL-6 (Figure 17, Supplementary figure 4). These assays were chosen to investigate the respective cytokines due to their roles in monocyte-mediated ALA immunopathology (CCL2[90,91], CXCL1[105], IL-23[90]), neutrophil recruitment during ALA (CCL3[91], CXCL1[105,106]), and inflammatory response of monocytes to *E. histolytica* antigens (IL-6[208], IL-12p40[208]). Since an effect of EV stimulation on cytokine release had already been observed, a heat inactivated (h.i.) control was added to the stimulation conditions to determine whether the observed effect was caused by EV components susceptible to heat.

ELISA of monocyte supernatants showed that A1 and B2 EV stimulation led to an increase in CCL3 and IL-6 but not CCL2 production by monocytes in comparison with mock controls for both male- and female-derived cells (Figure 16). Interestingly, heat inactivation of A1 EVs did not impair the observed effect, while heat inactivation of B2 EVs led to a decrease in CCL3 release by male monocytes when compared to non-inactivated B2 EVs (Figure 16 A).

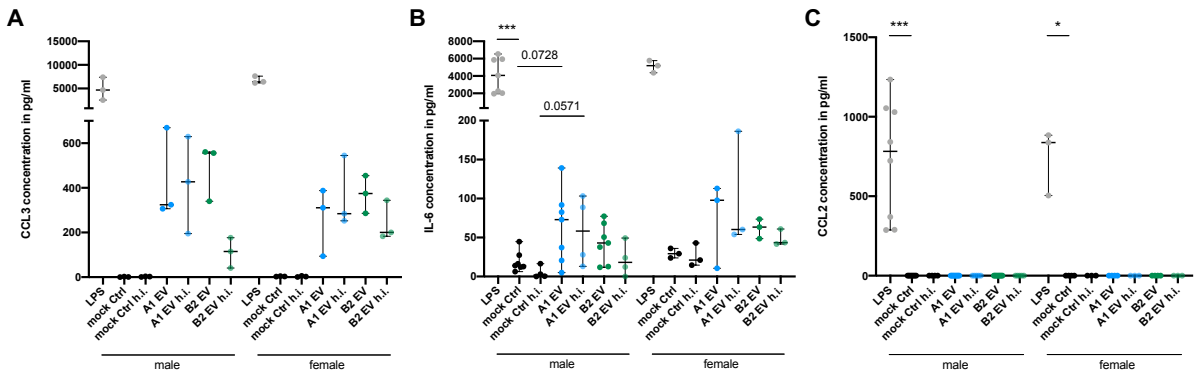

Figure 16: Analysis of CCL3, IL-6 and CCL2 secretion by EV stimulated monocytes using ELISA.
Male and female bone marrow-derived monocytes were stimulated for 24 h with LPS (positive control), mock control or 1000 EVs/cell of A1 or B2 EVs. Heat inactivation of EVs was performed at 95°C for 10 min as a separate control. Concentrations of CCL3 (A, n = 3), IL-6 (B, n = 3-7), and CCL2 (C, n = 3-8) in supernatants of stimulated monocytes were detected using ELISA. Graphs depict median with range. Significances were calculated using Mann-Whitney U test (* $p < 0.05$, *** $p < 0.001$).

Furthermore, LEGENDplex™ with M1 macrophage panel showed that EV stimulation led to increases in IL-12p40 and CXCL1 concentrations in supernatants of stimulated cells compared with mock controls and confirmed previous findings from ELISA and anti-virus response LEGENDplex™ on increased secretion of IL-6, TNFα, and IL-1β upon EV stimulation (Figure 17). IL-12p70, IL-18, and IL-23 could not be detected in any of the samples (data not shown). More precisely, IL-6 concentration was significantly increased upon A1 and B2 EV stimulation of male monocytes (** $p < 0.01$) and also increased in female monocytes, but not significantly (Figure 17 A). However, lack of statistical significance for female samples may be explained by lower sample number and thus lower statistical power. Again, heat inactivation of A1 EVs did not impair their stimulatory capacity, while heat inactivation of B2 EVs led to a decrease in the elicited cytokine concentration compared with intact B2 EVs. In samples from male monocytes, this effect was statistically significant (** $p < 0.01$). Analysis of IL-12p40 (Figure 17 B) and TNFα (Figure 17 C) revealed the same pattern and here, increase of IL-12p40 concentration upon A1 EV stimulation and TNFα concentration upon B2 EV stimulation of female monocytes were significant (* $p < 0.05$). In accordance with the previously performed LEGENDplex™, IL-1β concentrations were higher in EV stimulated male and female samples compared with mock controls, but the effect was not statistically significant (Figure 17 D). Again, concentrations of this cytokine were around the lower detection limit, especially in female samples. Nevertheless, the loss of the capacity of B2 EVs to induce IL-1β secretion upon heat inactivation was significant for male mice (* $p < 0.05$), mirroring the effect observed for other cytokines. CXCL1 was increased upon A1 and B2 EV stimulation of male (** $p < 0.01$) and B2 EV stimulation of female mice (* $p < 0.05$). The increase in CXCL1 concentration upon A1 EV stimulation of female monocytes was significant only when analyzing the MFI (* $p < 0.05$, Supplementary figure 4 E). Particularly for IL-1β and CXCL1, overall cytokine concentrations were higher in male monocyte samples compared with female samples.

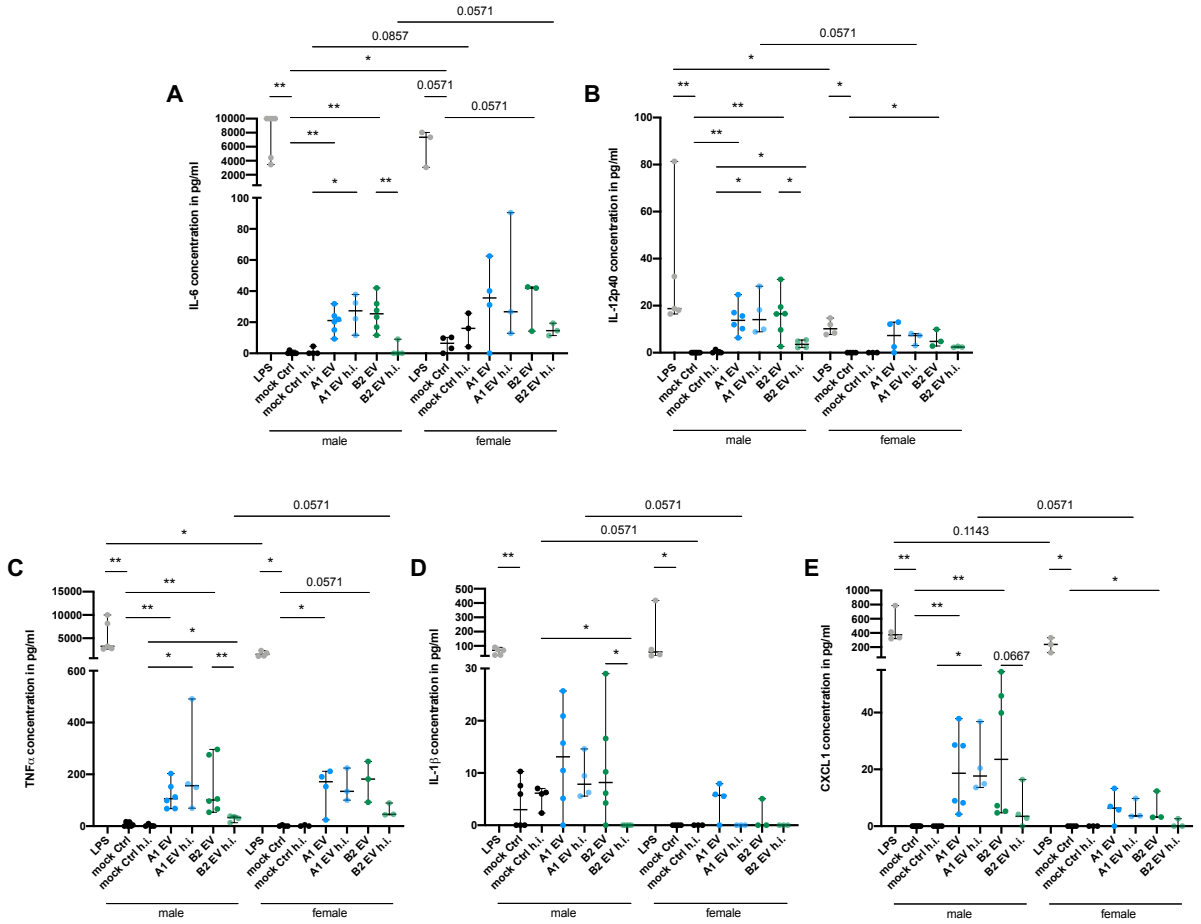

Figure 17: Cytokine profiling of EV-stimulated monocyte culture supernatants with LEGENDplex™ M1 macrophage panel.
Male and female bone marrow-derived monocytes were stimulated for 24 h with LPS (positive control), mock control or 1000 EVs/cell of A1 or B2 EVs. Heat inactivation (h.i.) of EVs was performed at 95°C for 10 min as a separate control. IL-6 (A), IL-12p40 (B), TNFα (C), IL-1β (D), and CXCL1 (E) were detected in supernatants after stimulation by LEGENDplex™. Graphs depict median with range (n = 3-6). Testing for significance was performed using Mann-Whitney U test (* $p < 0.05$, ** $p < 0.01$).

In summary, stimulation of both male and female monocytes with EVs derived from low pathogenic A1 and highly pathogenic B2 *E. histolytica* led to an increase in the concentration of multiple chemokines and cytokines with pro-inflammatory properties compared with mock controls. Apart from the effect of heat inactivation on the stimulatory capacity of B2 EVs, A1 and B2 EVs exhibited the same stimulatory pattern.

3.3.3 Myeloperoxidase release by EV stimulated monocytes and neutrophils

MPO is an enzyme stored in azurophilic granules of neutrophils and monocytes, which is released as part of the innate immune response by degranulation and catalyzes the formation of metabolites with microbicidal activity, such as hypochlorous acid[211]. MPO is described to be mainly secreted by neutrophils and only to a lesser extent by monocytes[211]. Hence, the release of MPO into the supernatants of both monocytes and neutrophils was studied in order to investigate the effect of EV stimulation on this effector function of the immune cells.

A significant increase in the release of MPO upon stimulation with A1 EVs compared to mock controls was observed for both male and female monocytes (* $p < 0.05$, Figure 18 A). In contrast, B2 EVs did not induce an increase in MPO release. Furthermore, heat inactivation of EVs did not have a significant effect on MPO release. Interestingly, heat inactivation of the mock control led to a decrease in MPO release (ns).

Neither stimulation with A1 EVs nor with B2 EVs resulted in an increase of MPO release by male or female BM-derived neutrophils when compared with mock controls (Figure 18 B). However, stimulation of peripheral neutrophils isolated from spleen and blood exhibited the same pattern as the stimulated monocytes (Figure 18 C). A1 EV stimulated male and female peripheral neutrophils both released significantly more MPO compared with mock controls (* $p < 0.05$, ** $p < 0.01$, respectively), but B2 EV stimulated neutrophils did not. Heat inactivated controls were not performed for peripheral neutrophils due to the much lower cell yield when isolating neutrophils out of blood and spleen compared with BM.

Overall, absolute MPO concentrations were comparable between supernatants of stimulated monocytes and BM as well as peripheral neutrophils.

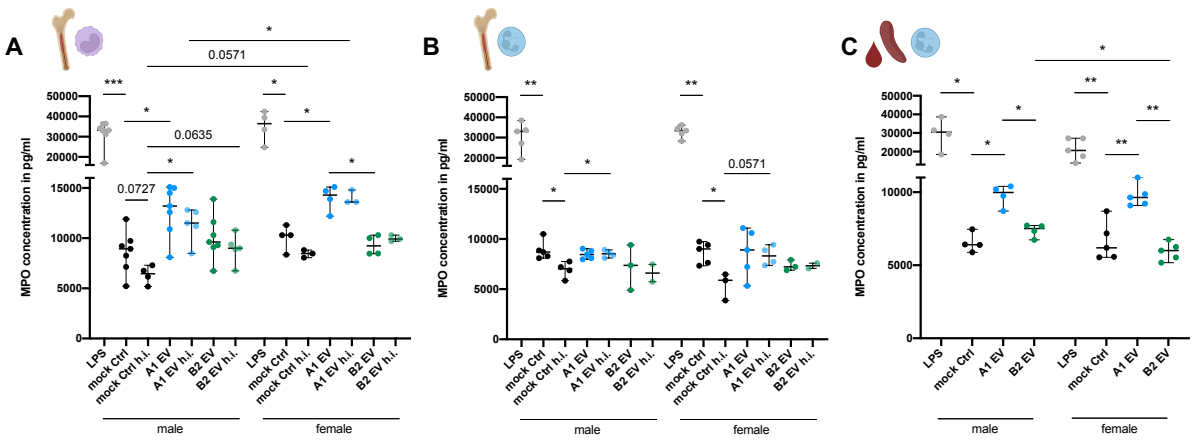

Figure 18: Detection of myeloperoxidase (MPO) in the supernatants of EV-stimulated monocytes and neutrophils.
Male and female bone marrow (BM)-derived monocytes (A), BM-derived neutrophils (B) or peripheral neutrophils (C) were stimulated for 24 h with either LPS (positive control), mock control or 1000 EVs/cell of A1 or B2 EVs. As a separate control employed in experiments on BM-derived cells, EVs were heat inactivated (h.i.) for 10 min at 95°C. Concentration of MPO in supernatants of stimulated cells was determined via ELISA. Depicted is the median with range ((A) n = 3-7, (B) n = 2-5, (C) n = 4-5). Testing for significance was performed using Mann-Whitney U test (* $p < 0.05$, ** $p < 0.01$, *** $p < 0.001$). B + C adapted from master thesis Valentin Bärreiter[166]. Icons created with BioRender.

3.3.4 Flow cytometry analysis of surface marker expression on EV stimulated monocytes

In order to determine the effect of EV stimulation on activation state of classical Ly6C^{hi} and non-classical Ly6C^{lo} monocytes, surface marker expression was analyzed. To this end, an antibody panel was designed (Figure 19 A), and cells were stained with fluorophore-coupled antibodies for spectral flow cytometry after stimulation. Of particular interest were CD38, CD69, and CD86, markers for activation of monocytes, that are upregulated in inflammatory conditions in general or during ALA[212–214]. In addition, CD62L, also called L-selectin, was investigated – a cell adhesion molecule important for adherence of circulating monocytes to the endothelium[215]. Major histocompatibility complex (MHC) II was included in the panel to determine antigen-presenting capacity of the investigated monocytes. Antibodies against CD11b, Ly6C, and Ly6G were used to identify monocytes as CD11b^{+}Ly6C^{+}Ly6G^{-} cells. CCR2 and CX_3CR1 were investigated as chemokine receptors present on monocytes during steady state that play a critical role in the immune response through the interaction with ligand chemokines[11,103]. Staining with Zombie UV™ was performed to determine viability of cells. Cytek® Full Spectrum Viewer with Similarity™ Index was used to assess similarity of the chosen fluorophores and dyes (Figure 19 B) and overlap of their emission spectra (Figure 19 C) to control quality of the designed panel. Low values for Similarity™ indices indicated uniqueness of the chosen dyes (Figure 19 B) and analysis of the emission spectra further showed that each fluorophore was characterized by peak emission in a different channel of the flow cytometer (Figure 19 C), hence proving successful panel design. Presence of the chosen markers on Ly6C^{hi} and Ly6C^{lo} monocytes was assessed according to the gating strategy shown in Figure 19 D. Gates were set according to FMO controls (not shown).

A

Antibody/Dye	Fluorophore	Dilution
Anti-CD11b	BV510	1:400
Anti-Ly6C	PE	1:800
Anti-Ly6G	APC	1:400
Anti-CCR2	PE-Cy7	1:100
Anti-CX_3CR1	PerCP-Cy5.5	1:200
Anti-CD38	BV421	1:800
Anti-CD62L	BV711	1:800
Anti-CD69	FITC	1:200
Anti-CD86	BV605	1:800
Anti-MHCII	APC-Cy7	1:100
Zombie UV	-	1:1000

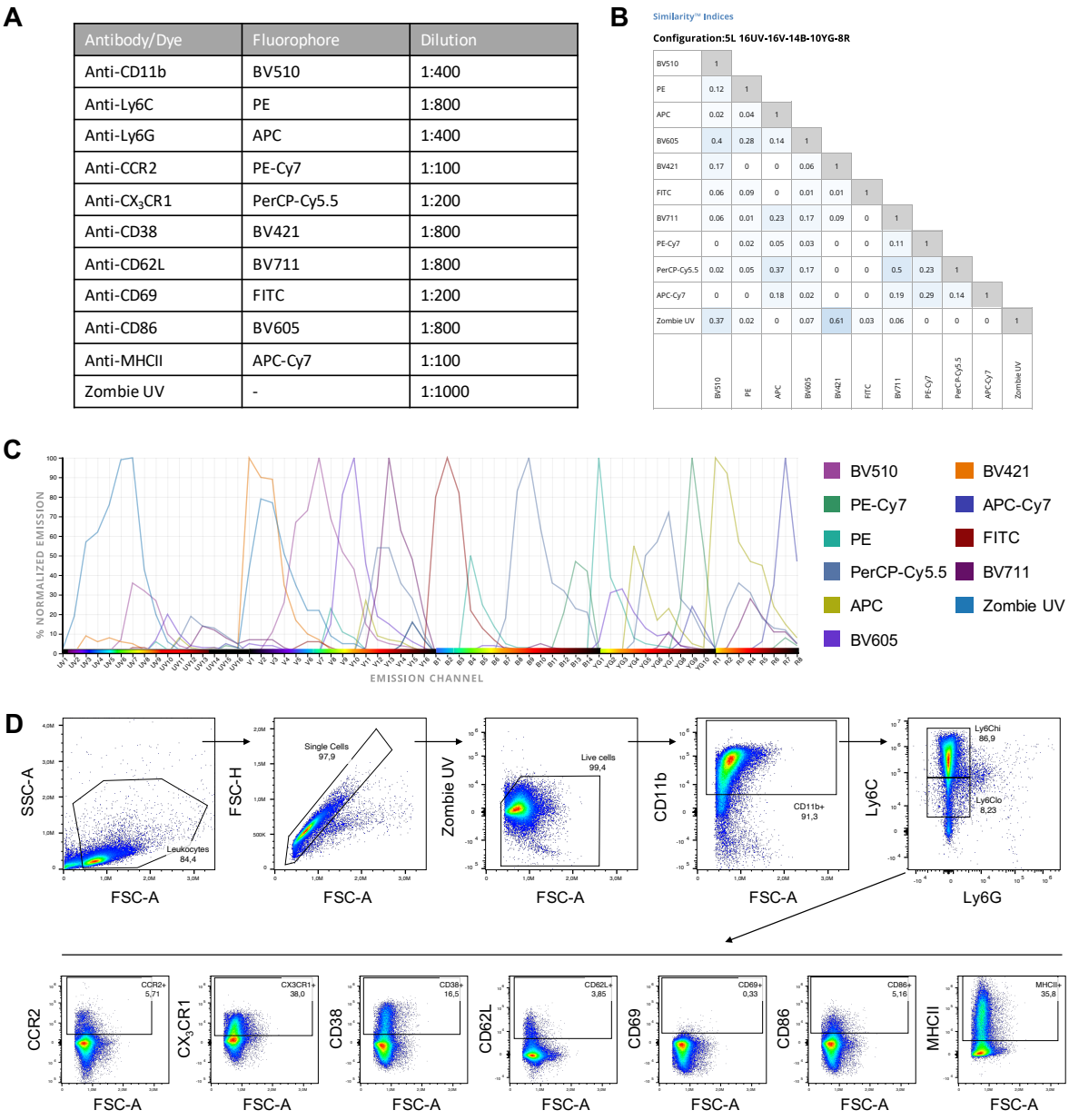

Figure 19: Antibody panel and gating strategy for the identification of surface marker expression on monocytes via flow cytometry.
(A) Antibody panel for the detection of surface markers on stimulated monocytes. (B) Similarity™ index of the designed panel showing similarity of two fluorophores/dyes on a scale of 0 to 1, where 0 stands for complete uniqueness and 1 indicates identity (Cytek® Full Spectrum Viewer). (C) Emission spectra of all fluorophores/dyes in the panel according to emission channels in the 5-laser Aurora flow cytometer, visualized by Cytek® Full Spectrum Viewer. (D) Gating strategy for the assessment of surface marker expression on stimulated monocytes. Shown is a representative sample. Gates for surface markers on monocytes were set according to FMO controls (not shown).

Stimulation of both male and female monocytes with A1 and B2 EVs resulted in an increased surface expression of CD38 on Ly6C^{hi} monocytes (Figure 20 A, B) and to a lesser extent also on Ly6C^{lo} monocytes (Figure 20 C, D) compared with mock controls. Similar to previous observations for secreted cytokines (3.3.2), heat inactivation of A1 EVs did not result in an alteration of the observed effect, while heat inactivation of B2 EVs led to lower CD38 expression compared to stimulation with intact B2 EVs especially on male Ly6C^{hi} monocytes (Figure 20 A, B).

EV stimulation did not lead to apparent alterations in the amount of the other analyzed markers in either male or female classical or non-classical monocytes (Supplementary figure 5), with the exception of a decrease in CX_3CR1 expression on male Ly6C^{hi} monocytes upon A1 and B2 EV stimulation (Supplementary figure 5 I) and slightly elevated CD86 levels on female Ly6C^{lo} monocytes (Supplementary figure 5 F). However, MFI of CCR2 was increased on male Ly6C^{hi} monocytes stimulated with both A1 and B2 EVs (Supplementary figure 6 G), even though the overall percentage of CCR2 positive cells was not affected (Supplementary figure 5 G). This finding indicates that cells that were already positive for CCR2 expressed more of this marker after stimulation with A1 or B2 EVs.

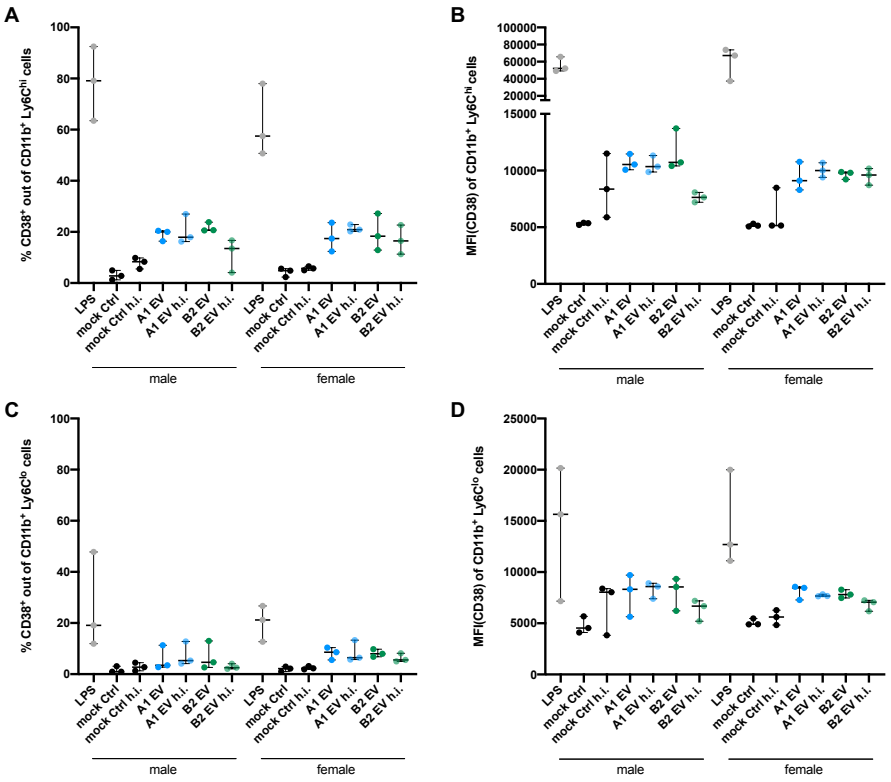

Figure 20: CD38 expression on the surface of stimulated classical and non-classical monocytes.
Male and female bone marrow-derived monocytes were stimulated for 24 h with LPS (positive control), mock control or 1000 EVs/cell of A1 or B2 EVs. Heat inactivation (h.i.) of EVs was performed at 95°C for 10 min as a separate control. After stimulation, cells were stained for flow cytometry. Expression of CD38 was examined on CD11b$^+$ cells with high Ly6C expression (Ly6C^{hi}, classical monocytes; A, B) or low Ly6C expression (Ly6C^{lo}, non-classical monocytes; C, D). Percent CD38 expression (A, C) and median fluorescence intensity (MFI; B, D) were examined. Depicted is median with range. Significances were calculated using Mann-Whitney U test.

3.3.5 The transcriptome of EV stimulated monocytes

For the determination of effects of EV stimulation on the transcriptome of male and female monocytes, bulk RNA-Seq was performed. RNA was isolated from A1 and B2 EV stimulated monocytes as well as LPS stimulated positive controls and mock controls and subjected to RNA integrity control with Agilent Bioanalyzer prior to sequencing (Figure 21 A). Only samples with high RNA integrity were sequenced. PCA of sequenced samples showed that LPS samples from both sexes clustered together with regard to PC 1, while all other EV stimulated samples and mock controls clustered together. Male and female samples differed from one another in PC 2 (Figure 21 B; n = 2). Between 45 and 83 genes were differentially expressed between A1 or B2 EV stimulated samples and corresponding mock controls (Figure 21 C).

When comparing A1 or B2 EV stimulated male or female monocytes with the corresponding mock controls, it was apparent that more genes were significantly (FDR $p < 0.05$) up- than down-regulated with a fold change ≥ |2| (Figure 22, Supplementary table 19 - Supplementary table 22). The top differentially expressed genes as determined by highest fold change between EV stimulated monocytes and their controls are shown in the heat map in Figure 21 D. The two female samples differed from each other in the expression level of most of the depicted genes, with one of the samples exhibiting lower expression levels and the other higher expression levels of the same gene (Figure 21 D). Overall, many of the genes were upregulated upon both A1 and B2 EV stimulation and in both male and female monocytes, such as *Tnf, Polo-like kinase 2 (Plk2)*, *Cxcl2, Ccl5, C-type lectin domain family 4 member E (Clec4e),* and *superoxide dismutase 2 (Sod2)* (Figure 21 D, Supplementary figure 7 - Supplementary figure 10, Supplementary table 19 - Supplementary table 22). *Aconitate decarboxylase 1* (*Acod1*) gene was the most significantly differentially expressed gene between EV stimulated monocytes and mock controls in all four pairwise comparisons (Figure 22, Supplementary table 19 - Supplementary table 22). Many of the upregulated genes are interferon-stimulated genes (ISGs), such as *2'-5' oligoadenylate synthetase-like 1* (*Oasl1), interferon induced protein with tetratricopeptide repeats 1 (Ifit1),* and *interferon activated gene 205 (Ifi205).*

When directly comparing A1 and B2 EV stimulated monocytes of the same sex to detect differences between the two subclones, close to no significant differences in gene expression could be detected. In female monocytes, only *glycoprotein nonmetastatic melanoma protein B* (*Gpnmb)* was significantly more highly expressed in B2 EV stimulated monocytes compared with A1 EV stimulated monocytes (fold change = 2.61) (Supplementary table 24). In males, only the predicted gene *Gm49388* was significantly more highly expressed in A1 EV stimulated monocytes compared with females (fold change = 6.12) (Supplementary table 23).

To determine cellular pathways and processes affected by EV stimulation, KEGG pathways analysis and GO term enrichment were performed for differentially expressed genes with shinyGO[177] and verified with g:profiler[216] as recommended by the developers (data not shown). KEGG pathways analysis of the upregulated genes in both A1 and B2 EV stimulated cells revealed that these genes are involved in several immunity related pathways such as NF-κB signaling, TNF signaling, NOD-like receptor signaling, IL-17 signaling, TLR signaling, and others (Figure 22). Affected pathways were similar in male and female monocytes. GO term enrichment analysis of genes upregulated upon EV stimulation in male and female monocytes revealed involvement of these genes in biological processes related to defense response, inflammatory response, response to other organism, cell motility, and other immune relevant biological processes (Supplementary figure 7 A - Supplementary figure 10 A). Molecular

function GO terms of the same genes were predominantly associated with cytokine activity (Supplementary figure 8 - Supplementary figure 10). Due to the low number of genes with decreased expression upon EV stimulation compared with mock controls, GO term enrichment and KEGG pathways analysis could not be performed for these genes in most comparisons. For genes downregulated upon B2 EV stimulation of female monocytes, associated biological process GO terms revealed functions in phagocytosis and T cell activation (Supplementary figure 10), the latter of which was also an enriched GO term for genes significantly downregulated in B2 EV stimulated male monocytes (Supplementary figure 8).

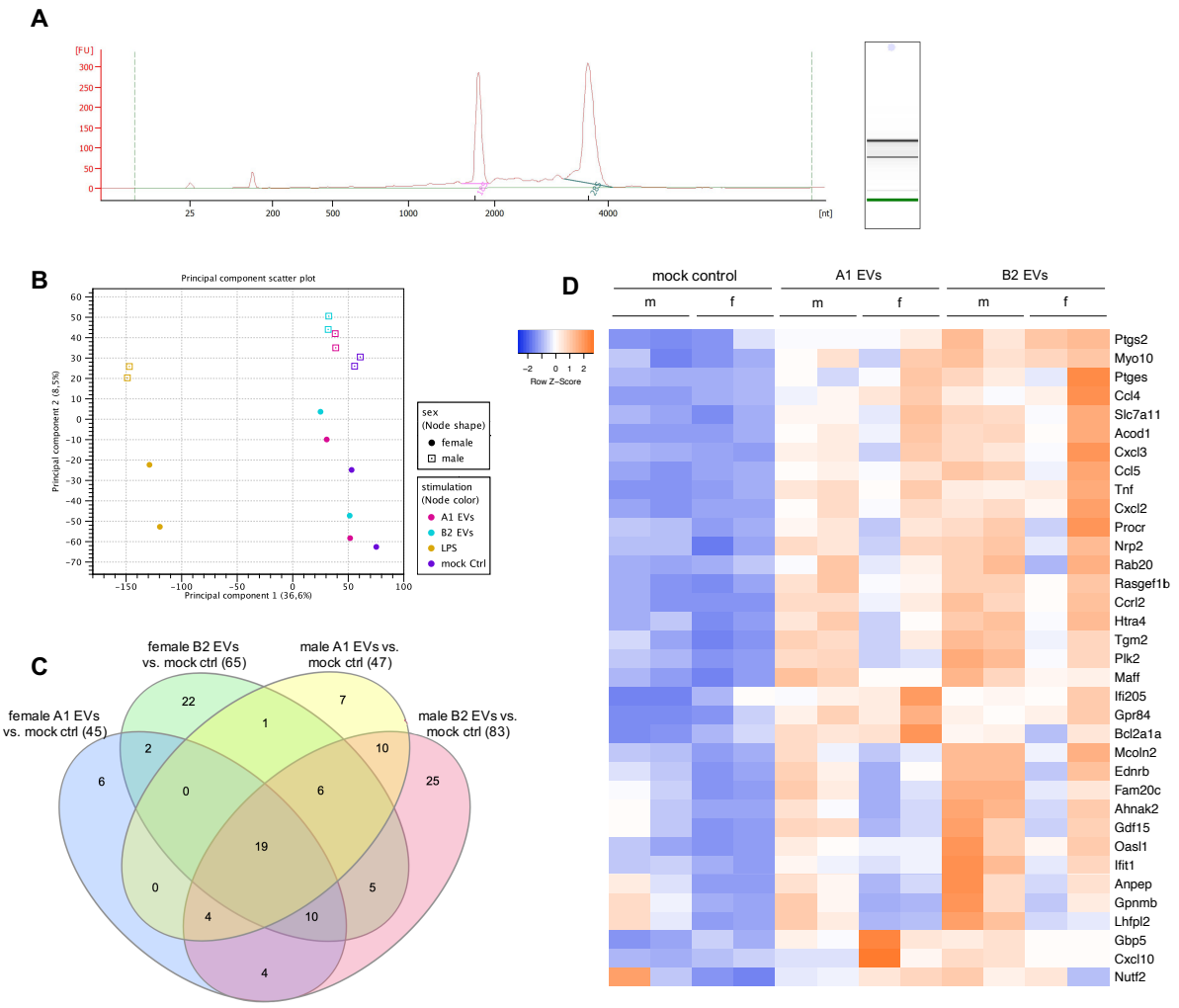

Figure 21: Transcriptome analysis of EV stimulated monocytes.
Male and female bone marrow-derived monocytes were stimulated for 8 h with LPS (positive control), mock control (ctrl) or 1000 EVs/cell of A1 or B2 EVs. After stimulation, cells were processed for RNA isolation and subsequent RNA sequencing via NGS. (A) Electropherogram (left) and gel image (right) of an RNA sample during integrity control with Agilent Bioanalyzer. Peak at 25 nt corresponds to the marker. RIN value is calculated based on 18S and 28S ribosomal RNA peaks. Shown is a representative sample with high RNA integrity. (B) PCA of sequenced monocytes according to biological sex (node shape) and stimulation condition (color). PCA was generated using CLC genomics. (n = 2) (C) Venn diagram depicting the number of significantly differentially regulated genes shared between or unique to four different pairwise comparisons (male / female A1 / B2 EVs versus corresponding mock control). Diagram was created with InteractiVenn[170]. (D) Heatmap depicting the z-score of the top differentially regulated genes between any of the EV stimulated conditions and the corresponding mock control. Shown are all genes significantly (FDR $p < 0.05$) regulated with a fold change ≥ |3| in at least one of the comparisons. RPKM normalized reads were used for mapping. Orange indicates high expression and blue indicates low expression of the gene. Heatmap created with Heatmapper[169].

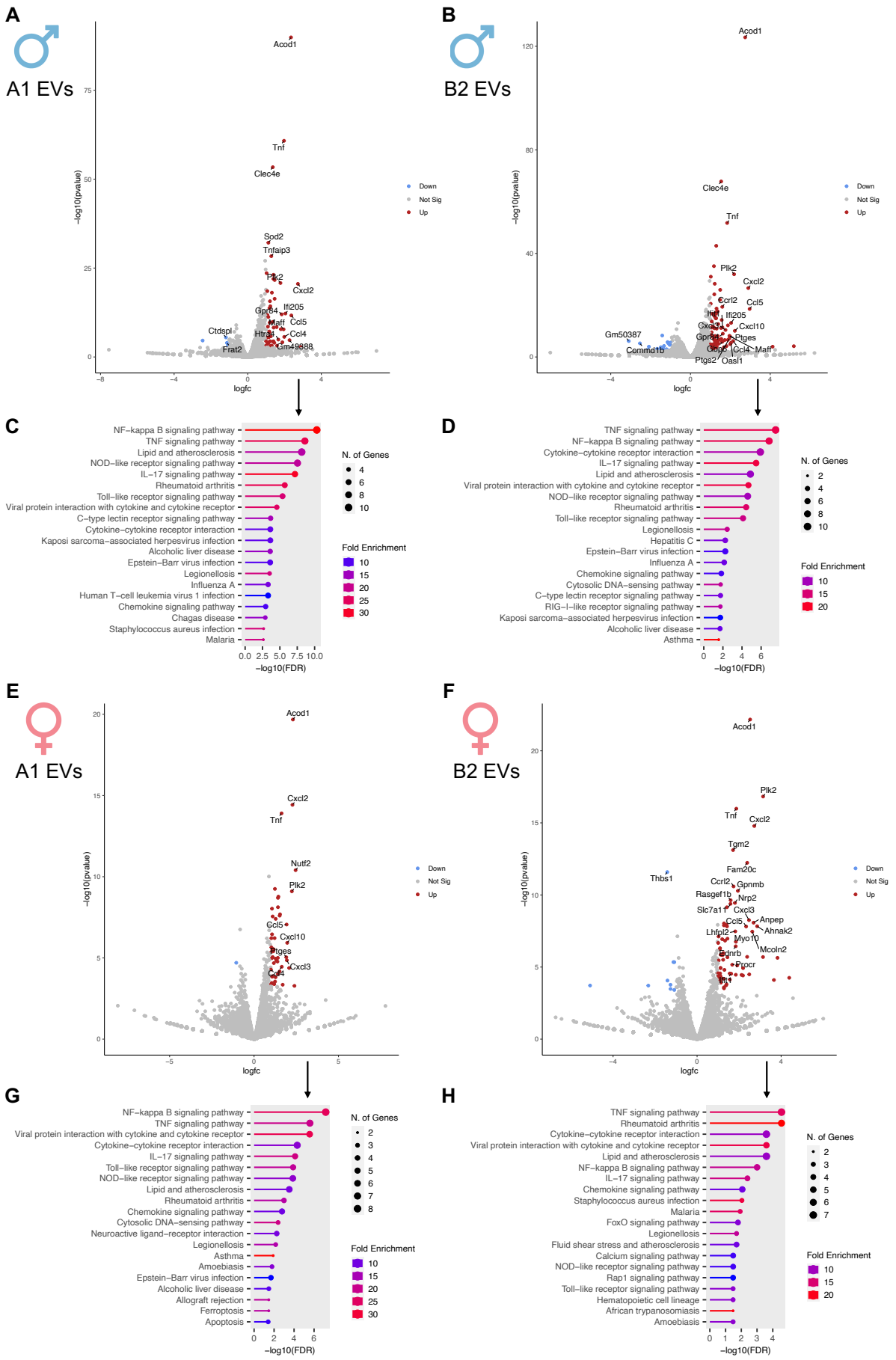

Figure 22: Analysis of differentially expressed genes between EV stimulated monocytes and mock controls.

(A, B, E, F) Volcano plots depicting relative gene expression between two sample sets according to statistical significance (-log10 of the FDR-adjusted *p* value) versus magnitude of change (logfc = log fold change). Depicted are male monocytes stimulated with A1 EVs versus mock control (A), B2 EVs versus mock control (B), as well as female monocytes stimulated with A1 EVs versus mock control (E) and B2 EVs versus mock control (F). Genes significantly regulated between the two conditions with a fold change ≥ |2| (logfc = 1) and FDR *p* value < 0.05 are colored in blue (downregulated in EV stimulated cells) or red (upregulated in EV stimulated cells). Genes not significantly regulated are colored in grey (not sig). Individual genes of interest are labeled. Volcano plots were created with Galaxy server[168]. (C, D, G, H) KEGG pathways analysis of genes significantly upregulated upon EV stimulation in male (C, D) and female (G, H) monocytes compared with mock controls. Shown are the top 20 pathways sorted by statistical significance (-log10(FDR)). KEGG pathways analysis was performed with shinyGO[177].

Differential expression analysis was furthermore performed between male and female samples of the same stimulation condition in order to determine sex differences in the response to A1 or B2 EVs. A total of 56 genes were detected to be significantly differentially regulated between the sexes upon EV stimulation that were not regulated between the sexes in mock controls (Figure 23 A, B). Out of these 56 genes, 28 were unique to A1 EV stimulated cells, 22 were unique to B2 EV stimulated cells and 6 were significantly differentially expressed in both. Genes that were only differentially expressed between the sexes upon A1 EV stimulation included *Cxcl10* and *Cd69*, which were both more highly expressed in female samples (Figure 23 B, F). Genes regulated only upon B2 EV stimulation included the ISGs *Ifit2, Ifit3,* and *Oasl2*, which were all more highly expressed in male samples than in females (Figure 23 B, G). GO term enrichment analysis showed that differentially expressed genes unique to EV stimulation were mainly immune-related genes involved in biological processes associated with immune response (Figure 23 C). Genes differentially expressed between the sexes also in mock controls included *Mpo, vascular cell adhesion molecule 1 (Vcam1), lipoma HMGIC fusion partner-like 2 protein* (*Lhfpl2), Gpnmb,* and *joining chain of multimeric IgA and IgM* (*Jchain)*, of which the first two were more highly expressed in females and the other three in males (Figure 23, Supplementary figure 11).

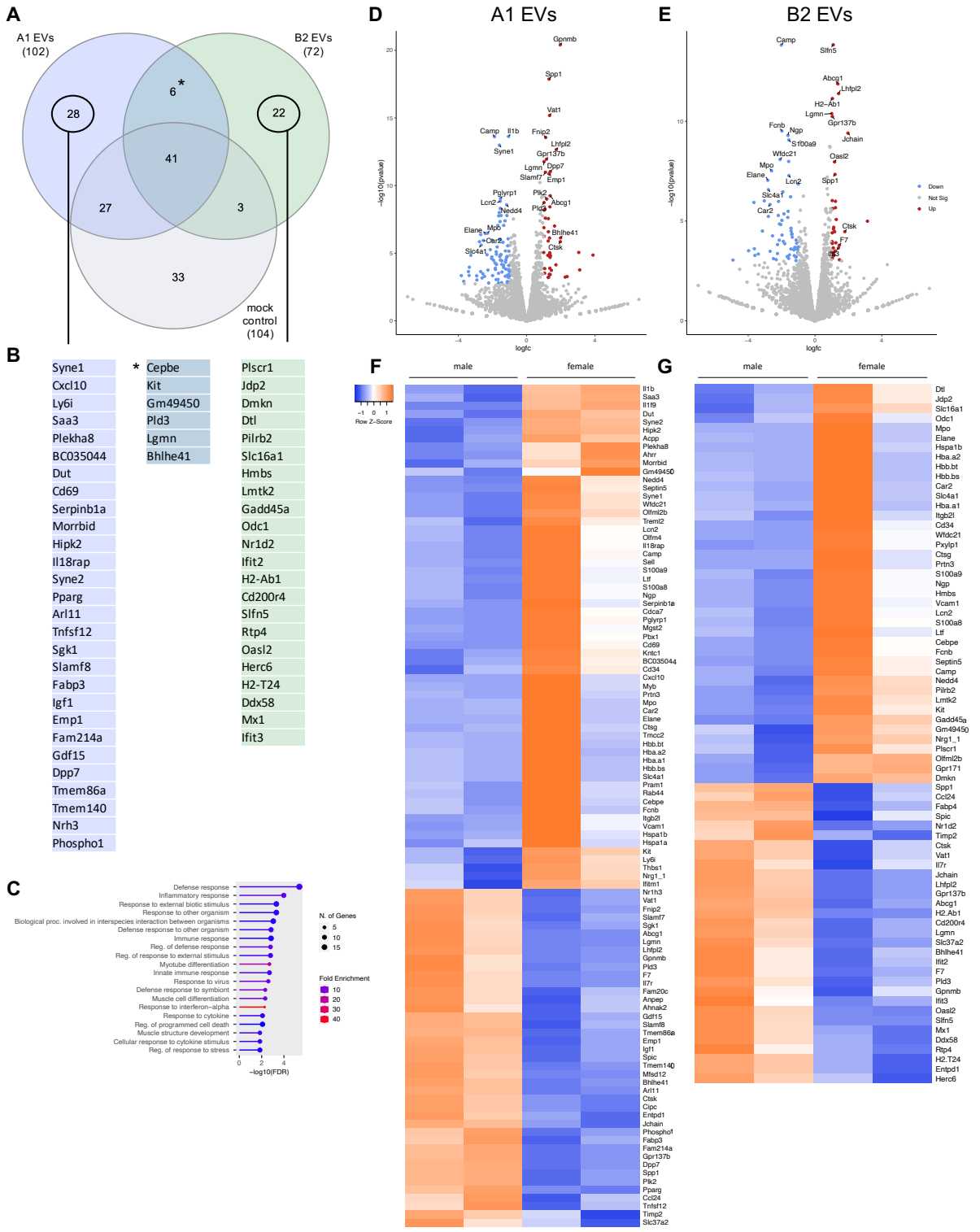

Figure 23: Analysis of differentially expressed genes between EV stimulated male and female monocytes.
(A) Venn diagram depicting the number of significantly differentially regulated genes between males and females shared between or unique to A1 EV stimulation, B2 EV stimulation and mock controls (fold change ≥ |2|, FDR $p < 0.05$). Venn diagram was created with InteractiVenn[170]. (B) List of genes regulated between the sexes only upon A1 EV stimulation (left), in both A1 and B2 EV stimulation (middle) and only upon B2 EV stimulation (right). (C) Biological process GO term enrichment of genes differentially regulated between the sexes only upon EV stimulation and not in mock controls as based on (B), sorted by statistical significance of enrichment (-log10(FDR)). Shown are the top 20 enriched GO terms. GO term enrichment was performed with shinyGO[177]. (D, E) Volcano plots depicting relative gene expression between two sample sets according to statistical significance (-log10 of the FDR-adjusted *p* value) versus magnitude of change (logfc = log fold change). Depicted are male versus female A1 EV stimulated monocytes (D) and B2 EV stimulated monocytes (E). Genes significantly regulated between the two conditions with a fold change ≥ |2| (logfc = 1) and FDR *p* value < 0.05 are colored in blue (downregulated in males/upregulated in females) or red (upregulated in males/downregulated in females). Genes not significantly regulated are colored in grey (not sig). Individual

genes of interest are labeled. Volcano plots were created with Galaxy server[168]. (F, G) Heatmaps depicting the z-score of all significantly differentially regulated genes between male and female A1 EV stimulated (F) and B2 EV stimulated (G) monocytes. RPKM normalized reads were used for mapping. Orange indicates high expression and blue indicates low expression of the gene. Heatmap created with Heatmapper[169].

Altogether, stimulation of both male and female monocytes with both A1 and B2 EVs led to the upregulation of immune relevant genes involved in key immunological pathways, such as NF-κB, TNF, and TLR signaling, with molecular functions predominantly related to cytokine signaling. Almost no significant differences could be detected between A1 and B2 EV stimulated cells of the same sex. A number of genes significantly differentially regulated between the sexes under the influence of *E. histolytica* EVs could be detected.

3.3.6 Comparison of the mRNA expression profile of genes of interest in EV stimulated monocytes by RT-qPCR and RNA-Seq

Since only two biological samples per stimulation condition were subjected to RNA-Seq and the two female samples differed from each other in the expression of many genes of interest as shown in 3.3.5, RT-qPCR was performed on 2-3 samples per condition to verify the previous findings. For this, six genes of interest were chosen based on the top differentially expressed genes as shown in Figure 21 D. The cytokine-encoding genes *Ccl5, Cxcl2,* and *Tnf* were chosen because they were among the most highly upregulated genes in both male and female A1 and B2 EV stimulated cells compared with controls (Figure 22, Supplementary table 19 - Supplementary table 22). In addition, *Oasl1* and *Ifit1* were chosen as ISGs upregulated upon EV stimulation (Supplementary table 19 - Supplementary table 22). Lastly, *Lhfpl2* was chosen for further investigation due to its significant upregulation upon B2 EV stimulation in females and differential expression between male and female samples (Figure 23, Supplementary figure 10, Supplementary table 19 - Supplementary table 21).

Primers for the chosen genes of interest were designed and tested for specificity and optimal annealing temperature via gradient RT-qPCR. Primer efficiency was determined by RT-qPCR on serial cDNA dilutions and was between 1.9975 and 2.1017 for all six primer pairs (data not shown). Values close to 2 (duplication of the template in every cycle) indicate efficient primers, which were achieved here. To assess the effect of 8 h incubation *in vitro* on gene expression, monocytes were isolated out of murine bone marrow and directly processed for RT-qPCR without stimulation (termed ‘0 h’ samples here). Genes of interest were then amplified by RT-qPCR on the samples, and fold changes between stimulated samples and 0 h controls were calculated according to Pfaffl[196] (2.2.10.4.5).

Furthermore, additional samples were subjected to RNA-Seq to investigate whether the previously observed effects on mRNA level were reproducible. To this end, two biological replicates for each of the four stimulation conditions were combined into one sample and sequenced at around 20 million reads per sample. The newly sequenced samples together with the samples from the first run (3.3.5) were used to control for gene expression of the genes of interest also investigated via RT-qPCR. RPKM normalized reads of these six genes in all sequenced samples were normalized to reads of *Rps9*, which was used as housekeeping gene in RT-qPCR.

For *Tnf, Oasl1, Ifit1, Ccl5,* and *Cxcl2*, RT-qPCR confirmed the previous finding from RNA-Seq that these genes were upregulated in both A1 and B2 EV stimulated male and female monocytes compared with mock controls, although the effect was not statistically significant (Figure 24 A, C, E, G, I). For *Tnf, Oasl1, Ifit1,* and *Ccl5*, the expression levels in 8 h mock control stimulated monocytes were comparable to naïve 0 h monocytes. Also, expression levels of genes of interest were comparable between male and female samples of the same stimulation condition (Figure 24 A, C, E, G). Interestingly, *Cxcl2* was expressed only at very low levels in 0 h controls (Cq values around 35; data not shown), and its expression was induced by 8 h *in vitro* culture in all stimulation conditions (Figure 24 I).

Normalized RPKM values for *Tnf* of the three sequenced samples showed a similar result as the RT-qPCR (Figure 24 B). It was apparent that expression levels of this gene were higher in EV stimulated male and female monocytes compared with mock controls of the same sequencing batch (as shown by the different shapes of the datapoints), but expression level ranges overlapped between the different batches. The same could be observed for normalized RPKM values of *Cxcl2* (Figure 24 J). For *Oasl1, Ifit1,* and *Ccl5*, stimulated male monocytes exhibited a similar pattern, but in female monocytes, gene expression was only visibly induced by EV stimulation in the two originally sequenced samples and not in the other (Figure 24 D, F, H).

Lhfpl2 was upregulated in male monocytes upon A1 and B2 EV stimulation compared with mock controls and, strikingly, more highly regulated by B2 EVs compared with the LPS positive control, as shown by RT-qPCR (Figure 24 K). In female monocytes, an upregulation of *Lhfpl2* upon EV stimulation compared with mock controls could not be detected. Here, gene expression was higher in 1 out of 3 mock control samples compared with the other 2. In comparison, normalized RPKM values of sequenced male samples exhibited the same pattern as observed for the other genes of interest, meaning an upregulation of gene expression in EV stimulated cells compared with the corresponding mock control according to sequencing batch (Figure 24 L). Meanwhile, *Lhfpl2* was upregulated upon EV stimulation in female monocytes only in the 2 originally sequenced samples and not in the third sample of each condition, as also seen for *Oasl1, Ifit1,* and *Ccl5* (Figure 24 L), thus mirroring the pattern observed in RT-qPCR (Figure 24 K). In addition, expression of *Lhfpl2* as detected by RNA-Seq was higher upon LPS stimulation in comparison with mock controls than upon EV stimulation (Figure 24 K), which did not correspond to the findings obtained via RT-qPCR (Figure 24 L).

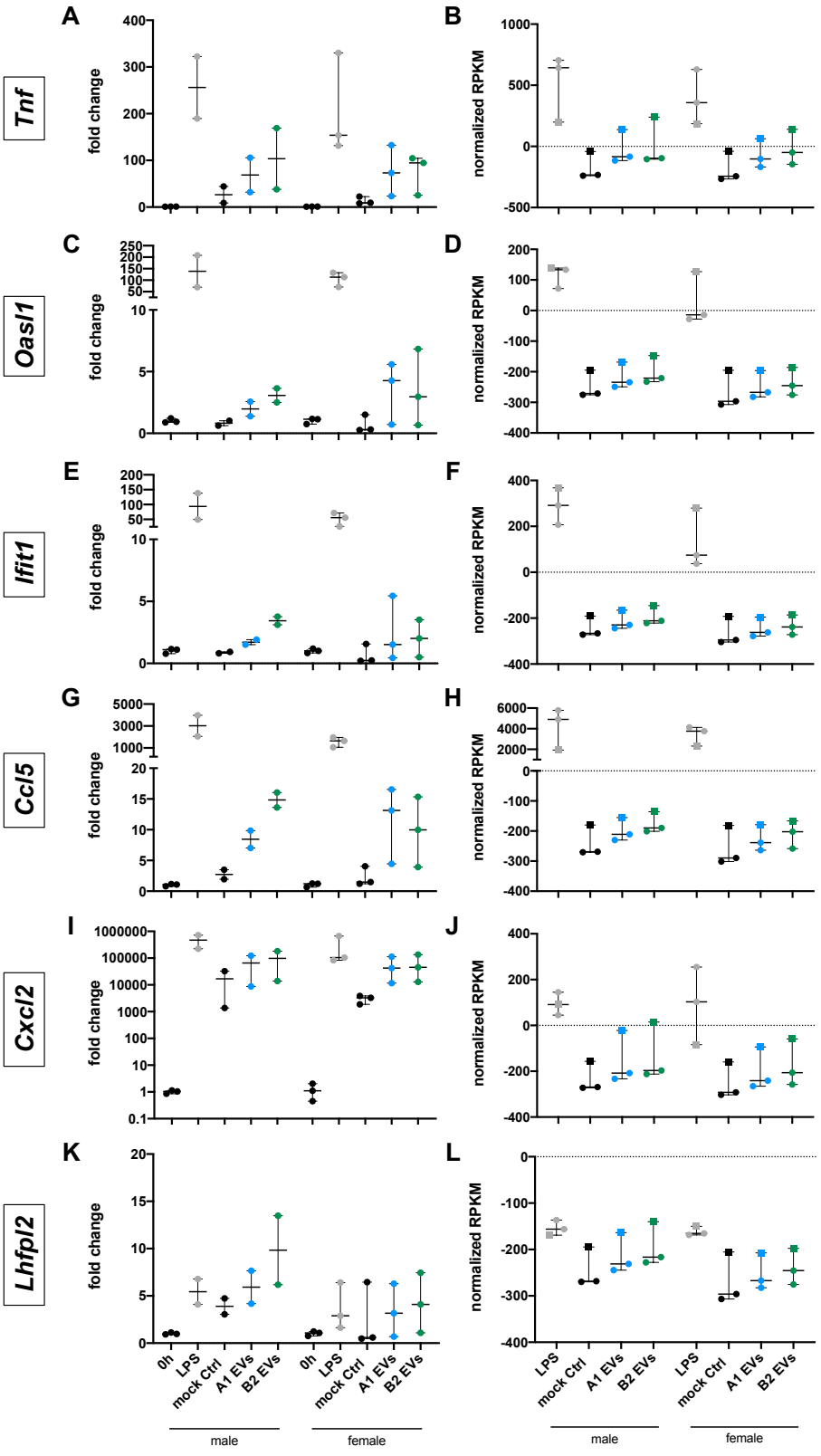

Figure 24: Investigation of the expression profile of genes of interest after EV stimulation in monocytes by RT-qPCR compared with RNA-Seq.

Male and female monocytes were isolated from bone marrow and processed directly for RNA isolation ('0 h' controls) or stimulated in *vitro* for 8 h with either LPS (positive control), mock control or 1000 EVs/cell of A1 or B2 EVs. *Tnf* (A), *Oasl1* (C), *Ifit1* (E), *Ccl5* (G), *Cxcl2* (I), and *Lhfpl2* (K) were detected via RT-qPCR. Fold changes were calculated with the mean of 0 h samples as calibrator. Depicted is the median with range (n = 2-3). For each gene of interest, RPKM normalized reads of three independent samples sequenced in two separate NGS runs were normalized to RPKM reads of *Rps9* housekeeping gene (dotted line in the graphs) (B, D, F, H, J, L). Round datapoints correspond to the first sequencing run, while squares correspond to the second sequencing run. Testing for significance was performed using Mann-Whitney U test.

Taken together, RT-qPCR could largely verify the findings previously obtained through sequencing of EV stimulated male and female monocytes. A sex difference in gene expression was observed only for *Lhfpl2*. Combined normalized RPKM values of the two NGS runs showed that relative gene expression was similar between the two runs for male samples, thus verifying the previous findings even further. However, for female samples, only some of the genes of interest previously determined also exhibited increased expression in the later sequenced sample compared to the corresponding mock control, underlining the limitations of the initial sequencing data and their validity.

4 Discussion

Parasite-derived EVs have been demonstrated to modulate host immune responses during infection, driving disease outbreak in some cases, while promoting parasite clearance in others. Invasive amebiasis, caused by infection with the protozoan parasite *E. histolytica*, is a disease with an underlying immunopathology and a bias towards the male sex. This sex dimorphism is particularly pronounced in the onset of ALA, and monocytes play a key role in this context. Most infections with this parasite remain asymptomatic, and it becomes invasive only in a minority of cases. The reasons for this are still not understood. The use of parasite clones with differing pathogenicity allows the further elucidation of underlying mechanisms. To this end, *E. histolytica* clones A1 (low pathogenicity in an ALA rodent model) and B2 (high pathogenicity) were previously generated from the human *E. histolytica* isolate HM-1:IMSS in our group[165]. In order to better understand the interaction of parasite and host immune system in the context of *E. histolytica* infection, parasite-derived EVs and their effect on monocytes as well as neutrophils were studied in this project. EVs from A1 and B2 clones were characterized with regard to their miRNA and protein content to elucidate putative parasitic pathogenicity factors. Isolated *E. histolytica* EVs were heterogeneous in size as determined by both NTA and TEM (Figure 6, Figure 7, Figure 8). The size distribution of *E. histolytica* EVs as determined by NTA was comparable to previous studies[144,145]. Immune cell stimulations were performed with EVs from both clones and with cells from male and female mice to investigate the immune response to A1 EVs compared with B2 EVs as well as putative sex differences. Monocytes were studied due to their pivotal role in disease manifestation. Additionally, experiments were carried out with neutrophils since they are also important in the host immune response against *E. histolytica.*

4.1 Isolation and handling of *E. histolytica* EVs

A differential ultracentrifugation-based protocol was established to isolate EVs from conditioned medium. Although a large variety of methods exist that allow for the enrichment of specific EV populations based on their size or density[217–219] including sucrose gradients following ultracentrifugation or size exclusion chromatography, a protocol yielding crude EV samples was used here in order to investigate all particles released by the amebae rather than just a specific subset. Moreover, it is unclear whether distinct subsets of *E. histolytica* EVs even exist because they have not been extensively studied yet. Since it was not practical to perform EV stimulation experiments with freshly isolated EVs, mostly due to the length of both EV and immune cell isolation protocols, EVs had to be stored after isolation. It is known that storage conditions such as temperature, duration and freeze-thaw cycles impact the integrity and functionality of EVs[182,220]. Since EV concentration is known to strongly decrease after the first freeze-thaw cycle[182], isolated EVs were aliquoted before storage to avoid multiple freeze-thaw cycles and each aliquot was only used once for stimulation or other experiments and not re-frozen. EVs are best stored over longer periods of time at – 80°C, but even at these low temperatures, particle size and concentration are significantly altered after 6 months of storage[220]. Consequently, EV aliquots used for immune cell stimulations in this project were not stored for more than 6 months. To minimize batch effects between different isolations, EVs were pooled prior to use in stimulation experiments (2.2.2.3). Nevertheless, it was evident that EV pools differed in their stimulatory capacity, as seen for example in the variance in cytokine concentrations after EV

stimulation (3.3.2). Although variance in the cytokine assays shown here may in part also be explained by the impact of freezing and thawing of samples between assays on cytokine stability, variance in IL-6 concentrations in supernatants of BM cells stimulated with fresh EV pools as quality control (data not shown) can not be explained by this. Since EV cargo depends on the state of the cell and *E. histolytica* growth *in vitro* is not always consistent even if culture conditions are kept the same, it is logical that EV composition differs between isolations and with it the stimulatory capacity. This constitutes a limitation to the reproducibility of EVs that needs to be considered especially in the context of putative therapeutic applications (refer also to 5).

4.2 The *E. histolytica* EV proteomes

Analysis of the protein content of EVs via mass spectrometry and comparison to whole cell proteomes revealed that EV proteomes were enriched in transmembrane proteins with signaling activity and depleted in proteins involved in nuclear processes (3.2.3), which is consistent with findings for other EV proteomes[198,221]. Many of the typical EV markers were found in both A1 and B2 EV proteomes, and the overall proteomes were similar to those of other organisms (3.2.3.1).

While Díaz-Godínez *et al.*[145] detected 597 proteins in their *E. histolytica* EVs and Sharma *et al.*[144] reported an EV proteome consisting of 359 proteins, a total of 900 proteins were detected between A1 and B2 EV proteomes in this study (Figure 9). Díaz-Godínez *et al.* reported the top 10 most abundant proteins found in their EV proteome[145]. Comparison of these with the EV proteomes presented here revealed that most of them were not even in the top 50 most abundant proteins in this study (data not shown). Differences in EV proteome constitution between the studies may be explained by different experimental setups. While EVs were precipitated chemically from cell culture media in the other two studies, a method that is associated with high co-precipitation of non-EV proteins[218], EVs characterized here were pelleted by ultracentrifugation. Furthermore, Sharma *et al.* cultured trophozoites for 16 h in serum-free TY-I-S-33 prior to EV isolation and Díaz-Godínez *et al.* cultured theirs in serum-free RPMI-1640 for only 1 h[144,145]. In contrast, in this study, amebae were cultured in EV-depleted TY-I-S-33 medium containing serum for 46 h, and, notably, were also stimulated with collagen during this time. It is well known that packaging of cargo into EVs depends on a multitude of factors, including stimuli and physiological state of the cell of origin. Hence, all the mentioned factors likely explain differences in EV proteomes found between the three studies. It should also be noted that EVs were isolated from the HM1:IMSS cell line in the other two studies, whereas here, clones previously established at BNITM[165] (also originating from HM1:IMSS) were used.

Nevertheless, there were also some key findings that were consistent among all three studies. Aldehyde-alcohol dehydrogenase 2 (EHI_150490), which was the most abundant protein in the Sharma *et al.* EV proteome[144], was also the most abundant in the A1 EV proteome in this study and the third most abundant in the B2 EV proteome (data not shown; Supplementary table 3). In the Díaz-Godínez *et al.* proteome[145], an aldehyde-alcohol dehydrogenase (EHI_160490) was also the second most abundant protein in amebic EVs. Another study previously characterized the excretory-secretory proteome of *E. histolytica* and also reported aldehyde-alcohol dehydrogenases as the most abundantly secreted proteins[222]. These dehydrogenases are essential for *E. histolytica* metabolism and catalyze the formation of acetate and ethanol[223,224].

Díaz-Godínez and colleagues furthermore characterized the proteome of amebic EVs after co-culture with human neutrophils and found increased amounts of pathogenicity factors, including CPs, Gal/GalNac lectin, and amebapore, compared to EVs from amebae culture alone[145]. This finding shows that the protein cargo of EVs is actively involved in and modulated during intercellular communication.

Interestingly, Sharma *et al.*[144] reported absence of tetraspanins from their EV proteome, a finding corroborated by Díaz-Godínez *et al.*[145], and suggested that EV biogenesis in *E. histolytica* might occur tetraspanin-independently. This study detected multiple tetraspanins in the A1 and B2 EV proteomes (Supplementary table 4) and therefore contradicts this theory. Components of the ESCRT machinery are known to be present in *E. histolytica*[200] and Galindo *et al.* described the secretion of the ESCRT-I component EhVPS23 (EHI_135460) in EVs[137,146,225]. EhVPS23 could also be detected in the proteome of this study alongside other proposed ESCRT proteins[200] (Supplementary table 5), as well as in the EV proteome of Sharma *et al.*[144]. The simultaneous presence of tetraspanins and ESCRT components in EVs indicates that EV biogenesis in *Entamoeba* involves both, similar to what is known from mammals (refer also to 1.3.1).

86 proteins were differentially expressed between A1 and B2 EV proteomes, out of which one was present in both and significantly regulated, and 85 were unique to one of the two proteomes (Figure 9, Supplementary table 1). Interestingly, out of these 86, only 15 were also differentially expressed between A1 and B2 whole amebae (Figure 11, Supplementary table 1). Analysis of these proteins is limited by the fact that many *E. histolytica* proteins are still uncharacterized. Nevertheless, this proteomic study reveals numerous proteins that may be interesting in the context of pathogenicity and worth further investigation. Especially the proteins that are differentially expressed between A1 and B2 EVs but not between corresponding whole cell proteomes hint at mechanisms of selective packaging into EVs that differ between A1 and B2 amebae. Interestingly, a CP (EHI_062480; EhCP-A10) was present uniquely in A1 EVs and not B2 EVs (Supplementary table 1). The same CP is also present in non-pathogenic *E. dispar*[226]. A previous study in our group showed that EhCP-A10 was upregulated in B2 trophozoites co-incubated with human intestinal organoids but not in A1 trophozoites (doctoral thesis Constantin König)[227]. Considering the fact that it is still unclear whether EVs originating from MVBs are secreted by cells actively or just accidentally escape lysosomal degradation, this finding could indicate that A1 amebae 'discard' this CP in EVs, while B2 amebae use it for intestinal invasion. Differentially expressed proteins also included Rab GTPases, a sphingomyelinase-like protein (EHI_100080), and a SNARE protein (EHI_181290)[228] (Supplementary table 1), which are protein classes associated with vesicle trafficking and EV biogenesis[229]. Rab GTPases were present at higher levels in A1 EVs than in B2 EVs, a finding that is consistent with previous transcriptome data of whole amebae[165]. Furthermore, 71 proteins were only detected in EVs and not whole amebae proteomes, most of which were hypothetical proteins (Figure 11 B, Supplementary table 12). In whole cell proteomes, these proteins were likely below the detection limit of the mass spectrometer due to low abundance. Consequently, they must be highly enriched in EVs, indicating importance of these proteins in intercellular communication.

In summary, the *E. histolytica* A1 and B2 EV proteomes contained typical EV markers, proteins likely involved in EV biogenesis and known pathogenicity factors of the parasite. Contrary to findings by other researchers, presence of tetraspanins was detected, which indicates a putative role of this protein class in the biogenesis of EVs in this parasite. Selective enrichment of proteins in EVs differing between A1 and B2 amebae was detected, and could be involved in parasite pathogenicity as the result of different EV-mediated communication with the host immune system.

4.3 The *E. histolytica* trophozoite proteomes

Mass spectrometry on whole trophozoites was performed primarily for the purpose of analyzing enrichment or depletion of certain protein groups in EVs compared with the whole cell (refer also to chapter 4.2). For the first time, whole cell proteomes were generated for *E. histolytica* A1 and B2 clones that differ in their pathogenicity. Moreover, to my knowledge, these proteomes are larger and more comprehensive than any other *E. histolytica* proteomes published to date[230,231]. Proteins differentially expressed between A1 and B2 trophozoite proteomes were compared to a transcriptome study[165] and proteome analysis of the A and B cell lines[232] previously performed in our group. Observations on differences in mRNA expression between the two clones correlated with differences on the protein level in this study. Furthermore, Biller *et al.*[232] reported higher amounts of the stress response proteins peroxiredoxin, Fe-hydrogenase, and SOD in cell line B in their study, a finding that could generally be reproduced here (Supplementary table 7 for Fe-hydrogenase EHI_005060 + data not shown). In addition, they reported higher expression of two signal transducing C2 domain containing proteins in cell line A (EHI_069320 and EHI_015290), which were both uniquely detected in A1 amebae proteomes and not in B2 amebae proteomes here (Supplementary table 8). There were, however, also some differences between the two proteome studies. For example, the previously reported hypothetical protein XP_651863 (EHI_011270) that was more abundant in cell line B was not differentially expressed between the two clones in this study (data not shown). Within the framework of the study that led to the cloning of A1 and B2, it was demonstrated that HM1:IMSS cell line B was very heterogeneous and contained amebae with varying degrees of pathogenicity[165]. The heterogeneity of the cell line in contrast with the clonality of B2 may explain the discrepancy in expression of EHI_011270. In-depth analysis of the two trophozoite proteomes will certainly reveal further interesting insight into mechanisms of *E. histolytica* pathogenicity.

4.4 The miRNA cargo of *E. histolytica* EVs

miRNA packaged into parasitic EVs can modulate the gene response of host target cells as shown for the nematode *Heligmosomoides polygyrus*, whose EVs repressed T helper 2 immune responses upon injection into mice[233]. A1 and B2 *E. histolytica* EVs in this study were shown to contain small RNAs (Figure 12 A). Similarly, Sharma *et al.* reported a small RNA population together with components of RISC in their study[144], indicating the capacity of *E. histolytica* EVs to modulate gene expression in target cells. Although none of the three *E. histolytica* argonaute proteins[234] could be detected in EVs by mass spectrometry here (data not shown), similar to findings by Sharma *et al.*[144], other members of the amebic RISC complex were detected, including elongation factors and heat shock protein 70 (Supplementary table 3 + data not shown). We were not able to detect any of the previously described mature *E. histolytica* miRNAs[192] in the dataset described here except for Ehi-miR-4. However, we detected 3' isomiRs of these miRNAs, two of which were significantly differentially expressed between A1 and B2 EVs (Figure 12 C, Supplementary table 17). Furthermore, *de novo* miRNA prediction using BrumiR algorithm[193] based on our sequencing data predicted new mature *E. histolytica* miRNAs (Supplementary table 18). Of these, one miRNA was significantly more highly expressed in A1 EVs than B2 EVs (Figure 12 D, Supplementary table 18). BLAST analysis using the seed sequence of the differentially expressed 3' isomiRs did not reveal target genes in either the *E. histolytica* or human genome, but possible targets for the differentially expressed mature miRNA could be detected. While

hits in the *E. histolytica* genome were predominantly hypothetical proteins, alignment to genes involved in GTPase activity or immune regulation was detected in the human genome (3.2.4). These results suggest that miRNA packaged into *E. histolytica* EVs can modulate cellular responses in human host target cells. Since *E. histolytica* miRNAs are not annotated in any database and, therefore, prediction of target genes for these miRNAs can not be carried out with any currently available tools, bioinformatics approaches to comprehensive target gene prediction should be performed in the future. They will provide valuable insight into EV-mediated gene regulation among parasites as well as between parasite and host.

4.5 *E. histolytica* EVs contain immunogenic molecules and induce pro-inflammatory responses in murine monocytes

A1 and B2 EV stimulation of male and female monocytes led to increases in the release of multiple cytokines as well as elevated expression of cytokine-encoding genes (chapters 3.3.2, 3.3.5). Although EVs are complex particles and the association of one molecule present in EVs with a specific observed host response is practically impossible, analysis of the EV cargo in the context of previously described immune responses to *E. histolytica* components can explain the monocyte reaction at least to some extent. First, immunogold labeling detected the PAMPs Gal/GalNac lectin (Figure 7; verified by proteomics, Supplementary table 3) and LPPG on *E. histolytica* EVs (Figure 8). LPPG is a highly immunogenic glycan that is recognized by monocytes and macrophages through TLR2 and TLR4 and induces the release of IL-6, IL-8, IL-10, IL-12p40, and TNFα via NF-κB signaling[208,235]. Murine macrophages exposed to Gal/GalNac lectin upregulate TLR2 expression via NF-κB and mitogen-activated protein kinase (MAPK) signaling and secrete elevated levels of TNFα[236,237]. Furthermore, binding of this lectin to macrophages results in the EhCP-A5-dependent activation of caspase-1 and the NLRP3 inflammasome, leading to secretion of IL-1β and CXCL10, among other cytokines[209,210,238]. Since elevated levels of IL-6, IL-1β, IL-12p40, CXCL10, and TNFα as well as the IL-8 homolog CXCL1[239] upon EV stimulation were detected in monocyte supernatants (Figure 15, Figure 16, Figure 17), RNA-Seq revealed activation of NF-κB signaling and NOD-like receptor signaling (Figure 22), and Gal/GalNAc lectin and LPPG were both detected on EVs, a link between their presence and the observed effect is likely. Interestingly, IL-10 release was not induced (Figure 15 B) despite the presence of LPPG. Furthermore, EhCP-A5 (EHI_168240) was detected in the proteomes of both A1 and B2 EVs (Supplementary table 3) and the simultaneous presence of Gal/GalNAc lectin and EhCP-A5 is probably a trigger for the release of IL-1β from monocytes as previously demonstrated for macrophages[210]. Peroxiredoxin, employed by the parasite to combat ROS released by the host, has also been shown to activate the NLRP3 inflammasome of macrophages in a TLR4-dependent manner[240] and was present in both A1 and B2 EV proteomes (EHI_001420; Supplementary table 3). Analysis of the transcriptome of EV stimulated monocytes furthermore revealed activation of IL-17 signaling (Figure 22). The IL-23/ IL-17 signaling pathway is a key immune axis involved in onset of invasive amebiasis and is known to induce CXCL1 and CCL3 secretion[90], both of which were present in elevated amounts in supernatants of EV stimulated monocytes (Figure 16 A, Figure 17 E).

Another highly immunogenic *E. histolytica* protein is a homolog for the cytokine macrophage migration inhibitory factor (MIF) (EHI_092370), a virulence factor involved in the induction of pro-inflammatory responses by host cells and tissue destruction during intestinal invasion[241]. It is known to induce IL-8

secretion by epithelial cells and thus contribute to neutrophil recruitment, resulting in increased MPO levels and increased inflammation[239]. *E. histolytica* MIF has been shown to trigger IL-6 and TNFα release by a murine macrophage cell line[242]. EV stimulation led to increases in the release of IL-6, TNFα, and the murine IL-8 homolog CXCL1[239] (Figure 15, Figure 16, Figure 17), and A1 EV stimulation led to increases in the release of MPO (Figure 18), but EHI_092370 was not detected in EV proteomes although it was present in whole cell proteomes (data not shown). Hence, a contribution of EhMIF to the observed effect can be excluded.

Overall, the pro-inflammatory profile of monocytes elicited by EV stimulation, particularly the elevated TNFα release by monocytes, suggests that *E. histolytica* EVs could trigger ALA immunopathology in a manner similar to live amebae. To test this, liver injection of EVs in mice analogous to the established injection of amebic trophozoites in the ALA model could be performed.

4.6 *E. histolytica* A1 EVs cause release of MPO by monocytes and peripheral neutrophils

Analysis of MPO concentrations in supernatants of stimulated monocytes and neutrophils was performed to investigate effects of EV stimulation on degranulation. Curiously, MPO release by monocytes and peripheral neutrophils was higher upon stimulation with EVs of the less pathogenic A1 clone compared with the pathogenic B2 clone, while no effect was observed on BM-derived neutrophils (Figure 18). Increased MPO levels are a hallmark of amebic colitis and associated with tissue damage[239]. Host MPO can kill amebic trophozoites by binding to them and using the hydrogen peroxide released by the parasite itself for the formation of cytotoxic HOCl[243]. MPO can also contribute to pathogen killing indirectly by activating macrophages and inducing increased TNFα release[244]. However, TNFα concentration in monocyte supernatants was not higher upon A1 EV stimulation compared with B2 EV stimulation (Figure 15, Figure 17). It seems counterintuitive that MPO levels are higher upon stimulation with EVs from the amebic clone that elicits smaller ALAs in a rodent model compared to the more destructive clone[74,165], as MPO concentrations are typically positively correlated with tissue damage and disease severity[211,239]. However, one study has proposed a putatively protective role of neutrophil-derived MPO in an ALA resistant mouse model compared to a susceptible hamster model[245]. The role of MPO in the onset of invasive amebiasis is clearly complex and warrants further investigation.

MPO is released by monocytes and neutrophils not just during degranulation, but also in the process of extracellular trap formation[32]. In order to refine the findings on MPO release upon EV stimulation, further experiments for the assessment of MET or NET formation by monocytes or neutrophils, respectively, in response to A1 and B2 EVs are needed. Previous studies have shown that human neutrophils release NETs *in vitro* upon contact with viable trophozoites and that purified LPPG triggers the same[79,246]. NETosis is triggered only by pathogenic *E. histolytica* and not by non-pathogenic *E. dispar*[247]. Díaz-Godínez *et al.* showed that *E. histolytica* EVs inhibited NET formation by human neutrophils upon stimulation with phorbol 12-myristate 13-acetate (PMA), A23187 ionophore or whole amebae *in vitro*[145]. Notably, EVs isolated from the human neutrophils themselves or from co-culture of neutrophils with amebae had the same effect and EVs from co-culture were the strongest inhibitors. To assess whether EVs isolated from A1 and B2 clones exert a similar effect and whether there are differences between the two clones, NETosis assays should be performed with them in the

future. METosis has not been investigated in the context of *E. histolytica* infection yet and would thus be interesting to study under the influence of EV stimulation.

4.7 Surface marker expression on Ly6C^{hi} and Ly6C^{lo} monocytes after EV stimulation

The expression of several markers on classical Ly6C^{hi} and non-classical Ly6C^{lo} monocytes upon EV stimulation was investigated to assess the cells' activation state. An increase in the expression of CD38 mainly on Ly6C^{hi} monocytes, but to a lesser extent also on Ly6C^{lo} monocytes, was detected by flow cytometry upon A1 and B2 EV stimulation of male and female monocytes (Figure 20). CD38 is an enzyme with cyclase and hydrolase functions that also serves as a receptor for CD31 and mediates the release of pro-inflammatory cytokines like IL-1β, IL-6, and IL-12p40 by monocytes and macrophages[212,248]. Its upregulation is a marker of monocyte activation, as seen in Ly6C^{hi} monocytes during ALA[214]. CD86 is a co-stimulatory molecule involved in T cell activation, thus bridging innate and adaptive immunity[249]. In ALA mice, Ly6C^{hi} monocytes express elevated levels of CD86, and this effect is stronger in male compared with female mice[105,214]. Here, a slight increase in the expression of CD86 on female Ly6C^{lo} monocytes could be observed upon EV stimulation, but not on males or on Ly6C^{hi} monocytes as might be expected (Supplementary figure 5 E, F). However, this effect was very marginal and repetitions would be needed in order to verify this. The expression of CD69 was not affected by EV stimulation (Supplementary figure 5 C, D). CD69 is a transmembrane lectin that is rapidly induced on leukocytes upon activation[213,250]. Since it is an early activation antigen, the time period of 24 h EV stimulation analyzed by flow cytometry herein may have been too long to capture putatvive changes in CD69 expression. No effect of EV stimulation on CD62L, a marker for monocyte adherence, or MHCII, which is involved in antigen presentation, could be detected. For both markers, a higher inter-experimental variance in the expression levels was observed, hindering the detection of putative stimulation effects.

Although non-classical Ly6C^{lo} monocytes are typically associated with high expression of CX_3CR1 and classical Ly6C^{hi} monocytes are described to have low CX_3CR1 levels, expression of this chemokine receptor was similar on both monocyte subsets in this study (Supplementary figure 5 I, J). In fact, the previously accepted description of CX_3CR1 expression pattern has been recently challenged by a single cell transcriptome study of classical, intermediate and non-classical human monocytes showing highest expression of CX_3CR1 in the classical monocyte subset[251]. Furthermore, a study on murine monocytes obtained similar results and the authors suggested not to use this marker for the discrimination of classical and non-classical monocytes subsets[252]. EV stimulation of male monocytes led to a decrease in CX_3CR1 expression on Ly6C^{hi} monocytes compared with mock controls, which was not observed on females (Supplementary figure 5 I). A decrease in the expression of CX_3CR1 was previously reported on male and female murine blood and hepatic Ly6C^{hi} monocytes at ALA day 3 compared to naïve controls[105]. Lower expression of this marker on male monocytes could be an indicator for a more pro-inflammatory phenotype, which coincides with a higher MFI for CCR2 on male EV stimulated monocytes compared with mock controls (Supplementary figure 6 G).

Taken together, A1 and B2 EV stimulation resulted in the activation of primarily pro-inflammatory Ly6C^{hi} monocytes, but also Ly6C^{lo} monocytes, as determined by the surface expression of CD38. The expression pattern of the receptors CX_3CR1 and CCR2 on Ly6C^{hi} monocytes indicated a more pro-inflammatory phenotype of male compared with female cells.

4.8 Changes in the monocyte transcriptome in response to *E. histolytica* EVs

Analysis of the transcriptome of stimulated monocytes through RNA-Seq and followed up by RT-qPCR revealed increased expression of multiple genes involved in chemokine activity and inflammatory response through several key immune pathways upon EV stimulation (Figure 21 D, Supplementary figure 7 - Supplementary figure 10), of which an overview is given in this paragraph. It should be noted that these methods determine the presence of transcripts at the timepoint of analysis but do not analyze regulation of transcription or translation.

Several of the cytokines that were detected to be increased in concentration upon EV stimulation by ELISA or LEGENDplex™ were also differentially expressed between EV stimulated monocytes and mock controls on mRNA level, namely *Tnf, Ccl3,* and *Cxcl10* (Figure 21 D, Supplementary figure 7 - Supplementary figure 10, Supplementary table 19 - Supplementary table 22). Further cytokines that are known to be involved in the immune response to *E. histolytica* but were not analyzed via ELISA or LEGENDplex™ in this study were regulated on mRNA level, including *Ccl4, Ccl5,* and *Cxcl2* (Figure 21 D, Figure 24, Supplementary figure 7 - Supplementary figure 10, Supplementary table 19 - Supplementary table 22). Genes upregulated upon EV stimulation included ISGs like *Ifi205* (Figure 21 D, Supplementary figure 7, Supplementary figure 8, Supplementary table 19, Supplementary table 20), which was previously already reported to be induced in the context of *E. histolytica* infection in another study[253]. In addition, several type I ISGs upregulated upon EV stimulation here (for example *Ifit1, Ifit2, Ifit3, Oasl1, Rsad2*; Supplementary figure 7 - Supplementary figure 10, Supplementary table 19 - Supplementary table 22) were found to be induced in blood neutrophils of ALA mice at day 3 post infection (Er-Lukowiak *et al.*, unpublished data).

Cd40 was significantly more highly expressed upon A1 and B2 EV stimulation of male monocytes and A1 EV stimulation of female monocytes compared with mock controls (Supplementary figure 7 - Supplementary figure 9, Supplementary table 19 - Supplementary table 21). Signaling through the co-stimulatory molecule CD40 leads to the activation of extracellular signal-regulated kinase 1 and 2, resulting in production of pro-inflammatory cytokines by monocytes[254,255]. DCs stimulated with *E. histolytica* LPPG exhibit increased expression of CD86 and CD40[256], thus, exposure to LPPG may also be involved in increased *Cd40* expression upon EV stimulation. Another key player of the innate immune response whose expression was increased upon EV stimulation on monocytes is *Clec4e*, also called Mincle, a receptor that recognizes PAMPs and DAMPs, initiates pro-inflammatory responses to bacterial, fungal, or parasitic infections as shown for *L. major,* and plays a role in phagocytosis[251,257]. *Plk2* was one of the most highly upregulated genes in both male and female monocytes stimulated with A1 or B2 EVs (Figure 22, Supplementary table 19 - Supplementary table 22). PLK2 is a kinase involved in multiple functions during homeostasis, such as cell cycle control, but is also involved in the immune response to infection by inducing pro-inflammatory cytokine release and ROS production[258]. Its functions in innate immunity are still not fully understood yet. *Plk2* is more highly expressed in males compared with females upon LPS or A1 EV stimulation and in mock controls (Figure 23 F, Supplementary figure 11 D, E; Supplementary table 25, Supplementary table 27, Supplementary table 28). In mice with hepatic infection of A1 and B2 *E. histolytica*, another kinase, *Plk3*, was upregulated in livers 6 h and 12 h after injection (unpublished data from our group, personal communication Iris Bruchhaus and Hanna Lotter). Monocytes stimulated with EVs also upregulated genes involved in oxidative stress response, like *Sod2* (Figure 22 A, Supplementary figure 7 - Supplementary figure 10, Supplementary table 19 - Supplementary table 22), which could be a mechanism of the cell to protect

itself against oxygen radicals generated in order to combat the infection[259]. *Acod1* was the most significantly upregulated gene upon EV stimulation in male and female monocytes (Figure 22, Supplementary table 19 - Supplementary table 22). *Acod1* expression is induced upon infection with a variety of bacterial, viral and parasitic pathogens through several TLRs, and is often one of the most highly upregulated genes in this context[260]. ACOD1 exerts numerous functions in the immune system, for example the mediation of ROS production or antigen processing[260].

Interestingly, increased expression of *Lhfpl2* was detected upon EV stimulation (Figure 23, Supplementary figure 10, Supplementary table 19 -Supplementary table 21), a gene that has not been studied in the context of infectious diseases yet. LHFPL2 is involved in reproductive tract development in male and female mice[261]. Furthermore, *Lhfpl2* is highly expressed in sarcoidosis patients[262], is a biomarker for depression[263], involved in onset of familial Parkinson's disease[264], overexpressed in brain tumors[264], and has been implicated in tumor regulation and cell proliferation in breast cancer[265], hepatocellular carcinoma[266], and acute myeloid leukemia[267]. Its function has not been elucidated yet. In this study, *Lhfpl2* was more highly expressed in male monocytes compared with female monocytes (Figure 23 D – G, Supplementary table 25 - Supplementary table 28). The induction of *Lhfpl2* expression upon EV stimulation in males that was detected by RNA-Seq could be verified by RT-qPCR (Figure 24 K, L). In a transcriptome study of hepatic monocytes of male mice during ALA previously conducted in our group, *Lhfpl2* was also upregulated in Ly6C^{hi} monocytes of ALA mice compared with naïve mice (fold change = 19.66; unpublished supplementary data)[214]. Interestingly, it was not upregulated in hepatic monocytes of mice infected with *Listeria monocytogenes*, a bacterium that can also cause liver abscess formation with an underlying monocyte-mediated immunopathology, which differs greatly from that in ALA[214]. Additionally, RT-qPCR results showed that induction of *Lhfpl2* expression by B2 EV stimulation in males was greater than in the LPS positive control (Figure 24 K). Although RNA-Seq data differed in this regard and showed higher *Lhfpl2* levels in LPS controls than in EV stimulated samples (Figure 24 L), this difference was not as prominent as for most other genes. Considering the fact that LPS is a very potent stimulator of monocytes through TLR4[268], it is striking that *E. histolytica* EVs seem to be almost equally as potent when it comes to the induction of *Lhfpl2* expression. This may indicate that its expression is caused, at least in part, by signaling through a receptor other than TLR4 that may get activated less potently by LPS but also by components on *E. histolytica* EVs. LPS has been described to signal independently of TLR4 through inflammatory caspases[269]. Overall, the role of LHFPL2 in the immune response to *E. histolytica* infection as well as the question of which receptors the parasite's secreted EVs bind to remain unclear and warrant further investigation.

In the ALA study mentioned previously[214], several other genes were significantly regulated between monocytes of ALA and naïve mice that were also differentially regulated upon EV stimulation. These included *solute carrier family 7 member 11 (Slc7a11), transglutaminase 2 (Tgm2),* and *endothelin receptor B* (*Ednrb)* (Figure 21 D, Supplementary figure 7 - Supplementary figure 10, Supplementary table 19 - Supplementary table 22). Researchers investigating wound healing during para-inflammation detected high levels of *Slc7a11* in M2 macrophages and associated it with tissue repair, although its function in this context is not fully elucidated yet[270]. Together with *prostaglandin E synthase (Ptges)*, a hypoxia-inducible factor (HIF) 1α target gene[271] also upregulated upon EV stimulation (Figure 21 D, Supplementary figure 8, Supplementary figure 9, Supplementary table 20, Supplementary table 21), *Slc7a11* was upregulated in mice on day 3 after induction of para-inflammation[270]. SLC7A11 is involved in cystine uptake and modulates ferroptosis[272]. TGM2 is involved in monocyte cytoadhesion, required for tissue extravasation and a marker for M2 macrophages[273–275]. Uptake of endothelins by EDNRA and

B plays a key role in vasoconstriction and fibrosis[276], and endothelin-1 stimulation of human monocytes *in vitro* was previously shown to result in increased secretion of IL-1β, IL-6, and TNFα[277]. Upregulated *Ednrb* expression correlates with increased levels of pro-inflammatory cytokines in this study.

Saa3, encoding for the apolipoprotein serum amyloid A3, was significantly more highly expressed in female monocytes stimulated with A1 EVs and male monocytes stimulated with B2 EVs compared with mock controls (Supplementary figure 8, Supplementary figure 9, Supplementary table 20, Supplementary table 21). Its expression was also increased in EV stimulated cells in the other two comparisons, but not statistically significant (data not shown). In a previous study investigating transcriptomes of male murine livers upon injection of A1 or B2 trophozoites, *Saa1* and *Saa2* were among the most highly expressed genes at 12 h and 24 h post injection (doctoral thesis Helena Fehling[278] and data not shown, personal communication Iris Bruchhaus and Hanna Lotter). SAAs are acute phase proteins, produced primarily in the liver but also in other tissues, by hepatocytes, monocytes and macrophages in response to pro-inflammatory stimuli like IL-1β, IL-6, and TNFα[279,280]. SAAs exert multiple biological functions of pro- or anti-inflammatory nature, are induced in response to infection or injury and have been implicated in a number of chronic inflammatory diseases such as rheumatoid arthritis and atherosclerosis[280]. SAAs can chemoattract leukocytes and induce for example release of pro-inflammatory cytokines through TLR2 on monocytes, but can also promote differentiation into M2 macrophages[280].

Ras Guanine Exchange Factor domain family member 1b (*Rasgef1b)* and *Family with sequence similarity 20, member C* (*Fam20c),* which were both increased in expression upon EV stimulation (Figure 21 D, Supplementary figure 7 - Supplementary figure 10, Supplementary table 19 - Supplementary table 22) were also previously differentially regulated upon injection of A1 and B2 trophozoites into livers (unpublished data, personal communication Iris Bruchhaus and Hanna Lotter). *Rasgef1b* was upregulated 6 h and 12 h after injection of both clones compared to the negative control, but the effect was gone after 24 h. RasGEF1b is a member of the Ras protein superfamily that catalyzes the exchange of guanosine diphosphate (GDP) and guanosine triphosphate (GTP), leading to the formation of Ras-GTP, which regulates gene expression[281]. Stimulation of TLR2, TLR3, or TLR4 in murine macrophages by specific ligands or infection with *Trypanosoma cruzi* previously led to induction of *Rasgef1b* expression[281–283]. Knockdown of *Rasgef1b* in LPS stimulated macrophages revealed a role in the inflammatory immune response and the release of IL-6 and CXCL1 via NF-κB[284]. Remarkably, *Fam20c* was downregulated at timepoints 6 h and 12 h in the previously mentioned liver study, in contrast to the findings here. FAM20C is a serine protein kinase involved in biomineralization processes and phosphorylation of the vast majority of secreted proteins, among them IL-6[285,286]. Its targets are involved in a variety of processes, including cell migration, wound repair and cholesterol metabolism[286]. The differences in regulation of *Fam20c* in response to whole trophozoites or EVs in the two studies may be explained by the fact that different cell types with differing tissue origins were analyzed. While BM-derived monocytes were used here, the other study investigated a conglomerate of cells in the liver. Due to the plethora of functions associated with FAM20C, it may be that its role in monocytes in the BM differs from that in the liver.

GO term enrichment for genes with lower expression upon EV stimulation revealed roles in iron ion transport (Supplementary figure 8 D) and phagocytosis (Supplementary figure 10 D), among others. However, due to the short list of genes, the informative value of GO term enrichment is limited here. *15-hydroxyprostaglandin dehydrogenase (Hpgd)*, the only gene significantly decreased in female A1 EV stimulated monocytes compared with mock controls (Supplementary figure 9 A, Supplementary table

21), has been described as a marker of DC-like monocytes[287]. *Signal-regulatory protein beta 1C* (*Sirpb1c)* was significantly decreased upon B2 EV stimulation in both male and female monocytes (Supplementary figure 8 A, Supplementary figure 10 A, Supplementary table 20, Supplementary table 22) and is enriched in neutrophil-like monocytes[287]. Its expression was also decreased by A1 EV stimulation, although with a fold change under the applied cutoff (data not shown). Although these results could suggest a role of *E. histolytica* EVs in the suppression of monocyte differentiation, this is contrasted by the finding that *Basic helix-loop-helix family member e40* (*Bhlhe40*), another neutrophil-like monocyte marker[288], is upregulated in the same samples in which *Sirpb1c* is downregulated (Supplementary figure 10 A, Supplementary table 22 + data not shown).

Due to the low sample number used for RNA-Seq in addition to the fact that the two female samples were quite different in terms of gene expression levels (Figure 21), these results should be interpreted with caution. Furthermore, samples were sequenced at a read depth of 5 million reads per sample, which is at the lower end of recommended sequencing depth for mammalian cells according to Illumina[289]. Although RT-qPCR on additional samples could largely verify previous findings for six genes of interest, a second sequencing run at a higher read depth revealed that not all previous results were reproducible, especially in female monocytes (Figure 24).

In summary, stimulation of male and female monocytes with A1 and B2 EVs triggered the increased expression of several genes encoding key mediators of the pro-inflammatory immune response, which act through several effector mechanism. This correlated with the observation of increased levels of pro-inflammatory cytokines in the supernatants of these cells. EV stimulation furthermore led to increases in the expression of type I ISGs, which were recently described to be involved in the neutrophil response to ALA but, to my knowledge, have not been investigated in the context of monocyte response to *E. histolytica* infection yet. Several of the detected genes were already previously reported in studies characterizing the immune response to *E. histolytica* infection in the liver and the findings correlated between the studies. This proves the validity of the results obtained here despite the abovementioned limitations of the transcriptome study on hand.

4.9 Differences in the immune response elicited by A1 and B2 EVs

The immune response of monocytes to A1 and B2 EVs was similar with regard to the secreted cytokines (3.3.2), CD38 surface expression (Figure 20) and changes on transcriptional level as determined by RNA-Seq (3.3.5). The main detected differences in the response to EVs from the two clones were the release of MPO (as discussed above, chapter 4.6) and the susceptibility to heat inactivation of B2 EVs. RNA-Seq revealed only one gene each differentially expressed between male or female monocytes stimulated with A1 compared to B2 EVs. *Gpnmb,* which was more highly expressed in female B2 EV stimulated cells compared to A1 EV stimulated cells (Supplementary table 24), encodes for a glycoprotein upregulated during the early phase of ALA as part of the hypoxia response[290,291]. *Gpnmb* is highly expressed in macrophages, both tissue-resident and infiltrating, in response to liver damage and in colitis[292–294]. The role of *Gm49388*, the only gene significantly differentially expressed between male A1 and B2 EVs (Supplementary table 23), is still unknown. As discussed above (4.8), RNA-Seq was performed at a depth of only 5 million reads per sample. Hence, there may be more differences in gene expression between A1 and B2 EV stimulated monocytes that may have been missed here due to insufficient sequencing depth. RNA-Seq results in this study should also be interpreted with caution

due to the low number of replicates and the apparent differences in gene expression between the two female samples.

The decrease in elicited cytokine release and CD38 expression upon heat inactivation of B2 EVs, which was not observed upon heat inactivation of A1 EVs, indicated further differences in the immune response to EVs of the different clones. Exposure of the EVs to heat was performed in order to denature proteins. The structure of EVs is generally relatively stable even during heat inactivation, although exposure to high temperatures for prolonged periods of time leads to rupture of some vesicles and release of contents[295], which could impact stimulatory capacity. miRNAs are stable even when exposed to boiling temperatures[296], in contrast to proteins. The persistence of the stimulatory effect of A1 EVs even after heat inactivation might indicate an involvement of heat stable miRNAs in the immune response. Indeed, miRNA cargo analysis revealed the differential expression of a novel mature miRNA as well as 3' isomiRs for Ehi-miR-35 and Ehi-miR-55 between A1 and B2 EVs, all of which were more highly expressed in A1 EVs (Figure 12 C, D; Supplementary table 17, Supplementary table 18). To elucidate whether the differences observed between A1 and B2 EVs were the result of an involvement of miRNAs, further analysis is needed. In addition to heat inactivation, A1 EVs should be subjected to ribonuclease (RNase) treatment prior to immune cell stimulation. If the stimulatory effect is ablated upon RNase treatment, an involvement of miRNAs is likely.

Although heat leads to denaturation of proteins, the molecular patterns that are recognized by target cells may not necessarily disappear by denaturation, as they may still be present in the primary structure of proteins. 86 proteins were found to be differentially expressed between A1 and B2 EV proteomes (Figure 9, Supplementary table 1). Any one of these proteins, a combination of several of them or non-protein EV cargo specific to one clone may also be the cause of the observed differences. RNase-treated controls will give insight into the extent to which miRNAs are involved and further studies are needed in order to investigate the other EV components.

4.10 Sex differences in the immune response of monocytes to *E. histolytica* EVs

The immune responses of male and female monocytes to EV stimulation analyzed in this study were similar with regard to surface marker expression and the elicited cytokine profile. Nevertheless, cytokine secretion differed in intensity between the sexes. EV stimulated male monocytes secreted higher amounts of some cytokines compared with female monocytes. This was especially prominent for CXCL1 and IL-1β (Figure 17 D, E). Furthermore, *Il-1β* was differentially expressed between male and female monocytes upon A1 EV stimulation and in mock controls as determined by RNA-Seq but, in contrast to LEGENDplex™ data, higher in females (Figure 23 F, Supplementary figure 11 E; Supplementary table 25, Supplementary table 27). It was not differentially expressed between the sexes upon LPS stimulation and differentially expressed with a fold change of 1.8 in B2 EV stimulated monocytes, thus under the applied cutoff (data not shown). Analysis of normalized reads of the additionally sequenced samples (refer to chapter 3.3.6) revealed the same pattern (data not shown). *Cxcl1* was not differentially expressed between the sexes as determined by RNA-Seq. Discrepancies in the results obtained by cytokine analysis and sequencing may be explained by dynamics in cytokine production and degradation in response to EV stimulation throughout time, which are not captured with the analysis of a single timepoint, as done here. This constitutes a limitation especially for bulk

RNA-Seq, which only gives information about the presence of a transcript at a given time and not whether it is subsequently translated or degraded.

In a previous study from our group, elevated amounts of CXCL1 in classical monocytes from male mice were reported both during steady state and on day 3 of ALA[105]. Human monocytes exhibited the same male bias, and CXCL1 concentration was shown to correlate positively with testosterone concentration[105]. In the same study, a sex difference biased towards males in the concentration of TNFα was reported as well but could not be seen here. To my knowledge, a sex difference in IL-1β secretion of monocytes has not been described in the context of *E. histolytica* infection yet. Bernin *et al.* investigated serum levels of several cytokines in male and female ALA patients and asymptomatic carriers, but did not detect a sex difference in the concentration of IL-1β[120]. However, elevated levels of IL-1β in men compared with women have been reported in other diseases, such as atherosclerosis[297].

Among the genes differentially expressed between the sexes under EV stimulation were *Lhfpl2*, which was already discussed in 4.8, and *Saa3*, which was more highly expressed in female A1 EV stimulated monocytes compared with males (Supplementary table 25). SAA3 has also been implicated in the sex dimorphism in atherosclerosis[298,299] and obesity-related inflammation[300] in mice. In both contexts, protective effects in female but not male mice were demonstrated. Since female mice regenerate faster from ALAs than males[93], higher expression of *Saa* in monocytes of females compared with males could also play a protective role in this context. A total of 56 genes were differentially expressed between the sexes under the influence of EV stimulation that were not differentially expressed in mock controls (Figure 23 A, B). *Cxcl10* was one of these genes that was more highly expressed in females than in males, and was also differentially expressed between the sexes under LPS stimulation (Supplementary figure 11 D), but CXCL10 concentrations in supernatants of stimulated monocytes were not significantly different between males and females (Figure 15 D). In addition, *Mpo* expression was significantly higher in female than male monocytes stimulated with EVs and mock controls (Figure 23 D – G, Supplementary figure 11 C, E; Supplementary table 25, Supplementary table 26, Supplementary table 27), but no sex differences in MPO concentration were determined by ELISA (Figure 18 A). In contrast, the higher expression levels of *Lhfpl2* in male monocytes compared with females detected by NGS could be verified by RT-qPCR (Figure 24 K, L).

Consequently, the results obtained by RNA-Seq in this study may provide interesting insight into sex differences in the response to *E. histolytica* EVs but should be interpreted with caution and verified by further analyses, particularly considering the low sample number analyzed here. For a few selected genes that were differentially expressed between the sexes under EV stimulation (Figure 23), RPKM values of the second sequencing run were analyzed as an initial verficiation step. For 6 of 9 genes, including *Cxcl10*, *Mpo* and *Il1b*, the same trends as previously were detected, while the previous results for *Oasl2*, *Saa3* and *Ly6i* could not be replicated (Supplementary table 29).

4.11 The effect of EV stimulation on the immune response of neutrophils

In addition to the release of MPO by neutrophils discussed above (4.6), we also studied the effect of EV stimulation on cytokine release by neutrophils and on the expression of surface markers for differentiation into N1 and N2 neutrophils as well as markers for activation (refer to master thesis Valentin Bärreiter[166]). We used neutrophils from the BM and the periphery since prior experiments in our group revealed remarkable differences in the responsiveness of neutrophils to stimuli based on the tissue of origin, which was evident also in the context of MPO release (Figure 18 B, C).

Apart from an initially observed increase in the secretion of CCL3 upon A1 and B2 EV stimulation of male BM neutrophils, which we were not able to replicate in further experiments, we did not observe any changes in cytokine profile or marker expression compared with mock controls. Other effector mechanisms of neutrophils, such as phagocytosis, ROS production or NETosis were not studied, but may be worth further investigation. For instance, next to the abovementioned effect of EV stimulation on extracellular trap formation (4.6), Díaz-Godínez *et al.* showed that pretreatment with amebic EVs, but also EVs isolated from neutrophils, inhibited the respiratory burst of human neutrophils in response to PMA, A23187 ionophore, or whole amebae stimulation[145]. Thus, EVs may not influence cytokine release by neutrophils or on the surface markers we studied but other effector mechanisms of this cell type. Since stimulation with amebic EVs did not have a significant impact on ROS production or NETosis of unstimulated neutrophils and only exerted a suppressive effect on stimulated neutrophils, it may be that we could not observe an effect on cytokine release or surface marker expression because we did not use an additional stimulatory agent together with the amebic EVs on our neutrophils. A potential suppressive effect of the amebic EVs may thus not have been detected as the result of the experimental setup.

The absence of detected effects upon EV stimulation may also be due to inherent difficulties of culturing neutrophils *in vitro*. Neutrophils are sensitive to isolation methods as shown by Blanter and colleagues, who demonstrated that neutrophils isolated by immunomagnetic selection were more quiescent in the absence of strong inflammatory stimuli compared with their density-gradient purified counterparts, but were more responsive to pro-inflammatory stimuli[301]. In addition, BM-derived neutrophils are less responsive than peripheral neutrophils as mentioned above, but peripheral neutrophils are less viable *in vitro* due to their pre-activated state[166]. This hinders the investigation of effects on cytokine release or surface marker expression over a time period of 24 h as performed for monocytes, but stimulation for a shorter amount of time may be insufficient for the detection of effects.

5 Conclusion

Taken together, this study revealed differences in the EV protein and miRNA cargo between A1 and B2 *E. histolytica* that will be interesting subjects for further studies on pathogenicity of the parasite. EV stimulation activated male and female monocytes to release pro-inflammatory mediators. Much evidence points to a recognition of antigens present on EVs by monocytes through TLR2 and TLR4 or other PRRs. It was not studied whether *E. histolytica* EVs were internalized by host monocytes through endocytosis, fused with their plasma membrane to deliver their cargo or remained bound to the surface membrane, a question that could be experimentally answered by fluorescent labeling of EVs and subsequent flow cytometry or confocal microscopy. *E. histolytica* EVs were previously shown to be internalized by human neutrophils, likely through membrane fusion[145].

While EVs had an activating effect on monocytes, the same could not be observed for neutrophils. Other researchers even showed a suppressive effect of *E. histolytica* EVs on neutrophils[145]. Although the role of neutrophils in invasive amebiasis is controversial[110], extensive evidence points to a protective role in ALA formation. In fact, recent findings from our group showed that neutrophils in male mice, which suffer from larger abscesses, exhibited a less activated phenotype (Er-Lukowiak *et al.*, unpublished data), highlighting the putatively protective role of neutrophil activation. When comparing the cytokine and mRNA profile elicited by EV stimulation to known immune responses to whole trophozoites in the context of invasive amebiasis, many of the same effects could be detected. Pro-inflammatory mediators released by monocytes and other immune cells in the liver are known to contribute to ALA immunopathology and *E. histolytica* EVs stimulated the release of such mediators (for example TNFα) by monocytes. A disparity in the large abscess size in humans compared with the relatively low number of trophozoites found in these abscesses has previously been described[40], hinting at a contribution of contact-independent mechanisms to tissue damage. These findings suggest that EVs can trigger monocyte-mediated liver pathology also in the absence of direct parasite-immune cell contact and over larger distances and may suppress the protective effects of neutrophils. Interestingly, EVs of both low pathogenic A1 and highly pathogenic B2 amebae caused similar effects, except for the differences in monocyte and neutrophil MPO release, which warrants further investigation. If MPO indeed plays a protective role during invasive amebiasis (as mentioned in 4.6), this may explain in part why abscesses caused by A1 compared with B2 amebae are smaller even though the EV-mediated activation of monocytes was very similar in this study.

However, whether EVs play a role in the immune response to *E. histolytica* infection *in vivo* remains to be determined. The experimental setup used in this project was artificial and a high concentration of EVs per target cell was used, which may not mirror the ratio of parasite-derived EVs to host cells present *in vivo*. Isolation of both host- and parasite-derived EVs from livers of ALA mice or from serum of infected mice or humans will be interesting tools for the further analysis of the role of EVs during infection. Alterations in the content of serum EVs and contribution to pathological processes have been described for several viral and other parasitic infections[302–304].

In addition, the parallels detected between immune response to *E. histolytica* EVs and whole amebae could open up new experimental possibilities. For instance, intestinal organoid monolayers constitute a promising new tool for the investigation of invasion mechanisms of parasites such as *G. intestinalis*[305], but also *E. histolytica*. Co-incubation experiments of these organoids with amebic trophozoites are

limited in their timeframe by the rapid destruction of the monolayer caused by the parasite[227]. EVs could be used instead of whole parasites for co-culture of organoids, EVs, and immune cells over longer periods of time to investigate immune mechanisms at play in this context. Since intestinal monolayers are grown in transwell systems, different culture media can be used for intestinal cells and parasites. However, the use of transwell systems makes less sense for other organoids, such as hepatic organoids, that may also be interesting to study in co-culture with *E. histolytica* and immune cells. Again, the use of EVs instead of whole parasites could here solve culture medium issues, as organoids and parasites require vastly different culture media.

Several studies have investigated the potential of parasite-derived EVs as vaccines. For example, EVs secreted by the nematode *Heligmosomoides polygyrus* were shown to be taken up by host macrophages and resulted in the suppression of the inflammatory response, hence they may constitute promising vaccine candidates[306]. Conversely, *Toxoplasma gondii* EVs induced immune response characterized by higher IFN-γ, TNFα, IL-10, and IL-17 concentrations in several tissues of vaccinated mice and thus conferred protection characterized by higher survival rates[307]. *L. donovani*-derived EVs suppressed TNFα release by monocytes, induced IL-10 and led to disease exacerbation upon vaccination of mice due to immunosuppression[159–161]. Efforts for the development of vaccines against *E. histolytica* infection have focused primarily on Gal/GalNac lectin, although other proteins have been studies as well[308]. Several studies using native or recombinant forms of this lectin reported varying degrees of protection against amebic colitis and ALA in animal models, and while vaccination was protective in most cases, some animals exhibited higher pathology after vaccination[308–311]. No clinical studies on humans have been performed with lectin-based vaccines to date. LPPG was also proposed by Wong-Baeza *et al.* as a putatively promising vaccine candidate due to its capacity to activate both innate and adaptive immunity[312]. A good vaccine is highly immunogenic and results in the formation of immunological memory[308]. *E. histolytica* EVs were shown in this study to contain several immunogenic molecules and trigger an immune response by monocytes. Therefore, they could act as their own adjuvants, an advantage over vaccines based on a single protein[313]. Whether *E. histolytica* EVs would constitute good vaccine candidates would have to be tested in animal experiments in future studies. Despite some advantages of using EVs as vaccines, their properties also constitute some challenges in large-scale production and commercialization. These include significant discrepancies between batches of EVs, as observed also in this study.

6 Supplementary Data

6.1 Supplementary figures

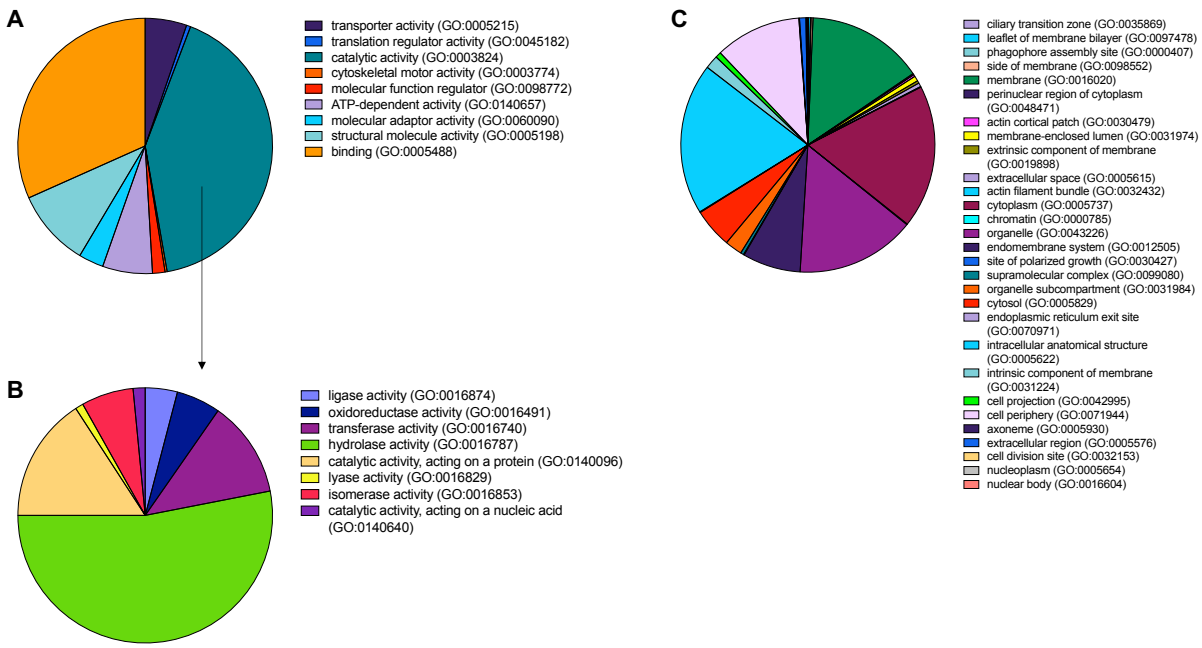

Supplementary figure 1: GO term enrichment analysis of the B2 EV proteome.
Pie charts depicting the relative amount of proteins in the B2 EV proteome with GO terms for (A) molecular function, (B) molecular function sublevel 1 catalytic activity and (C) cellular component, sublevel 1 cellular anatomical entity. Pie charts were created with Panther knowledgebase[173].

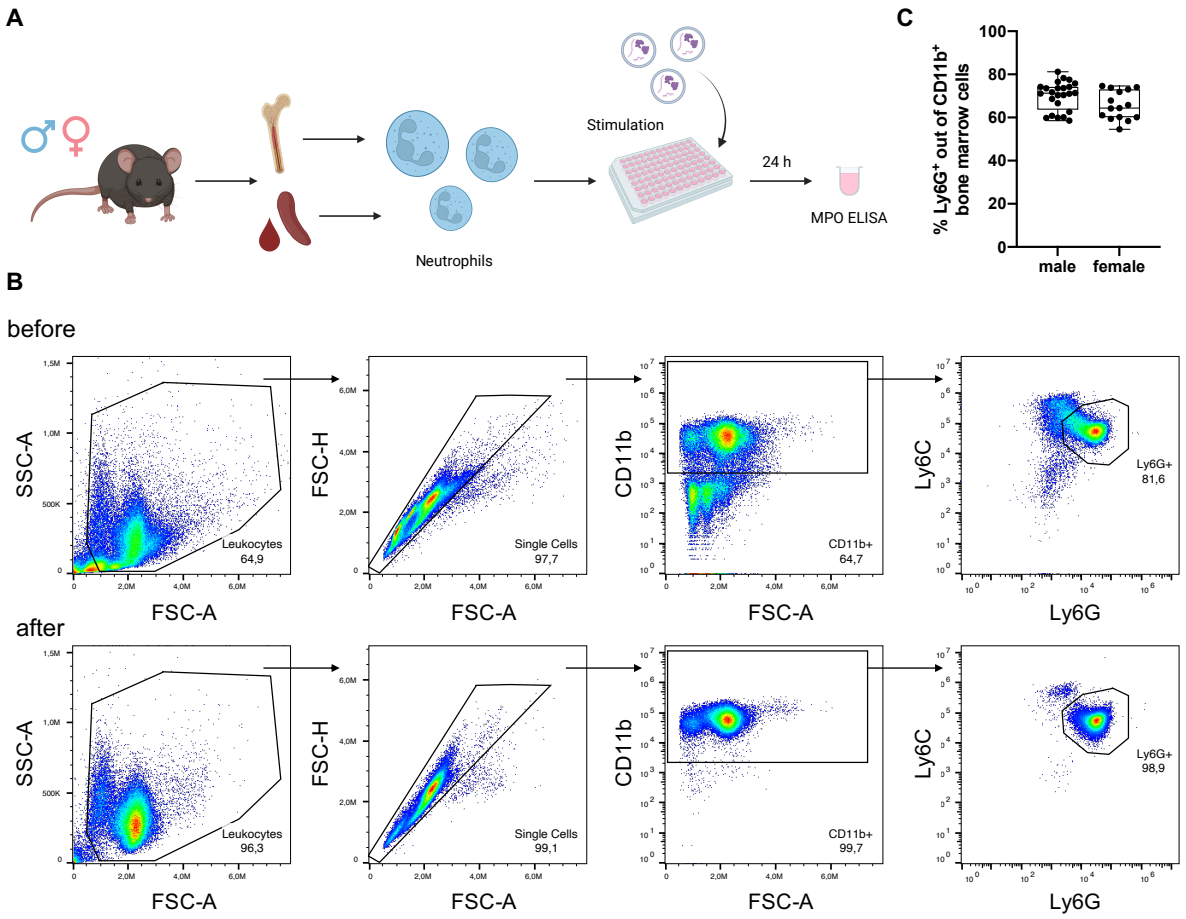

Supplementary figure 2: Experimental setup of EV stimulation of primary murine neutrophils.
(A) Schematic depiction of the workflow of stimulation experiments on neutrophils. The bones or spleen and blood of male and female C57BL/6J mice were harvested and neutrophils isolated out of these tissues via antibody-mediated negative selection. Isolated neutrophils were then stimulated with 1000 EVs/cell, together with positive and negative controls, for 24 h and supernatants of stimulated cells were used for the detection of myeloperoxidase using ELISA. (B) Efficacy control of neutrophil isolation using flow cytometry. Cells before and after isolation were stained with anti-CD11b, anti-Ly6C and anti-Ly6G antibodies to identify $CD11b^+Ly6C^+Ly6G^+$ neutrophils, labeled simply '$Ly6G^+$' here. Shown is one representative experiment. (C) Quantification of the relative amount of $Ly6G^+$ neutrophils in male and female mice (n = 15-24). Percentage of cells was determined based on 'before enrichment' samples (B). Testing for statistical significance was performed with Mann-Whitney U test.

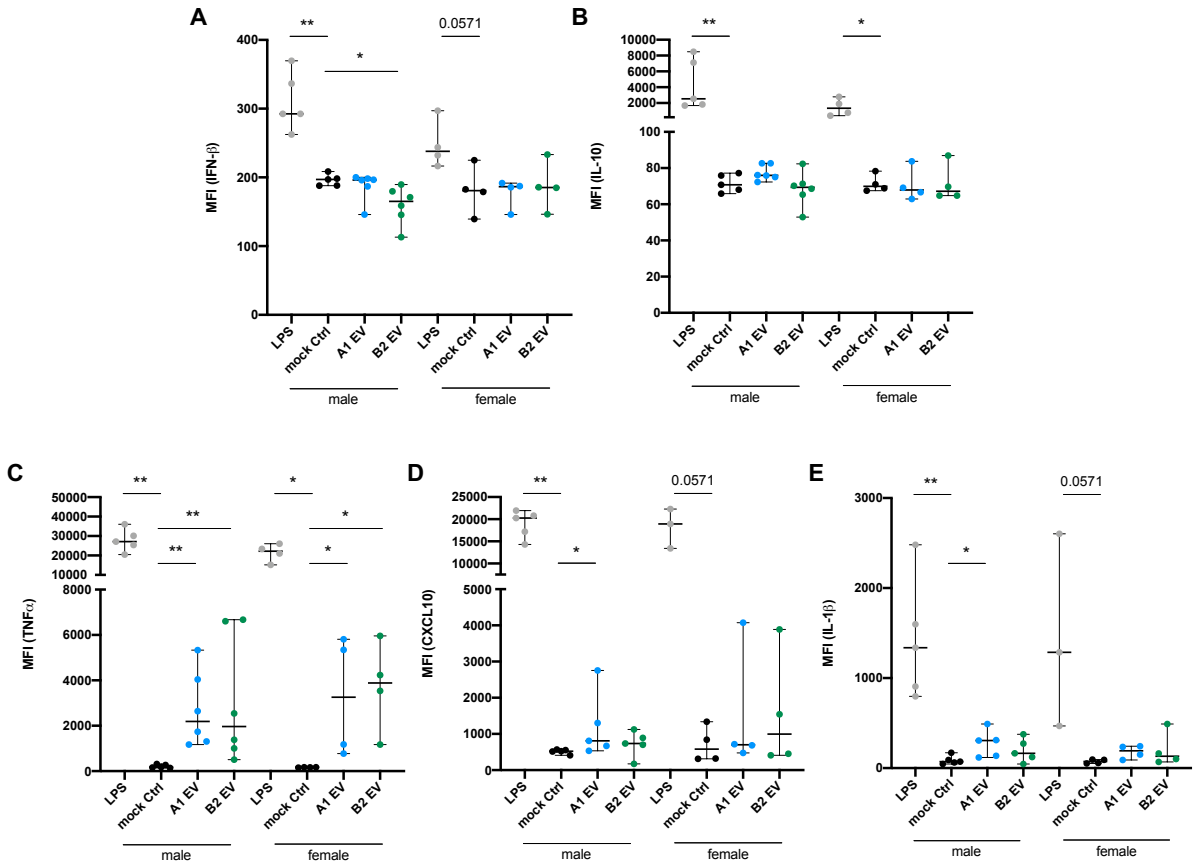

Supplementary figure 3: Median fluorescence intensities of cytokines present in supernatants of EV-stimulated monocytes (anti-virus response LEGENDplex™ panel).

Male and female bone marrow-derived monocytes were stimulated for 24 h with LPS (positive control), mock control or 1000 EVs/cell of A1 or B2 EVs. IFN-β (A), IL-10 (B), TNFα (C), CXCL10 (D), and IL-1β (E) were detected in supernatants after stimulation by LEGENDplex™. Depicted is the median with range of median fluorescence intensities (MFIs) for each cytokine. Testing for significance was performed using Mann-Whitney U test (* $p < 0.05$, ** $p < 0.01$).

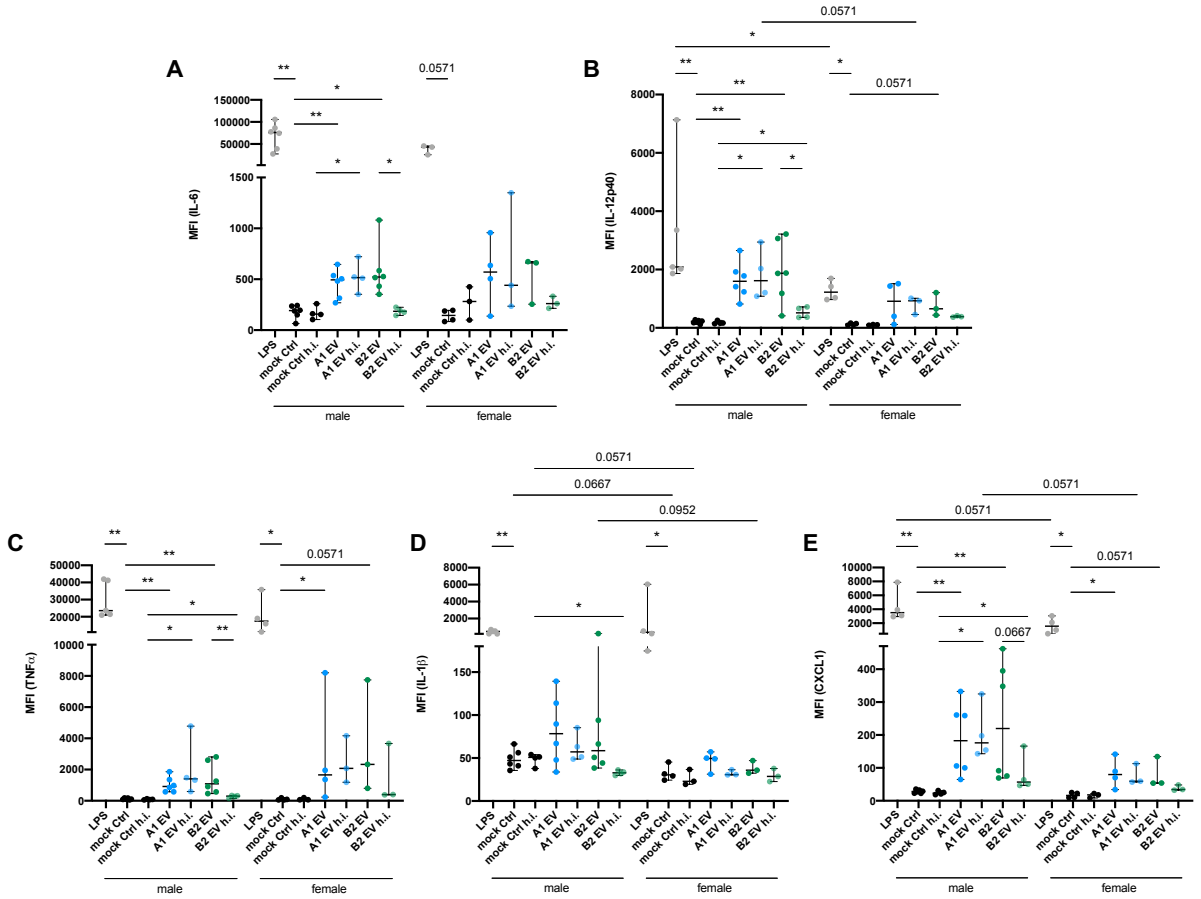

Supplementary figure 4: Median fluorescence intensities of cytokines present in supernatants of EV-stimulated monocytes (LEGENDplex™ M1 macrophage panel).

Male and female bone marrow-derived monocytes were stimulated for 24 h with LPS (positive control), mock control or 1000 EVs/cell of A1 or B2 EVs. Heat inactivation (h.i.) of EVs was performed at 95°C for 10 min as a separate control. IL-6 (A), IL-12p40 (B), TNFα (C), IL-1β (D), and CXCL1 (E) were detected in supernatants after stimulation by LEGENDplex™. Graphs depict median with range of median fluorescence intensities (MFIs) for each cytokine (n = 3-6). Testing for significance was performed using Mann-Whitney U test (* $p < 0.05$, ** $p < 0.01$).

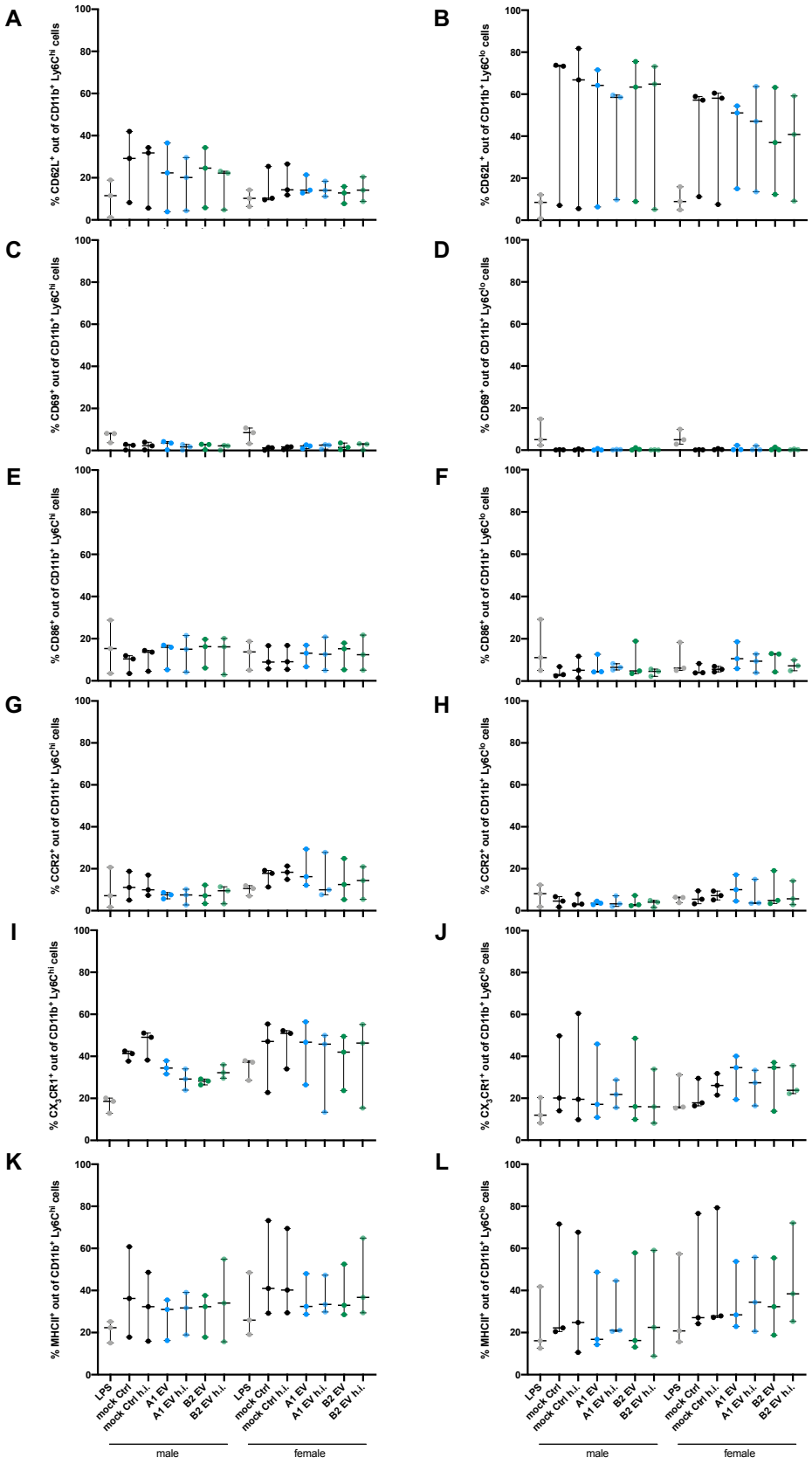

Supplementary figure 5: Surface marker expression on stimulated classical and non-classical monocytes.
Male and female bone marrow-derived monocytes were stimulated for 24 h with LPS (positive control), mock control or 1000 EVs/cell of A1 or B2 EVs. Heat inactivation (h.i.) of EVs was performed at 95°C for 10 min as a separate control. After stimulation, cells were stained for flow cytometry. Percent expression of CD62L (A, B), CD69 (C, D), CD86, (E, F), CCR2 (G, H), CX_3CR1 (I, J), and MHCII (K, L) was analyzed on $Ly6C^{hi}$ (A, C, E, G, I, K) and $Ly6C^{lo}$ (B, D, F, H, J, L) monocytes. Graphs depict median with range. Testing for significance was done using Mann-Whitney U test.

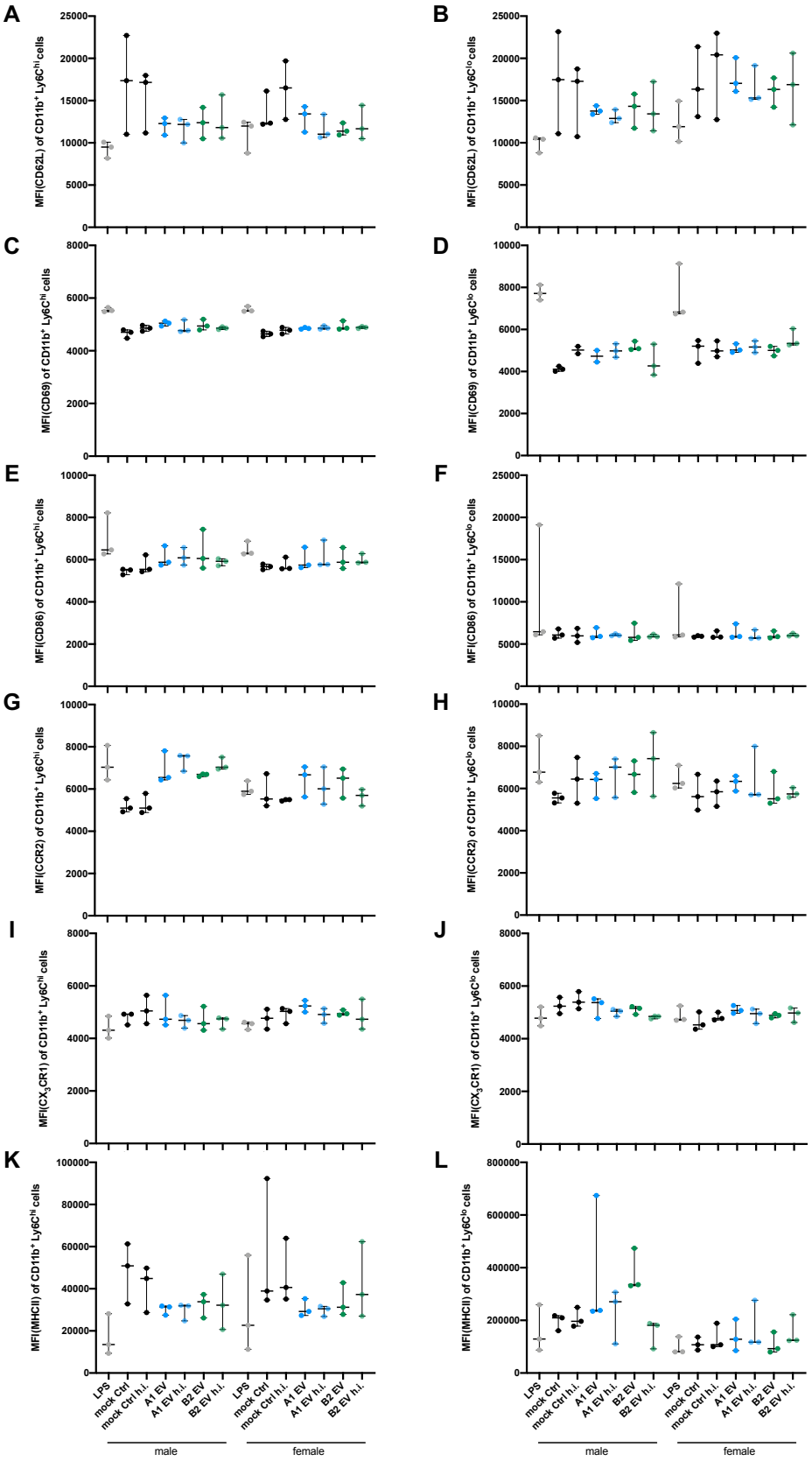

Supplementary figure 6: Median fluorescence intensities of surface markers on stimulated classical and non-classical monocytes.
Male and female bone marrow-derived monocytes were stimulated for 24 h with LPS (positive control), mock control or 1000 EVs/cell of A1 or B2 EVs. Heat inactivation (h.i.) of EVs was performed at 95°C for 10 min as a separate control. After stimulation, cells were stained for flow cytometry. Median fluorescence intensity (MFI) of CD62L (A, B), CD69 (C, D), CD86, (E, F), CCR2 (G, H), CX_3CR1 (I, J), and MHCII (K, L) was analyzed in positive gates for each marker on $Ly6C^{hi}$ (A, C, E, G, I, K) and $Ly6C^{lo}$ (B, D, F, H, J, L) monocytes. Graphs depict median with range. Testing for significance was done using Mann-Whitney U test.

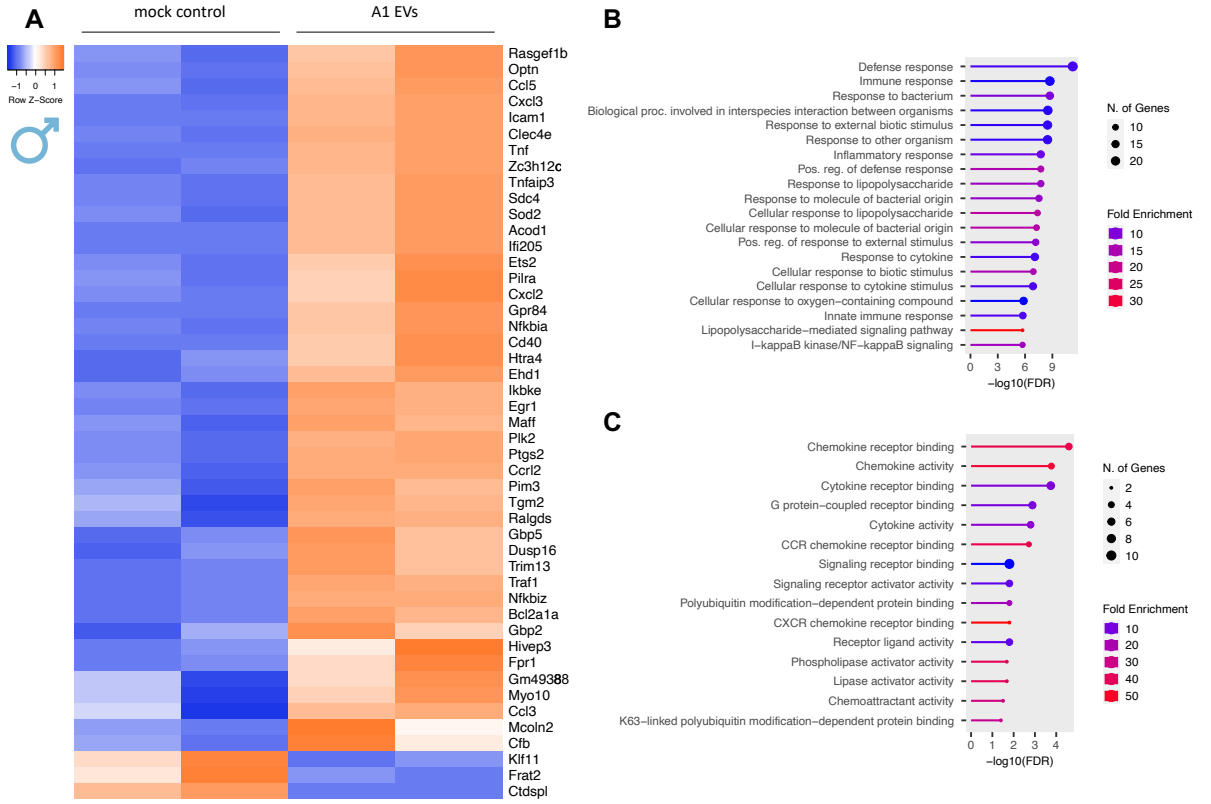

Supplementary figure 7: Transcriptome of A1 EV stimulated male monocytes compared to mock controls.
(A) Heatmap depicting the z-score of all significantly differentially expressed genes (fold change ≥ |2|, FDR $p < 0.05$) between male A1 EV stimulated monocytes and mock controls. RPKM normalized reads were used for mapping. Orange indicates high expression and blue indicates low expression of the gene. Heatmap created with Heatmapper[169]. (B, C) GO term enrichment analysis of biological process (B) and molecular function (C) GO terms associated with genes upregulated in male A1 EVs versus mock controls. Shown are the top 20 enriched biological process GO terms (B) and all significantly enriched molecular function GO terms (C) sorted by statistical significance (-log10(FDR)). GO term enrichment was performed with shinyGO[177].

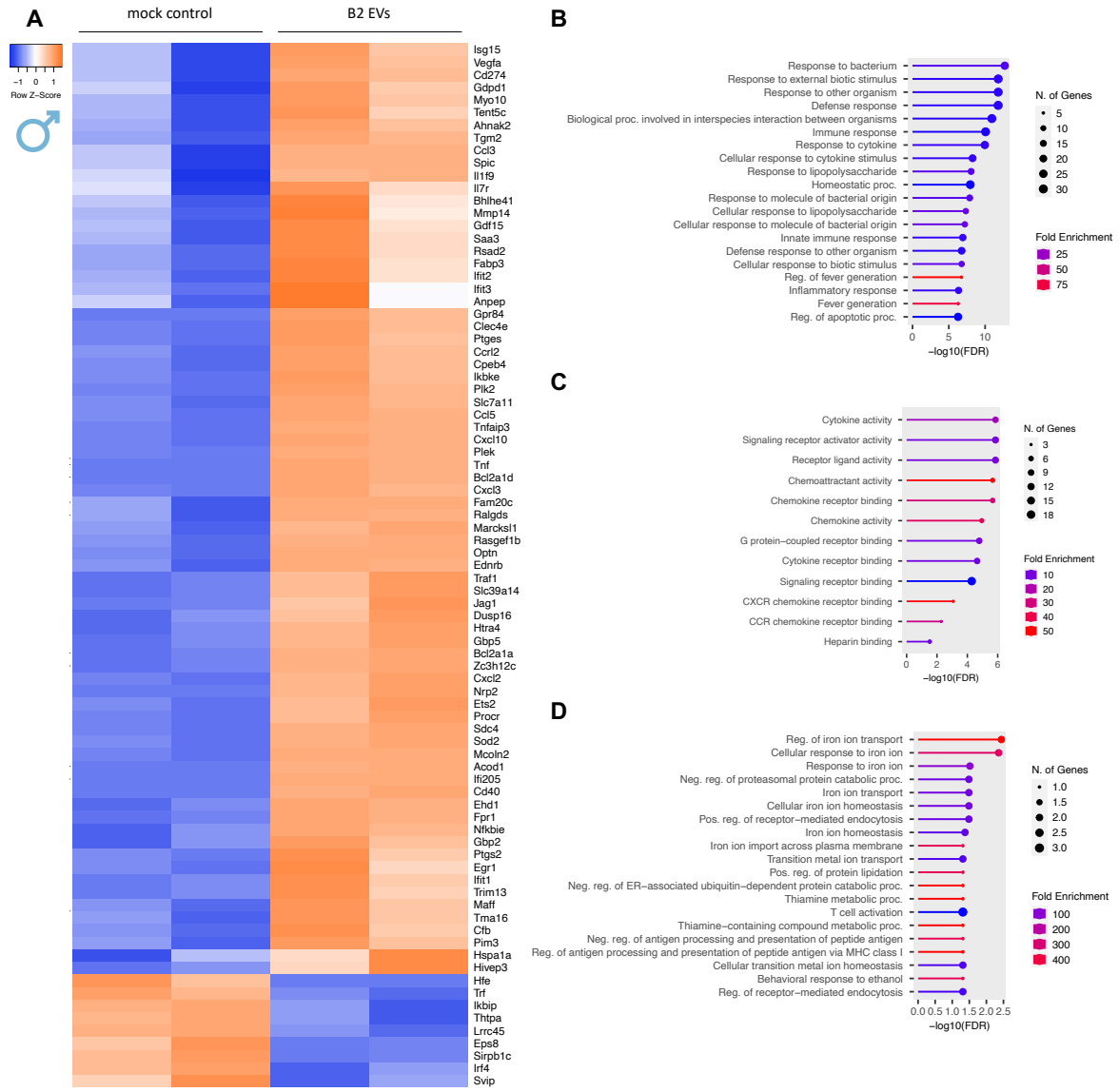

Supplementary figure 8: Transcriptome of B2 EV stimulated male monocytes compared to mock controls.
(A) Heatmap depicting the z-score of all significantly differentially expressed genes (fold change ≥ |2|, FDR $p < 0.05$) between male B2 EV stimulated monocytes and mock controls. RPKM normalized reads were used for mapping. Orange indicates high expression and blue indicates low expression of the gene. Heatmap created with Heatmapper[169]. (B, C, D) GO term enrichment analysis of biological process (B) and molecular function (C) GO terms associated with genes upregulated in male B2 EVs versus mock controls, as well as biological process GO terms of downregulated genes (D). Shown are the top 20 enriched biological process GO terms (B, D) and all significantly enriched molecular function GO terms (C) sorted by statistical significance (-log10(FDR)). GO term enrichment was performed with shinyGO[177].

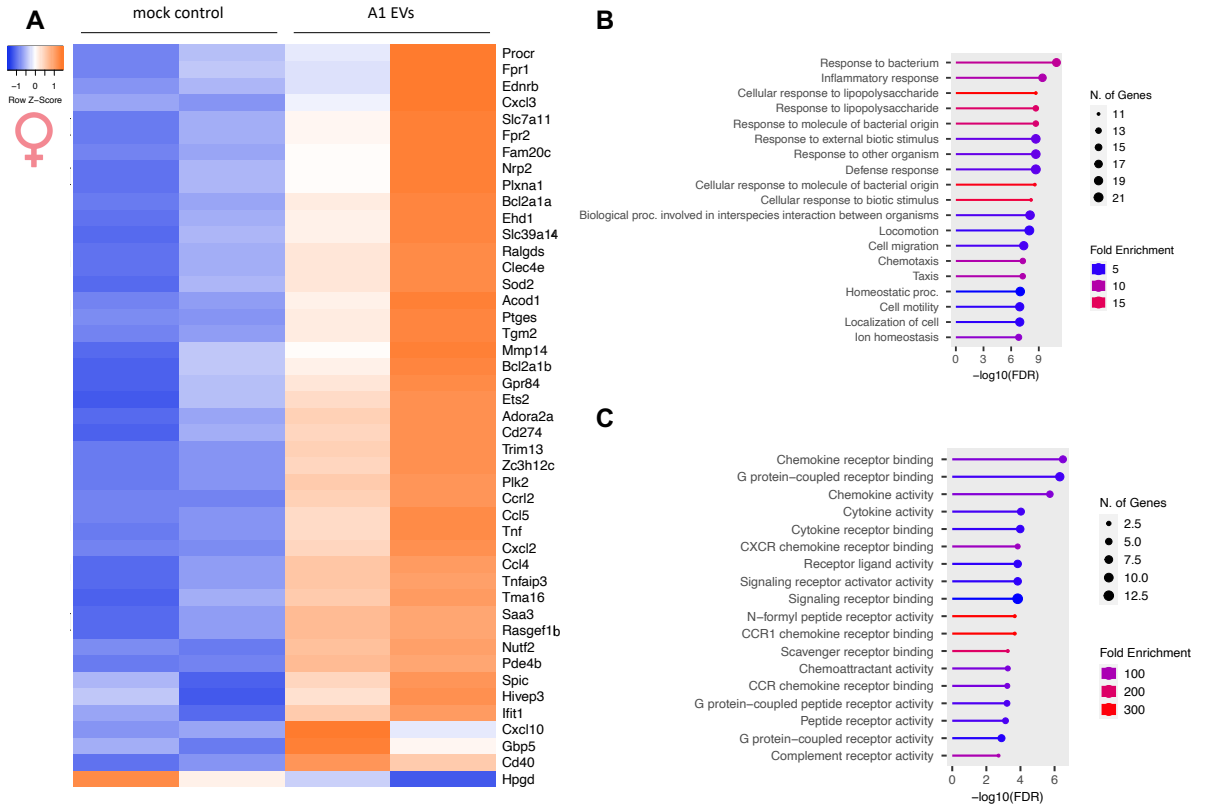

Supplementary figure 9: Transcriptome of A1 EV stimulated female monocytes compared to mock controls.
(A) Heatmap depicting the z-score of all significantly differentially expressed genes (fold change ≥ |2|, FDR $p < 0.05$) between female A1 EV stimulated monocytes and mock controls. RPKM normalized reads were used for mapping. Orange indicates high expression and blue indicates low expression of the gene. Heatmap created with Heatmapper[169]. (B, C) GO term enrichment analysis of biological process (B) and molecular function (C) GO terms associated with genes upregulated in female A1 EVs versus mock controls. Shown are the top 20 enriched biological process GO terms (B) and all significantly enriched molecular function GO terms (C) sorted by statistical significance (-log10(FDR)). GO term enrichment was performed with shinyGO[177].

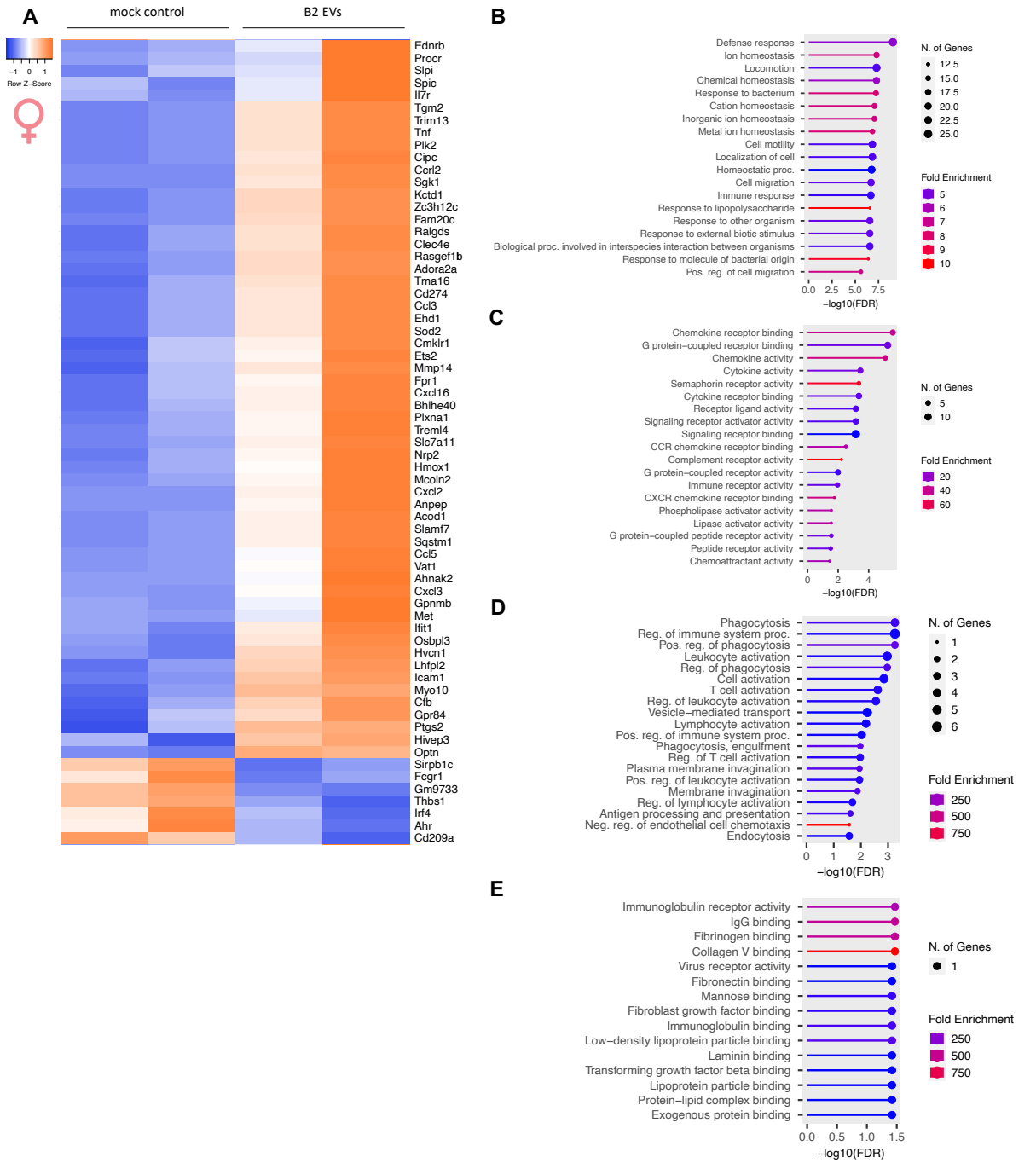

Supplementary figure 10: Transcriptome of B2 EV stimulated female monocytes compared to mock controls.
(A) Heatmap depicting the z-score of all significantly differentially expressed genes (fold change ≥ |2|, FDR $p < 0.05$) between female B2 EV stimulated monocytes and mock controls. RPKM normalized reads were used for mapping. Orange indicates high expression and blue indicates low expression of the gene. Heatmap created with Heatmapper[169]. (B, C, D, E) GO term enrichment analysis of biological process (B, D) and molecular function (C, E) GO terms associated with genes upregulated (B, C) or downregulated (D, E) in female B2 EVs versus mock controls. Shown are the top 20 enriched terms or less, if less than 20 were significantly enriched (FDR 0.05), sorted by statistical significance (-log10(FDR)). GO term enrichment was performed with shinyGO[177].

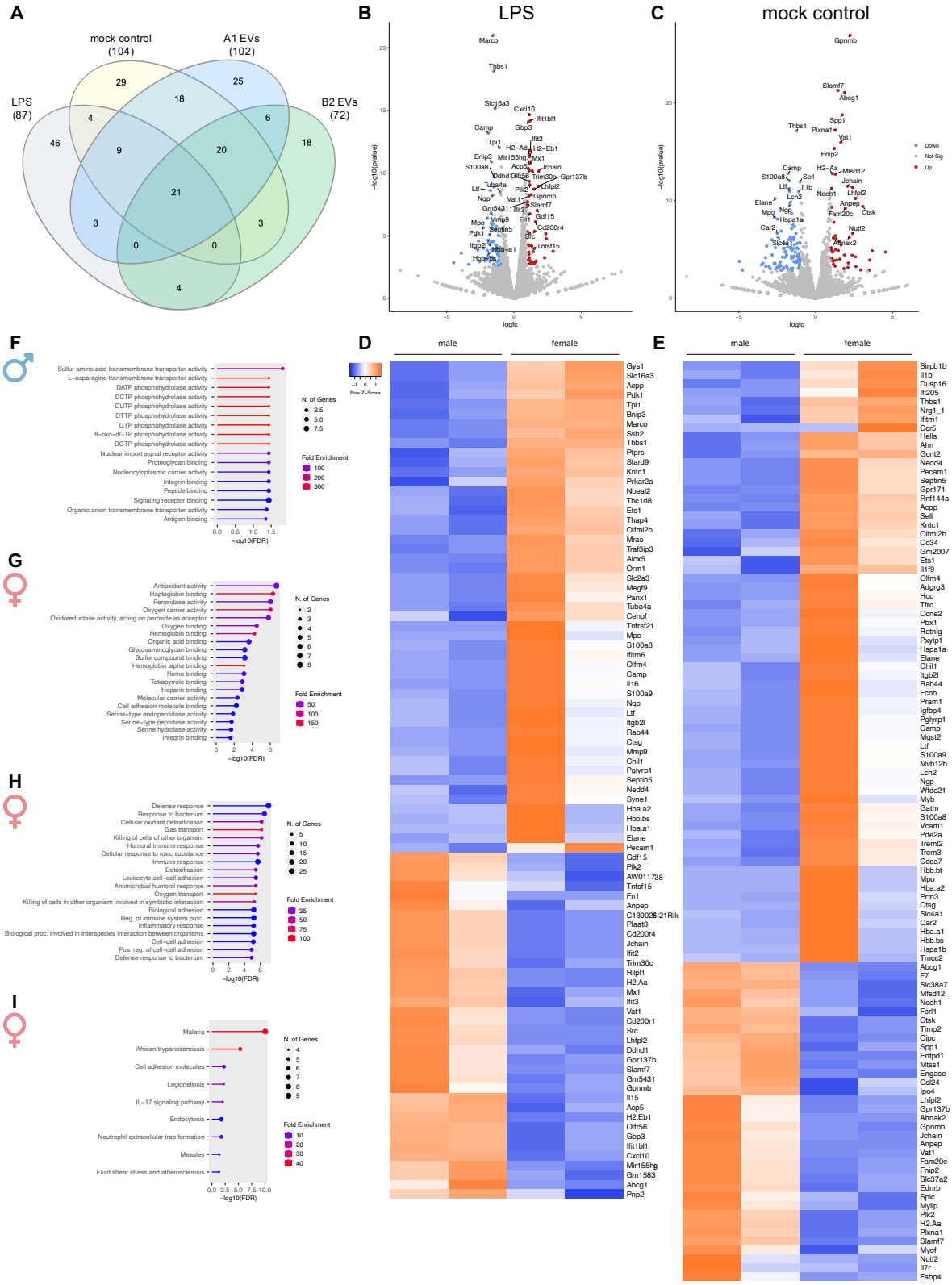

Supplementary figure 11: Analysis of genes differentially expressed between male and female LPS stimulated monocytes and mock controls.

(A) Venn diagram depicting the number of differentially expressed genes shared between or unique to pairwise comparisons of male and female monocytes under LPS stimulation (grey), mock controls (yellow), A1 EV stimulation (blue) or B2 EV stimulation (green). Diagram was created with InteractiVenn[170]. (B, C) Volcano plots depicting relative gene expression between two sample sets according to statistical significance (-log10 of the FDR-adjusted *p* value) versus magnitude of change (logfc = log fold change). Depicted are male versus female LPS stimulated monocytes (B) and mock controls (C). Genes significantly differentially expressed between the two conditions with a fold change ≥ |2| (logfc = 1) and FDR *p* value < 0.05 are colored in blue (downregulated in males/upregulated in females) or red (upregulated in males/downregulated in females). Genes not significantly differentially expressed are colored in grey (not sig). Individual genes of interest

are labeled. Volcano plots were created with Galaxy server[168]. (D, E) Heatmaps depicting the z-score of all significantly differentially expressed genes between male and female LPS stimulated monocytes (D) and mock controls (E). RPKM normalized reads were used for mapping. Orange indicates high expression and blue indicates low expression of the gene. Heatmap created with Heatmapper[169]. (F – I) GO term enrichment analysis of significantly differentially expressed genes. Shown are the top 20 significantly enriched GO terms (or less, if less were statistically significant (FDR 0.05)) sorted by statistical significance (-log10(FDR)). (F) Enriched molecular function GO terms for genes more highly expressed in male mock controls compared with females. (G-I) Enriched molecular function (G), biological process (H) GO terms and KEGG pathways (I) for genes with significantly higher expression in female mock controls compared with males. No significant enrichment for biological process GO terms and KEGG pathways could be detected in genes upregulated in males. GO term enrichment analysis was performed with shinyGO[177].

6.2 Supplementary tables

Supplementary table 1: List of proteins differentially expressed between A1 and B2 EV proteomes.

Identifier	Description	Fold change	-log FDR *p*-value	Sample data binary logarithm					
				A1 - 1	A1 - 2	A1 - 3	B2 - 1	B2 - 2	B2 - 3
EHI_161930	hypothetical protein	-3.18	3.697166	23.52	23.50	23.21	25.01	25.24	24.99
EHI_072010	hypothetical protein	NA	0	X	X	X	22.59	24.67	23.59
EHI_023070	hypothetical protein, conserved	NA	0	X	X	X	23.12	X	22.79
EHI_029580	mannosyltransferase, putative	NA	0	X	X	X	24.20	25.75	X
EHI_130950	hypothetical protein	NA	0	X	X	X	22.35	X	22.69
EHI_148130	beta-N-acetylhexosaminidase, alpha subunit	NA	0	X	X	X	20.00	X	21.59
EHI_181290	syntaxin, putative	NA	0	X	X	X	21.69	X	21.27
EHI_095850	hypothetical protein, conserved	NA	0	X	X	X	20.88	21.74	X
EHI_000610	nucleotide binding protein 2, putative	NA	0	21.59	20.82	20.21	X	X	X
EHI_005910	Rho guanine nucleotide exchange factor, putative	NA	0	19.98	19.96	20.51	X	X	X
EHI_015120	leucine rich repeat protein, BspA family	NA	0	21.28	21.76	21.84	X	X	X
EHI_023500	calmodulin, putative	NA	0	21.41	21.13	20.01	X	X	X
EHI_024230	cysteine synthase A, putative	NA	0	21.19	21.67	21.51	X	X	X
EHI_027710	calcium-transporting P-type ATPase, putative	NA	0	19.97	20.77	19.77	X	X	X
EHI_053130	protein kinase 2, putative	NA	0	22.39	22.26	22.53	X	X	X
EHI_062480	cysteine protease, putative	NA	0	22.06	22.92	22.74	X	X	X
EHI_065490	hypothetical protein	NA	0	21.03	21.30	20.99	X	X	X
EHI_079270	hypothetical protein	NA	0	20.87	22.32	22.52	X	X	X
EHI_094000	hypothetical protein	NA	0	20.70	21.56	21.30	X	X	X
EHI_118160	WD repeat protein	NA	0	20.63	21.10	20.56	X	X	X
EHI_118260	formin homology 2 family protein	NA	0	20.44	21.28	20.92	X	X	X
EHI_119300	Ras family protein	NA	0	21.49	22.76	23.53	X	X	X
EHI_125300	diaphanous protein, putative	NA	0	20.84	20.65	21.20	X	X	X
EHI_125720	hypothetical protein	NA	0	22.35	22.04	22.88	X	X	X
EHI_129740	Rab family GTPase	NA	0	20.00	21.41	20.94	X	X	X
EHI_131970	competence protein ComEC, putative	NA	0	21.41	22.11	21.91	X	X	X
EHI_136210	soluble NSF attachment protein gamma isoform, putative	NA	0	20.40	20.81	21.39	X	X	X
EHI_140680	hypothetical protein	NA	0	21.09	21.25	21.07	X	X	X
EHI_153770	phosphatidylinositol-4-phosphate 5-kinase, putative	NA	0	19.52	21.79	21.82	X	X	X
EHI_169580	nucleoside transporter, putative	NA	0	22.19	23.54	24.11	X	X	X
EHI_185600	citrate transporter, putative	NA	0	21.18	21.57	21.24	X	X	X
EHI_192760	copine, putative	NA	0	20.28	21.45	21.61	X	X	X
EHI_001070	LIM zinc finger domain containing protein	NA	0	X	20.38	21.85	X	X	X
EHI_004370	hypothetical protein	NA	0	20.41	X	19.89	X	X	X
EHI_009940	clathrin adaptor complex small chain, putative	NA	0	X	22.70	21.51	X	X	X
EHI_012330	serine-threonine-isoleucine rich protein, putative	NA	0	X	22.01	21.43	X	X	X
EHI_012510	hypothetical protein	NA	0	X	20.51	21.08	X	X	X
EHI_013040	adaptor protein (AP) family protein	NA	0	X	20.26	19.72	X	X	X
EHI_015300	hypothetical protein, conserved	NA	0	X	22.37	22.39	X	X	X
EHI_016410	hypothetical protein	NA	0	X	20.43	20.35	X	X	X
EHI_022260	hypothetical protein	NA	0	X	21.87	22.72	X	X	X
EHI_038800	actin binding protein, putative	NA	0	X	22.69	23.76	X	X	X
EHI_040620	hypothetical protein	NA	0	X	20.31	20.66	X	X	X
EHI_042210	hypothetical protein	NA	0	X	19.78	21.28	X	X	X

EHI_042870	cell surface protease gp63, putative	NA	0	X	24.00	24.55	X	X	X
EHI_049320	hypothetical protein	NA	0	X	22.46	21.02	X	X	X
EHI_050690	hypothetical protein	NA	0	20.33	20.45	X	X	X	X
EHI_052870	ENTH domain protein, putative	NA	0	20.50	20.44	X	X	X	X
EHI_059860	C2 domain containing protein	NA	0	X	24.02	24.55	X	X	X
EHI_064680	alpha-soluble NSF attachment protein, putative	NA	0	X	19.72	21.23	X	X	X
EHI_069320	C2 domain containing protein	NA	0	X	24.53	23.99	X	X	X
EHI_074060	Rap/Ran GTPase-activating protein, putative	NA	0	X	21.53	22.09	X	X	X
EHI_081790	protein kinase domain containing protein	NA	0	X	20.10	20.29	X	X	X
EHI_082070	Rab family GTPase	NA	0	X	23.57	23.36	X	X	X
EHI_092680	hypothetical protein, conserved	NA	0	X	23.49	23.29	X	X	X
EHI_094360	hypothetical protein	NA	0	X	20.91	22.59	X	X	X
EHI_100080	acid sphingomyelinase-like phosphodiesterase, putative	NA	0	19.76	20.30	X	X	X	X
EHI_103730	threonyl-tRNA synthetase, putative	NA	0	20.88	X	20.94	X	X	X
EHI_104420	hypothetical protein	NA	0	21.50	X	20.32	X	X	X
EHI_113950	hypothetical protein, conserved	NA	0	X	19.74	19.63	X	X	X
EHI_121780	enhancer binding protein-1	NA	0	21.19	X	20.74	X	X	X
EHI_124860	protein kinase, putative	NA	0	X	22.19	21.93	X	X	X
EHI_125020	hypothetical protein	NA	0	X	20.97	22.19	X	X	X
EHI_125930	protein kinase, putative	NA	0	22.00	X	21.46	X	X	X
EHI_126270	Ras GTPase-activating protein, putative	NA	0	X	21.35	21.90	X	X	X
EHI_131540	Rho guanine nucleotide exchange factor, putative	NA	0	X	18.93	20.25	X	X	X
EHI_134660	hypothetical protein	NA	0	20.45	X	20.83	X	X	X
EHI_136460	hypothetical protein	NA	0	X	19.60	19.79	X	X	X
EHI_140740	hypothetical protein	NA	0	19.87	X	20.86	X	X	X
EHI_143440	calmodulin, putative	NA	0	20.86	X	20.39	X	X	X
EHI_148870	hypothetical protein	NA	0	X	20.22	20.55	X	X	X
EHI_150120	hypothetical protein	NA	0	23.56	X	23.29	X	X	X
EHI_151380	hypothetical protein, conserved	NA	0	20.41	X	22.89	X	X	X
EHI_152570	60S ribosomal protein L26, putative	NA	0	20.60	X	20.97	X	X	X
EHI_153480	translation initiation factor 2 beta subunit, putative	NA	0	20.66	X	21.41	X	X	X
EHI_156230	transporter, major facilitator family	NA	0	21.13	22.39	X	X	X	X
EHI_161020	hypothetical protein	NA	0	X	21.34	20.90	X	X	X
EHI_168300	hypothetical protein	NA	0	21.90	22.27	X	X	X	X
EHI_169280	Rab family GTPase	NA	0	X	23.32	23.06	X	X	X
EHI_172170	hypothetical protein	NA	0	X	19.42	19.07	X	X	X
EHI_189140	ARF GTPase activating protein, putative	NA	0	X	21.14	20.97	X	X	X
EHI_189940	60S ribosomal protein L34	NA	0	22.98	X	24.25	X	X	X
EHI_192540	serine/threonine protein kinase STE20, putative	NA	0	X	21.40	21.45	X	X	X
EHI_192960	PH domain containing protein	NA	0	X	21.19	21.17	X	X	X
EHI_200080	purine nucleoside phosphorylase, putative	NA	0	19.85	19.11	X	X	X	X
EHI_201420	predicted protein	NA	0	20.30	X	19.89	X	X	X

Marked in yellow are proteins that are not also differentially expressed in whole amoeba proteomes. NA = not applicable

Supplementary table 2: Molecular function GO term enrichment analysis of EV proteins unique to A1.

GO term	Hits back-ground	Hits EV list	Protein ID	Fold enrich-ment	*p*-value	FDR *p*-value
GO:0005215 transporter activity	156	8	EHI_009940,EHI_027710,EHI_064680, EHI_104420,EHI_136210,EHI_156230, EHI_169580,EHI_185600	4.6	0.000281	0.033502
GO:0004829 threonine-tRNA ligase activity	1	1	EHI_103730	89.69	0.011149	0.222155
GO:0022857 transmembrane transporter activity	132	5	EHI_027710,EHI_104420,EHI_156230, EHI_169580,EHI_185600	3.4	0.015079	0.222155
GO:0005509 calcium ion binding	50	3	EHI_023500,EHI_050690,EHI_143440	5.38	0.017727	0.222155
GO:0017048 Rho GTPase binding	2	1	EHI_125300	44.85	0.022176	0.222155
GO:0016308 1-phosphatidylinositol-4-phosphate 5-kinase activity	2	1	EHI_153770	44.85	0.022176	0.222155
GO:0016307 phosphatidylinositol phosphate kinase activity	2	1	EHI_153770	44.85	0.022176	0.222155
GO:0004767 sphingomyelin phosphodiesterase activity	60	3	EHI_100080,EHI_129740,EHI_169280	4.48	0.028640	0.222155
GO:0003924 GTPase activity	213	6	EHI_052870,EHI_082070,EHI_094000, EHI_119300,EHI_129740,EHI_169280	2.53	0.029816	0.222155
GO:0004124 cysteine synthase activity	3	1	EHI_024230	29.9	0.033083	0.222155
GO:0005337 nucleoside transmembrane transporter activity	3	1	EHI_169580	29.9	0.033083	0.222155
GO:0005544 calcium-dependent phospholipid binding	3	1	EHI_192760	29.9	0.033083	0.222155
GO:0008081 phosphoric diester hydrolase activity	68	3	EHI_100080,EHI_129740,EHI_169280	3.96	0.039431	0.222155
GO:0005525 GTP binding	294	7	EHI_052870,EHI_082070,EHI_094000, EHI_119300,EHI_129740,EHI_169280, EHI_192960	2.14	0.042875	0.222155
GO:0032561 guanyl ribonucleotide binding	294	7	EHI_052870,EHI_082070,EHI_094000, EHI_119300,EHI_129740,EHI_169280, EHI_192960	2.14	0.042875	0.222155
GO:0019001 guanyl nucleotide binding	295	7	EHI_052870,EHI_082070,EHI_094000, EHI_119300,EHI_129740,EHI_169280, EHI_192960	2.13	0.043545	0.222155
GO:0140312 cargo adaptor activity	4	1	EHI_009940	22.42	0.043870	0.222155
GO:0022884 macromolecule transmembrane transporter activity	4	1	EHI_104420	22.42	0.043870	0.222155
GO:0035615 clathrin adaptor activity	4	1	EHI_009940	22.42	0.043870	0.222155
GO:0008320 protein transmembrane transporter activity	4	1	EHI_104420	22.42	0.043870	0.222155
GO:0140318 protein transporter activity	4	1	EHI_104420	22.42	0.043870	0.222155
GO:0004620 phospholipase activity	72	3	EHI_100080,EHI_129740,EHI_169280	3.74	0.045501	0.222155

Supplementary table 3: List of selected EV markers and other proteins of interest in *E. histolytica* EV proteomes.

Identifier	Description	Fold change	-log FDR *p*-value	Sample data binary logarithm					
				A1 - 1	A1 - 2	A1 - 3	B2 - 1	B2 - 2	B2 - 3
EHI_025360	14-3-3 protein 1	-1.47	1.911130	21.74	21.70	21.81	22.35	22.49	22.07
EHI_098280	14-3-3 protein 2	-1.22	0.362881	23.51	22.57	22.56	23.10	23.35	23.05
EHI_006810	14-3-3 protein 3	1.34	0.592581	24.53	24.74	24.99	24.40	23.81	24.79
EHI_199590	70 kDa heat shock protein, putative	-1.21	0.290534	26.04	26.26	25.29	26.45	25.69	26.26
EHI_163480	90 kDa heat shock protein, putative	1.11	0.132491	25.95	26.53	25.84	26.55	25.35	25.98
EHI_137720	ADP-ribosylation factor 1, putative	-1.20	1.069917	25.04	25.06	24.95	25.22	25.13	25.50
EHI_194500	ADP-ribosylation factor, putative	1.74	2.001923	22.98	22.81	22.90	22.37	21.80	22.13
EHI_134840	ADP-ribosylation factor, putative	1.52	0	19.70	X	20.84	X	X	19.66
EHI_150490	aldehyde-alcohol dehydrogenase 2, putative	1.44	0.705846	29.49	30.08	28.93	28.84	29.13	28.94
EHI_168240	Cysteine proteinase, putative	-1.40	0.159425	29.35	27.83	26.14	28.84	29.04	26.91
EHI_012270	Gal/GalNac lectin heavy subunit	1.76	0.689024	24.81	26.30	26.16	24.45	25.33	25.03
EHI_046650	Gal/GalNac lectin heavy subunit, putative	-1.91	1.316241	22.80	22.23	21.67	23.12	23.10	23.29
EHI_148790	Gal/GalNac lectin light subunit	1.11	0.090855	24.80	25.35	25.07	24.35	26.07	24.35
EHI_006980	Gal/GalNac lectin subunit lgl1	2.27	0.363295	24.65	22.94	22.41	24.26	22.00	20.19
EHI_065330	Gal/GalNac lectin subunit lgl2	1.83	1.373059	26.46	26.39	26.92	25.39	26.20	25.56
EHI_001950	heat shock protein 70 family	-1.07	0.112292	24.62	24.69	24.26	25.00	24.08	24.78
EHI_052860	heat shock protein 70, putative	-1.49	0.716831	23.42	22.75	22.39	23.24	23.20	23.85
EHI_148990	heat shock protein 70, putative	-1.39	0.629844	22.88	22.73	22.38	23.63	22.58	23.21
EHI_196940	heat shock protein 90, putative	-1.10	0.137722	22.12	21.06	21.40	21.65	21.95	21.38
EHI_001420	Peroxiredoxin	-1.30	0.413273	24.15	23.39	22.91	23.57	23.90	24.11

Supplementary table 4: Detection of known and putative tetraspanins in the *E. histolytica* EV and whole cell proteomes.

Identifier	Name[199]	EV proteomes – sample data binary logarithm						Whole cell proteomes – sample data binary logarithm					
		A1 -1	A1 -2	A1 -3	B2 -1	B2 -2	B2 -3	A1 -1	A1 -2	A1 -3	B2 -1	B2 -2	B2 -3
EHI_022890	TSPAN1	24.27	24.51	23.86	24.26	24.77	24.95	25.01	24.89	24.66	25.06	25.09	25.19
EHI_174220	TSPAN2	X	X	X	X	X	X	24.37	24.92	24.67	24.84	25.00	24.83
EHI_075690	TSPAN4	X	23.16	22.46	X	X	21.77	24.96	24.84	24.71	20.95	20.35	X
EHI_133990	TSPAN7	X	X	X	X	X	X	23.37	23.41	23.43	21.83	21.84	X
EHI_091490	TSPAN12	23.91	23.48	23.22	24.29	24.21	24.79	X	X	21.90	23.64	23.78	23.41
EHI_107790	TSPAN13	22.18	X	X	X	X	X	X	X	X	X	X	X
EHI_016390	TSPAN15	X	X	X	X	X	X	22.70	22.45	22.57	23.58	23.51	23.64

Supplementary table 5: Detection of proposed ESCRT proteins in the *E. histolytica* EV proteomes.

Identifier	Predicted protein[200]	Putative ESCRT complex[200]	Sample data binary logarithm					
			A1 - 1	A1 - 2	A1 - 3	B2 - 1	B2 - 2	B2 - 3
EHI_091530	EhHSE1	ESCRT-0	22.19	21.63	20.74	20.40	X	22.03
EHI_135460	EhVPS23	ESCRT-I	26.44	23.06	22.78	26.20	25.96	25.98
EHI_137860	EhVPS25	ESCRT-II	23.02	X	X	22.08	X	22.46
EHI_045320	EhVPS36	ESCRT-II	21.13	X	X	X	X	22.47

Supplementary table 6: Proteins detected in negative control samples.

Identifier	Description	Sample data binary logarithm		
		Control 1	Control 2	Control 3
EHI_008200	glyceraldehyde-3-phosphate dehydrogenase, putative	18.93	19.72	21.69
EHI_052860	heat shock protein 70, putative	18.11	20.10	18.80
EHI_133900	galactose-inhibitable lectin 170 kDa subunit, putative	17.49	17.25	18.61
EHI_182900	actin	18.66	20.66	20.98
EHI_033710	cysteine proteinase 2	19.07	X	21.88
EHI_035690	galactose-inhibitable lectin 35 kda subunit precursor	19.70	X	20.26
EHI_051060	pyruvate:ferredoxin oxidoreductase	18.66	X	16.89
EHI_148790	Gal/GalNAc lectin light subunit	18.99	X	19.14
EHI_164810	Adapter-related protein complex 3 (AP-3) subunit, putative	X	26.87	27.11
EHI_168240	cysteine proteinase, putative	20.65	X	21.61
EHI_005150	hypothetical protein, conserved	X	X	18.06
EHI_006810	14-3-3 protein 3	X	X	19.39
EHI_009530	pyruvate phosphate dikinase	X	X	19.96
EHI_011210	elongation factor 1-alpha 1	X	X	17.93
EHI_015380	immuno-dominant variable surface antigen	X	X	18.85
EHI_047800	hypothetical protein	X	X	18.54
EHI_068340	hypothetical protein	X	19.24	X
EHI_074180	cysteine proteinase 1, putative	X	X	22.93
EHI_099260	hypothetical protein	X	24.18	X
EHI_116360	serine-rich protein	X	X	23.00
EHI_130700	enolase, putative	X	X	21.43
EHI_135190	protein kinase, putative	18.11	X	X
EHI_144270	AIG1 family protein	21.76	X	X
EHI_148900	protein kinase, putative	X	26.94	X
EHI_150490	aldehyde-alcohol dehydrogenase 2, putative	X	X	18.36
EHI_152650	type A flavoprotein, putative	X	X	19.10
EHI_165350	malate dehydrogenase, putative	X	17.84	X
EHI_178960	acetyl-CoA synthetase, putative	X	X	17.08
EHI_188180	phosphoglycerate kinase, putative	X	X	18.10
EHI_198760	alcohol dehydrogenase 3, putative	X	X	18.64

Supplementary table 7: List of the top 50 differentially expressed proteins present in both A1 and B2 trophozoite proteomes.

Identifier	Description	Fold change	-log FDR *p*-value	Sample data binary logarithm					
				A1 - 1	A1 - 2	A1 - 3	B2 - 1	B2 - 2	B2 - 3
EHI_144490	hypothetical protein, conserved	-14.61	5.279277	22.77	23.02	22.83	26.61	26.70	26.92
EHI_159870	galactose-inhibitable lectin small subunit, putative	-10.69	1.836876	X	19.99	21.53	24.27	23.68	24.59
EHI_050570	cysteine proteinase, putative	-10.52	2.150279	20.69	X	21.87	24.81	24.27	24.95
EHI_144610	methionine gamma-lyase	-8.58	1.821689	20.18	20.87	22.43	23.88	23.90	25.00
EHI_156310	Ribonuclease, putative	-7.20	2.731532	20.05	X	20.63	23.45	23.09	23.04
EHI_039610	cysteine proteinase, putative	-5.59	2.893405	21.54	21.45	21.83	24.55	24.15	23.57
EHI_179830	hypothetical protein	-5.40	2.495273	21.06	20.08	20.98	23.58	22.89	22.95
EHI_026480	(2r)-phospho-3-sulfolactate synthase, putative	-5.23	4.404144	24.21	23.92	24.22	26.37	26.51	26.62
EHI_029230	hydrolase yafV, putative	-5.20	3.693129	22.03	21.92	22.45	24.67	24.50	24.37
EHI_073380	carbonic anhydrase, putative	-4.98	2.098846	20.22	19.84	X	21.90	22.34	22.80
EHI_095180	hypothetical protein	-4.81	1.975212	22.61	21.56	22.09	25.09	24.23	23.73
EHI_186820	protein kinase domain containing protein	-4.79	3.949310	23.71	23.92	24.10	26.33	26.19	25.99
EHI_074180	cysteine proteinase 1, putative	-4.73	4.154596	26.97	27.01	26.85	29.41	29.14	29.00
EHI_005060	Fe-hydrogenase, putative	-4.51	4.122509	24.59	24.53	24.28	26.81	26.57	26.53
EHI_071590	protein disulfide isomerase, putative	4.61	2.902496	28.37	28.68	28.18	26.53	26.31	25.77
EHI_098750	hypothetical protein	4.90	1.314062	21.54	23.03	21.25	19.65	19.63	X
EHI_065330	Gal/GalNAc lectin subunit Igl2	4.95	4.016052	27.89	28.06	27.63	25.66	25.59	25.40
EHI_086690	hypothetical protein	4.99	2.851672	26.71	27.35	26.48	24.78	24.31	24.50
EHI_038860	40S ribosomal protein S28, putative	5.14	3.231979	27.74	27.92	27.35	25.17	25.10	25.65
EHI_093330	Helix-turn-helix protein, putative	5.37	2.609755	26.05	26.65	25.58	23.59	24.01	23.41
EHI_158570	actobindin, putative	5.69	2.157767	26.10	27.14	25.97	23.45	24.53	23.71
EHI_119330	serine protease inhibitor, putative	5.80	3.126146	23.95	24.15	23.40	21.43	20.99	21.47
EHI_098570	fructose-1,6-bisphosphate aldolase, putative	5.85	3.406391	30.89	31.34	30.64	28.59	28.22	28.42
EHI_110530	hypothetical protein	5.91	2.621039	23.32	23.32	22.73	20.66	19.96	21.06
EHI_151990	RNA-binding protein, putative	5.93	3.706684	23.80	23.71	23.67	21.34	21.36	20.77
EHI_126870	40S ribosomal protein S21, putative	6.06	1.903807	24.92	25.69	24.07	22.91	22.37	21.60
EHI_048560	hypothetical protein	6.08	2.157813	27.05	27.60	26.79	25.10	24.88	23.65
EHI_118920	Rab family GTPase	6.15	3.868138	23.67	24.00	23.80	20.98	21.50	21.13
EHI_140150	hypothetical protein, conserved	6.51	2.452777	22.59	22.84	21.92	20.36	19.71	19.18
EHI_126880	methionine aminopeptidase, putative	6.56	3.309284	26.75	27.11	26.25	24.15	23.91	23.91
EHI_170060	ubiquitin like protein	6.69	3.543801	26.45	26.06	26.60	23.45	23.47	23.95
EHI_021450	40S ribosomal protein S28, putative	6.95	3.377255	23.55	23.60	23.38	20.40	20.53	21.21
EHI_075660	CAAX prenyl protease, putative	7.02	4.569087	26.01	26.04	25.66	23.18	23.07	23.03
EHI_063040	hypothetical protein	7.31	2.482714	23.92	24.35	23.26	21.44	21.15	20.33
EHI_169820	SNF7 family protein	7.59	2.163746	26.41	26.38	25.19	23.50	23.44	22.27
EHI_119920	DEAD/DEAH box helicase, putative	7.65	2.148017	23.33	23.57	23.37	20.69	21.36	19.41
EHI_119950	leucine-rich repeat containing protein	8.14	3.683536	24.47	24.25	24.36	21.32	20.95	21.73
EHI_017690	hypothetical protein	8.31	1.310009	22.87	24.70	24.04	21.50	22.02	18.93
EHI_119930	protein kinase domain containing protein	8.52	2.828329	23.12	22.69	23.18	19.65	X	20.16
EHI_156560	heat shock protein, putative	8.62	3.718222	23.83	24.61	24.19	21.03	21.22	21.05
EHI_158050	Hsc70-interacting protein, putative	8.90	3.102329	25.40	26.27	25.17	22.44	22.32	22.62
EHI_184220	hypothetical protein	10.38	2.109251	24.79	24.50	24.62	21.41	22.35	20.02
EHI_088060	hypothetical protein	11.58	3.943730	24.29	24.29	24.17	20.88	X	20.56
EHI_057670	20 kDa antigen	12.19	2.523194	25.41	26.96	25.20	22.24	22.40	22.11
EHI_013895	4F5 family protein	14.03	2.225213	25.39	25.85	25.27	21.03	22.35	X
EHI_075640	protein phosphatase domain-containing protein	14.42	3.981081	24.36	24.05	24.46	20.03	20.51	20.77
EHI_114330	hypothetical protein	14.74	1.920091	24.62	22.86	23.11	X	19.63	19.66
EHI_039330	hypothetical protein, conserved	16.20	2.050549	23.43	24.37	22.48	20.24	19.84	18.14
EHI_075690	hypothetical protein	18.21	3.388307	24.96	24.84	24.71	20.95	20.35	X
EHI_068650	hypothetical protein	23.19	3.044325	23.67	24.53	23.68	18.72	19.36	20.19

Supplementary table 8: List of proteins detected in A1, but not B2 amebae proteomes.

Identifier	Description	Sample data binary logarithm					
		A1 - 1	A1 - 2	A1 - 3	B2 - 1	B2 - 2	B2 - 3
EHI_000570	hypothetical protein	23.34	23.42	23.80	X	X	X
EHI_000590	40S ribosomal protein S6, putative	23.04	23.16	22.37	X	X	X
EHI_001140	hypothetical protein	21.42	21.45	20.89	X	X	X
EHI_001980	hypothetical protein	20.59	20.27	20.60	X	X	X
EHI_004940	hypothetical protein	20.30	20.22	20.22	X	X	X
EHI_006160	signal recognition particle 19 kDa protein, putative	18.54	18.40	18.78	X	X	X
EHI_006830	hypothetical protein	22.64	22.39	22.19	X	X	X
EHI_006840	hypothetical protein	21.82	21.67	21.78	X	X	X
EHI_006950	hypothetical protein, conserved	21.71	22.35	21.37	X	X	X
EHI_007280	hypothetical protein	17.99	18.26	18.46	X	X	X
EHI_009800	phosphatidylserine synthase, putative	23.28	23.29	23.30	X	X	X
EHI_010060	RNA recognition motif domain containing protein	24.19	24.72	23.27	X	X	X
EHI_012080	hypothetical protein	19.92	20.57	20.40	X	X	X
EHI_014260	small GTP-binding protein domain, pseudogene	22.77	22.23	23.35	X	X	X
EHI_015290	C2 domain protein, putative	27.73	27.60	27.60	X	X	X
EHI_020070	hypothetical protein	22.04	22.50	22.75	X	X	X
EHI_021240	hypothetical protein	21.03	21.72	21.18	X	X	X
EHI_021460	hypothetical protein	21.45	21.13	21.65	X	X	X
EHI_024670	hypothetical protein, conserved	20.47	20.33	20.42	X	X	X
EHI_025700	serine-threonine-isoleucine rich protein, putative	22.49	22.51	22.57	X	X	X
EHI_027760	DEAD/DEAH box helicase, putative	18.84	18.53	18.88	X	X	X
EHI_037160	hypothetical protein	24.65	25.67	24.51	X	X	X
EHI_038600	splicing factor 3A subunit 3, putative	20.26	20.69	20.53	X	X	X
EHI_042870	cell surface protease gp63, putative	22.36	22.45	22.66	X	X	X
EHI_045200	hypothetical protein	21.69	21.53	21.66	X	X	X
EHI_048670	WH2 motif domain containing protein	21.03	20.80	20.79	X	X	X
EHI_049590	adaptor protein (AP) family protein	21.25	20.78	22.04	X	X	X
EHI_049970	RNA recognition motif domain containing protein	21.03	21.98	21.39	X	X	X
EHI_050980	hypothetical protein	22.82	22.77	22.67	X	X	X
EHI_051760	hypothetical protein	22.36	23.10	21.86	X	X	X
EHI_053030	hypothetical protein	20.46	20.35	21.07	X	X	X
EHI_053610	apyrase, putative	21.34	21.29	21.20	X	X	X
EHI_054130	hypothetical protein	21.45	21.69	21.59	X	X	X
EHI_055350	SH3 domain containing protein	22.15	22.03	22.35	X	X	X
EHI_055690	hypothetical protein	21.22	21.41	21.07	X	X	X
EHI_056450	Rho GTPase activating protein, putative	20.09	20.92	20.22	X	X	X
EHI_058810	mRNA decapping protein, putative	20.45	20.20	20.98	X	X	X
EHI_059860	C2 domain containing protein	25.59	25.69	25.59	X	X	X
EHI_060430	Uro-adherence factor A precursor, putative	22.46	22.50	22.37	X	X	X
EHI_062500	hypothetical protein	20.94	21.47	21.47	X	X	X
EHI_065720	hypothetical protein, conserved	21.23	20.91	21.36	X	X	X
EHI_067940	hypothetical protein, conserved	22.20	22.56	22.48	X	X	X
EHI_068670	hypothetical protein	23.08	23.33	22.84	X	X	X
EHI_069320	C2 domain containing protein	27.21	27.12	27.39	X	X	X
EHI_069370	vesicle-associated membrane protein, putative	21.44	21.91	21.03	X	X	X
EHI_075700	casein kinase II regulatory subunit family protein	22.71	22.13	22.84	X	X	X
EHI_075840	hypothetical protein	20.67	20.68	20.56	X	X	X
EHI_078180	hypothetical protein	21.58	22.30	21.85	X	X	X
EHI_082070	Rab family GTPase	24.39	24.34	24.36	X	X	X
EHI_085950	hypothetical protein	21.36	21.15	21.17	X	X	X
EHI_086580	vacuolar protein sorting-associated protein 35, putative	22.37	22.46	22.90	X	X	X
EHI_087340	hypothetical protein	22.24	22.39	21.38	X	X	X
EHI_091060	ATPase, AAA family protein	20.21	20.00	20.23	X	X	X
EHI_092200	hypothetical protein	23.23	22.80	23.26	X	X	X
EHI_092520	hypothetical protein	22.01	22.66	22.18	X	X	X
EHI_093880	DNA repair protein Rad21, putative	21.74	21.87	21.81	X	X	X

EHI_095830	hypothetical protein	20.89	20.98	20.97	X	X	X
EHI_098620	hypothetical protein	21.84	21.61	21.79	X	X	X
EHI_098810	ribosome biogenesis regulatory protein, putative	22.88	23.38	23.08	X	X	X
EHI_100500	hypothetical membrane-spanning protein	21.16	21.38	21.44	X	X	X
EHI_103530	DNA primase small subunit, putative	21.31	21.37	21.34	X	X	X
EHI_103650	phosphoglycerate mutase family protein, putative	21.65	21.87	21.98	X	X	X
EHI_107120	RNA recognition motif domain containing protein	22.42	22.42	22.56	X	X	X
EHI_109000	hypothetical protein	21.93	21.18	21.38	X	X	X
EHI_110460	hypothetical protein	22.61	23.03	22.40	X	X	X
EHI_111800	hypothetical protein	21.57	21.85	21.53	X	X	X
EHI_115280	hypothetical protein	21.11	21.28	20.82	X	X	X
EHI_115340	hypothetical protein	20.87	20.89	21.02	X	X	X
EHI_115350	chromodomain-helicase-DNA-binding protein, putative	20.48	20.58	20.66	X	X	X
EHI_118130	C2 domain containing protein	23.83	23.85	24.24	X	X	X
EHI_119350	hypothetical protein	20.24	20.15	20.22	X	X	X
EHI_119370	hypothetical protein	21.07	20.50	21.28	X	X	X
EHI_119530	kinesin, putative	22.82	22.84	23.09	X	X	X
EHI_119620	DEAD/DEAH box helicase, putative	20.90	21.06	20.94	X	X	X
EHI_121770	hypothetical protein	22.18	22.94	22.26	X	X	X
EHI_121790	ser/thr protein phosphatase family protein	20.97	21.05	21.26	X	X	X
EHI_122720	hypothetical protein	22.16	21.87	21.74	X	X	X
EHI_124620	hypothetical protein	22.16	22.88	22.10	X	X	X
EHI_133330	5'-3' exonuclease domain containing protein	21.42	20.83	21.07	X	X	X
EHI_134670	hypothetical protein	21.20	21.76	21.54	X	X	X
EHI_134800	ankyrin repeat protein, putative	21.47	21.80	21.22	X	X	X
EHI_135140	hypothetical protein, conserved	20.79	20.93	20.84	X	X	X
EHI_137970	proteasome subunit beta Type 4 precursor, putative	19.75	19.08	19.67	X	X	X
EHI_138350	hypothetical protein	21.89	22.05	22.14	X	X	X
EHI_138370	hypothetical protein, conserved	21.17	21.66	20.78	X	X	X
EHI_138760	hypothetical protein	22.32	22.10	22.12	X	X	X
EHI_138970	hypothetical protein	21.57	21.67	21.31	X	X	X
EHI_140140	gtpase activating protein, putative	22.72	22.74	22.58	X	X	X
EHI_141010	hypothetical protein	21.40	21.53	21.11	X	X	X
EHI_141380	leucine-rich repeat containing protein	21.32	21.58	21.17	X	X	X
EHI_141870	protein kinase domain containing protein	22.27	21.71	21.97	X	X	X
EHI_143080	hypothetical protein	22.26	22.41	22.17	X	X	X
EHI_145610	hypothetical protein, conserved	21.38	21.99	21.42	X	X	X
EHI_147560	hypothetical protein	21.74	21.69	21.30	X	X	X
EHI_148020	hypothetical protein, conserved	23.14	23.01	23.21	X	X	X
EHI_148140	hypothetical protein	21.55	22.18	21.43	X	X	X
EHI_152980	C2 domain containing protein	20.76	20.75	21.64	X	X	X
EHI_153280	hypothetical protein, conserved	21.53	21.74	21.70	X	X	X
EHI_159750	hypothetical protein	23.02	24.15	23.09	X	X	X
EHI_165150	myosin heavy chain, putative	22.35	22.81	22.62	X	X	X
EHI_167680	hypothetical protein	21.01	20.76	21.05	X	X	X
EHI_168230	hypothetical protein	23.16	23.11	23.16	X	X	X
EHI_168290	hypothetical protein	21.24	21.52	21.21	X	X	X
EHI_169080	hypothetical protein	22.06	21.97	21.82	X	X	X
EHI_169280	Rab family GTPase	25.56	25.74	25.63	X	X	X
EHI_170050	hypothetical protein	21.53	22.26	21.45	X	X	X
EHI_170130	hypothetical protein	22.84	23.92	22.05	X	X	X
EHI_174210	serine/threonine-protein kinase, putative	21.25	20.61	20.64	X	X	X
EHI_177350	hypothetical protein	21.86	21.69	21.97	X	X	X
EHI_177580	citrate transporter, putative	21.42	21.16	21.33	X	X	X
EHI_183120	centromeric protein E, putative	22.17	22.48	22.02	X	X	X
EHI_184540	protein kinase, putative	23.58	23.39	23.27	X	X	X
EHI_184560	hypothetical protein, conserved	22.14	22.48	22.01	X	X	X
EHI_187090	Rab family GTPase	23.21	23.51	22.71	X	X	X
EHI_188090	hypothetical protein, conserved	21.55	21.37	21.25	X	X	X
EHI_188830	DnaJ domain containing protein	22.07	22.26	21.41	X	X	X

EHI_189500	calponin homology domain protein, putative	20.08	20.22	19.93	X	X	X
EHI_189540	hypothetical protein	22.86	23.86	22.24	X	X	X
EHI_189950	co-chaperone protein, putative	21.25	21.33	20.85	X	X	X
EHI_190870	hypothetical protein	22.12	22.83	22.02	X	X	X
EHI_194240	hypothetical protein	23.43	24.07	23.02	X	X	X
EHI_194320	hypothetical protein	21.49	21.38	21.24	X	X	X
EHI_194360	hypothetical protein	21.04	21.11	21.12	X	X	X
EHI_194400	SNF7 family protein	22.02	22.76	21.73	X	X	X
EHI_196550	Rap/Ran GTPase-activating protein, putative	21.34	20.87	20.97	X	X	X
EHI_196580	phosphoribulokinase /uridine kinase family protein	22.33	22.30	21.86	X	X	X
EHI_196940	heat shock protein 90, putative	24.28	24.37	24.35	X	X	X
EHI_198590	hypothetical protein	20.59	20.88	20.47	X	X	X
EHI_200800	hypothetical protein	21.16	21.65	21.07	X	X	X
EHI_002200	hypothetical protein, conserved	X	22.41	21.74	X	X	X
EHI_006780	Rab GTPase activating protein, putative	19.78	X	19.55	X	X	X
EHI_008050	ankyrin repeat protein, putative	21.00	X	20.89	X	X	X
EHI_009590	serine/threonine protein kinase, putative	20.28	X	19.42	X	X	X
EHI_010010	hypothetical protein	X	19.24	19.87	X	X	X
EHI_010020	calmodulin, putative	21.56	21.40	X	X	X	X
EHI_010680	Sand family protein	23.54	X	23.59	X	X	X
EHI_011860	hypothetical protein	18.63	X	19.39	X	X	X
EHI_014000	Retinoblatoma-binding protein 6, putative	20.86	20.69	X	X	X	X
EHI_014250	hypothetical protein	22.43	23.21	X	X	X	X
EHI_014320	adenosine deaminase, putative	19.74	20.93	X	X	X	X
EHI_017720	zinc finger protein, putative	22.94	23.04	X	X	X	X
EHI_018610	hypothetical protein	20.37	21.03	X	X	X	X
EHI_019090	hypothetical protein, conserved	21.44	22.74	X	X	X	X
EHI_019640	caldesmon, putative	X	23.02	21.70	X	X	X
EHI_020210	Ras guanine nucleotide exchange factor, putative	20.48	X	19.79	X	X	X
EHI_029570	methyltransferase, putative	21.67	X	21.49	X	X	X
EHI_030720	cysteine protease, putative	19.80	X	20.25	X	X	X
EHI_045010	hypothetical protein, conserved	22.37	21.86	X	X	X	X
EHI_045170	U5 snRNP-specific 200kd protein, putative	20.03	20.22	X	X	X	X
EHI_049730	hypothetical protein	19.57	19.34	X	X	X	X
EHI_050900	N-system amino acid transporter 1, putative	21.68	X	21.66	X	X	X
EHI_054790	tRNA nucleotidyltransferase, putative	21.58	21.64	X	X	X	X
EHI_065290	acetyltransferase, GNAT family	19.33	18.34	X	X	X	X
EHI_067880	hypothetical protein	21.32	21.85	X	X	X	X
EHI_068160	tyrosine kinase, putative	19.86	20.03	X	X	X	X
EHI_068400	major facilitator superfamily transporter, putative	20.98	X	21.03	X	X	X
EHI_069240	hypothetical protein	X	22.11	21.85	X	X	X
EHI_070800	hypothetical protein	19.21	X	19.39	X	X	X
EHI_072030	nucleosome assembly protein, putative	20.49	20.56	X	X	X	X
EHI_072050	Viral A-type inclusion protein repeat, putative	20.23	20.00	X	X	X	X
EHI_073330	phospholipase, patatin family protein	20.02	X	20.34	X	X	X
EHI_074080	hypothetical protein	X	22.78	21.84	X	X	X
EHI_079280	hypothetical protein	21.90	X	22.00	X	X	X
EHI_079960	hypothetical protein, conserved	21.00	21.25	X	X	X	X
EHI_081380	hypothetical protein	23.46	X	23.09	X	X	X
EHI_086200	hypothetical protein	22.86	23.24	X	X	X	X
EHI_086560	hypothetical protein	20.48	20.66	X	X	X	X
EHI_087710	hypothetical protein, conserved	X	22.67	22.72	X	X	X
EHI_088450	inositol polyphosphate 5-phosphatase, putative	25.20	X	24.32	X	X	X
EHI_090010	ubiquitin-like protein 5, putative	21.12	21.86	X	X	X	X
EHI_092400	hypothetical protein	20.78	21.32	X	X	X	X
EHI_099340	hypothetical protein	X	22.00	21.31	X	X	X
EHI_099750	hypothetical protein	22.10	22.09	X	X	X	X
EHI_104760	hypothetical protein	21.31	X	21.66	X	X	X
EHI_105240	BAR/SH3 domain containing protein	21.17	X	20.95	X	X	X
EHI_105300	cell division protein kinase, putative	22.87	X	23.13	X	X	X

EHI_109870	hypothetical protein	22.69	23.00	X	X	X	X
EHI_111770	hypothetical protein	19.28	X	19.70	X	X	X
EHI_111850	transporter, auxin efflux carrier (AEC) family	X	22.39	21.94	X	X	X
EHI_120470	hypothetical protein	21.43	X	20.75	X	X	X
EHI_124470	leucine-rich repeat containing protein	21.14	X	21.52	X	X	X
EHI_124600	ubiquitin-protein ligase, putative	19.45	X	19.59	X	X	X
EHI_125600	hypothetical protein	20.65	21.23	X	X	X	X
EHI_126210	histone H2A, putative	X	23.02	22.48	X	X	X
EHI_129370	hypothetical protein	24.34	X	24.38	X	X	X
EHI_131070	Pten 3-phosphoinositide phosphatase, putative	X	19.82	20.22	X	X	X
EHI_134980	hypothetical protein	X	21.30	20.65	X	X	X
EHI_137820	hypothetical protein	22.55	X	21.59	X	X	X
EHI_138050	hypothetical protein, conserved	22.24	21.87	X	X	X	X
EHI_143120	hypothetical protein	23.07	21.95	X	X	X	X
EHI_147530	DNA primase large subunit, putative	X	21.31	22.03	X	X	X
EHI_148930	helicase, putative	X	20.81	19.80	X	X	X
EHI_150430	villidin, putative	X	20.19	20.61	X	X	X
EHI_151470	hypothetical protein	20.89	20.43	X	X	X	X
EHI_152060	hypothetical protein	20.28	20.04	X	X	X	X
EHI_152670	malate dehydrogenase, putative	X	23.91	23.84	X	X	X
EHI_156210	Ras GTPase-activating protein, putative	X	20.33	20.43	X	X	X
EHI_158610	Activator 1 140 kDa subunit, putative	20.75	20.63	X	X	X	X
EHI_160890	hypothetical protein	20.79	X	21.12	X	X	X
EHI_170370	hypothetical protein	20.96	21.40	X	X	X	X
EHI_174960	60S ribosomal protein L24, putative	20.88	X	21.22	X	X	X
EHI_177610	hypothetical protein, conserved	22.34	22.49	X	X	X	X
EHI_178680	Rho family GTPase	19.52	X	19.78	X	X	X
EHI_179020	hypothetical protein	20.73	20.83	X	X	X	X
EHI_179870	hypothetical protein	20.92	X	20.60	X	X	X
EHI_179880	hypothetical protein	22.90	X	23.12	X	X	X
EHI_181150	hypothetical protein	20.49	X	19.78	X	X	X
EHI_183050	DnaJ domain containing protein	20.67	21.82	X	X	X	X
EHI_186320	hypothetical protein	21.84	21.82	X	X	X	X
EHI_186980	hypothetical protein	X	21.75	20.96	X	X	X
EHI_193840	protein kinase, putative	22.81	22.92	X	X	X	X
EHI_196540	IBR domain containing protein	19.27	X	19.87	X	X	X
EHI_201080	protein kinase domain containing protein	21.63	20.94	X	X	X	X
EHI_202470	arginine N-methyltransferase protein, putative	22.28	22.38	X	X	X	X

Supplementary table 9: List of proteins detected in B2, but not A1 amebae proteomes.

Identifier	Description	Sample data binary logarithm					
		A1 - 1	A1 - 2	A1 - 3	B2 - 1	B2 - 2	B2 - 3
EHI_002560	heat shock protein 70, putative	X	X	X	24.67	25.49	X
EHI_012040	poly(A) polymerase, putative	X	X	X	X	21.84	21.85
EHI_014140	hypothetical protein	X	X	X	23.27	23.42	X
EHI_020330	hypothetical protein	X	X	X	24.57	24.98	X
EHI_021400	exosome component 10, putative	X	X	X	X	20.31	20.08
EHI_040340	hypothetical protein	X	X	X	25.67	X	25.52
EHI_049500	SAC3/GANP family protein	X	X	X	19.40	19.49	X
EHI_054720	CDP-alcohol phosphatidyltransferase family protein	X	X	X	X	21.85	22.31
EHI_058110	hypothetical protein	X	X	X	20.97	20.98	X
EHI_092530	protein kinase, putative	X	X	X	X	20.62	21.22
EHI_096640	EF-hand calcium-binding domain containing protein	X	X	X	X	20.75	21.20
EHI_096770	acetyltransferase, putative	X	X	X	22.23	X	22.39
EHI_100130	hypothetical protein	X	X	X	22.39	X	22.82
EHI_113900	prefoldin subunit 2, putative	X	X	X	20.99	20.11	X
EHI_114950	hypothetical protein, conserved	X	X	X	X	21.43	21.92
EHI_117590	tyrosine kinase, putative	X	X	X	18.54	19.01	X
EHI_146500	Rho GTPase activating protein, putative	X	X	X	19.87	20.04	X
EHI_152120	hypothetical protein	X	X	X	X	20.37	21.37
EHI_152880	alpha-amylase family protein	X	X	X	21.47	X	21.84
EHI_163660	hypothetical protein	X	X	X	X	21.28	21.45
EHI_166440	zinc finger domain containing protein	X	X	X	20.91	20.90	X
EHI_178090	ankyrin repeat protein, putative	X	X	X	19.32	20.03	X
EHI_180780	hypothetical protein	X	X	X	22.00	21.86	X
EHI_182690	hypothetical protein	X	X	X	20.40	20.47	X
EHI_183480	60S ribosomal protein L27, putative	X	X	X	26.56	26.39	X
EHI_193480	serine/threonine protein phosphatase PP2A catalytic subunit, putative	X	X	X	X	19.45	19.64
EHI_197440	hypothetical protein	X	X	X	20.87	20.64	X
EHI_011840	hypothetical protein	X	X	X	21.42	21.49	21.67
EHI_012440	hypothetical protein	X	X	X	23.01	22.29	22.10
EHI_013240	hypothetical protein	X	X	X	22.60	22.81	23.01
EHI_013870	dimethyladenosine transferase, putative	X	X	X	21.17	21.30	21.27
EHI_014170	hypothetical protein	X	X	X	22.71	22.86	22.28
EHI_022490	AIG family protein	X	X	X	22.77	22.63	23.19
EHI_031360	lecithin:cholesterol acyltransferase domain-containing protein	X	X	X	21.04	21.29	22.25
EHI_031950	hypothetical protein	X	X	X	21.78	21.91	22.44
EHI_038670	protein kinase domain containing protein	X	X	X	20.21	20.42	20.97
EHI_039600	hypothetical protein	X	X	X	20.84	21.10	20.85
EHI_040380	hypothetical protein, conserved	X	X	X	20.35	20.39	20.46
EHI_049370	LSM domain containing protein	X	X	X	19.87	20.14	20.07
EHI_062960	hypothetical protein	X	X	X	25.08	24.70	24.45
EHI_067860	malate dehydrogenase, putative	X	X	X	21.62	21.28	21.69
EHI_079910	Rap/Ran GTPase-activating protein, putative	X	X	X	21.28	21.60	21.90
EHI_086030	hypothetical protein	X	X	X	20.64	20.62	20.67
EHI_087390	Rho family GTPase	X	X	X	22.74	22.51	22.06
EHI_096240	hypothetical protein	X	X	X	22.08	22.00	22.57
EHI_104570	ubiquitin ligase, putative	X	X	X	20.42	20.70	20.82
EHI_125820	PH domain containing protein kinase, putative	X	X	X	20.78	20.86	21.17
EHI_153100	alpha-amylase, putative	X	X	X	21.74	21.74	21.10
EHI_166020	TBC domain containing protein	X	X	X	21.91	21.79	21.83
EHI_169670	hypothetical protein	X	X	X	24.24	23.84	23.28
EHI_180390	AIG1 family protein, putative	X	X	X	21.41	21.58	21.80
EHI_194540	pore-forming peptide amoebapore B precursor, putative	X	X	X	20.43	20.58	22.97
EHI_195010	hypothetical protein	X	X	X	21.59	21.42	21.05

Supplementary table 10: Molecular function GO term enrichment analysis of proteins more highly expressed in A1 amebae compared with B2 amebae.

GO term	Hits back-ground	Hits EV list	Protein ID	Fold enrich-ment	*p* value	FDR *p* value
GO:0003676 nucleic acid binding	593	50	EHI_006160,EHI_009470,EHI_010060,EHI_014000, EHI_017720,EHI_019640,EHI_026330,EHI_026440, EHI_027760,EHI_038600,EHI_045170,EHI_045480, EHI_048210,EHI_049970,EHI_053830,EHI_054790, EHI_055430,EHI_055640,EHI_056380,EHI_058810, EHI_063040,EHI_067880,EHI_085970,EHI_086110, EHI_086540,EHI_093330,EHI_099740,EHI_103830, EHI_107120,EHI_115350,EHI_119620,EHI_119920, EHI_121770,EHI_121780,EHI_126210,EHI_133330, EHI_138050,EHI_148140,EHI_148930,EHI_151990, EHI_158610,EHI_175030,EHI_177650,EHI_178890, EHI_179390,EHI_183460,EHI_188830,EHI_192520, EHI_192780,EHI_194320	1.63	0.000241	0.068879
GO:0008092 cytoskeletal protein binding	69	11	EHI_007480,EHI_048670,EHI_068510,EHI_080740, EHI_110180,EHI_119530,EHI_150430,EHI_156420, EHI_158570,EHI_197480,EHI_197550	3.07	0.000732	0.104355
GO:0003779 actin binding	59	9	EHI_007480,EHI_048670,EHI_080740,EHI_110180, EHI_150430,EHI_156420,EHI_158570,EHI_197480, EHI_197550	2.94	0.003023	0.287229
GO:0005488 binding	2442	145	EHI_004790,EHI_006160,EHI_007480,EHI_008050, EHI_009470,EHI_009590,EHI_010020,EHI_010060, EHI_010510,EHI_014000,EHI_017720,EHI_019640, EHI_023300,EHI_024640,EHI_026330,EHI_026420, EHI_026440,EHI_026470,EHI_027760,EHI_035800, EHI_038600,EHI_042870,EHI_045170,EHI_045200, EHI_045480,EHI_048210,EHI_048670,EHI_049970, EHI_050980,EHI_051760,EHI_053020,EHI_053200, EHI_053420,EHI_053610,EHI_053830,EHI_054790, EHI_055350,EHI_055430,EHI_055640,EHI_056380, EHI_058810,EHI_060380,EHI_063040,EHI_067880, EHI_068160,EHI_068510,EHI_069240,EHI_073330, EHI_080740,EHI_082070,EHI_085950,EHI_085970, EHI_086110,EHI_086530,EHI_086540,EHI_090010, EHI_091060,EHI_092640,EHI_093330,EHI_093880, EHI_094100,EHI_098570,EHI_099740,EHI_103430, EHI_103830,EHI_104560,EHI_105240,EHI_105300, EHI_107120,EHI_110180,EHI_110530,EHI_115350, EHI_118800,EHI_118920,EHI_119300,EHI_119530, EHI_119620,EHI_119920,EHI_119930,EHI_119950, EHI_121770,EHI_121780,EHI_122720,EHI_124470, EHI_124880,EHI_126210,EHI_130700,EHI_131200, EHI_133330,EHI_134800,EHI_138050,EHI_138970, EHI_140350,EHI_141380,EHI_141870,EHI_146180, EHI_148140,EHI_148280,EHI_148930,EHI_150430, EHI_151990,EHI_152060,EHI_155570,EHI_156420, EHI_156560,EHI_158050,EHI_158150,EHI_158570, EHI_158610,EHI_161940,EHI_163480,EHI_164900, EHI_169280,EHI_170050,EHI_170060,EHI_174210, EHI_175030,EHI_176700,EHI_177520,EHI_177650, EHI_178680,EHI_178850,EHI_178890,EHI_179390, EHI_179880,EHI_183050,EHI_183460,EHI_184540, EHI_187090,EHI_188830,EHI_189950,EHI_192520, EHI_192780,EHI_192810,EHI_193840,EHI_194320, EHI_196580,EHI_196940,EHI_197480,EHI_197550, EHI_197810,EHI_200740,EHI_201080,EHI_201270, EHI_202460	1.14	0.009150	0.436004
GO:0003756 protein disulfide isomerase activity	9	3	EHI_021560,EHI_042900,EHI_071590	6.42	0.009179	0.436004
GO:0016864 intramolecular oxidoreductase activity, transposing S-S bonds	9	3	EHI_021560,EHI_042900,EHI_071590	6.42	0.009179	0.436004
GO:0051015 actin filament binding	19	4	EHI_007480,EHI_110180,EHI_150430,EHI_156420	4.06	0.014785	0.472735

GO:0005515 protein binding	826	55	EHI_007480,EHI_008050,EHI_010510,EHI_019640, EHI_023300,EHI_024640,EHI_026470,EHI_035800, EHI_045200,EHI_048670,EHI_051760,EHI_053200, EHI_055350,EHI_063040,EHI_068510,EHI_069240, EHI_073330,EHI_080740,EHI_085950,EHI_086530, EHI_090010,EHI_093880,EHI_103430,EHI_104560, EHI_105240,EHI_110180,EHI_110530,EHI_119530, EHI_119950,EHI_122720,EHI_124470,EHI_126210, EHI_131200,EHI_134800,EHI_138970,EHI_141380, EHI_150430,EHI_152060,EHI_156420,EHI_156560, EHI_158050,EHI_158570,EHI_163480,EHI_170050, EHI_170060,EHI_178850,EHI_183050,EHI_188830, EHI_189950,EHI_196940,EHI_197480,EHI_197550, EHI_197810,EHI_200740,EHI_202460	1.28	0.024495	0.472735
GO:1901363 heterocyclic compound binding	1458	89	EHI_004790,EHI_006160,EHI_009470,EHI_009590, EHI_010060,EHI_014000,EHI_017720,EHI_019640, EHI_026330,EHI_026420,EHI_026440,EHI_027760, EHI_038600,EHI_045170,EHI_045480,EHI_048210, EHI_049970,EHI_053020,EHI_053420,EHI_053830, EHI_054790,EHI_055430,EHI_055640,EHI_056380, EHI_058810,EHI_063040,EHI_067880,EHI_068160, EHI_082070,EHI_085970,EHI_086110,EHI_086540, EHI_091060,EHI_092640,EHI_093330,EHI_094100, EHI_099740,EHI_103830,EHI_105300,EHI_107120, EHI_110180,EHI_115350,EHI_118800,EHI_118920, EHI_119300,EHI_119530,EHI_119620,EHI_119920, EHI_119930,EHI_121770,EHI_121780,EHI_126210, EHI_133330,EHI_138050,EHI_140350,EHI_141870, EHI_146180,EHI_148140,EHI_148280,EHI_148930, EHI_151990,EHI_155570,EHI_156560,EHI_158610, EHI_163480,EHI_164900,EHI_169280,EHI_174210, EHI_175030,EHI_176700,EHI_177520,EHI_177650, EHI_178680,EHI_178850,EHI_178890,EHI_179390, EHI_183460,EHI_184540,EHI_187090,EHI_188830, EHI_192520,EHI_192780,EHI_192810,EHI_193840, EHI_194320,EHI_196580,EHI_196940,EHI_201080, EHI_201270	1.18	0.034895	0.472735
GO:0097159 organic cyclic compound binding	1460	89	EHI_004790,EHI_006160,EHI_009470,EHI_009590, EHI_010060,EHI_014000,EHI_017720,EHI_019640, EHI_026330,EHI_026420,EHI_026440,EHI_027760, EHI_038600,EHI_045170,EHI_045480,EHI_048210, EHI_049970,EHI_053020,EHI_053420,EHI_053830, EHI_054790,EHI_055430,EHI_055640,EHI_056380, EHI_058810,EHI_063040,EHI_067880,EHI_068160, EHI_082070,EHI_085970,EHI_086110,EHI_086540, EHI_091060,EHI_092640,EHI_093330,EHI_094100, EHI_099740,EHI_103830,EHI_105300,EHI_107120, EHI_110180,EHI_115350,EHI_118800,EHI_118920, EHI_119300,EHI_119530,EHI_119620,EHI_119920, EHI_119930,EHI_121770,EHI_121780,EHI_126210, EHI_133330,EHI_138050,EHI_140350,EHI_141870, EHI_146180,EHI_148140,EHI_148280,EHI_148930, EHI_151990,EHI_155570,EHI_156560,EHI_158610, EHI_163480,EHI_164900,EHI_169280,EHI_174210, EHI_175030,EHI_176700,EHI_177520,EHI_177650, EHI_178680,EHI_178850,EHI_178890,EHI_179390, EHI_183460,EHI_184540,EHI_187090,EHI_188830, EHI_192520,EHI_192780,EHI_192810,EHI_193840, EHI_194320,EHI_196580,EHI_196940,EHI_201080, EHI_201270,	1.17	0.036069	0.472735
GO:0044877 protein-containing complex binding	37	5	EHI_007480,EHI_110180,EHI_140350,EHI_150430, EHI_156420	2.6	0.040468	0.472735
GO:0016886 ligase activity, forming phosphoric ester bonds	7	2	EHI_158610,EHI_184560	5.51	0.047365	0.472735

Supplementary table 11: Molecular function GO term enrichment analysis of proteins more highly expressed in B2 amebae compared with A1 amebae.

GO term	Hits back-ground	Hits EVs	Protein ID	Fold enrich-ment	*p*-value	FDR *p*-value
GO:0016491 oxidoreductase activity	203	16	EHI_001420,EHI_002560,EHI_005060,EHI_025710, EHI_067860,EHI_106330,EHI_120640,EHI_123390, EHI_125740,EHI_145840,EHI_150770,EHI_152130, EHI_159160,EHI_165070,EHI_174070,EHI_200770	3.14	0.000038	0.007545
GO:0016616 oxidoreductase activity, acting on the CH-OH group of donors, NAD or NADP as acceptor	41	6	EHI_067860,EHI_125740,EHI_152130,EHI_165070, EHI_174070,EHI_200770	5.83	0.000481	0.033236
GO:0016614 oxidoreductase activity, acting on CH-OH group of donors	43	6	EHI_067860,EHI_125740,EHI_152130,EHI_165070, EHI_174070,EHI_200770	5.56	0.000626	0.033236
GO:0004197 cysteine-type endopeptidase activity	17	4	EHI_033710,EHI_039610,EHI_050570,EHI_074180	9.38	0.000695	0.033236
GO:0016209 antioxidant activity	19	4	EHI_001420,EHI_123390,EHI_145840,EHI_159160	8.39	0.001089	0.033236
GO:0051920 peroxiredoxin activity	9	3	EHI_001420,EHI_123390,EHI_145840	13.29	0.001157	0.033236
GO:0016684 oxidoreductase activity, acting on peroxide as acceptor	9	3	EHI_001420,EHI_123390,EHI_145840	13.29	0.001157	0.033236
GO:0008831 dTDP-4-dehydrorhamnose reductase activity	3	2	EHI_152130,EHI_174070	26.58	0.001841	0.046264
GO:0016829 lyase activity	38	5	EHI_073380,EHI_127160,EHI_144610,EHI_156310, EHI_174070	5.25	0.002361	0.052732
GO:0004553 hydrolase activity, hydrolyzing O-glycosyl compounds	40	5	EHI_007330,EHI_152880,EHI_153100,EHI_192590, EHI_199110	4.98	0.002974	0.059784
GO:0016798 hydrolase activity, acting on glycosyl bonds	45	5	EHI_007330,EHI_152880,EHI_153100,EHI_192590, EHI_199110	4.43	0.004552	0.083186
GO:0033897 ribonuclease T2 activity	6	2	EHI_127160,EHI_156310	13.29	0.005000	0.083745
GO:0008374 O-acyltransferase activity	19	3	EHI_031360,EHI_099180,EHI_136400	6.29	0.008762	0.135470
GO:0016849 phosphorus-oxygen lyase activity	7	2	EHI_127160,EHI_156310	11.39	0.011120	0.151583
GO:0035091 phosphatidylinositol binding	7	2	EHI_004400,EHI_186740	11.39	0.012066	0.151583
GO:0033764 steroid dehydrogenase activity, acting on the CH-OH group of donors, NAD or NADP as acceptor	10	2	EHI_165070,EHI_174070	7.97	0.012066	0.151583
GO:0018271 biotin-protein ligase activity	1	1	EHI_167730	39.86	0.024616	0.162653
GO:0042887 amide transmembrane transporter activity	1	1	EHI_101230	39.86	0.025086	0.162653
GO:0047560 3-dehydrosphinganine reductase activity	1	1	EHI_200770	39.86	0.025086	0.162653
GO:0050112 inositol 2-dehydrogenase activity	1	1	EHI_125740	39.86	0.025086	0.162653

GO:0016433 rRNA (adenine) methyltransferase activity	1	1	EHI_013870	39.86	0.025086	0.162653
GO:0016721 oxidoreductase activity, acting on superoxide radicals as acceptor	1	1	EHI_159160	39.86	0.025086	0.162653
GO:0000179 rRNA (adenine-N6,N6-)-dimethyltransferase activity	1	1	EHI_013870	39.86	0.025086	0.162653
GO:1904680 peptide transmembrane transporter activity	1	1	EHI_101230	39.86	0.025086	0.162653
GO:0015440 ABC-type peptide transporter activity	1	1	EHI_101230	39.86	0.025086	0.162653
GO:0004077 biotin-[acetyl-CoA-carboxylase] ligase activity	1	1	EHI_167730	39.86	0.025086	0.162653
GO:0004089 carbonate dehydratase activity	1	1	EHI_073380	39.86	0.025086	0.162653
GO:0004784 superoxide dismutase activity	1	1	EHI_159160	39.86	0.025086	0.162653
GO:0008988 rRNA (adenine-N6-)-methyltransferase activity	1	1	EHI_013870	39.86	0.025086	0.162653
GO:0008667 2,3-dihydro-2,3-dihydroxybenzoate dehydrogenase activity	1	1	EHI_200770	39.86	0.025086	0.162653
GO:0016836 hydro-lyase activity	11	2	EHI_073380,EHI_174070	7.25	0.025086	0.162653
GO:0050662 obsolete coenzyme binding	11	2	EHI_152130,EHI_174070	7.25	0.029599	0.180286
GO:0016229 steroid dehydrogenase activity	12	2	EHI_165070,EHI_174070	6.64	0.029599	0.180286
GO:0016835 carbon-oxygen lyase activity	12	2	EHI_073380,EHI_174070	6.64	0.034945	0.190624
GO:0016160 amylase activity	12	2	EHI_152880,EHI_192590	6.64	0.034945	0.190624
GO:0003824 catalytic activity	2107	63	EHI_001420,EHI_002560,EHI_005040,EHI_005060, EHI_007330,EHI_012040,EHI_013870,EHI_021400, EHI_025710,EHI_026360,EHI_026480,EHI_031360, EHI_033710,EHI_038670,EHI_039610,EHI_040380, EHI_045470,EHI_046670,EHI_050570,EHI_050690, EHI_054720,EHI_067860,EHI_070720,EHI_073380, EHI_074180,EHI_087390,EHI_092530,EHI_096770, EHI_099180,EHI_101230,EHI_101280,EHI_104570, EHI_106330,EHI_109840,EHI_117590,EHI_120640, EHI_123390,EHI_125740,EHI_125820,EHI_127160, EHI_134960,EHI_136400,EHI_144610,EHI_145840, EHI_150770,EHI_151380,EHI_152130,EHI_152880, EHI_153100,EHI_154240,EHI_156310,EHI_159160, EHI_165070,EHI_167730,EHI_174070,EHI_174180, EHI_178580,EHI_186820,EHI_187180,EHI_192590, EHI_193480,EHI_199110,EHI_200770	1.19	0.034945	0.190624
GO:0008234 cysteine-type peptidase activity	51	4	EHI_033710,EHI_039610,EHI_050570,EHI_074180	3.13	0.035090	0.190624
GO:0005543 phospholipid binding	13	2	EHI_004400,EHI_186740	6.13	0.038043	0.201229
GO:0005089	53	4	EHI_011390,EHI_051820,EHI_138390,EHI_182740	3.01	0.040633	0.209417

Rho guanyl-nucleotide exchange factor activity						
GO:0003955 NAD(P)H dehydrogenase (quinone) activity	2	1	EHI_025710	19.93	0.042925	0.211895
GO:0008460 dTDP-glucose 4,6-dehydratase activity	2	1	EHI_174070	19.93	0.049547	0.211895
GO:0004512 inositol-3-phosphate synthase activity	2	1	EHI_070720	19.93	0.049547	0.211895
GO:0016655 oxidoreductase activity, acting on NAD(P)H, quinone or similar compound as acceptor	2	1	EHI_025710	19.93	0.049547	0.211895
GO:0016872 intramolecular lyase activity	2	1	EHI_070720	19.93	0.049547	0.211895
GO:0004123 cystathionine gamma-lyase activity	2	1	EHI_144610	19.93	0.049547	0.211895
GO:0004648 O-phospho-L-serine:2-oxoglutarate aminotransferase activity	2	1	EHI_026360	19.93	0.049547	0.211895

Supplementary table 12: List of proteins uniquely detected in EV and not whole cell proteomes.

Identifier	Description	Sample data binary logarithm					
		A1 - 1	A1 - 2	A1 - 3	B2 - 1	B2 - 2	B2 - 3
EHI_000260	RNA recognition motif domain containing protein	27.29	28.12	X	28.19	X	26.08
EHI_008630	hypothetical protein	19.85	18.32	23.91	19.79	20.91	X
EHI_008750	hypothetical protein	21.65	X	X	19.39	X	20.61
EHI_012020	hypothetical protein	23.25	24.26	25.60	22.51	25.32	23.23
EHI_014010	myosin-2 heavy chain, putative	23.29	22.57	23.28	22.45	22.95	22.56
EHI_015250	lysozyme, putative	23.51	24.38	23.25	20.48	23.68	22.84
EHI_019630	hypothetical protein	20.43	X	21.08	X	21.21	X
EHI_020250	lecithin:cholesterol acyltransferase domain-containing protein	21.14	20.84	X	21.77	X	X
EHI_021350	hypothetical protein	19.42	20.21	20.78	21.69	X	21.30
EHI_029580	mannosyltransferase, putative	X	X	X	24.20	25.75	X
EHI_030420	tyrosine kinase, putative	20.54	20.37	20.67	21.58	X	21.31
EHI_035750	lecithin:cholesterol acyltransferase domain-containing protein	20.92	21.70	19.92	20.84	X	X
EHI_038800	actin binding protein, putative	X	22.69	23.76	X	X	X
EHI_040620	hypothetical protein	X	20.31	20.66	X	X	X
EHI_044490	hypothetical protein	21.48	21.02	21.10	20.96	22.42	22.27
EHI_049060	hypothetical protein	X	21.92	21.26	X	X	20.94
EHI_049320	hypothetical protein	X	22.46	21.02	X	X	X
EHI_052870	ENTH domain protein, putative	20.50	20.44	X	X	X	X
EHI_053320	hypothetical protein	23.03	X	X	22.23	23.16	21.89
EHI_054480	hypothetical protein	22.46	23.24	22.71	22.82	24.13	23.90
EHI_062480	cysteine protease, putative	22.06	22.92	22.74	X	X	X
EHI_065250	Lecithin:cholesterol acyltransferase, putative	20.34	X	X	20.91	X	21.13
EHI_065310	Skp1 family protein	19.95	X	20.40	X	X	20.81
EHI_078310	hypothetical protein, conserved	24.62	X	23.43	24.30	X	X
EHI_081690	hypothetical protein	22.79	X	X	21.88	23.81	22.66
EHI_092670	hypothetical membrane-spanning protein	21.01	X	20.42	X	21.81	21.84
EHI_094360	hypothetical protein	X	20.91	22.59	X	X	X
EHI_095190	hypothetical protein, conserved	21.54	22.18	21.24	21.90	22.70	22.37
EHI_095510	hypothetical protein	21.63	X	20.16	X	23.30	X
EHI_096280	endo-1,4-beta-xylanase, putative	21.63	22.60	22.41	X	22.58	22.69
EHI_096360	hypothetical protein	22.13	22.46	24.78	23.53	24.16	23.51

EHI_098200	beta-amylase, putative	21.67	23.13	22.36	21.58	X	X
EHI_099780	hypothetical protein	22.85	23.52	24.02	22.98	24.28	24.67
EHI_100080	acid sphingomyelinase-like phosphodiesterase, putative	19.76	20.30	X	X	X	X
EHI_101290	hypothetical protein, conserved	23.41	23.96	23.99	23.37	23.38	24.21
EHI_106240	hypothetical protein	X	21.78	21.82	22.23	23.12	X
EHI_110730	nucleoside transporter, putative	X	22.05	22.37	X	X	20.84
EHI_111550	hypothetical protein, conserved	22.36	24.20	23.95	22.36	24.39	X
EHI_119910	lipid phosphate phosphatase, putative	X	21.82	22.29	19.99	X	X
EHI_120600	hypothetical protein	23.93	23.11	23.98	23.97	24.79	24.82
EHI_125020	hypothetical protein	X	20.97	22.19	X	X	X
EHI_125400	hypothetical protein	23.67	24.21	22.65	24.69	25.02	25.26
EHI_126890	hypothetical protein	21.40	X	21.49	21.01	22.82	22.34
EHI_126900	hypothetical protein	21.52	21.85	X	21.53	22.22	23.09
EHI_127670	hypothetical protein	26.01	X	X	24.22	X	22.83
EHI_128070	protein kinase, putative	22.26	20.52	19.33	20.14	X	21.05
EHI_129910	hypothetical protein	22.00	22.57	23.46	22.21	X	22.14
EHI_131970	competence protein ComEC, putative	21.41	22.11	21.91	X	X	X
EHI_134840	ADP-ribosylation factor, putative	19.70	X	20.84	X	X	19.66
EHI_135460	hypothetical protein	26.44	23.06	22.78	26.20	25.96	25.98
EHI_137860	hypothetical protein	23.02	X	X	22.08	X	22.46
EHI_143070	hypothetical protein	X	24.11	25.42	21.63	23.36	23.51
EHI_143440	calmodulin, putative	20.86	X	20.39	X	X	X
EHI_148360	hypothetical protein	21.79	21.68	X	22.85	X	22.45
EHI_156230	transporter, major facilitator family	21.13	22.39	X	X	X	X
EHI_156430	NUF1 protein, putative	X	20.83	X	20.78	X	22.22
EHI_164890	rab GDP dissociation inhibitor alpha, putative	22.87	22.95	22.97	22.08	21.90	23.28
EHI_168300	hypothetical protein	21.90	22.27	X	X	X	X
EHI_170420	thioredoxin, putative	24.28	23.50	X	24.06	24.88	24.33
EHI_172170	hypothetical protein	X	19.42	19.07	X	X	X
EHI_175040	hypothetical protein	21.58	22.35	22.95	21.15	22.17	21.96
EHI_177180	hypothetical protein	22.38	X	20.40	22.58	X	X
EHI_178640	Yos1-like domain-containing protein	X	21.13	X	21.48	X	22.31
EHI_180660	protein kinase domain containing protein	21.00	20.92	20.76	20.45	X	20.30
EHI_183250	hypothetical protein	26.50	25.26	25.20	26.26	X	27.47
EHI_185600	citrate transporter, putative	21.18	21.57	21.24	X	X	X
EHI_187760	hypothetical protein, conserved	19.07	X	18.86	20.45	X	X
EHI_188720	hypothetical protein	24.07	24.78	26.59	24.03	26.08	24.81
EHI_192610	sericin 1 precursor, putative	21.48	24.66	23.80	21.10	22.40	22.66
EHI_194280	Rab family GTPase	21.54	X	21.05	21.51	21.72	21.23
EHI_199580	hypothetical protein	23.72	23.15	24.83	22.62	23.39	23.14

Supplementary table 13: PANTHER statistical overrepresentation test of annotated biological process GO terms of EV proteomes compared with whole cell proteomes.

GO term	A1				B2			
	Hits whole cell	Hits EVs	Fold enrichment	FDR *p*-value	Hits whole cell	Hits EVs	Fold enrichment	FDR *p*-value
lipid metabolic process (GO:0006629)	86	53	1.94	9.34E-03	83	44	1.86	4.48E-02
localization (GO:0051179)	378	169	1.4	6.72E-03	341	138	1.42	1.84E-02
transport (GO:0006810)	362	161	1.4	9.45E-03	328	134	1.43	1.65E-02
establishment of localization (GO:0051234)	363	161	1.39	1.11E-02	328	134	1.43	1.72E-02
transmembrane transport (GO:0055085)	50	34	2.14	2.94E-02	-	-	-	-
organelle membrane fusion (GO:0090174)	-	-	-	-	13	14	3.78	3.91E-02
vesicle-mediated transport (GO:0016192)	-	-	-	-	199	86	1.52	4.48E-02
DNA-templated transcription (GO:0006351)	34	0	< 0.01	8.77E-03	31	0	< 0.01	3.85E-02
nucleic acid-templated transcription (GO:0097659)	34	0	< 0.01	9.03E-03	31	0	< 0.01	3.96E-02
RNA biosynthetic process (GO:0032774)	36	0	< 0.01	6.76E-03	31	0	< 0.01	3.76E-02
cellular nitrogen compound metabolic process (GO:0034641)	503	108	0.67	2.72E-03	466	92	0.69	2.16E-02
regulation of molecular function (GO:0065009)	187	28	0.47	4.16E-03	179	15	0.29	1.64E-05
regulation of catalytic activity (GO:0050790)	185	27	0.46	2.81E-03	177	15	0.3	2.07E-05
heterocycle metabolic process (GO:0046483)	369	50	0.43	2.16E-08	334	43	0.45	6.45E-06
organic cyclic compound metabolic process (GO:1901360)	369	50	0.43	1.80E-08	334	43	0.45	5.38E-06
cellular aromatic compound metabolic process (GO:0006725)	367	48	0.41	8.60E-09	332	41	0.43	4.25E-06
nucleobase-containing compound metabolic process (GO:0006139)	365	48	0.41	9.06E-09	330	41	0.44	3.90E-06
ncRNA metabolic process (GO:0034660)	165	18	0.34	1.15E-04	146	14	0.34	1.01E-03
positive regulation of catalytic activity (GO:0043085)	74	8	0.34	4.98E-02	66	5	0.27	4.15E-02
positive regulation of molecular function (GO:0044093)	75	8	0.34	3.80E-02	67	5	0.26	4.25E-02
tRNA metabolic process (GO:0006399)	74	7	0.3	2.33E-02	73	5	0.24	1.90E-02
RNA metabolic process (GO:0016070)	249	23	0.29	6.02E-09	220	20	0.32	3.10E-06
ncRNA processing (GO:0034470)	138	12	0.27	5.48E-05	119	11	0.32	4.58E-03
nucleic acid metabolic process (GO:0090304)	290	25	0.27	2.32E-11	258	21	0.29	3.07E-08
regulation of gene expression (GO:0010468)	92	7	0.24	1.38E-03	86	6	0.24	5.66E-03
regulation of macromolecule metabolic process (GO:0060255)	129	9	0.22	9.94E-06	121	9	0.26	4.99E-04
RNA processing (GO:0006396)	171	12	0.22	6.76E-08	147	12	0.29	1.57E-04
regulation of cellular metabolic process (GO:0031323)	106	7	0.21	8.45E-05	99	6	0.21	1.01E-03
regulation of metabolic process (GO:0019222)	137	9	0.21	2.22E-06	128	9	0.25	1.76E-04
regulation of nitrogen compound metabolic process (GO:0051171)	106	7	0.21	9.15E-05	100	7	0.25	2.07E-03
regulation of primary metabolic process (GO:0080090)	108	7	0.2	6.68E-05	102	7	0.24	1.51E-03
regulation of cellular biosynthetic process (GO:0031326)	70	4	0.18	2.50E-03	66	3	0.16	6.19E-03
regulation of macromolecule biosynthetic process (GO:0010556)	70	4	0.18	2.75E-03	66	3	0.16	6.91E-03
regulation of RNA metabolic process (GO:0051252)	53	3	0.18	1.83E-02	49	2	0.14	3.08E-02

regulation of nucleobase-containing compound metabolic process (GO:0019219)	58	3	0.16	7.49E-03	53	2	0.13	1.66E-02
regulation of DNA-templated transcription (GO:0006355)	41	2	0.15	3.75E-02	39	1	0.09	4.21E-02
regulation of nucleic acid-templated transcription (GO:1903506)	41	2	0.15	3.69E-02	39	1	0.09	4.11E-02
regulation of RNA biosynthetic process (GO:2001141)	41	2	0.15	3.63E-02	39	1	0.09	4.02E-02
DNA metabolic process (GO:0006259)	44	2	0.14	2.90E-02	40	1	0.09	4.17E-02
nucleobase-containing compound biosynthetic process (GO:0034654)	74	3	0.13	2.78E-04	65	3	0.16	7.46E-03
aromatic compound biosynthetic process (GO:0019438)	76	3	0.12	2.06E-04	67	3	0.16	5.66E-03
heterocycle biosynthetic process (GO:0018130)	76	3	0.12	2.19E-04	67	3	0.16	5.94E-03
organic cyclic compound biosynthetic process (GO:1901362)	76	3	0.12	1.94E-04	67	3	0.16	5.40E-03
methylation (GO:0032259)	28	0	< 0.01	2.59E-02	-	-	-	-
mRNA processing (GO:0006397)	33	0	< 0.01	9.12E-03	-	-	-	-
positive regulation of nucleobase-containing compound metabolic process (GO:0045935)	28	0	< 0.01	2.54E-02	-	-	-	-
regulation of catabolic process (GO:0009894)	31	0	< 0.01	1.85E-02	-	-	-	-
tRNA modification (GO:0006400)	35	0	< 0.01	6.82E-03	-	-	-	-
gene expression (GO:0010467)	368	78	0.67	1.83E-02	-	-	-	-
cellular macromolecule catabolic process (GO:0044265)	121	18	0.47	3.89E-02	-	-	-	-
ubiquitin-dependent protein catabolic process (GO:0006511)	88	11	0.39	4.16E-02	-	-	-	-
modification-dependent protein catabolic process (GO:0019941)	90	11	0.38	3.38E-02	-	-	-	-
rRNA processing (GO:0006364)	93	11	0.37	2.70E-02	-	-	-	-
modification-dependent macromolecule catabolic process (GO:0043632)	95	11	0.36	2.12E-02	-	-	-	-
rRNA metabolic process (GO:0016072)	97	11	0.36	1.71E-02	-	-	-	-
positive regulation of biological process (GO:0048518)	62	5	0.25	2.89E-02	-	-	-	-
regulation of protein metabolic process (GO:0051246)	62	4	0.2	1.09E-02	-	-	-	-
positive regulation of cellular metabolic process (GO:0031325)	49	3	0.19	3.31E-02	-	-	-	-
positive regulation of nitrogen compound metabolic process (GO:0051173)	53	3	0.18	1.87E-02	-	-	-	-
mRNA metabolic process (GO:0016071)	57	3	0.17	7.67E-03	-	-	-	-
positive regulation of macromolecule metabolic process (GO:0010604)	54	3	0.17	1.28E-02	-	-	-	-
positive regulation of metabolic process (GO:0009893)	56	3	0.17	9.70E-03	-	-	-	-
RNA modification (GO:0009451)	50	2	0.13	8.08E-03	-	-	-	-
tRNA processing (GO:0008033)	45	1	0.07	6.31E-03	-	-	-	-
biological regulation (GO:0065007)	-	-	-	-	475	95	0.7	2.39E-02
protein modification by small protein conjugation or removal (GO:0070647)	-	-	-	-	58	3	0.18	2.82E-02
regulation of GTPase activity (GO:0043087)	-	-	-	-	71	5	0.25	2.44E-02
regulation of hydrolase activity (GO:0051336)	-	-	-	-	80	6	0.26	1.62E-02

Shown are all GO terms significantly enriched (> 1) or depleted (< 1) with FDR $p < 0.05$.

Supplementary table 14: PANTHER statistical overrepresentation test of annotated molecular function GO terms of EV proteomes compared with whole cell proteomes.

GO term	A1				B2			
	Hits whole cell	Hits EVs	Fold enrichment	FDR *p*-value	Hits whole cell	Hits EVs	Fold enrichment	FDR *p*-value
GTPase activity (GO:0003924)	127	91	2.25	3.79E-06	125	74	2.08	3.11E-04
guanyl nucleotide binding (GO:0019001)	148	96	2.04	2.16E-05	147	80	1.91	5.73E-04
GTP binding (GO:0005525)	147	95	2.03	1.99E-05	146	79	1.9	6.58E-04
guanyl ribonucleotide binding (GO:0032561)	147	95	2.03	1.49E-05	146	79	1.9	5.64E-04
ribonucleoside triphosphate phosphatase activity (GO:0017111)	191	107	1.76	3.16E-04	184	87	1.66	7.96E-03
pyrophosphatase activity (GO:0016462)	204	110	1.69	7.91E-04	194	89	1.61	1.27E-02
hydrolase activity, acting on acid anhydrides, in phosphorus-containing anhydrides (GO:0016818)	205	110	1.69	7.38E-04	195	89	1.6	1.23E-02
hydrolase activity, acting on acid anhydrides (GO:0016817)	205	110	1.69	6.64E-04	195	89	1.6	1.15E-02
nucleic acid binding (GO:0003676)	328	59	0.57	6.72E-04				
catalytic activity, acting on RNA (GO:0140098)	97	10	0.32	1.05E-02	85	6	0.25	7.62E-03
catalytic activity, acting on a nucleic acid (GO:0140640)	126	10	0.25	6.81E-05	109	6	0.19	5.49E-04
DNA binding (GO:0003677)	64	2	0.10	5.22E-04	58	2	0.12	6.09E-03
molecular function regulator activity (GO:0098772)	158	24	0.48	1.75E-02	156	14	0.31	3.29E-04
enzyme regulator activity (GO:0030234)	154	22	0.45	1.01E-02	152	13	0.3	2.53E-04
GTPase regulator activity (GO:0030695)	-	-	-	-	123	11	0.31	2.14E-03
nucleoside-triphosphatase regulator activity (GO:0060589)	-	-	-	-	123	11	0.31	1.90E-03
guanyl-nucleotide exchange factor activity (GO:0005085)	-	-	-	-	67	4	0.21	1.44E-02

Shown are all GO terms significantly enriched (> 1) or depleted (< 1) with FDR $p < 0.05$.

Supplementary table 15: PANTHER statistical overrepresentation test of annotated cellular component GO terms of EV proteomes compared with whole cell proteomes.

GO term	A1				B2			
	Hits whole cell	Hits EVs	Fold enrichment	FDR *p*-value	Hits whole cell	Hits EVs	Fold enrichment	FDR *p*-value
integral component of endoplasmic reticulum membrane (GO:0030176)	14	14	3.14	4.09E-02	-	-	-	-
intrinsic component of endoplasmic reticulum membrane (GO:0031227)	14	14	3.14	3.99E-02	-	-	-	-
endoplasmic reticulum subcompartment (GO:0098827)	53	42	2.49	5.02E-04	49	37	2.65	7.99E-04
endoplasmic reticulum membrane (GO:0005789)	53	42	2.49	4.70E-04	49	37	2.65	7.27E-04
endoplasmic reticulum protein-containing complex (GO:0140534)	37	27	2.29	2.43E-02	49	37	2.65	6.66E-04
organelle subcompartment (GO:0031984)	70	50	2.24	5.02E-04	65	43	2.32	1.09E-03
integral component of membrane (GO:0016021)	355	252	2.23	1.31E-23	322	225	2.45	5.26E-26
endoplasmic reticulum (GO:0005783)	118	75	2.00	1.41E-04	115	68	2.07	1.27E-04
membrane (GO:0016020)	597	352	1.85	2.09E-23	547	303	1.94	2.86E-24
plasma membrane (GO:0005886)	127	71	1.76	3.78E-03	-	-	-	-
ribosomal subunit (GO:0044391)	91	51	1.76	2.40E-02	-	-	-	-
cytosolic ribosome (GO:0022626)	88	49	1.75	2.94E-02	-	-	-	-
ribosome (GO:0005840)	101	55	1.71	2.50E-02	-	-	-	-
cell periphery (GO:0071944)	145	77	1.67	5.70E-03	-	-	-	-
organelle membrane (GO:0031090)	122	64	1.65	2.49E-02	110	60	1.91	2.15E-03
endomembrane system (GO:0012505)	275	142	1.62	5.67E-05	258	122	1.66	1.22E-04
cellular anatomical entity (GO:0110165)	1689	587	1.09	3.02E-02	1563	491	1.1	3.85E-02
cellular_component (GO:0005575)	1712	591	1.08	4.95E-02	-	-	-	-
intracellular anatomical structure (GO:0005622)	1386	381	0.86	6.95E-03	1286	317	0.86	2.42E-02
protein-containing complex (GO:0032991)	608	144	0.74	5.64E-03	560	120	0.75	2.86E-02
catalytic complex (GO:1902494)	174	24	0.43	5.25E-04	166	23	0.49	1.02E-02
transferase complex (GO:1990234)	78	9	0.36	2.50E-02	-	-	-	-
membrane-enclosed lumen (GO:0031974)	146	12	0.26	3.71E-06	126	13	0.36	3.16E-03
intracellular organelle lumen (GO:0070013)	146	12	0.26	3.29E-06	126	13	0.36	2.96E-03
organelle lumen (GO:0043233)	146	12	0.26	2.97E-06	126	13	0.36	2.79E-03
nucleus (GO:0005634)	464	36	0.24	1.46E-23	408	32	0.27	5.58E-17
nucleolus (GO:0005730)	90	5	0.17	5.63E-05	75	5	0.23	4.81E-03
preribosome (GO:0030684)	49	2	0.13	4.52E-03	39	0	< 0.01	3.15E-03
intracellular protein-containing complex (GO:0140535)	127	5	0.12	1.04E-08	121	7	0.2	1.69E-05
nuclear lumen (GO:0031981)	133	5	0.12	3.24E-09	112	6	0.19	2.68E-05
chromosome (GO:0005694)	38	1	0.08	9.11E-03	-	-	-	-
transferase complex, transferring phosphorus-containing groups (GO:0061695)	39	1	0.08	6.20E-03	-	-	-	-
nuclear protein-containing complex (GO:0140513)	114	2	0.06	9.96E-10	104	1	0.03	1.64E-08
nucleoplasm (GO:0005654)	37	0	< 0.01	1.47E-03	-	-	-	-
proteasome complex (GO:0000502)	33	0	< 0.01	3.68E-03	-	-	-	-
nuclear DNA-directed RNA polymerase complex (GO:0055029)	25	0	< 0.01	2.55E-02	-	-	-	-
RNA polymerase complex (GO:0030880)	25	0	< 0.01	2.47E-02	-	-	-	-
DNA-directed RNA polymerase complex (GO:0000428)	25	0	< 0.01	2.40E-02	-	-	-	-

Shown are all GO terms significantly enriched (> 1) or depleted (< 1) with FDR $p < 0.05$.

Supplementary table 16: Comparison of the *E. histolytica* EV proteomes to the top 100 mammalian EV proteins (Vesiclepedia).

Gene name (human)	UniProt ID	Orthologs found	Presence in EV proteomes		
			A1	B2	Ctrl
PDCD6IP	Q8WUM4	no significant similarity found	-	-	-
GAPDH	P04406	EHI_008200	yes	yes	yes
HSPA8	P11142	EHI_052860;EHI_113410;EHI_188610;EHI_104330;EHI_192440 (top 5 hits)	yes	yes	yes
ACTB	P60709	EHI_182900	yes	yes	yes
ANXA2	P07355	no significant similarity found	-	-	-
CD9	P21926	no significant similarity found	-	-	-
PKM	P14618	no significant similarity found	-	-	-
HSP90AA1	P07900	EHI_102270;EHI_196940;EHI_163480	yes	yes	no
ENO1	P06733	EHI_130700	yes	yes	1/3
ANXA5	P08758	no significant similarity found	-	-	-
HSP90AB1	P08238	EHI_102270;EHI_196940;EHI_163480	yes	yes	no
CD63	P08962	no significant similarity found	-	-	-
YWHAZ	P63104	EHI_025360;EHI_006810;EHI_098280	yes	yes	no
YWHAE	P62258	EHI_025360;EHI_006810;EHI_098280	yes	yes	no
EEF1A1	P68104	EHI_011210;EHI_102170;EHI_004230;EHI_044230	yes	yes	no
PGK1	P00558	EHI_188180	yes	yes	1/3
CLTC	Q00160	no significant similarity found	-	-	-
PPIA	P62937	EHI_125840;EHI_128100;EHI_083580;EHI_020340	yes	yes	no
SDCBP	O00560	no significant similarity found	-	-	-
ALDOA	P04075	no significant similarity found	-	-	-
EEF2	P13639	EHI_189490;EHI_164510;EHI_166810;EHI_155660	yes	yes	no
ALB	P43652	no significant similarity found	-	-	-
TPI1	P60174	EHI_054680	no	no	no
VCP	P55072	EHI_045120;EHI_176970	yes	1/3	no
CFL1	P23528	EHI_197480	yes	yes	no
MSN	P26038	no significant similarity found	-	-	-
ATP1A1	P05023	EHI_027710;EHI_016480;EHI_030830;EHI_054830;EHI_001150 (top 5 hits)	yes	yes	no
PRDX1	Q06830	EHI_123390;EHI_201250;EHI_001420;EHI_114010;EHI_122310;EHI_061980; EHI_139570;EHI_145840;EHI_084260 (top 9 hits)	yes	yes	no
MYH9	P35579	EHI_110180	yes	yes	no
EZR	P15311	no significant similarity found	-	-	-
CD81	P60033	no significant similarity found	-	-	-
ANXA6	P08133	no significant similarity found	-	-	-
FLOT1	O75955	no significant similarity found	-	-	-
YWHAB	P31946	EHI_025360;EHI_006810;EHI_098280	yes	yes	no
LDHB	P07195	EHI_152670;EHI_030810	no	no	no
SLC3A2	P08195	only 2 hits with very low query cover found	-	-	-
GNB1	P62873	EHI_000240;EHI_130870 (top 2 hits)	yes	yes	no
PFN1	P07737	no significant similarity found	-	-	-
TSG101	Q99816	EHI_178530;EHI_135460;EHI_131530	yes	yes	no
YWHAQ	P27348	EHI_025360;EHI_006810;EHI_098280	yes	yes	no
GNAI2	P04899	EHI_140350	yes	yes	no
CLIC1	O00299	no significant similarity found	-	-	-
ANXA1	P04083	no significant similarity found	-	-	-
ITGB1	P05556	one hit with very low query cover found	-	-	-
LDHA	P00338	EHI_152670;EHI_030810	no	no	no
FASN	A0A0U1RQF0	no significant similarity found	-	-	-
CDC42	P60953	EHI_181250 (top hit)	yes	yes	no
RAP1B	P61224	EHI_058090;EHI_049030;EHI_137700;EHI_124610;EHI_004860;EHI_154240; EHI_074750;EHI_198330;EHI_068120;EHI_124520 (top 10 hits)	yes	yes	no
CCT2	P78371	EHI_044940;EHI_155450;EHI_155220;EHI_114120;EHI_140600;EHI_005760; EHI_071600;EHI_103270	no	no	no
YWHAG	P61981	EHI_025360;EHI_006810;EHI_098280	yes	yes	no
GNB2	P62879	EHI_040300;EHI_130870;EHI_092070;EHI_050550 (top 4 hits)	yes	yes	no
ACTN4	O43707	EHI_199000;EHI_146140;EHI_094060 (top 3 hits)	yes	yes	no
RAB5C	P51148	EHI_026420;EHI_108610;EHI_107250;EHI_005460;EHI_129740 (top 5 hits)	yes	yes	no

C3	P01024	no significant similarity found	-	-	-
RAB10	P61026	EHI_146510;EHI_199820;EHI_056100;EHI_021210;EHI_143650 (top 5 hits)	yes	yes	no
HIST1H4A	P62805	EHI_023230	no	no	no
*KRT1**	P04264	no significant similarity found	-	-	-
FN1	P02751	no significant similarity found	-	-	-
AHCY	P23526	EHI_068250	no	no	no
A2M	P01023	no significant similarity found	-	-	-
BSG	P35613	no significant similarity found	-	-	-
ACTN1	P12814	EHI_199000;EHI_146140;EHI_094060 (top3)	yes	yes	no
ANXA7	P20073	no significant similarity found	-	-	-
ACLY	P53396	no significant similarity found	-	-	-
HIST1H4B	P62805	EHI_023230	no	no	no
GDI2	P50395	EHI_167060;EHI_164890;EHI_074100	yes	yes	no
FLNA	P21333	EHI_104630	yes	yes	no
UBA1	P22314	EHI_020270;EHI_038690;EHI_035540;EHI_098550	no	no	no
GNAS	O95467	no significant similarity found	-	-	-
GSN	P06396	EHI_021270;EHI_150430	no	no	no
CCT4	P50991	EHI_114120;EHI_155450;EHI_155220;EHI_083260;EHI_044940;EHI_091130 (top 6 hits)	no	no	no
RAN	P62826	EHI_148190;EHI_164900;EHI_117960;EHI_143650;EHI_187090 (top 5 hits)	yes	yes	no
PRDX2	P32119	EHI_201250;EHI_001420;EHI_114010;EHI_139570;EHI_061980;EHI_145840; EHI_123390;EHI_122310;EHI_084260;EHI_121620	yes	yes	no
RHOA	P61586	EHI_013260;EHI_129750;EHI_140190;EHI_181250;EHI_012240 (top 5 hits)	yes	yes	no
CCT3	P49368	EHI_155450;EHI_155220;EHI_114120;EHI_044940;EHI_103270;EHI_140600	no	no	no
RAC1	P63000	EHI_181250;EHI_197840;EHI_140190;EHI_129750;EHI_067220 (top 5 hits)	yes	yes	no
LGALS3BP	Q08380	no significant similarity found	-	-	-
TCP1	P17987	EHI_155450;EHI_155220;EHI_114120;EHI_044940;EHI_103270;EHI_140600	no	no	no
KRT10	P13645	no significant similarity found	-	-	-
CAP1	Q01518	EHI_136150;EHI_081430	yes	yes	no
RAB7A	P51149	EHI_192810;EHI_189990;EHI_081330;EHI_169280;EHI_082070 (top 5 hits)	yes	yes	no
TUBB4B	P68371	EHI_008240;EHI_049920	no	no	no
HSPA5	P11021	EHI_199590;EHI_052860;EHI_104330;EHI_192440;EHI_188610 (top 5 hits)	yes	yes	no
IQGAP1	P46940	EHI_035800	1/3	1/3	no
GPI	P06744	EHI_072240;EHI_047730	no	no	no
RALA	P11233	EHI_137700;EHI_124610;EHI_154240;EHI_124520;EHI_015350 (top 5 hits)	yes	yes	no
KPNB1	Q14974	EHI_171760	no	no	no
HIST1H4I	P62805	EHI_023230	no	no	no
TFRC	P02786	no significant similarity found	-	-	-
EIF4A1	P60842	EHI_093900;EHI_106300;EHI_151600;EHI_036900;EHI_069410;EHI_013960; EHI_096390;EHI_175030;EHI_021440;EHI_111040 (top 10 hits)	yes	no	no
HIST4H4	P62805	EHI_023230	no	no	no
CCT8	P50990	EHI_140600;EHI_071600;EHI_155220;EHI_114120;EHI_155450;EHI_044940; EHI_103270	no	no	no
TLN1	Q9Y490	only 2 hits with low query cover found	-	-	-
HIST1H4K	P62805	EHI_023230	no	no	no
HIST1H4H	P62805	EHI_023230	no	no	no
CCT6A	P40227	EHI_125800;EHI_178980;EHI_158250;EHI_155450;EHI_155220;EHI_083260; EHI_114120;EHI_044940;EHI_103270;EHI_140600	no	no	no
ANXA11	P50995	no significant similarity found	-	-	-
HIST1H4J	P62805	EHI_023230	no	no	no
HIST1H4F	P62805	EHI_023230	no	no	no
HIST1H4D	P62805	EHI_023230	no	no	no

For genes with multiple orthologs, only some of the top hits are shown. Hits with low query cover (for example 20 %) were excluded and not counted as true hits. If samples were present in at least 2/3 samples, the protein was considered to be part of the EV proteome ('yes'). Ctrl = Control

*Human keratin is described as a common contaminant in EV proteomes according to Vesiclepedia.

Supplementary table 17: Differential expression analysis of 3' isomiRs of annotated mature miRNAs in A1 and B2 EVs.

3' isomiR of miRNA[192]	Seed sequence	Fold change	Log fold change	FDR *p*-value	A1 - 1 - CPM	A1 - 2 - CPM	A1 - 3 - CPM	B2 - 1 - CPM	B2 - 2 - CPM	B2 - 3 - CPM
Ehi-miR-35	TTTGTTT	-3.8017	-1.9266	0.0079	2541.3248	4677.2877	2304.9641	1140.7441	858.8815	481.9622
Ehi-miR-55	TTAAAAA	-5.0498	-2.3362	0.0088	4190.6615	7740.7743	17622.993	825.5385	1329.8810	3713.9441
Ehi-miR-67	TGATGGA	-1.8775	-0.9088	0.0766	6580.5166	9600.7483	6878.5937	4097.6729	4443.3263	3713.9441
Ehi-miR-132	AAGGGAT	-1.8902	-0.9185	0.2134	3416.4831	9422.9567	5299.6025	2694.2575	3605.2242	3302.8587
Ehi-miR-187	TGGTTTT	-2.5320	-1.3403	0.2134	2002.7659	2530.1117	3684.3127	1718.6211	1004.3372	496.1376
Ehi-miR-43	AACAATG	2.1474	1.1026	0.2134	8263.5132	5347.4254	3648.0141	8593.1053	13354.222	15139.284
Ehi-miR-127	TCAGTAT	-2.3712	-1.2456	0.2477	1868.1262	3706.2718	1941.9776	1050.6854	1115.1606	1006.4505
Ehi-miR-130	TGCAAGA	2.0232	1.0166	0.4142	8179.3634	5620.9509	5898.5302	6619.3178	11016.540	22255.314
Ehi-miR-133	AAAGATA	1.9928	0.9948	0.4142	1985.9360	1600.1247	1143.4074	2153.9050	2427.7255	4904.6743
Ehi-miR-163	AGACATA	-1.8843	-0.9140	0.4142	3702.5925	7316.8096	5063.6613	3317.1638	2853.7030	2353.1096
Ehi-miR-189	TTGAGGT	2.2089	1.1433	0.5200	2995.7339	1189.8363	1016.3621	2724.2770	3300.4599	5485.8640
Ehi-miR-39	TATTGTT	-1.9022	-0.9277	0.5200	2474.0050	4225.9704	2377.5614	1088.2098	1856.2922	1842.7967
Ehi-miR-49	ACGAAAG	2.1058	1.0744	0.5200	9441.6108	11351.312	9147.2592	9133.4577	18195.820	35764.431
Ehi-miR-80	TCCTTTT	1.7126	0.7762	0.5200	1329.5673	943.6633	2940.1904	2889.3847	2850.2397	3161.1051
Ehi-miR-83	GAAGATG	1.4772	0.5629	0.5200	4880.6901	5087.5760	4319.5391	5388.5149	5530.7811	10277.135
Ehi-miR-86	ACTGTTT	-1.8058	-0.8526	0.5200	4762.8803	9067.3734	10018.427	5883.8380	4938.5685	2353.1096
Ehi-miR-89	GCAAAAA	-2.4459	-1.2903	0.5200	12874.924	28474.014	41434.90	8337.9388	6936.8532	18598.071
Ehi-miR-94	TAATGGT	2.3227	1.2158	0.5200	1396.8872	1518.0670	2069.0229	3317.1638	1620.7925	6676.5941
Ehi-miR-125	GGGTCAT	-1.7858	-0.8366	0.5604	6462.7069	9026.3446	6842.2951	4232.7610	3414.7465	4961.3757
Ehi-miR-156	ACAATAA	1.5327	0.6161	0.5604	3971.8719	3364.3648	3157.9823	6694.3667	5277.9652	4054.1527
Ehi-miR-195	GGAAAGA	1.5378	0.6209	0.5604	9811.8701	9655.4535	12087.450	13643.900	12370.664	22581.347
Ehi-miR-197	TGAGATT	-1.4841	-0.5695	0.5604	4358.9612	4595.2300	3103.5344	3429.7372	2386.1667	2310.5835
Ehi-miR-29	AATTAAG	1.7223	0.7843	0.5604	6243.9173	7590.3352	6769.6978	5245.9219	12200.965	18073.583
Ehi-miR-112	CAGAAAG	1.7927	0.8421	0.5881	4847.0302	1777.9164	2758.6972	3759.9526	3546.3493	9540.0167
Ehi-miR-82	ATGTAAT	-2.3194	-1.2137	0.5881	2574.9848	6400.4989	1760.4844	2814.3358	1281.3957	524.4883
Ehi-miR-192	AGAACAA	1.5033	0.5881	0.6245	8280.3432	4868.7556	6642.6525	12968.459	10659.827	6067.0537
Ehi-miR-101	TATAGAC	2.1306	1.0913	0.6516	454.4091	765.8717	2032.7243	1868.7190	2493.5269	2551.5646
Ehi-miR-102	CAGTTTT	-2.2236	-1.1529	0.6516	2877.9242	3131.8680	2377.5614	1470.9595	2167.9831	113.4029
Ehi-miR-138	AACAAAG	1.2629	0.3367	0.6516	3164.0336	3501.1276	3448.3715	3872.5260	4086.6135	5003.9018
Ehi-miR-152	AGTGCTC	-1.4728	-0.5586	0.6516	11730.486	15303.757	17350.754	12180.445	11245.114	6648.2434
Ehi-miR-155	ACCTTTA	-1.4015	-0.4870	0.6516	4544.0908	5402.1305	3375.7742	3850.0113	2209.5419	3501.3137
Ehi-miR-168	GATTGGA	1.4062	0.4918	0.6516	7556.6547	7672.3929	5934.8289	7144.6604	12336.032	10277.135
Ehi-miR-178	CTTAAAT	-1.9091	-0.9329	0.6516	1110.7777	3542.1564	1379.3486	1328.3665	1129.0135	694.5926
Ehi-miR-180	TGCAGCA	1.6928	0.7594	0.6516	4611.4106	2557.4643	2304.9641	5028.2799	5897.8837	5088.9539
Ehi-miR-191	AAAATAT	-1.9633	-0.9733	0.6516	2507.6649	1887.3266	1197.8554	1065.6951	1042.4328	708.7680
Ehi-miR-26	GAGAAAC	1.5715	0.6521	0.6516	4560.9207	5812.4189	3157.9823	5748.7499	6673.6476	8930.4762
Ehi-miR-41	CATCAGT	1.5343	0.6176	0.6516	2608.6447	2365.9964	2994.6384	4045.1386	5454.5900	2636.6168
Ehi-miR-46	TACCTCC	-1.5070	-0.5917	0.6516	19640.570	9887.9502	6551.9059	5703.7205	6524.7286	11737.197
Ehi-miR-71	GGAAAAA	-1.5480	-0.6304	0.6516	13447.143	17478.285	23884.510	9328.5850	8422.5796	17705.024
Ehi-miR-90	TTGTGGA	1.4442	0.5302	0.6516	3753.0824	4034.5025	3847.6566	8525.5612	3816.4814	4465.2381
Ehi-miR-63	AAGGAAG	-1.6716	-0.7412	0.6530	21525.526	35763.471	13376.052	15895.369	10012.203	16400.891
Ehi-miR-142	GATTTCA	-1.6238	-0.6993	0.6596	14759.880	27379.912	20962.469	9913.9668	12284.083	16712.748
Ehi-miR-116	AGGTGAA	1.4815	0.5670	0.6601	7371.5250	9997.3604	5281.4532	11212.314	8928.2114	13509.117
Ehi-miR-73	TGACATT	1.5868	0.6661	0.6601	2238.3855	1053.0735	998.2128	2754.2966	2379.2402	1644.3417
Ehi-miR-137	TGAGTTG	1.4394	0.5255	0.6656	2457.1750	1887.3266	1415.6473	3332.1736	2496.9901	2466.5125
Ehi-miR-145	CCTACTG	1.6145	0.6911	0.6793	1514.6969	3747.3006	1833.0817	4382.8589	4942.0317	2126.3039
Ehi-miR-144	TTAGTGG	-1.6656	-0.7360	0.7360	2322.5353	4349.0569	1669.7378	2131.3903	2289.1962	567.0144
Ehi-miR-166	TAATTGC	-2.5204	-1.3336	0.7360	2086.9158	957.3396	2159.7695	675.4406	1343.7339	28.3507
Ehi-miR-58	CATAATC	-1.7469	-0.8048	0.7360	4291.6413	2584.8169	3938.4033	1718.6211	3300.4599	1119.8534
Ehi-miR-174	CCAAAAA	-1.6777	-0.7465	0.7417	13228.353	8875.9055	41217.114	9928.9766	8135.1314	19689.574
Ehi-miR-64	AGCATCT	1.9476	0.9617	0.7417	36874.455	29048.418	25953.533	26544.815	28464.302	123963.52
Ehi-miR-98	TAGAGAT	1.5745	0.6549	0.7704	1817.6363	492.3461	1324.9006	2221.4490	1721.2262	1757.7445
Ehi-miR-104	CCTGTTG	-1.4519	-0.5380	0.7986	6294.4072	8916.9344	9219.8565	5238.4170	5762.8176	5840.2480
Ehi-miR-110	GAGACAA	1.6115	0.6884	0.7986	9121.8415	3145.5443	4119.8965	4202.7414	4509.1277	17719.199
Ehi-miR-61	AGAGAAT	1.5773	0.6575	0.7986	3820.4022	943.6633	4609.9282	7264.7388	4308.2603	3189.4558
Ehi-miR-8	AATAAAT	-1.5395	-0.6224	0.7986	2827.4343	1764.2401	2123.4709	945.6168	2223.3948	1148.2041

Ehi-miR-23	GTGATAG	1.2875	0.3645	0.8405	5486.5689	4704.6402	5372.1998	6236.5681	4419.0837	9454.9645
Ehi-miR-147	TATACAT	2.1043	1.0733	0.8422	504.8990	123.0865	471.8824	382.7497	1059.7489	850.5215
Ehi-miR-165	TTATTGG	1.2942	0.3721	0.8422	5957.8079	2311.2913	4664.3762	4562.9764	5437.2738	6733.2956
Ehi-miR-91	ATTCTTC	-1.3311	-0.4126	0.8422	7489.3348	12965.113	10345.115	8833.2619	6590.5300	7753.9214
Ehi-miR-120	TGGATTT	1.2779	0.3538	0.8754	3466.9730	2940.4001	3611.7154	5320.9708	4086.6135	3317.0340
Ehi-miR-123	TGTAACA	-1.5311	-0.6146	0.8887	3298.6733	6988.5789	1724.1858	1943.7679	3352.4083	2551.5646
Ehi-miR-20	TAATATC	-2.1758	-1.1215	0.8887	1514.6969	82.0577	2649.8013	878.0728	266.6688	807.9955
Ehi-miR-105	TCGTGAA	1.3905	0.4756	0.8998	4729.2204	4608.9063	7060.0869	5636.1765	6836.4195	10362.188
Ehi-miR-170	AATTATT	1.6741	0.7434	0.8998	807.8384	1901.0029	1397.4979	1313.3567	2202.6154	3402.0862
Ehi-miR-69	AGGAGCA	1.2739	0.3492	0.8998	2221.5555	3952.4448	2976.4891	3504.7862	2916.0411	5315.7597
Ehi-miR-107	TAAACAA	1.4718	0.5576	0.9141	3046.2238	984.6921	1070.8101	3459.7568	3134.2247	893.0476
Ehi-miR-12	ATAAACG	-1.3245	-0.4055	0.9141	3197.6935	3090.8392	6624.5032	3414.7274	4761.9437	1530.9388
Ehi-miR-121	CCTTGTA	-1.5463	-0.6289	0.9141	2474.0050	4034.5025	3194.2810	4007.6142	1956.7259	297.6825
Ehi-miR-126	TTGGAAG	-1.5018	-0.5866	0.9141	6698.3264	15098.613	3448.3715	3489.7764	3667.5624	9681.7703
Ehi-miR-129	CAAGTAT	-1.3445	-0.4270	0.9141	2103.7457	2830.9899	3412.0729	1876.2239	1980.9686	2395.6357
Ehi-miR-136	TTCGAGA	-1.3662	-0.4502	0.9141	2373.0252	6509.9091	2232.3668	3347.1834	2666.6884	2126.3039
Ehi-miR-154	GTGTAGA	1.2511	0.3232	0.9141	1985.9360	1504.3908	2559.0546	2911.8994	1863.2187	2806.7211
Ehi-miR-157	GGATCTG	1.5476	0.6300	0.9141	25901.317	30771.629	22251.071	27610.510	22154.294	72436.085
Ehi-miR-164	AGACAAT	1.2341	0.3035	0.9141	6597.3466	8151.0627	9020.2139	7062.1066	7650.2789	14685.672
Ehi-miR-171	AATGCGA	1.3655	0.4494	0.9141	1817.6363	2530.1117	4101.7472	3234.6099	3660.6360	4649.5178
Ehi-miR-19	GATCTGA	1.3513	0.4344	0.9141	4729.2204	8533.9985	7259.7295	6461.7150	4363.6720	16953.730
Ehi-miR-196	TTGGTAT	-1.4768	-0.5625	0.9141	959.3081	3254.9546	707.8236	1163.2588	619.9185	1573.4649
Ehi-miR-24	GTTCAAT	1.5463	0.6288	0.9141	3416.4831	410.2884	2794.9959	2521.6449	3051.1072	4663.6932
Ehi-miR-45	CTGTCTA	1.4430	0.5290	0.9141	1211.7575	451.3172	2504.6067	2146.4001	2112.5714	1729.3938
Ehi-miR-54	AATGAAA	1.4151	0.5009	0.9141	3365.9932	1012.0447	6025.5755	5118.3387	5468.4429	4110.8541
Ehi-miR-72	AACTATA	-1.5533	-0.6354	0.9141	1346.3973	3637.8904	635.2263	983.1413	1284.8590	1360.8345
Ehi-miR-81	TTGGTTT	1.6972	0.7631	0.9141	1649.3367	300.8782	889.3169	1178.2686	1374.9030	2268.0575
Ehi-miR-93	TATGGAT	-1.6279	-0.7030	0.9141	1699.8266	3788.3295	5081.8107	3167.0659	1797.4173	1516.7634
Ehi-miR-96	TAATAGA	-1.3199	-0.4004	0.9141	1144.4377	2352.3201	2613.5026	825.5385	1800.8805	2012.9010
Ehi-miR-106	GTTCTCG	-1.3303	-0.4118	0.9262	8633.7725	8123.7101	6461.1593	5133.3485	5374.9357	7059.3288
Ehi-miR-111	TTTAGGG	1.2086	0.2734	0.9262	3248.1834	4294.3518	4428.4350	3692.4085	5430.3474	5358.2857
Ehi-miR-50	ATGAATA	-1.5662	-0.6472	0.9262	891.9882	3719.9481	635.2263	1298.3469	1800.8805	240.9811
Ehi-miR-31	CATCGAC	1.2023	0.2658	0.9348	7489.3348	3993.4737	4918.4667	5763.7597	6406.9787	7555.4664
Ehi-miR-167	CGTAGAT	1.3038	0.3828	0.9448	2204.7255	5744.0375	3030.9371	2866.8700	8374.0944	3061.8776
Ehi-miR-1	GATTGAA	-1.1405	-0.1896	0.9635	4628.2406	5292.7202	5971.1275	4367.8491	4398.3043	5287.4090
Ehi-miR-109	CCAGATA	1.1295	0.1756	0.9635	1514.6969	2037.7657	2813.1452	1853.7092	3456.3053	1828.6213
Ehi-miR-113	TACTTCT	1.1775	0.2358	0.9635	2339.3653	1832.6215	1923.8283	2371.5470	1880.5348	3019.3515
Ehi-miR-114	ACAGATA	1.2255	0.2933	0.9635	2675.9646	1586.4484	3448.3715	4435.3932	3930.7680	1048.9766
Ehi-miR-117	TGCTGAT	1.2361	0.3058	0.9635	3147.2036	971.0159	2577.2040	3347.1834	3847.6505	1048.9766
Ehi-miR-131	ATTAAAA	-1.3195	-0.4000	0.9635	185.1296	3487.4513	2268.6655	690.4504	1537.6749	2282.2328
Ehi-miR-134	TCAAACT	-1.2691	-0.3438	0.9635	5772.6783	6304.7649	6370.4126	4818.1429	5371.4724	4139.2049
Ehi-miR-135	TGAATGT	-1.2458	-0.3171	0.9635	2221.5555	3063.4866	2177.9189	1193.2784	1994.8215	2849.2472
Ehi-miR-140	AGTGTTG	-1.1667	-0.2225	0.9635	8263.5132	9819.5688	12795.273	8510.5514	9800.9458	8079.9547
Ehi-miR-141	TTTCCAA	-1.2024	-0.2659	0.9635	1009.7980	3213.9257	2141.6202	2191.4295	1444.1676	1672.6924
Ehi-miR-143	TAATGAA	-1.1513	-0.2033	0.9635	4409.4511	3760.9769	4446.5843	2491.6253	3418.2097	5103.1293
Ehi-miR-149	GACCATA	-1.3307	-0.4122	0.9635	1514.6969	7152.6943	1597.1405	3024.4729	2680.5414	2012.9010
Ehi-miR-153	GTAAGAA	-1.2141	-0.2798	0.9635	13076.884	30689.572	13031.215	19580.272	14074.574	13140.558
Ehi-miR-158	TGATTCT	-1.1327	-0.1798	0.9635	4746.0504	5429.4830	5063.6613	3714.9232	6566.2874	3104.4036
Ehi-miR-16	TTGCAAG	1.2421	0.3128	0.9635	2608.6447	1285.5703	3230.5796	1786.1651	1388.7559	5698.4944
Ehi-miR-161	TAGAAAA	-1.2643	-0.3383	0.9635	3079.8838	2748.9322	2577.2040	2679.2477	2372.3137	1516.7634
Ehi-miR-162	TTCCATT	1.2311	0.3000	0.9635	622.7087	1053.0735	2014.5749	1268.3273	1219.0576	2069.6024
Ehi-miR-172	ACAAATT	-1.3070	-0.3863	0.9635	2356.1952	3884.0634	3121.6837	2941.9190	3875.3563	326.0333
Ehi-miR-175	AGAATAT	1.1681	0.2242	0.9635	2406.6851	4171.2653	1415.6473	4277.7904	1845.9025	3246.1572
Ehi-miR-181	AGAGATG	1.1392	0.1880	0.9635	8616.9425	10612.793	12178.196	11512.510	11591.437	12715.297
Ehi-miR-182	AATTGGA	1.1942	0.2560	0.9635	16779.476	8547.6748	14519.459	13005.984	19023.532	15507.843
Ehi-miR-184	TAAGTCA	-1.2070	-0.2714	0.9635	3635.2726	3337.0122	2994.6384	2041.3316	2368.8505	3926.5745
Ehi-miR-198	TAATTCC	1.2092	0.2741	0.9635	5149.9695	3391.7174	2740.5479	6499.2394	3854.5769	3274.5080
Ehi-miR-199	AGGATTT	1.1642	0.2194	0.9635	5015.3298	7713.4217	3974.7019	7189.6898	5998.3174	6308.0348
Ehi-miR-2	CTAGGAT	1.1303	0.1767	0.9635	3887.7221	4622.5825	4882.1681	6446.7052	4962.8111	3671.4180
Ehi-miR-27	GAGATTC	-1.1499	-0.2015	0.9635	6041.9577	10325.591	3920.2539	8653.1444	4897.0097	4096.6788

Ehi-miR-33	ATTGAGG	-1.1511	-0.2030	0.9635	4661.9005	5238.0151	3484.6702	3842.5065	4152.4149	3628.8919
Ehi-miR-40	TATTGTA	-1.6083	-0.6855	0.9635	1346.3973	1764.2401	399.2851	1238.3077	834.6389	99.2275
Ehi-miR-47	CATTTAC	-1.3958	-0.4811	0.9635	3096.7137	1381.3042	1833.0817	960.6266	1222.5208	2367.2850
Ehi-miR-48	CTGAGGC	-1.1656	-0.2211	0.9635	6126.1076	11829.982	4464.7336	7212.2045	6032.9497	6010.3523
Ehi-miR-51	GTCATAG	1.1765	0.2344	0.9635	4241.1514	7084.3129	3139.8330	5118.3387	6767.1548	5145.6554
Ehi-miR-53	CAAATTC	-1.1608	-0.2151	0.9635	4022.3618	8602.3799	10435.861	4270.2855	7369.7572	8235.8836
Ehi-miR-65	AGACTTA	-1.2624	-0.3362	0.9635	5452.9089	2434.3778	2958.3398	3039.4826	2292.6594	3274.5080
Ehi-miR-66	AACAGTA	1.1655	0.2209	0.9635	3921.3820	4143.9127	1669.7378	3159.5610	5226.0167	2948.4747
Ehi-miR-68	TATCCAC	-1.1800	-0.2387	0.9635	2844.2642	3268.6308	4083.5978	3077.0071	2628.5929	2962.6501
Ehi-miR-7	AGGAGAA	1.1774	0.2356	0.9635	2339.3653	7713.4217	4591.7789	5433.5443	5904.8101	5925.3001
Ehi-miR-76	TAAATGC	1.2700	0.3448	0.9635	942.4781	1490.7145	1669.7378	2476.6155	1852.8290	850.5215
Ehi-miR-85	TAGAAGG	-1.2379	-0.3078	0.9635	3433.3130	2270.2624	4501.0323	2829.3456	3885.7460	1474.2373
Ehi-miR-88	TAAACAT	-1.3639	-0.4477	0.9635	891.9882	328.2307	1179.7060	1238.3077	467.5363	42.5261
Ehi-miR-9	TCAAAAT	-1.3314	-0.4129	0.9635	3601.6127	2160.8522	3684.3127	2364.0421	2729.0266	1927.8488
Ehi-miR-95	AGGAGTA	-1.1294	-0.1756	0.9635	4157.0016	5990.2105	4664.3762	4645.5303	4858.9141	3558.0151
Ehi-miR-13	TCGTCTA	1.3157	0.3958	0.9781	1952.2760	506.0223	308.5385	1485.9693	1281.3957	864.6969
Ehi-miR-139	GAGTGTC	1.1183	0.1613	0.9781	2760.1144	4499.4960	2758.6972	2514.1400	3421.6730	5329.9350
Ehi-miR-151	GGATTGG	1.0970	0.1335	0.9781	8061.5536	10722.203	10581.056	11249.838	11404.422	9483.3153
Ehi-miR-4	TAAAGAG	-1.0887	-0.1226	0.9781	4476.7709	8684.4376	5589.9917	5711.2254	6341.1773	5174.0061
Ehi-miR-77	CTAATAA	1.1187	0.1618	0.9781	3635.2726	2502.7592	2486.4574	2634.2183	2919.5044	4153.3802
Ehi-miR-159	ATTCCAA	1.0753	0.1047	0.9897	3483.8029	5744.0375	4228.7924	4833.1526	3729.9006	5996.1769
Ehi-miR-21	ATTAGTG	-1.1332	-0.1803	0.9897	3786.7423	6632.9956	3212.4303	3925.0603	3387.0406	4777.0960
Ehi-miR-10	GAGAATC	1.0503	0.0708	0.9947	4375.7911	3788.3295	3920.2539	4795.6282	3245.0481	4734.5699
Ehi-miR-103	TATGGAG	-1.0225	-0.0320	0.9947	14170.831	24425.836	9873.2321	17328.804	14192.324	15918.928
Ehi-miR-108	TTAGGCT	-1.0409	-0.0578	0.9947	4173.8315	1135.1312	2450.1587	2904.3945	2961.0631	1559.2895
Ehi-miR-11	TGCTGAG	-1.0245	-0.0350	0.9947	7775.4442	6044.9156	10871.445	5718.7303	7934.2639	10461.415
Ehi-miR-115	CCGGTGC	-1.0298	-0.0423	0.9947	15231.119	14688.324	7005.6390	10747.010	8363.7047	16797.801
Ehi-miR-119	GGAACAT	1.0500	0.0704	0.9947	2541.3248	4280.6755	5408.4985	2168.9148	4190.5104	6506.4898
Ehi-miR-122	GGCATAA	1.1202	0.1638	0.9947	1396.8872	1559.0959	1978.2763	2454.1008	1696.9836	1332.4838
Ehi-miR-124	AAATGAG	-1.0219	-0.0313	0.9947	4358.9612	2324.9675	4900.3174	3504.7862	5364.5460	2409.8111
Ehi-miR-128	TTCCAGC	-1.0442	-0.0623	0.9947	5318.2692	4841.4030	5717.0370	6326.6268	4322.1132	4536.1149
Ehi-miR-14	TACTTGT	-1.1291	-0.1752	0.9947	2877.9242	2666.8745	3430.2222	3880.0309	2881.4088	1148.2041
Ehi-miR-148	GAATTGA	1.0826	0.1146	0.9947	4560.9207	2981.4290	6225.2180	4900.6967	5520.3914	4422.7120
Ehi-miR-15	ATGAGAC	-1.0243	-0.0346	0.9947	3248.1834	724.8428	3593.5661	2071.3511	2763.6589	2537.3893
Ehi-miR-150	TTGTTGA	1.1423	0.1919	0.9947	4426.2810	191.4679	3230.5796	2964.4337	2961.0631	3033.5269
Ehi-miR-160	AGAGATT	-1.0262	-0.0373	0.9947	3164.0336	3760.9769	4900.3174	4247.7708	4547.2233	2650.7922
Ehi-miR-169	ATAGACT	-1.1301	-0.1764	0.9947	2339.3653	3090.8392	2159.7695	3294.6491	3006.0852	396.9101
Ehi-miR-17	TAAAGGA	1.0286	0.0406	0.9947	5856.8281	8752.8190	5009.2134	6146.5093	6850.2724	7243.6085
Ehi-miR-173	GTAGTAA	1.0242	0.0346	0.9947	2002.7659	1791.5926	2304.9641	3437.2421	1693.5203	1091.5027
Ehi-miR-176	ATATCCA	-1.0396	-0.0560	0.9947	2675.9646	1203.5126	2776.8465	1786.1651	3452.8421	1119.8534
Ehi-miR-177	GGAGTTG	-1.0259	-0.0368	0.9947	8583.2826	3364.3648	7078.2363	4818.1429	8162.8372	5528.3901
Ehi-miR-179	ATTTTAA	1.0779	0.1083	0.9947	1716.6565	2338.6438	2559.0546	2836.8505	2774.0486	1460.0620
Ehi-miR-183	TGGATTG	1.0566	0.0794	0.9947	2760.1144	971.0159	1923.8283	1883.7287	1845.9025	2239.7067
Ehi-miR-186	AAATTGT	1.0798	0.1108	0.9947	2928.4141	1066.7498	4682.5255	3257.1246	1963.6524	4153.3802
Ehi-miR-188	AGGATTC	1.0297	0.0422	0.9947	7169.5655	11474.399	9129.1098	7955.1891	9014.7922	11708.847
Ehi-miR-190	ATTTGCT	-1.0554	-0.0778	0.9947	1598.8468	1600.1247	2849.4438	2671.7428	2199.1522	822.1708
Ehi-miR-194	CGAATAT	-1.0759	-0.1055	0.9947	2894.7541	1394.9805	2177.9189	1688.6015	1752.3953	2594.0907
Ehi-miR-22	GTGTACT	-1.0835	-0.1157	0.9947	1901.7861	847.9293	1052.6608	1463.4546	1780.1011	240.9811
Ehi-miR-25	ATGATAA	1.0296	0.0421	0.9947	2591.8147	1559.0959	1288.6020	2769.3064	1745.4688	1063.1519
Ehi-miR-28	CACGAAA	1.1335	0.1808	0.9947	5638.0386	1066.7498	8094.5984	3452.2519	8682.3220	4621.1671
Ehi-miR-3	TGAAATT	1.0116	0.0166	0.9947	4291.6413	3719.9481	4156.1951	3084.5120	4827.7451	4366.0106
Ehi-miR-30	TCACGAG	-1.0471	-0.0664	0.9947	3483.8029	5730.3612	2359.4121	2896.8896	4592.2453	3572.1905
Ehi-miR-32	ATTGGGA	1.0188	0.0269	0.9947	7876.4240	7275.7808	6769.6978	7234.7192	6084.8982	9157.2820
Ehi-miR-36	ACGCAAA	1.0363	0.0514	0.9947	3197.6935	998.3684	2849.4438	3242.1148	2192.2257	1842.7967
Ehi-miR-37	TATGGTC	1.0303	0.0430	0.9947	4274.8113	4526.8486	4773.2721	4825.6478	4287.4809	5088.9539
Ehi-miR-38	GCGATTT	-1.0420	-0.0594	0.9947	5419.2490	4061.8551	4446.5843	5523.6030	3158.4674	4720.3946
Ehi-miR-42	TGAATAA	1.0775	0.1077	0.9947	2743.2844	2352.3201	3266.8783	3122.0365	3511.7170	2253.8821
Ehi-miR-5	ATGATCT	1.1428	0.1926	0.9947	656.3687	2201.8810	1706.0364	1425.9301	1797.4173	2012.9010
Ehi-miR-52	GACATAA	1.1127	0.1541	0.9947	858.3283	95.7340	1088.9594	637.9161	626.8449	1006.4505
Ehi-miR-56	TTTTAAG	1.0532	0.0748	0.9947	3096.7137	6605.6431	5698.8877	3016.9680	5045.9287	8193.3576

Ehi-miR-59	CAGCAGA	1.0195	0.0279	0.9947	4358.9612	6072.2682	4736.9735	4247.7708	4841.5980	6478.1391
Ehi-miR-70	AAGAAGG	-1.0232	-0.0330	0.9947	7152.7355	3706.2718	7314.1775	5703.7205	4536.8336	7541.2911
Ehi-miR-75	GTGATCC	-1.0735	-0.1023	0.9947	64946.838	40563.846	25753.890	22679.794	18476.341	81153.931
Ehi-miR-78	ACGAAAT	1.1599	0.2140	0.9947	6429.0470	1969.3843	889.3169	2356.5372	3532.4964	4890.4989
Ehi-miR-79	TAATAAT	1.1500	0.2017	0.9947	2743.2844	136.7628	2268.6655	442.7888	2091.7920	3387.9108
Ehi-miR-92	CACATCC	1.0764	0.1062	0.9947	3988.7019	5949.1817	3393.9235	4562.9764	6621.6991	3132.7544
Ehi-miR-97	CTTCGTA	-1.1845	-0.2442	0.9947	1144.4377	1148.8075	598.9277	1553.5134	595.6759	283.5072
Ehi-miR-99	CAGGATT	1.1127	0.1541	0.9947	4948.0100	4814.0504	5245.1546	6611.8129	4000.0327	6152.1059
Ehi-miR-100	ATCATGG	-1.0054	-0.0077	0.9977	8246.6833	3925.0923	6842.2951	5568.6324	7206.9853	6095.4044
Ehi-miR-118	TCGACTA	1.0012	0.0017	0.9977	2086.9158	2448.0541	780.4209	2904.3945	1617.3292	793.8201
Ehi-miR-185	TTGAGGA	-1.0018	-0.0026	0.9977	6429.0470	4308.0281	2722.3986	3001.9582	4422.5469	6038.7030
Ehi-miR-62	GTTGCTG	-1.0011	-0.0016	0.9977	3315.5033	4458.4672	5027.3627	5125.8436	5717.7956	1899.4981
Ehi-miR-74	GTGCTGG	1.0008	0.0011	0.9977	4560.9207	10079.418	6261.5167	7347.2926	7882.3155	5684.3190
Ehi-miR-84	CTACTTC	-1.0137	-0.0196	0.9977	3685.7625	2352.3201	2014.5749	2446.5959	2884.8720	2594.0907
Ehi-miR-87	AACATAA	-1.0253	-0.0360	0.9977	2204.7255	328.2307	889.3169	2251.4686	820.7859	255.1565

CPM = counts per million (sequenced reads) (normalization method). isomiRs are sorted by statistical significance (FDR *p* value). For mature miRNAs with identical seed sequence as reported by Mar-Aguilar *et al.*[192], only one identifier is stated.

Supplementary table 18: Differential expression analysis of novel mature miRNAs between A1 and B2 EVs.

Mature miRNA sequence	Fold Change	Fold change (tagwise dispersions)	Log fold change	FDR *p*-value	A1 - 1 - CPM	A1 - 2 - CPM	A1 - 3 - CPM	B2 - 1 - CPM	B2 -2 - CPM	B2 - 3 - CPM
GGACCTTCCAAGGCCCTTG	NA	-696.5583	-9.4441	0.000941	15672.851738	14052.490184	3737.422137	0	0	0
TCAAACTCTCCGTGTTGCACG	NA	-55.0293	-5.7821	0.683299	960.787846	1859.888407	0	0	0	0
AAATACCACAATGCAATCATATGTT	13.7887	7.5140	2.9096	0.929528	420.344683	413.308535	95.831337	878.477306	8287.292818	3650.659927
ACTGTAGAACTATTAACGTGTACTC	-6.9157	-13.1599	-3.7181	0.948865	45577.373446	826.617070	1437.470053	1756.954612	2071.823204	3089.019938
AAGCCATGCATGGGTAAGTATAAAG	-3.5213	-4.0564	-2.0202	1	360.295442	0	670.819358	292.825769	0	0
GAGCTAATACATGGCTCTGGAAT	-4.9132	-5.4632	-2.4497	1	480.393923	0	958.313368	292.825769	0	0
GACAGAATCCTAGGATTTCACCTC	-3.3869	-3.4692	-1.7946	1	360.295442	1239.925604	383.325347	585.651537	0	0
ACCGAACGTCGTGATAAAGTGCCAA	-2.1508	-2.3584	-1.2378	1	240.196962	1033.271337	1245.807379	1171.303075	0	0
GGCGTGAAATGTTTAGGACATT	-2.0325	-3.3145	-1.7288	1	4443.643788	206.654267	2491.614758	3513.909224	0	0
AACGGGTAAATGAAGGCATACGA	-2.1063	-3.9746	-1.9908	1	780.640125	619.962802	670.819358	292.825769	690.607735	0
TTCGTTTCCTTAGTCGTTAAAATG	-2.3763	-3.9041	-1.9650	1	360.295442	826.617070	1149.976042	292.825769	690.607735	0
CTGTCATGTACTGTCTTTTGAGTTT	-1.5217	-2.4437	-1.2891	1	540.443163	826.617070	574.988021	585.651537	690.607735	0
CTGCGGACGGTTCATTATAACAGT	-1.2231	-1.9775	-0.9837	1	300.246202	206.654267	1054.144705	585.651537	690.607735	0
AATGGCGTAAGGATAACAAAAGTAA	-2.0230	-3.7505	-1.9071	1	1321.083288	206.654267	1054.144705	585.651537	690.607735	0
TTGACAATAGGACAGTGGCCATGG	-1.7470	-3.1736	-1.6661	1	1561.280250	413.308535	766.650695	878.477306	690.607735	0
TCAAAAAGCAAGGTCGCTATGAGCG	-1.2053	-1.9728	-0.9803	1	540.443163	1033.271337	1149.976042	878.477306	1381.215470	0
CTTTCATGATTTACTGGGTAGTGGT	2.3393	1.2284	0.2968	1	420.344683	0	670.819358	1171.303075	1381.215470	0
ATTCGGAGGCGTAGGTTGCCA	3.3267	1.5868	0.6661	1	360.295442	206.654267	766.650695	292.825769	4143.646409	0
GTGAAACCACCGTCAAGGGAACGG	-6.5533	-6.2019	-2.6327	1	300.246202	1446.579872	2012.458074	292.825769	0	280.819994
GATCAGGCTCTCCGCATCTTTACTT	-1.3396	-1.7674	-0.8217	1	660.541644	413.308535	479.156684	878.477306	0	280.819994
CTGCCCTTTGTAGACACCGCCCGT	-1.9997	-2.3212	-1.2149	1	660.541644	1859.888407	383.325347	1171.303075	0	280.819994
TAGAGCCTGATTAGTACCATTATGT	-1.9767	-2.3270	-1.2185	1	540.443163	413.308535	1916.626737	1171.303075	0	280.819994
GTACCGAGATTGATATACACC	1.1716	-1.0133	-0.0191	1	360.295442	1033.271337	95.831337	1464.128843	0	280.819994

GGGACGTATTCAT ATCGAGTTAATG	-1.0374	-1.5546	-0.6365	1	420.344 683	619.962 802	574.988 021	585.651 537	690.607 735	280.819 994
TTGACGAGGCTTA CACTCTCTCTGG	1.6035	-1.0745	-0.1036	1	300.246 202	0	670.819 358	585.651 537	690.607 735	280.819 994
ACGTTCGGTTCTTA CCGCATCGCCA	-1.1205	-1.8356	-0.8762	1	660.541 644	413.308 535	670.819 358	585.651 537	690.607 735	280.819 994
GAAATTACGGTTA CGTCTCAGCAAA	-1.0122	-1.4973	-0.5823	1	300.246 202	413.308 535	862.482 032	585.651 537	690.607 735	280.819 994
AGCTATGTTGCGG TCTTCCCTTACC	1.1519	-1.1711	-0.2279	1	300.246 202	826.617 070	479.156 684	878.477 306	690.607 735	280.819 994
GCATTCAGCAATCA CAGGTCTGTGA	1.0405	-1.3652	-0.4491	1	660.541 644	619.962 802	1341.63 8716	1756.95 4612	690.607 735	280.819 994
AATCCGTTCAAGTG TAGTTCACCA	-1.1572	-1.8356	-0.8762	1	1681.37 8731	1239.92 5604	574.988 021	2049.78 0381	690.607 735	280.819 994
ATTGACAATAGGA TGGTGGCCATGG	-1.7412	-2.5452	-1.3478	1	1801.47 7211	1446.57 9872	2012.45 8074	2049.78 0381	690.607 735	280.819 994
GAGTTTGGCTGTG TCGGCACATCTG	-1.1147	-1.9083	-0.9323	1	720.590 885	826.617 070	958.313 368	585.651 537	1381.21 5470	280.819 994
ATTAATCTTATTCT CTTTCAATC	1.5132	-1.2267	-0.2948	1	720.590 885	0	958.313 368	878.477 306	1381.21 5470	280.819 994
AGAGATAGACGTG TAGTTTGGCTGG	1.2727	-1.4939	-0.5791	1	300.246 202	206.654 267	1341.63 8716	0	2071.82 3204	280.819 994
GGTTAGATCGTCG GACTG	1.6834	-1.2234	-0.2909	1	720.590 885	826.617 070	670.819 358	0	3453.03 8674	280.819 994
CACGACGGTCTTAT CCCAGCTCACG	-3.3447	-3.2629	-1.7062	1	300.246 202	619.962 802	958.313 368	0	0	561.639 989
CAATTCATTGCGGA CTTCATCGCC	-1.3648	-1.7259	-0.7873	1	480.393 923	206.654 267	479.156 684	292.825 769	0	561.639 989
CTCTCTCTGGCTTA ATATTCGTTCT	-1.6202	-1.7776	-0.8300	1	300.246 202	413.308 535	670.819 358	292.825 769	0	561.639 989
AGTTTGTATGAGTC CAAAATGGC	-2.2755	-2.4410	-1.2875	1	300.246 202	206.654 267	1437.47 0053	292.825 769	0	561.639 989
CCCGCCGTTCCCAG CAAGCCCGTTC	-1.7782	-1.8101	-0.8560	1	240.196 962	1033.27 1337	766.650 695	585.651 537	0	561.639 989
GGTGAACCGGGGA CCCTCA	1.3766	1.0525	0.0739	1	360.295 442	206.654 267	479.156 684	878.477 306	0	561.639 989
ATTAAAAGGAACC ATTGGGGTGAT	-3.1243	-3.3315	-1.7362	1	480.393 923	1239.92 5604	2779.10 8769	878.477 306	0	561.639 989
CCCCCCCTCCCGGA GGATCGT	1.1725	-1.1657	-0.2212	1	600.492 404	206.654 267	670.819 358	1171.30 3075	0	561.639 989
GGCGATTGAAAGA AATAGACGGGG	-1.4211	-1.5657	-0.6468	1	360.295 442	1239.92 5604	862.482 032	1171.30 3075	0	561.639 989
AACACGGAAGTAG AGATGCTTAGAG	1.2766	-1.0218	-0.0311	1	540.443 163	413.308 535	862.482 032	1756.95 4612	0	561.639 989
GAATGCTTCCTATA TCTTTTTCCCA	-1.8671	-2.9850	-1.5777	1	840.689 365	826.617 070	670.819 358	0	690.607 735	561.639 989
TCGGACTGTCGAA GTCTGAACGT	-2.6590	-4.4474	-2.1530	1	2161.77 2654	413.308 535	1533.30 1390	292.825 769	690.607 735	561.639 989
AATTGCGATAACT GATAGGAACAAT	-1.2333	-1.6632	-0.7340	1	540.443 163	1033.27 1337	1054.14 4705	878.477 306	690.607 735	561.639 989
CAGGTAAGGGACT TCGGCAACATAG	-1.4696	-1.9976	-0.9983	1	660.541 644	1033.27 1337	1437.47 0053	878.477 306	690.607 735	561.639 989
GCACTTTATCTCGG CGTTCGGTTCA	-2.0557	-2.5781	-1.3663	1	600.492 404	2273.19 6942	2108.28 9411	1171.30 3075	690.607 735	561.639 989
TGAAACGATTTACT GAGACTTAAC	1.0641	-1.2514	-0.3235	1	480.393 923	826.617 070	1245.80 7379	1464.12 8843	690.607 735	561.639 989
TACACCACTTAGTA TCCTTAATTAT	-1.3372	-1.9002	-0.9261	1	1080.88 6327	826.617 070	1724.96 4063	1464.12 8843	690.607 735	561.639 989
ATGGTACTGATCAC GCTCTAAGCAT	-2.7011	-3.4443	-1.7842	1	1140.93 5567	3513.12 2546	2683.27 7432	1464.12 8843	690.607 735	561.639 989
CCCCAATTCCTGGT TATCCGTTAT	1.3379	-1.0212	-0.0303	1	240.196 962	1033.27 1337	1054.14 4705	1171.30 3075	1381.21 5470	561.639 989
CCATCTTTCGGATC CTAACATATTT	1.1095	-1.2799	-0.3560	1	300.246 202	206.654 267	2299.95 2084	1171.30 3075	1381.21 5470	561.639 989
AATTCCAATCATTG ATCCCTGTCAT	1.2551	-1.1070	-0.1466	1	420.344 683	1239.92 5604	1054.14 4705	1464.12 8843	1381.21 5470	561.639 989
CGGAAGTAAAGAC GCTTAGAGCCTG	1.0517	-1.3907	-0.4758	1	840.689 365	1239.92 5604	1437.47 0053	1756.95 4612	1381.21 5470	561.639 989
ACGCAATGAATTCC GATAAGTGATA	1.2020	-1.1507	-0.2025	1	600.492 404	1239.92 5604	1724.96 4063	2342.60 6149	1381.21 5470	561.639 989
AAGCATATCAATG AGGGAAGGAAGA	-1.0696	-1.7415	-0.8004	1	960.787 846	2066.54 2674	3258.26 5453	1171.30 3075	4143.64 6409	561.639 989
AATTTCACCTCTGT ATTCAATCGGT	-4.4514	-4.4754	-2.1620	1	540.443 163	1446.57 9872	3066.60 2779	292.825 769	0	842.459 983
GAGCTATGTTGACT ACTTCCCTTAC	1.0402	-1.1923	-0.2538	1	480.393 923	413.308 535	479.156 684	585.651 537	0	842.459 983
TTAATCCTTCTCGC GAAATGTCTTA	-2.2637	-2.4212	-1.2757	1	540.443 163	1446.57 9872	1245.80 7379	585.651 537	0	842.459 983
CATTTCAGAGTTAG TGATTGTAC	1.0593	-1.1894	-0.2502	1	540.443 163	413.308 535	670.819 358	878.477 306	0	842.459 983

ACTTCCCTTACATTCGTTATTCTAT	2.3989	1.6311	0.7059	1	360.295442	0	479.156684	1171.303075	0	842.459983
GTGGCCATGGACGACGGAAACCGCT	1.0076	-1.1705	-0.2271	1	420.344683	619.962802	958.313368	1171.303075	0	842.459983
GATGGTGAACTGTACTTGAACGGA	1.1807	1.0151	0.0216	1	360.295442	826.617070	766.650695	1464.128843	0	842.459983
GCCAAACTCCCGGGCTATCTCTTTC	-1.3738	-1.5995	-0.6776	1	540.443163	826.617070	2204.120747	1756.954612	0	842.459983
AAACCACATTTTACTTCAACTACGA	1.1944	-1.2710	-0.3459	1	540.443163	413.308535	574.988021	292.825769	690.607735	842.459983
AAATATGTTAGGAGCCGAAAGATGG	-1.0797	-1.4547	-0.5407	1	480.393923	206.654267	1916.626737	878.477306	690.607735	842.459983
CGCGTGCGGCCAAAGATGTCTAAGG	-1.7657	-2.1417	-1.0988	1	540.443163	2893.159744	1341.638716	1171.303075	690.607735	842.459983
AACCTGTCTCACGCCGGTCTAAACC	-3.1839	-3.7823	-1.9193	1	540.443163	1239.925604	7762.338285	1464.128843	690.607735	842.459983
TTGAATGAAACGGTTTGCTGAGACT	-1.1645	-1.7190	-0.7815	1	540.443163	1239.925604	1149.976042	292.825769	1381.215470	842.459983
TTGCCGACTTCACGTACCTGCGTTA	1.2051	-1.2592	-0.3325	1	480.393923	413.308535	1437.470053	585.651537	1381.215470	842.459983
TCTAAGCATCTTGACTTCCGTGTTC	1.2637	-1.2480	-0.3196	1	780.640125	619.962802	1054.144705	878.477306	1381.215470	842.459983
ACGGCGGGGACAGAAGACCCTGT	-1.0604	-1.4578	-0.5438	1	420.344683	1239.925604	1629.132726	878.477306	1381.215470	842.459983
ATAATGGTACTGAGCAGGCTCTAAG	2.8718	2.1281	1.0896	1	420.344683	1033.271337	1054.144705	4978.038067	1381.215470	842.459983
ACTTACAGAGCTAAGTTGCCGACTT	1.0969	-1.3917	-0.4768	1	840.689365	1446.579872	1437.470053	1171.303075	2071.823204	842.459983
CGCAGTCAGGCACAGGCCTGATCG	2.3910	1.4887	0.5741	1	540.443163	619.962802	670.819358	1464.128843	2071.823204	842.459983
AGACGGGGAGTTACGCTGGGGCGGC	1.1960	-1.2004	-0.2636	1	1080.886327	1653.234139	2395.783421	3221.083455	2071.823204	842.459983
ATAGACGGGGAGAATGGCTGGGGCG	-1.0484	-1.6565	-0.7282	1	1200.984808	3099.814011	4216.578821	1756.954612	5524.861878	842.459983
GGCGGGAGTAACGATGACTCTCTTA	3.3676	1.5424	0.6252	1	4503.693028	1446.579872	1533.301390	878.477306	23480.662983	842.459983
ATTGGGGTTCTCCATCGGAGAGGG	-2.1370	-2.2654	-1.1797	1	540.443163	1239.925604	1245.807379	292.825769	0	1123.279978
CGGTTCATCCCTCTTCGCCAGTCCT	-1.7685	-2.1973	-1.1357	1	1261.034048	1033.271337	1245.807379	878.477306	0	1123.279978
GGCTCTAAGCATGTTTACTTCCGTG	-1.2082	-1.4621	-0.5480	1	780.640125	1033.271337	958.313368	1171.303075	0	1123.279978
AAATACTCTCTAGCAACTCCATTGT	2.0630	1.6514	0.7237	1	420.344683	826.617070	574.988021	2635.431918	0	1123.279978
GGGTTCGACATAGTAGAGGGAGCTT	-1.1804	-1.5047	-0.5894	1	720.590885	1653.234139	1149.976042	1171.303075	690.607735	1123.279978
TAGGCCATCATCTCAGAGTTATTGA	-1.6995	-2.2431	-1.1655	1	1561.280250	2686.505476	1820.795400	1756.954612	690.607735	1123.279978
GGGGAATTGTGAGCGGATAAC	-1.0300	-1.3656	-0.4496	1	540.443163	2273.196942	670.819358	878.477306	1381.215470	1123.279978
AGAACGCAATGGATTGCGATAAGTG	1.0721	-1.3554	-0.4387	1	780.640125	1033.271337	1341.638716	878.477306	1381.215470	1123.279978
ATAACGCAGGTATCCAAAGATGAAC	-1.0686	-1.5640	-0.6453	1	1261.034048	1446.579872	1533.301390	1464.128843	1381.215470	1123.279978
TTCCATGGCCAGCGTCCTATTGTCA	-1.2841	-1.6973	-0.7632	1	840.689365	1653.234139	3354.096790	2049.780381	1381.215470	1123.279978
AGAAGTGGAATCTATTGGCTTTGT	2.5742	1.5255	0.6093	1	480.393923	413.308535	574.988021	585.651537	2071.823204	1123.279978
AACAGATGTGCCGACCCAGCCAAAC	-1.7460	-2.4315	-1.2819	1	1681.378731	3099.814011	4887.398179	2342.606149	2071.823204	1123.279978
AAGCATCTTTACCTCCGTGTTCGGA	1.3481	1.0866	0.1198	1	600.492404	619.962802	1341.638716	2049.780381	0	1404.099972
AAGTCTGGTGCCCGCAGCCGCGGTA	1.1760	-1.0640	-0.0895	1	540.443163	1239.925604	1245.807379	1464.128843	690.607735	1404.099972
GCATCTTTACTTTCGTGTTCGGATG	1.0194	-1.2095	-0.2745	1	540.443163	1033.271337	2779.108769	2342.606149	690.607735	1404.099972
CCAATAAATCATTAAAGAACTCTTA	1.5079	1.2030	0.2667	1	540.443163	1446.579872	1149.976042	2635.431918	690.607735	1404.099972
TGAATCACCCCAGTTGTTCCTTTT	-1.0090	-1.5953	-0.6738	1	3122.560500	619.962802	1916.626737	3513.909224	690.607735	1404.099972
CCAAACTCCCCTTATATCTCTTTCA	1.6426	1.2195	0.2863	1	420.344683	619.962802	1724.964063	1756.954612	1381.215470	1404.099972
GCTTAGAGCCTAATCAGTACCATTA	-1.1488	-1.5297	-0.6132	1	720.590885	2273.196942	3354.096790	2049.780381	2071.823204	1404.099972
GGAGTTTGGCTTGTGCGGCACATCT	1.4478	-1.0236	-0.0336	1	600.492404	1446.579872	1437.470053	878.477306	2762.430939	1404.099972
TGCCGCCCCAGACTAACTCCCCGTC	-1.3217	-1.7802	-0.8320	1	720.590885	1859.888407	3545.759463	878.477306	2071.823204	1684.919966
ACGGATAACGAGGGATTGGGGTTCG	1.5930	1.1097	0.1501	1	1200.984808	1446.579872	1916.626737	3513.909224	2071.823204	1684.919966

CGCAGGTAAGGTACGTCGGCAACAT	1.2350	-1.1451	-0.1955	1	1020.837086	2273.196942	2204.120747	2342.606149	2762.430939	1684.919966
ATAACGAGGAATCGGGGTTCGACAT	1.5010	1.0425	0.0601	1	1501.231009	3513.122546	1724.964063	4978.038067	3453.038674	1684.919966
ACGGGTAACTGAACGCATACGCCCC	-1.6134	-2.4752	-1.3075	1	2101.723413	8886.133499	4120.747484	1464.128843	6215.469613	1684.919966
GGTGGCCATGGCCGTCGGAAACCGC	1.7943	1.5440	0.6267	1	300.246202	826.617070	1437.470053	2635.431918	0	1965.739961
TAGACGGGGAGATGGGCTGGGGCGG	-1.4091	-1.6943	-0.7607	1	900.738606	2893.159744	2012.458074	1464.128843	690.607735	1965.739961
CCCAGCCAAACACGCCGTCTATCTC	-1.5840	-1.7881	-0.8384	1	300.246202	3719.776813	2970.771442	1756.954612	690.607735	1965.739961
CTGGGGCGGCACAACTGTTACCCCC	-1.4702	-2.0513	-1.0365	1	2101.723413	2479.851209	2491.614758	1464.128843	1381.215470	1965.739961
TGGTGCATGGCCCTTCTTAGTTGG	1.3723	-1.0408	-0.0576	1	1381.132529	2686.505476	1724.964063	3221.083455	2762.430939	1965.739961
GGCGTCCCGTCCTCTCGTCTG	1.8847	1.3025	0.3813	1	720.590885	2686.505476	766.650695	1756.954612	4143.646409	1965.739961
GCACTAATGTTCCGGCGTTATTT	1.2715	-1.3817	-0.4664	1	4563.742269	2066.542674	1629.132726	4392.386530	4143.646409	1965.739961
CGGCTCGGCCGCTTCGCAGCG	-1.4648	-2.3164	-1.2119	1	3182.609740	6199.628022	5174.892190	1756.954612	6215.469613	1965.739961
CCCCATCGGCTCAGGGGAC	1.5570	-1.0794	-0.1103	1	2822.314298	3719.776813	2299.952084	3513.909224	8287.292818	1965.739961
CTGAATCACCCCGATTGTTCCTTTT	-1.2516	-1.8066	-0.8532	1	3783.102144	1653.234139	3737.422137	4392.386530	690.607735	2246.559955
TCTACCCTTAGACGACAAATGCGGT	1.7785	1.0955	0.1316	1	2161.772654	826.617070	862.482032	3221.083455	1381.215470	2246.559955
CCCGTCTATCTGTTTCAATCGCCTG	-1.1907	-1.4897	-0.5750	1	1080.886327	3719.776813	3354.096790	3221.083455	1381.215470	2246.559955
ATAGTTCACCATGTTTCGGGTCCTA	-1.4294	-1.7515	-0.8086	1	1020.837086	3099.814011	7762.338285	4685.212299	1381.215470	2246.559955
CAGAGTTCTTCACGCCGACGATC	1.7564	1.2355	0.3050	1	720.590885	1239.925604	1724.964063	1464.128843	2762.430939	2246.559955
CAATTTAACTGTGATAAACTACCG	2.7009	1.3638	0.4476	1	2101.723413	206.654267	1149.976042	878.477306	6215.469613	2246.559955
TCGGACTGTAGAGATCTGAACGTG	-1.7535	-2.7840	-1.4772	1	7145.859605	1653.234139	2491.614758	3221.083455	690.607735	2527.379949
CAGTCCGACGATCAAACC	1.7883	1.1171	0.1597	1	1321.083288	619.962802	958.313368	585.651537	2071.823204	2527.379949
AGTCCGACGATCACCCCCCC	1.6042	-1.0818	-0.1135	1	2221.821894	1239.925604	383.325347	878.477306	2762.430939	2527.379949
GGAAGCATTCAACAATAACAGGTCT	1.1641	-1.1675	-0.2234	1	1561.280250	3306.468279	3449.928126	4392.386530	2762.430939	2527.379949
CTGTAGAACTCTGCACGTGT	1.3555	-1.3539	-0.4371	1	3663.003663	1033.271337	2108.289411	1171.303075	5524.861878	2527.379949
CACACACGTTCTGCGTTCTACAGTC	2.6353	1.4448	0.5308	1	2942.412778	826.617070	4408.241495	1756.954612	17265.193370	2527.379949
TGAGCCGTCCGCAATTTCATCCTAC	1.2488	-1.1291	-0.1751	1	3302.708221	3306.468279	5270.723527	9956.076135	2071.823204	2808.199944
CCAGTTTGTCTTACTACAAAATG	1.3292	1.0309	0.0439	1	720.590885	1859.888407	4024.916148	2928.257687	2762.430939	3089.019938
CGCCACAGGCGGTTGAAAGAGATA	-1.1172	-1.5460	-0.6285	1	1861.526452	2686.505476	6804.024916	2928.257687	4143.646409	3089.019938
GTTCTACAGTCCGGCGATC	1.1867	-1.3411	-0.4235	1	3663.003663	3099.814011	2874.940105	3513.909224	4834.254144	3089.019938
ACGGTGGCCATGTAAGTCGGAAACC	-1.6843	-2.3027	-1.2033	1	2221.821894	14879.107254	9103.977000	5563.689605	6906.077348	3089.019938
TCCCCGTCTATATCTTTCAATCGCC	1.2905	1.1019	0.1400	1	600.492404	3099.814011	2395.783421	3806.734993	690.607735	3369.839933
CATTTTGTACGAAGACAAACTGGA	1.1915	-1.0455	-0.0642	1	780.640125	2273.196942	4216.578821	3221.083455	2071.823204	3369.839933
GGTAAGCGGCAGGGTCGGAACAGGC	-1.5495	-2.0441	-1.0314	1	1741.427971	11572.638975	1341.638716	2635.431918	3453.038674	3369.839933
CTCTCCGATGTCAAACCCCAATTCC	-1.2527	-1.7378	-0.7973	1	4023.299105	8059.516429	9199.808337	8784.773060	4834.254144	3369.839933
GTGTCTGTCCGTTTACCACGCGG	1.1055	-1.6097	-0.6868	1	7386.056566	4546.393883	3929.084811	3806.734993	10359.116022	3369.839933
CGAAAATGACCCATAGCGCTGCCGG	1.7723	1.3844	0.4692	1	900.738606	1033.271337	1341.638716	1464.128843	690.607735	3650.659927
GATCGTTAGGCTATCATTTCAGAGT	-1.3157	-1.6259	-0.7012	1	1981.624932	4133.085348	3449.928126	2928.257687	690.607735	3650.659927
GCCCGTTCCCTGGACTGTGGTTTCA	-1.0175	-1.2408	-0.3112	1	1080.886327	3099.814011	4216.578821	3221.083455	1381.215470	3650.659927
ACGTTCAGAGGTCGACAGTCCGAC	1.3274	-1.2492	-0.3210	1	4443.643788	2273.196942	3354.096790	3221.083455	6215.469613	3931.479921
GTATTAAGGATCCGGCTGCTAACA	1.8878	1.2081	0.2727	1	2401.969615	5579.665220	2491.614758	4099.560761	11740.331492	3931.479921
ACGAGGAATTGGCGTTCGACATCGG	1.5335	1.0874	0.1209	1	2041.674173	3719.776813	4216.578821	5563.689605	5524.861878	4212.299916

TGGTGCACTTGCC GGGAAACGAA	2.5926	2.0924	1.0652	1	720.590 885	413.308 535	1149.97 6042	585.651 537	0	5335.57 9893
CGCGCGTGCGGGC CAAGATGTCTAA	-1.5221	-2.1901	-1.1310	1	5644.62 8595	3926.43 1081	4983.22 9516	1464.12 8843	2762.43 0939	5335.57 9893
GAAGTAATCTGCC ATTCCTTCTAC	3.0585	1.7581	0.8141	1	3843.15 1384	826.617 070	2395.78 3421	6734.99 2679	8977.90 0552	5897.21 9882
ACGGGCTTGATTC GAACGGCGGGGA	-1.1159	-1.4765	-0.5622	1	3242.65 8980	6612.93 6557	9295.63 9674	6149.34 1142	4834.25 4144	6178.03 9876
CGATGGGGAAGAT AGGGCTCGCCAA	2.6054	1.6349	0.7092	1	2582.11 7336	2893.15 9744	2108.28 9411	3221.08 3455	10359.1 16022	6178.03 9876
CGCAGACGCGCCG AGACAGAACTT	1.3154	-1.2295	-0.2981	1	6125.02 2518	4753.04 8150	5558.21 7537	4392.38 6530	11049.7 23757	6178.03 9876
CGGCCATGCACGA CTACCCAATAAA	3.3647	2.5785	1.3665	1	960.787 846	619.962 802	2395.78 3421	4978.03 8067	1381.21 5470	7020.49 9860
GTGGCTCTTCAACG GGGATCGTCGG	-1.6469	-2.2500	-1.1699	1	8466.94 2893	8679.47 9231	4695.73 5506	5270.86 3836	690.607 735	7301.31 9854
GGGTGGCGACTGT GGCAGGATCGT	1.9753	1.1848	0.2447	1	7085.81 0364	206.654 267	2683.27 7432	11713.0 30747	690.607 735	7301.31 9854
TCGTCGGACTGGA CAACTCTGAACG	1.1876	-1.3437	-0.4262	1	10808.8 63268	7646.20 7894	9774.79 6358	8784.77 3060	15193.3 70166	9547.87 9809
CGTCGGACTGTCG TACTCTGAACGT	-1.2117	-1.9314	-0.9497	1	15252.5 07056	8679.47 9231	18974.6 04696	7906.29 5754	17955.8 01105	9547.87 9809
CTTCACGTTTGTAC CCCGGGTTCGT	1.0701	-1.3036	-0.3825	1	7866.45 0489	4959.70 2418	7762.33 8285	10541.7 27672	1381.21 5470	10109.5 19798
ACATCTTGGGCCG AACGCGCGCTA	2.8604	1.8686	0.9020	1	3122.56 0500	413.308 535	1533.30 1390	1756.95 4612	2071.82 3204	10671.1 59787
AGAGTTCTACACTA CGACGATCCCC	1.2311	-1.1663	-0.2220	1	10989.0 10989	13019.2 18847	26161.9 54959	22840.4 09956	23480.6 62983	15445.0 99691
GTCGGACTGTATA CCTCTGAACGTG	-1.1417	-1.8483	-0.8862	1	26481.7 15006	11779.2 93242	12458.0 73790	13762.8 11127	13812.1 54696	16849.1 99663
GGGATCGTCGGCC GGTAGAACTCTG	1.1825	-1.1892	-0.2499	1	14111.5 71489	32238.0 65716	39290.8 48107	40409.9 56076	38674.0 33149	22184.7 79556
CAGAGTTCTACCG ACCGACGATCCC	1.0582	-1.3034	-0.3823	1	16513.5 41104	34097.9 54123	41878.2 94202	40117.1 30307	31077.3 48066	26677.8 99466
GGACTGTAGAAAT ATGAACGTGTAC	-1.1023	-1.8831	-0.9131	1	36509.9 38149	2893.15 9744	4599.90 4169	4392.38 6530	8287.29 2818	27239.5 39455
TTCAGAGTTCTCCC GTCCGACGATC	1.2752	-1.1809	-0.2399	1	25520.9 27160	30378.1 77309	31049.3 53138	31625.1 83016	46961.3 25967	32294.2 99354
ACACGTTCAGATTA CTACAGTCCGA	1.2713	-1.3080	-0.3873	1	37110.4 30553	7646.20 7894	14662.1 94538	10541.7 27672	26243.0 93923	38753.1 59225
GCCCCCCCCTCCCT GGGGATCGT	-1.2304	-1.8829	-0.9129	1	73620.3 68702	41950.8 16284	64973.6 46382	71742.3 13324	33149.1 71271	41842.1 79163
CAAGGTGGAGATC AGGGTTCTCC	-1.2794	-1.7737	-0.8267	1	43895.9 94716	87208.1 00847	68423.5 74509	60907.7 59883	42817.6 79558	52232.5 18955
GATCCCCTGGGTA CGGGACCCC	-1.0321	-1.6582	-0.7296	1	154206. 449288	35544.5 33995	108097. 747964	130600. 292826	66988.9 50276	90985.6 78180
CGATCCCCTGGGTC GGGGACCCC	-1.0197	-1.6423	-0.7157	1	155107. 187894	35751.1 88262	111931. 001437	131771. 595900	73895.0 27624	91266.4 98175

NA = not applicable, CPM = counts per million (sequenced reads). miRNAs are sorted by statistical significance (FDR *p* value). Log fold changes are calculated based on tagwise dispersions fold changes.

Supplementary table 19: Differentially expressed genes between male A1 EV stimulated monocytes and mock controls.

Gene name	Fold change	Log fold change	FDR *p*-value	male control 1 - RPKM	male control 2 - RPKM	male A1 EVs 1 - RPKM	male A1 EVs 2 - RPKM
Cxcl2	6.627358	2.728434	2.22E-18	4.406675	2.925364	19.26392	28.44981
Ccl5	5.175555	2.371713	5.92E-10	6.206773	3.150861	22.2858	25.72484
Acod1	5.110519	2.35347	1.42E-86	25.38888	23.49632	112.6434	130.5655
Gm49388	4.835144	2.273559	0.001221	1.137119	0	2.182237	3.257478
Ifi205	4.146524	2.051903	2.03E-10	1.762151	1.629365	6.358277	7.390424
Tnf	3.929854	1.974476	8.51E-58	37.2099	38.29478	136.1595	152.2274
Maff	3.863828	1.950031	2.23E-06	2.161913	1.311846	6.96783	6.300245
Gpr84	3.599596	1.847835	3.28E-10	5.486089	5.260567	16.8931	20.84304
Bcl2a1a	3.485815	1.801496	2.04E-06	6.419416	7.386633	24.32099	22.61524
Plk2	3.437106	1.781194	1.4E-18	4.292475	3.367653	12.64879	13.10047
Htra4	3.171404	1.665122	0.000879	1.457987	2.044652	4.756622	6.042831
Cxcl3	2.973415	1.572121	6.25E-07	2.304603	2.161826	6.221622	6.748519
Rasgef1b	2.760678	1.465023	2.17E-19	2.640494	1.999387	5.664621	6.839933
Ccrl2	2.757351	1.463283	2.39E-14	9.578718	7.131278	22.71707	22.36638
Ptgs2	2.726695	1.447154	0.005085	0.994869	0.825553	2.416169	2.458166
Optn	2.659884	1.411363	8.27E-07	3.455504	2.921661	7.568043	8.999519
Ehd1	2.644408	1.402945	8.88E-21	9.8386	12.24626	26.58242	29.99495
Zc3h12c	2.639792	1.400424	1.17E-19	5.325349	5.744739	13.57996	14.80286
Myo10	2.635519	1.398087	0.002253	0.900316	0.336191	1.421248	1.793984
Clec4e	2.575697	1.364963	1.49E-50	88.87808	80.18988	205.8679	217.8313
Gbp5	2.574591	1.364343	0.00248	0.73934	0.911504	2.223103	1.915187
Ets2	2.562515	1.35756	2.88E-08	3.274569	2.878295	6.828533	8.545274
Traf1	2.489611	1.31592	5.4E-16	3.775656	4.030129	9.578281	9.306878
Tnfaip3	2.433319	1.282925	9.47E-26	11.83532	10.62205	25.3195	27.89395
Hivep3	2.389722	1.256843	0.000137	0.636297	0.729308	1.25558	1.916106
Sdc4	2.345853	1.230112	2.29E-12	12.24755	11.13378	25.19949	28.23262
Mcoln2	2.314026	1.210405	0.002209	3.091394	2.529888	7.965224	4.74954
Nfkbiz	2.313855	1.210299	1E-13	6.915009	7.45959	16.2455	16.06709
Fpr1	2.289914	1.195293	4.41E-08	19.32516	21.13266	38.16841	51.84283
Cd40	2.273211	1.184731	1.49E-05	4.527894	4.551449	9.097165	10.98266
Ralgds	2.267426	1.181055	6.97E-12	11.82144	7.806388	21.917	21.46419
Trim13	2.253965	1.172465	8.09E-06	9.983943	10.77021	24.14411	21.35024
Ccl3	2.222045	1.151888	0.000217	30.19975	13.3274	46.22894	48.36
Cfb	2.21782	1.149143	0.004333	3.473984	2.676837	7.964946	5.399403
Sod2	2.178723	1.123483	1.97E-29	25.14579	22.25248	47.73027	52.76331
Ikbke	2.176847	1.12224	1.42E-09	3.264805	2.893006	6.708185	6.362998
Pilra	2.139819	1.097489	4.82E-07	10.09531	8.68781	17.42873	21.74344
Pim3	2.133239	1.093046	0.007331	3.89926	2.804227	7.295296	6.73376
Tgm2	2.101233	1.071236	4.7E-10	18.40734	11.97983	32.09988	30.10688
Icam1	2.092196	1.065018	2.15E-16	17.28384	16.82386	33.67193	35.73434
Egr1	2.079304	1.056101	0.000256	3.595675	3.288588	7.074639	6.884434
Nfkbia	2.037983	1.027142	3.58E-21	97.96587	93.70386	176.6444	203.2422
Dusp16	2.017297	1.012424	0.021103	0.943896	1.115206	2.128633	1.909482
Gbp2	2.007149	1.005148	0.002301	4.318563	5.860901	10.84907	8.949442
Klf11	-2.099	-1.0697	0.017973	3.068895	4.094667	1.529869	1.757294
Frat2	-2.18689	-1.12888	0.005404	6.97432	10.32304	4.096641	3.529226
Ctdspl	-2.26724	-1.18094	0.000256	3.984491	4.443988	1.776823	1.819369

Supplementary table 20: Differentially expressed genes between male B2 EV stimulated monocytes and mock controls.

Gene name	Fold change	Log fold change	FDR *p*-value	male control 1 - RPKM	male control 2 - RPKM	male B2 EVs 1 - RPKM	male B2 EVs 2 - RPKM
Ccl5	7.817049	2.966624	1.37E-16	6.206773	3.150861	37.2677	35.2383
Cxcl2	7.464318	2.900011	2.46E-24	4.406675	2.925364	25.76638	28.21791
Acod1	6.695935	2.743286	3.7E-120	25.38888	23.49632	157.147	161.6958
Cxcl10	4.676307	2.22537	1.08E-08	2.178953	1.846863	9.464455	9.012994
Plk2	4.558377	2.18852	1.87E-29	4.292475	3.367653	17.88197	16.19502
Ifi205	4.105996	2.037732	1.83E-11	1.762151	1.629365	6.742845	6.883997
Oasl1	4.085549	2.03053	0.00017	1.478336	0.869870	5.545644	3.891346
Maff	3.9582	1.984844	9.63E-07	2.161913	1.311846	7.483007	6.031537
Ptges	3.87547	1.954371	5.99E-07	1.337446	1.15422	5.131553	4.30282
Ptgs2	3.859676	1.94848	5.04E-06	0.994869	0.825553	3.905785	2.954478
Mcoln2	3.675604	1.877982	1.28E-10	3.091394	2.529888	10.07079	10.15995
Htra4	3.665591	1.874046	1.64E-05	1.457987	2.044652	6.016239	6.508239
Tnf	3.579617	1.839805	5.84E-49	37.2099	38.29478	133.7579	128.7413
Cxcl3	3.385345	1.759303	5.07E-09	2.304603	2.161826	7.616478	7.132281
Myo10	3.295028	1.720291	1.82E-05	0.900316	0.336191	2.218511	1.796381
Gpr84	3.077831	1.621914	1.08E-07	5.486089	5.260567	16.98938	15.19843
Gbp5	3.042444	1.605231	6.7E-05	0.73934	0.911504	2.351191	2.548499
Ifit1	3.038792	1.603498	7.15E-10	4.750755	5.40961	16.62286	13.21436
Ccrl2	3.026979	1.597879	2.29E-17	9.578718	7.131278	26.07695	23.27518
Bcl2a1a	2.981363	1.575972	7.68E-05	6.419416	7.386633	19.51827	20.65248
Cd40	2.967424	1.569211	1.4E-12	4.527894	4.551449	12.96252	13.2842
Isg15	2.913941	1.542971	6.79E-06	20.94026	8.067638	44.93645	37.89496
Clec4e	2.909745	1.540893	7.98E-65	88.87808	80.18988	253.4309	224.6735
Ahnak2	2.892004	1.53207	1.07E-09	2.069214	1.066112	4.728653	4.13582
Ehd1	2.814328	1.49279	1.1E-23	9.8386	12.24626	30.51014	29.67436
Rasgef1b	2.809532	1.49033	5.69E-20	2.640494	1.999387	6.31357	6.43249
Cfb	2.682173	1.423402	1.66E-05	3.473984	2.676837	8.892041	7.184871
Bhlhe41	2.647258	1.404499	0.000367	1.981995	0.843981	4.417751	2.894575
Rsad2	2.620877	1.39005	4.4E-11	7.115112	4.884379	17.73529	12.876
Gbp2	2.599617	1.378299	7.7E-07	4.318563	5.860901	13.61469	11.93284
Ifit2	2.586862	1.371203	2.17E-05	4.10568	2.503358	9.885877	6.783844
Fam20c	2.574107	1.364072	1.03E-15	5.5846	3.614644	11.55103	11.6142
Hspa1a	2.562861	1.357755	5.99E-05	2.835188	5.862066	9.107869	12.54184
Ralgds	2.530995	1.339704	1.35E-15	11.82144	7.806388	24.29402	24.12532
Ifit3	2.489507	1.31586	0.003317	5.824931	3.683528	15.04976	7.996772
Ets2	2.483364	1.312296	1.76E-09	3.274569	2.878295	7.045826	7.901183
Zc3h12c	2.477402	1.308828	9.77E-17	5.325349	5.744739	13.01123	13.65259
Slc7a11	2.451022	1.293383	2.92E-40	19.51139	16.48532	44.15164	41.67242
Tgm2	2.437133	1.285185	6.66E-15	18.40734	11.97983	37.25118	34.87124
Tma16	2.434872	1.283846	3.26E-13	7.752195	5.789567	17.53349	14.55465
Ednrb	2.425877	1.278506	2.25E-15	9.530711	7.267808	20.07417	19.72552
Sdc4	2.410058	1.269068	3.55E-13	12.24755	11.13378	27.0474	27.8918
Pim3	2.409646	1.268821	0.000464	3.89926	2.804227	8.468372	7.317719
Ccl3	2.408129	1.267913	2.9E-05	30.19975	13.3274	51.17813	51.33935
Jag1	2.354574	1.235466	6.64E-07	3.067703	3.17952	6.597088	7.764884
Gdpd1	2.344999	1.229587	0.000631	6.451843	2.913467	11.73102	9.775008
Nrp2	2.326279	1.218024	6.01E-26	8.879416	8.812406	19.38064	20.6752
Gdf15	2.32385	1.216517	0.000235	8.894982	5.103986	18.49599	13.2429
Optn	2.31327	1.209934	1.08E-05	3.455504	2.921661	7.200385	7.211035
Procr	2.310074	1.207939	5.96E-14	19.15584	17.68578	39.72847	43.30616
Bcl2a1d	2.299449	1.201288	1.36E-09	26.80534	26.72572	60.86172	58.79856
Tnfaip3	2.291611	1.196362	5.33E-22	11.83532	10.62205	25.28245	24.81213
Tent5c	2.290631	1.195745	2.12E-05	3.276777	1.922454	6.429793	5.201652
Trim13	2.273998	1.185231	4.65E-06	9.983943	10.77021	25.37375	20.24601
Sod2	2.262951	1.178205	1.69E-32	25.14579	22.25248	51.45487	52.98421
Il7r	2.230268	1.157217	0.000577	9.470945	3.729949	16.2429	12.42371

Ikbke	2.2197	1.150365	4.92E-10	3.264805	2.893006	7.006059	6.283343
Fabp3	2.206284	1.141619	0.007765	10.64703	8.269574	23.58557	16.95549
Il1f9	2.167278	1.115884	0.012959	5.529735	2.523748	8.545165	8.724046
Cd274	2.15422	1.107165	3.72E-10	20.51519	12.10933	35.51765	32.92281
Cpeb4	2.147258	1.102495	7.11E-15	9.355475	8.133168	19.00342	17.52786
Saa3	2.144868	1.100889	0.004505	4.169418	2.611611	8.03275	6.166027
Hivep3	2.125514	1.087812	0.000641	0.636297	0.729308	1.230757	1.607284
Vegfa	2.125056	1.087501	0.008001	2.208519	1.323582	3.908209	3.453929
Nfkbie	2.098256	1.069191	5.19E-12	13.35239	16.14234	30.74849	29.16273
Fpr1	2.087018	1.061443	3.53E-08	19.32516	21.13266	41.39525	40.56131
Traf1	2.085768	1.060579	7.85E-10	3.775656	4.030129	7.509411	8.343075
Dusp16	2.080193	1.056717	0.009114	0.943896	1.115206	1.952328	2.223294
Mmp14	2.061718	1.043847	3.4E-07	20.64187	13.89339	40.87047	28.30889
Anpep	2.052044	1.037061	0.001406	7.544017	4.389107	14.9113	8.896926
Spic	2.049811	1.035491	1.03E-06	10.58527	6.201642	16.74628	16.84393
Slc39a14	2.030356	1.021733	0.001081	1.229242	1.29021	2.381044	2.605296
Plek	2.027471	1.019681	1.39E-28	125.9488	122.0449	246.3845	242.3478
Marcksl1	2.021197	1.01521	1.73E-18	81.89255	65.49079	141.8084	148.5937
Egr1	2.009637	1.006935	0.000563	3.595675	3.288588	7.469526	5.941159
Hfe	-2.01773	-1.01273	0.000153	11.57867	10.05594	5.221083	5.208797
Eps8	-2.0553	-1.03935	0.00089	2.099313	2.448261	1.047399	1.095225
Lrrc45	-2.05978	-1.04249	0.000699	8.621473	8.955984	4.507636	3.723938
Trf	-2.14824	-1.10315	0.000284	9.07922	8.54149	4.241697	3.693653
Irf4	-2.21434	-1.14687	9.28E-05	6.076384	6.632038	2.406444	3.191068
Svip	-2.50668	-1.32578	0.001991	4.330808	5.627485	1.496346	2.374949
Ikbip	-2.5898	-1.37284	0.00692	2.34472	2.452728	1.080172	0.685765
Sirpb1c	-2.66911	-1.41636	4.77E-07	8.852936	10.06359	3.307822	3.560198
Thtpa	-2.80218	-1.48655	0.0052	3.963252	4.275373	1.748368	1.045943

Supplementary table 21: Differentially expressed genes between female A1 EV stimulated monocytes and mock controls.

Gene name	Fold change	Log fold change	FDR *p*-value	female Ctrl 1 - RPKM	female Ctrl 2 - RPKM	female A1 EVs 1 - RPKM	female A1 EVs 2 - RPKM
Nutf2	5.506677	2.461182	9.84E-08	2.754476	1.999396	11.86002	13.76843
Acod1	4.941556	2.304965	2.1E-16	24.16296	35.37793	98.25278	185.917
Cxcl2	4.845261	2.276574	1.88E-11	4.741082	5.363246	19.05288	28.34806
Plk2	4.724437	2.240143	1.13E-06	1.013608	1.481789	4.923849	6.485235
Cxcl10	3.905519	1.965514	0.000453	2.954304	3.775865	18.74589	7.129749
Cxcl3	3.846591	1.943581	0.003061	1.801867	1.479671	3.563092	8.646481
Ccl5	3.808799	1.929336	5.49E-05	6.200798	7.702217	20.52154	30.7277
Ptges	3.763186	1.911955	0.002452	1.158004	1.410734	3.375173	5.984277
Ccl4	3.126156	1.64439	0.006352	6.366595	10.0829	22.53943	27.15636
Tnf	3.096896	1.630823	4.17E-11	41.23332	53.23411	116.2745	166.7655
Nrp2	2.905008	1.538542	1.72E-05	3.637056	6.556185	10.04967	18.57225
Saa3	2.866185	1.519132	1.92E-05	4.031037	6.100298	13.42239	14.61504
Fam20c	2.856428	1.514212	0.010301	1.062709	1.402528	2.379383	4.419604
Ccrl2	2.717942	1.442514	2.1E-06	6.873864	6.830603	15.93981	20.12163
Tgm2	2.674964	1.419519	2.23E-06	7.750998	9.146382	17.10128	26.57881
Slc7a11	2.673311	1.418628	7.54E-06	12.65133	17.73911	28.64806	49.85996
Gbp5	2.672302	1.418083	0.013612	1.477257	1.058373	4.240444	2.419195
Gpr84	2.6566	1.409581	0.00261	5.683801	11.14477	17.48064	25.75918
Slc39a14	2.619456	1.389267	0.003407	0.896151	1.576947	2.400895	3.857876
Spic	2.50093	1.322465	0.003184	3.737743	2.117558	6.175794	8.068782
Rasgef1b	2.435251	1.284071	2.62E-05	1.674085	2.303133	4.514196	4.841621
Adora2a	2.430251	1.281106	0.002752	3.316368	4.467386	8.00958	10.2435
Bcl2a1a	2.416948	1.273187	0.018043	10.68873	14.44518	23.07273	35.56189
Ednrb	2.373828	1.247215	0.029909	3.365371	4.419837	5.560531	12.2541
Tma16	2.358886	1.238105	9.35E-07	4.995123	7.451222	12.99666	15.44227
Ralgds	2.324027	1.216627	0.000269	5.518719	7.749559	12.16619	17.65484
Ifit1	2.288274	1.19426	0.039722	3.427798	2.50554	6.05504	7.169953
Mmp14	2.253822	1.172374	0.003992	7.226513	12.96454	16.19012	27.81704
Trim13	2.237455	1.161859	0.000978	10.39877	11.65135	21.19925	26.47745
Sod2	2.199807	1.137377	0.001265	22.67241	32.7298	48.48921	69.50879
Procr	2.180809	1.124863	0.016501	10.86177	15.29066	19.00406	36.03465
Zc3h12c	2.15155	1.105376	2E-05	6.292187	7.129473	12.27603	15.65607
Ets2	2.1505	1.104672	0.002452	3.150253	5.181007	7.51244	9.819513
Cd274	2.127263	1.088998	0.000949	9.377633	13.26942	20.53565	26.08232
Ehd1	2.098774	1.069547	0.000176	17.01195	22.85095	32.12097	48.77882
Bcl2a1b	2.096912	1.068266	0.016867	30.0017	49.77687	63.97443	97.80609
Tnfaip3	2.09074	1.064014	8.4E-06	12.01776	15.29784	25.92824	29.40279
Cd40	2.073456	1.052037	0.002672	5.345996	6.078555	12.51256	10.52448
Fpr1	2.072606	1.051446	0.035	22.21576	32.3912	36.44	72.76221
Plxna1	2.040405	1.028856	0.000798	6.961486	9.636703	12.6558	20.08458
Pde4b	2.038803	1.027723	0.000269	3.945963	4.061169	7.614672	8.203482
Fpr2	2.028781	1.020613	0.001376	62.95364	77.02217	108.2693	166.2436
Hivep3	2.014732	1.010588	0.040346	1.013122	0.629216	1.39135	1.821773
Clec4e	2.004694	1.003382	0.008454	88.01674	112.215	164.5468	224.1151
Hpgd	-2.07241	-1.05131	0.003895	68.4513	45.25224	35.11707	18.41485

Supplementary table 22: Differentially expressed genes between female B2 EV stimulated monocytes and mock controls.

Gene name	Fold change	Log fold change	FDR *p*-value	female Ctrl 1 - RPKM	female Ctrl 2 - RPKM	female B2 EVs 1 - RPKM	female B2 EVs 2 - RPKM
Plk2	8.82579	3.141725	8.07E-14	1.013608	1.481789	7.971869	13.25327
Ahnak2	7.253566	2.85869	7.56E-06	0.339395	0.358337	1.301276	3.562339
Cxcl2	6.604629	2.723478	4.46E-12	4.741082	5.363246	20.77466	43.26298
Anpep	6.449127	2.689104	6.05E-06	1.016192	0.9835	4.004418	8.41931
Mcoln2	6.183758	2.628484	1.57E-05	0.958475	1.686617	4.899863	10.81585
Acod1	5.757695	2.525491	7.36E-19	24.16296	35.37793	112.7759	216.3565
Cxcl3	5.540636	2.470052	4.3E-06	1.801867	1.479671	5.37332	12.09282
Fam20c	5.228077	2.38628	1.06E-09	1.062709	1.402528	4.957362	7.441405
Ccl5	5.045696	2.335053	7.56E-06	6.200798	7.702217	20.0452	47.18274
Gpnmb	3.848686	1.944366	6.25E-08	14.35269	10.32953	27.27445	63.44397
Tnf	3.653086	1.869116	3.73E-13	41.23332	53.23411	132.1538	200.0756
Myo10	3.601277	1.848508	6.17E-05	0.449725	0.730501	1.945358	2.145017
Ednrb	3.582844	1.841105	0.000119	3.365371	4.419837	7.343286	19.30505
Lhfpl2	3.527165	1.818509	1.57E-05	0.790623	1.274092	3.031335	3.959177
Nrp2	3.490607	1.803478	3.52E-07	3.637056	6.556185	11.90416	22.28605
Ccrl2	3.334912	1.737649	3.48E-08	6.873864	6.830603	17.5701	26.36823
Tgm2	3.277836	1.712744	1.67E-10	7.750998	9.146382	21.26889	32.00758
Procr	3.190689	1.673868	0.001233	10.86177	15.29066	20.27174	59.34922
Ifit1	3.079301	1.622603	0.004094	3.427798	2.50554	6.571277	10.99349
Rasgef1b	3.030924	1.599758	2.51E-07	1.674085	2.303133	4.765343	6.833342
Slc7a11	3.012796	1.591103	3.71E-07	12.65133	17.73911	32.11272	55.9013
Spic	2.946504	1.559004	0.008196	3.737743	2.117558	4.893484	11.5977
Cfb	2.936519	1.554107	0.003991	1.611368	3.009999	5.70292	7.288083
Ccl3	2.726087	1.446832	4.31E-05	21.02805	32.81989	56.08616	85.0334
Adora2a	2.72357	1.445499	0.000504	3.316368	4.467386	8.47688	11.85866
Vat1	2.683182	1.423945	7.56E-06	14.81166	15.772	27.66669	51.02209
Ralgds	2.673557	1.41876	5.97E-07	5.518719	7.749559	14.03572	20.11832
Ptgs2	2.640719	1.400931	0.013821	0.993912	2.018048	3.713055	3.923239
Plxna1	2.640308	1.400706	7.1E-06	6.961486	9.636703	15.61924	26.50248
Il7r	2.604541	1.381029	0.015572	3.30413	2.299268	4.318772	9.633517
Trim13	2.516329	1.33132	5.49E-05	10.39877	11.65135	21.9692	31.30864
Cmklr1	2.465392	1.301817	0.002437	5.753848	11.3906	15.75777	24.93419
Slamf7	2.433969	1.283311	6.32E-06	13.54136	15.34722	26.20397	41.38459
Kctd1	2.431315	1.281737	0.022042	1.017272	1.214143	2.261063	2.931569
Slpi	2.430182	1.281065	0.019242	209.8009	348.088	394.0459	904.7666
Tma16	2.4276	1.279531	7.33E-06	4.995123	7.451222	12.00651	17.09796
Gpr84	2.406161	1.266733	0.007543	5.683801	11.14477	16.8631	22.13503
Mmp14	2.380824	1.251461	0.000312	7.226513	12.96454	18.77185	27.57321
Sqstm1	2.365811	1.242335	0.000679	163.0823	177.8028	301.2364	474.5091
Sod2	2.331276	1.22112	0.000388	22.67241	32.7298	50.43999	74.06055
Osbpl3	2.292977	1.197222	4.52E-05	4.541519	3.729441	7.540535	10.70617
Cd274	2.262594	1.177978	0.000388	9.377633	13.26942	20.38678	28.93867
Hivep3	2.19577	1.134727	0.01114	1.013122	0.629216	1.650244	1.847608
Met	2.174074	1.120401	0.005598	5.745606	5.344109	7.984158	15.11214
Sgk1	2.172985	1.119678	0.000384	6.856134	6.710967	11.77446	16.56788
Clec4e	2.170802	1.118228	0.001886	88.01674	112.215	176.4845	242.776
Optn	2.164726	1.114184	0.001886	4.665104	4.235911	9.539479	9.176526
Ets2	2.143297	1.099832	0.009263	3.150253	5.181007	6.73604	10.42719
Fpr1	2.140419	1.097893	0.003984	22.21576	32.3912	43.94086	68.4221
Zc3h12c	2.134617	1.093977	0.000157	6.292187	7.129473	12.16054	15.42214
Ehd1	2.116993	1.082016	0.000177	17.01195	22.85095	33.69995	47.58847
Cipc	2.114261	1.080154	0.007469	3.528269	3.801217	6.165719	8.698477
Treml4	2.040484	1.028911	0.000714	23.49615	28.51016	40.33738	61.67184
Icam1	2.034604	1.024748	3.17E-05	17.2672	19.33327	33.35878	38.46454
Bhlhe40	2.033535	1.02399	0.005205	6.474848	8.643508	11.8895	17.66292
Hmox1	2.008271	1.005954	0.008007	184.5804	222.7529	305.4183	481.6639

Hvcn1	2.006883	1.004956	7.21E-05	29.18842	25.62938	47.47765	58.62562
Cxcl16	2.005906	1.004254	0.003934	11.47505	16.154	21.33168	31.96966
Cd209a	-2.11893	-1.08334	0.000884	28.31385	23.58834	14.70062	9.459063
Irf4	-2.12255	-1.0858	0.027658	5.356354	8.068241	3.833546	2.36684
Sirpb1c	-2.1848	-1.1275	0.000884	9.985629	11.84828	4.254	5.286748
Ahr	-2.39838	-1.26206	0.023797	3.124931	4.979009	2.033195	1.275546
Fcgr1	-2.40489	-1.26597	0.014509	7.43876	10.99552	3.111384	4.193098
Gm9733	-2.65676	-1.40967	0.009083	26.6305	29.91152	10.86216	9.691713
Thbs1	-2.6742	-1.4191	4.01E-09	33.49984	37.50027	16.21185	9.800831

Supplementary table 23: Differentially expressed genes between male A1 EV and B2 EV stimulated monocytes.

Gene name	Fold change	Log fold change	FDR *p*-value	male A1 EVs 1 - RPKM	male A1 EVs 2 - RPKM	male B2 EVs - RPKM	male B2 EVs - RPKM
Gm49388	6.12398	2.61447	0.006086	2.182237	3.257478	0	0.887682

Supplementary table 24: Differentially expressed genes between female A1 EV and B2 EV stimulated monocytes.

Gene name	Fold change	Log fold change	FDR *p*-value	female A1 EVs - RPKM	female A1 EVs - RPKM	female B2 EVs - RPKM	female B2 EVs - RPKM
Gpnmb	-2.61326	-1.38585	0.010165	15.18352	19.83364	27.27445	63.44397

Supplementary table 25: Differentially expressed genes between male and female A1 EV stimulated monocytes.

Gene name	Fold change	Log fold change	FDR *p*-value	male A1 EVs 1 - RPKM	male A1 EVs 2 - RPKM	female A1 EVs 1 - RPKM	female A1 EVs 2 - RPKM
Bhlhe41	3.967004	1.98805	0.000123	2.470101	2.107707	0.478637	0.666786
Ctsk	3.919685	1.970738	0.0002	10.97823	9.127392	2.925001	2.222618
Gpnmb	3.906495	1.965875	4.12E-17	82.84533	53.07672	15.18352	19.83364
Lhfpl2	3.334015	1.737261	2.87E-10	7.67106	5.740007	1.863355	2.174283
Phospho1	3.281472	1.714343	0.004541	5.453944	6.443701	1.387079	2.208378
Nr1h3	3.096369	1.630577	2.34E-05	12.46673	9.81942	2.557803	4.602543
Tmem140	2.728141	1.447918	0.009603	2.457862	2.047625	0.755613	0.893149
Tmem86a	2.623512	1.391499	0.00132	9.187501	9.045673	2.769852	4.155484
Dpp7	2.602345	1.379812	8.96E-09	16.02814	16.65138	5.542258	7.049503
Abcg1	2.598742	1.377814	3.88E-07	8.642984	6.419494	2.809645	3.018717
F7	2.597905	1.377349	0.01627	8.53219	6.056158	2.595296	3.012909
Ahnak2	2.586287	1.370883	0.001667	2.99021	1.984034	0.602249	1.316063
Jchain	2.570424	1.362006	1.71E-06	15.09473	13.99598	6.708898	4.747237
Ccl24	2.568876	1.361137	0.000995	28.19921	37.01852	7.761673	17.58872
Timp2	2.557736	1.354867	0.007285	5.586046	4.847293	3.095903	1.05426
Gdf15	2.547346	1.348995	0.000917	12.74707	12.1581	3.690567	6.048594
Vat1	2.534079	1.341461	2.3E-12	72.14671	57.64044	21.22197	30.23918
Entpd1	2.529668	1.338948	0.000123	5.618963	4.686118	2.449795	1.672939
Fam214a	2.51515	1.330645	0.015435	1.83406	1.969906	0.666355	0.843905
Emp1	2.496301	1.319792	1.1E-08	20.38565	18.11281	6.096869	9.374319
Spp1	2.481351	1.311126	7.1E-15	112.1378	117.679	40.01029	53.01916
Igf1	2.438414	1.285943	0.022128	1.415287	1.246761	0.446547	0.640933
Fam20c	2.422942	1.27676	5.77E-05	9.403625	7.054065	2.379383	4.419604
Il7r	2.413552	1.271158	8.1E-06	12.49865	9.190339	4.224893	4.804631
Fabp3	2.403134	1.264917	0.023558	15.23879	18.5338	5.373756	8.620411
Slamf8	2.396867	1.26115	0.000187	14.37616	13.44653	4.309128	7.276386
Anpep	2.361319	1.239593	0.001286	8.474606	6.411539	2.139106	4.153904
Plk2	2.262497	1.177916	5.48E-07	12.64879	13.10047	4.923849	6.485235
Gpr137b	2.232952	1.158952	1.32E-09	21.13691	22.54483	8.959435	10.69829
Fnip2	2.164496	1.114031	4.88E-11	24.34243	19.74953	9.290985	11.20457
Slamf7	2.141908	1.098896	9.01E-09	59.4767	46.41837	21.17002	28.55363
Cipc	2.138442	1.09656	7.73E-06	11.30195	10.00727	5.291281	4.760599

Sgk1	2.111857	1.078512	2.37E-06	23.09659	17.55502	8.692187	10.66204
Slc37a2	2.078742	1.055711	0.007689	4.775355	3.553563	2.602491	1.461448
Tnfsf12	2.069862	1.049535	0.01395	14.36517	18.69807	6.1038	9.858743
Arl11	2.041427	1.029578	0.0001	20.77418	19.12318	9.388639	10.25824
Mfsd12	2.030534	1.021859	2.66E-06	20.15725	17.19384	9.213542	9.309138
Lgmn	2.025083	1.017981	1.79E-09	97.49685	77.23118	42.92275	44.04286
Pld3	2.02417	1.01733	9.05E-07	34.18719	25.33773	13.75016	15.83502
Spic	2.012363	1.00889	3.03E-05	15.26948	13.33183	6.175794	8.068782
Pparg	2.004036	1.002908	0.000908	10.4927	11.68356	5.718353	5.437249
Gm49450	-2.00524	-1.00377	0.019254	22.97734	15.35108	28.62236	48.59598
Syne2	-2.0112	-1.00806	0.010587	0.400254	0.462019	0.902615	0.852256
Il18rap	-2.02702	-1.01936	0.015435	2.185239	1.721204	5.001865	3.041616
Kntc1	-2.03984	-1.02845	0.008614	1.478616	1.819738	4.079472	2.759689
Pram1	-2.05486	-1.03904	0.047092	6.891936	5.015402	17.31023	7.583263
Hipk2	-2.05641	-1.04012	0.000761	1.502859	1.849574	3.549147	3.422973
Kit	-2.06153	-1.04372	0.009903	1.573	1.059648	2.977848	2.514195
Cd34	-2.07297	-1.0517	0.004994	1.467378	2.291634	4.68788	3.226913
Il1b	-2.08407	-1.0594	4.88E-11	77.75831	60.75121	139.5701	151.3572
Morrbid	-2.09228	-1.06508	0.023558	0.350741	0.490727	0.804834	0.971714
Thbs1	-2.1212	-1.08488	0.00014	13.0589	6.398754	23.10507	18.63003
Serpinb1a	-2.15061	-1.10475	0.000348	21.78294	18.76584	58.48385	29.99521
Cd69	-2.18535	-1.12787	0.017719	1.303422	1.339097	3.644373	2.237302
Fcnb	-2.18879	-1.13013	0.041753	18.18171	12.20525	50.14423	17.56848
Cebpe	-2.20047	-1.13781	0.048639	12.18663	7.901452	32.07366	12.93811
Il1f9	-2.21182	-1.14524	0.001462	6.938665	6.831552	14.88188	15.86043
Sell	-2.22183	-1.15175	5.43E-06	26.8336	21.99566	70.39868	39.54463
Nedd4	-2.25184	-1.1711	1.25E-06	2.224744	2.017474	5.711276	3.970763
Ifitm1	-2.26112	-1.17704	0.001723	24.6137	10.62301	43.36604	37.20346
Treml2	-2.3057	-1.2052	0.008354	2.625665	1.477218	5.805548	3.79703
Dut	-2.32714	-1.21856	0.002461	4.13255	3.315283	9.175521	8.366636
Rab44	-2.35473	-1.23556	0.003367	8.375097	5.807918	24.36935	9.583808
BC035044	-2.36084	-1.2393	0.000751	6.753272	9.171064	23.60548	14.6154
Plekha8	-2.37368	-1.24713	0.02019	0.789868	0.93321	1.721861	2.398714
Ahrr	-2.40668	-1.26705	1.09E-05	2.1489	2.346533	4.556705	6.328141
Mgst2	-2.53401	-1.34142	0.00668	2.390721	2.157664	7.708853	4.033485
Saa3	-2.53675	-1.34298	2.17E-05	6.935745	4.041462	13.42239	14.61504
Cdca7	-2.55127	-1.35122	0.004808	2.649586	2.381842	8.412761	4.664583
Itgb2l	-2.61285	-1.38562	0.000213	4.265361	4.619468	16.08591	7.512902
Ly6i	-2.71999	-1.4436	0.011747	5.743625	3.141645	14.25972	10.33633
Hspa1a	-2.73776	-1.453	0.00272	4.599977	8.078697	25.88218	9.438824
Cxcl10	-2.73986	-1.4541	0.004446	4.586286	4.676754	18.74589	7.129749
S100a8	-2.81724	-1.49428	5.43E-06	784.5097	479.8713	2422.177	1191.221
Olfml2b	-2.8382	-1.50497	0.001233	2.145277	1.642791	6.23542	4.705201
Acpp	-2.88706	-1.5296	0.00124	0.553554	0.941379	2.358574	2.037653
Pglyrp1	-2.8873	-1.52972	5.21E-07	11.84716	11.26888	43.99183	23.78214
Myb	-2.89142	-1.53178	0.002444	1.527833	1.422937	6.481123	2.215403
Septin5	-2.89896	-1.53554	0.000151	2.261262	2.13359	8.010284	4.95959
S100a9	-2.91461	-1.5433	2.16E-06	2738.247	1608.541	8785.896	4070.917
Lcn2	-2.92727	-1.54955	7.54E-07	97.03362	58.29063	303.9552	157.1611
Ngp	-2.94814	-1.5598	1.21E-05	766.715	435.6901	2436.017	1160.84
Ctsg	-2.97128	-1.57109	0.001514	16.78298	19.33647	83.6803	25.66446
Syne1	-3.02098	-1.59502	1.55E-10	0.665022	0.502278	2.144768	1.429379
Olfm4	-3.03804	-1.60314	0.000152	4.358674	2.574834	14.11671	7.311679
Wfdc21	-3.04419	-1.60606	3.72E-06	39.94658	28.45143	126.9159	84.3161
Ltf	-3.10371	-1.63399	5.43E-06	79.65419	45.47572	273.5137	120.7867
Hspa1b	-3.21545	-1.68502	2.17E-05	8.159058	10.23573	44.32212	15.85251
Nrg1_1	-3.30391	-1.72417	0.000415	1.051656	0.235323	2.500956	1.814617
Pbx1	-3.4049	-1.76761	0.001175	0.39967	0.341033	1.742508	0.836131
Prtn3	-3.44215	-1.78331	0.000836	9.370791	7.338969	45.96237	12.71974
Hba-a2	-3.56092	-1.83225	0.007246	369.4214	277.1449	2025.946	323.0161

Tmcc2	-3.59776	-1.8471	0.00364	2.20336	2.041738	12.78494	2.820835
Camp	-3.67545	-1.87792	4.88E-11	188.3273	113.0727	750.007	373.8925
Hbb-bs	-4.09998	-2.03562	0.001585	296.8238	207.5956	1812.387	297.553
Vcam1	-4.11	-2.03914	0.000165	0.582205	0.736994	3.988817	1.557587
Hba-a1	-4.13842	-2.04908	0.001905	223.0473	163.6967	1419.075	214.2911
Hbb-bt	-4.37332	-2.12873	0.000616	42.50119	36.16243	301.398	49.92829
Mpo	-4.89048	-2.28998	6.97E-05	7.325657	8.273243	65.7566	12.10496
Elane	-5.34429	-2.418	7.29E-05	9.371656	11.07238	93.5676	18.21463
Car2	-5.79185	-2.53402	0.000172	3.045982	3.898649	35.19223	6.012632
Slc4a1	-6.34423	-2.66545	0.000325	4.449649	2.153353	38.47098	4.427968

Supplementary table 26: Differentially expressed genes between male and female B2 EV stimulated monocytes.

Gene name	Fold change	Log fold change	FDR *p*-value	male B2 EVs 1 - RPKM	male B2 EVs 2 - RPKM	female B2 EVs 1 - RPKM	female B2 EVs 2 - RPKM
Jchain	3.930773	1.974813	4.24E-07	17.69207	13.60812	2.844789	5.056672
Ctsk	3.452453	1.787622	0.004897	12.33446	10.06809	0.887938	5.446781
F7	2.744691	1.456644	0.015065	9.827381	6.141587	2.166588	3.624617
Lhfpl2	2.676444	1.420318	8.82E-09	10.2671	8.341616	3.031335	3.959177
Ifit3	2.648595	1.405227	0.019229	15.04976	7.996772	3.590425	5.148549
Abcg1	2.590622	1.373298	3.62E-09	9.595993	8.633336	2.820767	4.206095
Mx1	2.425166	1.278083	0.001593	10.45787	7.820389	4.374708	3.362653
Bhlhe41	2.37454	1.247648	0.012336	4.417751	2.894575	1.065526	2.005406
Ddx58	2.34156	1.22747	0.000321	7.396179	5.458188	3.300863	2.336321
H2-T24	2.340575	1.226863	0.000612	14.65212	12.98423	7.383478	4.803661
Timp2	2.303693	1.203949	0.023188	3.907662	4.992696	2.297335	1.633424
Spp1	2.296868	1.199668	2.49E-05	112.011	124.1894	35.03045	68.14486
Herc6	2.264805	1.179387	0.004908	3.80934	3.185555	2.070964	1.128023
Oasl2	2.255253	1.173289	6.52E-06	12.47987	9.685834	5.125356	4.874556
Rtp4	2.210054	1.144082	0.033397	12.50232	7.937299	5.460132	4.040298
Slc37a2	2.177765	1.122848	0.003329	4.984607	3.819295	1.818916	2.254056
Fabp4	2.155618	1.108102	0.0039	8.478643	8.760513	3.090476	4.836681
Ccl24	2.137918	1.096206	0.019229	24.98188	29.71446	8.639398	16.76592
Slfn5	2.13313	1.092972	5.43E-11	45.18421	33.75658	18.60543	18.93607
Gpnmb	2.124573	1.087173	0.028161	118.2018	73.61419	27.27445	63.44397
Pld3	2.099689	1.070176	0.00063	33.97341	25.59718	10.71356	17.79535
Cd200r4	2.078452	1.05551	0.036294	12.09751	9.511757	4.376732	6.040733
H2-Ab1	2.062658	1.044505	1.31E-08	63.87901	56.48008	29.10279	30.02903
Il7r	2.057083	1.0406	0.013062	16.2429	12.42371	4.318772	9.633517
Gpr137b	2.056227	1.039999	7.79E-08	26.42889	23.13697	11.0411	13.25765
Ifit2	2.052224	1.037188	0.041006	9.885877	6.783844	3.190879	4.956915
Vat1	2.048759	1.03475	0.000318	85.17545	75.21581	27.66669	51.02209
Entpd1	2.046902	1.033442	0.005421	4.979258	4.471096	2.726829	2.012594
Nr1d2	2.041119	1.02936	0.011869	5.136672	6.175986	2.48209	3.045122
Spic	2.034957	1.024999	0.01105	16.74628	16.84393	4.893484	11.5977
Lgmn	2.002887	1.002081	6.37E-08	102.5654	85.5549	40.26339	54.46739
Nedd4	-2.00642	-1.00462	6.28E-05	2.657992	1.946342	5.362721	4.129323
Odc1	-2.01695	-1.01218	0.028969	4.91826	7.327083	16.56024	8.685184
Gadd45a	-2.02447	-1.01755	0.018067	6.472896	5.992908	13.95331	11.88389
Lmtk2	-2.02506	-1.01797	0.026942	1.454128	1.250756	3.254095	2.399039
Hmbs	-2.05853	-1.04161	0.020918	5.452533	4.435212	13.28023	7.661139
Gm49450	-2.13887	-1.09685	0.012967	19.05148	9.407333	35.34369	27.48231
Slc16a1	-2.17906	-1.12371	0.036843	1.461886	2.197418	4.550031	3.552278
Cebpe	-2.18981	-1.1308	0.009881	11.04096	9.200008	28.84904	16.89216
Pilrb2	-2.19585	-1.13478	0.049179	3.500722	2.808981	8.003693	6.312366
Olfml2b	-2.20857	-1.14311	0.03763	2.582466	1.776147	4.916222	4.958979
Gpr171	-2.30041	-1.20189	0.020444	3.763298	2.850739	7.643052	7.907458
Nrg1_1	-2.30411	-1.20421	0.018514	0.789179	0.410996	1.565873	1.309823
Dtl	-2.35761	-1.23732	0.034443	0.416449	0.586063	1.468994	0.955721

Itgb2l	-2.40252	-1.26455	0.02175	5.809439	3.422777	16.55951	6.319842
Dmkn	-2.56388	-1.35833	0.007567	3.299051	2.507835	7.962277	7.343396
Kit	-2.60031	-1.37868	0.005897	0.982375	0.854166	3.01327	1.932415
Jdp2	-2.61811	-1.38853	0.006236	3.012247	5.118413	13.33395	8.365194
Septin5	-2.69742	-1.43158	0.004709	2.333219	1.944182	7.544412	4.398404
Cd34	-2.70526	-1.43577	0.003618	1.931747	1.740163	6.998268	3.235058
Plscr1	-2.70584	-1.43607	0.020444	3.401031	1.374036	8.179706	5.321683
Ltf	-2.75006	-1.45946	0.000213	77.77607	45.84043	243.9961	104.7074
Lcn2	-2.95779	-1.56452	2.7E-05	91.12495	48.68609	287.1435	136.7213
S100a9	-2.96986	-1.5704	7.79E-07	2611.747	1639.594	8727.513	4200.237
S100a8	-2.98439	-1.57744	6.52E-06	755.7283	432.6085	2426.543	1205.016
Ctsg	-3.05039	-1.60899	0.00076	17.31703	16.78339	78.84684	28.26593
Ngp	-3.07842	-1.62219	5.05E-07	688.642	435.317	2419.982	1124.253
Prtn3	-3.09246	-1.62875	0.001322	8.570234	8.300939	39.27434	14.48091
Pxylp1	-3.6224	-1.85695	0.000929	0.92861	1.0317	5.022598	2.313763
Hspa1b	-3.80106	-1.9264	0.000138	7.875549	7.844702	48.37631	13.22151
Fcnb	-3.9399	-1.97816	3.69E-07	12.22261	8.842472	58.15431	27.39773
Hba-a1	-3.94041	-1.97835	0.0017	224.9889	161.9573	1322.722	251.252
Camp	-4.04407	-2.01581	5.43E-11	179.7586	90.37369	735.6345	383.7257
Hba-a2	-4.12267	-2.04358	0.002553	300.7189	245.9813	2004.786	323.2702
Wfdc21	-4.24969	-2.08736	5.57E-06	26.30919	22.40961	151.5796	62.10289
Hbb-bs	-4.36559	-2.12618	0.002446	265.1359	189.4059	1784.256	267.1089
Vcam1	-4.54207	-2.18335	0.000321	0.772369	0.429057	4.086718	1.603722
Hbb-bt	-4.59112	-2.19885	0.001088	39.52242	29.47386	283.2813	44.72939
Mpo	-6.06399	-2.60027	1.73E-05	6.447186	7.162926	73.06195	12.24485
Car2	-6.47345	-2.69453	0.000434	4.085782	2.269684	37.3242	5.564132
Slc4a1	-6.92922	-2.79269	0.000112	3.968702	1.902047	37.24003	5.051441
Elane	-7.0748	-2.82269	4.28E-05	9.669875	6.875766	105.0582	16.73889

Supplementary table 27: Differentially expressed genes between male and female mock control stimulated monocytes.

Gene name	Fold change	Log fold change	FDR *p*-value	male Ctrl 1 - RPKM	male Ctrl 2 - RPKM	female Ctrl 1 - RPKM	female Ctrl 2 - RPKM
Ctsk	8.336964	3.059522	1.49E-07	11.12699	10.75294	0.694767	1.956119
Anpep	6.027578	2.591578	2.97E-08	7.544017	4.389107	1.016192	0.9835
Nutf2	5.254169	2.393463	4.17E-05	18.78295	5.948528	2.754476	1.999396
Lhfpl2	5.171159	2.370488	3.06E-09	6.8309	3.684429	0.790623	1.274092
Gpnmb	4.711878	2.236302	1.34E-23	70.9717	43.41745	14.35269	10.32953
Ahnak2	4.545794	2.184532	8.77E-05	2.069214	1.066112	0.339395	0.358337
Jchain	4.196969	2.069348	2.69E-09	24.6478	14.27088	5.147406	4.259629
Fam20c	3.797051	1.924879	2.11E-07	5.5846	3.614644	1.062709	1.402528
Abcg1	3.6732	1.877038	3.18E-18	10.56591	9.740123	2.926819	2.684905
Spp1	3.295775	1.720618	4.67E-16	103.7889	116.0924	24.22242	43.52126
Plk2	3.132667	1.647391	0.000383	4.292475	3.367653	1.013608	1.481789
Vat1	3.104462	1.634343	1.77E-13	57.0228	36.36134	14.81166	15.772
Spic	2.906554	1.53931	0.000201	10.58527	6.201642	3.737743	2.117558
Fabp4	2.752721	1.460859	0.001161	9.369573	4.548358	2.340139	2.800182
Slamf7	2.738533	1.453403	3.12E-18	41.65874	36.0177	13.54136	15.34722
F7	2.574565	1.364329	0.006825	7.35315	6.915283	3.013773	2.585359
Timp2	2.512249	1.32898	0.000118	7.107164	6.599339	2.51657	3.036603
Ccl24	2.467578	1.303096	0.000941	31.39615	36.20448	8.111878	19.69864
Plxna1	2.43081	1.281437	1.36E-14	22.18208	17.49782	6.961486	9.636703
Entpd1	2.424057	1.277424	6.69E-05	5.025091	5.624117	2.196361	2.252691
Mfsd12	2.409271	1.268597	2.04E-10	22.77236	20.09061	10.31706	7.727432
Il7r	2.393746	1.25927	0.020616	9.470945	3.729949	3.30413	2.299268
Fnip2	2.310997	1.208515	6.36E-13	23.04968	16.3013	8.051569	9.266038
Ipo4	2.259317	1.175887	0.007492	4.12883	4.292027	1.349953	2.454679
Gpr137b	2.259151	1.175781	3.78E-06	24.40809	15.5725	8.290761	9.709758
Engase	2.224752	1.153645	0.0147	2.907312	3.355083	1.48603	1.35502

Cipc	2.209055	1.143429	9.93E-05	7.856162	8.086108	3.528269	3.801217
Ednrb	2.203444	1.13976	0.001407	9.530711	7.267808	3.365371	4.419837
Fcrl1	2.176581	1.122064	0.008168	5.41503	5.204231	3.04917	1.869302
H2-Aa	2.117059	1.082061	1.98E-10	49.64957	42.40969	19.73008	24.53028
Slc38a7	2.106851	1.075089	0.001542	8.711755	8.759149	4.64743	3.747024
Slc37a2	2.08677	1.061272	0.004981	5.117946	3.756558	1.950327	2.393102
Nceh1	2.05187	1.036939	3.88E-09	30.49278	25.62436	15.26504	12.52765
Mtss1	2.047582	1.033921	1.77E-07	7.414723	8.465248	3.734658	4.138626
Myof	2.042896	1.030616	0.001094	11.51369	7.890277	3.278521	6.36565
Mylip	2.003842	1.002769	0.000695	19.51439	14.1511	9.531185	7.547362
Sirpb1b	-2.01463	-1.01052	0.005928	5.482275	4.862642	9.250041	12.07939
Sell	-2.01633	-1.01173	1.03E-09	37.8903	30.19197	75.7669	63.92149
Nedd4	-2.03008	-1.02154	0.000272	2.308667	2.130413	5.14087	4.019505
Kntc1	-2.03358	-1.02402	0.006918	1.580609	1.278816	3.245903	2.686079
Ets1	-2.05901	-1.04195	0.008966	2.935997	1.605913	5.411906	4.143713
Tfrc	-2.06714	-1.04763	0.000248	5.270253	6.541156	15.05955	9.743273
Hdc	-2.06745	-1.04785	0.014879	1.810378	1.893771	4.76822	3.009036
Ccr5	-2.07779	-1.05505	0.021475	5.028517	5.648686	5.978591	16.52589
Pde2a	-2.09944	-1.07	0.009059	3.249066	2.398118	7.459964	4.629597
Treml2	-2.11554	-1.08103	0.010494	2.281067	1.768634	5.127459	3.609092
Gpr171	-2.12116	-1.08485	0.005357	4.725844	4.928088	11.80324	8.97265
Pram1	-2.13964	-1.09737	0.009316	8.114747	6.296602	20.62291	10.81189
Il1b	-2.15675	-1.10886	7.28E-09	53.30102	43.22313	87.40297	124.2694
Mvb12b	-2.17318	-1.11981	0.030641	0.962362	0.865126	2.563827	1.480348
Gcnt2	-2.19173	-1.13207	0.002487	1.292441	1.501474	3.079009	3.145991
Olfml2b	-2.20293	-1.13942	0.010009	2.264944	2.93198	6.562016	5.017017
Cdca7	-2.22465	-1.15358	0.003587	3.940664	3.306337	9.842176	6.581282
Trem3	-2.23233	-1.15855	0.007598	11.98894	8.368483	27.82984	18.5969
Pecam1	-2.24706	-1.16804	0.000843	2.307403	2.124858	5.791066	4.333424
Chil1	-2.25105	-1.1706	0.003495	8.125003	5.39377	20.10564	10.94352
Olfm4	-2.29273	-1.19706	0.003781	4.023297	3.82954	11.5854	6.74009
Hells	-2.31495	-1.21098	0.000302	1.605344	1.941682	4.471197	3.848436
Rnf144a	-2.33783	-1.22517	0.000712	1.528066	1.493869	3.959606	3.223598
Thbs1	-2.36996	-1.24486	1.4E-14	17.02578	12.38968	33.49984	37.50027
Ccne2	-2.41768	-1.27362	0.007734	2.60744	3.029154	9.317635	4.548605
Retnlg	-2.43531	-1.2841	0.010576	12.41231	17.2155	49.01097	24.31459
Ahrr	-2.43701	-1.28511	4.09E-05	1.522138	2.042503	4.710377	4.072605
Dusp16	-2.51185	-1.32875	0.001582	0.943896	1.115206	2.245209	3.034266
Il1f9	-2.5921	-1.37412	0.003414	5.529735	2.523748	11.2613	10.31947
Ifitm1	-2.59915	-1.37804	9.9E-06	29.47533	14.51585	52.4924	64.20861
Septin5	-2.62457	-1.39208	0.000383	2.417242	2.02814	6.886981	5.004965
Igfbp4	-2.66292	-1.41301	0.009157	1.825522	1.284318	5.709175	2.762752
Rab44	-2.69147	-1.4284	8.63E-05	9.618858	6.046667	29.93494	13.06564
Acpp	-2.6964	-1.43103	0.000137	1.099796	1.186409	3.535067	2.723622
Adgrg3	-2.74911	-1.45897	0.000822	1.269008	1.31419	4.716167	2.516466
Cd34	-2.79174	-1.48117	6.88E-06	1.682785	3.319425	8.59796	5.57856
Pbx1	-2.79844	-1.48462	0.004502	0.430403	0.518922	1.795836	0.907976
Tmcc2	-2.83943	-1.5056	0.030129	3.386772	2.391377	13.78012	2.987789
Myb	-2.8688	-1.52045	0.004742	1.922591	1.142817	6.546197	2.441809
Mgst2	-2.91078	-1.54141	0.001161	2.650285	1.940038	9.267067	4.392947
Pglyrp1	-2.93862	-1.55514	1.5E-05	12.59282	9.468019	44.60429	21.53434
Nrg1_1	-2.94754	-1.55951	6.21E-07	1.112843	0.73499	2.473125	3.114225
Gatm	-2.9563	-1.56379	0.005049	2.1023	1.511909	7.000921	3.942221
Pxylp1	-2.95783	-1.56454	0.003587	1.197219	1.660506	6.208155	2.405377
Fcnb	-2.98032	-1.57547	0.000112	16.75281	11.01272	59.36291	25.12568
Ifi205	-3.00266	-1.58624	0.000843	1.762151	1.629365	3.688571	6.726762
Prtn3	-3.04499	-1.60644	0.000611	12.3444	11.78844	56.40612	18.5707
Ctsg	-3.05713	-1.61218	0.000822	21.7154	20.8634	101.693	31.13694
Wfdc21	-3.14859	-1.6547	8.63E-05	41.1878	24.39376	141.1947	69.85236
Lcn2	-3.15875	-1.65935	7.29E-08	90.0637	55.64158	315.9875	152.9285

Ngp	-3.16725	-1.66323	1.02E-07	784.7532	478.0438	2741.986	1332.093
S100a8	-3.2415	-1.69666	9.08E-10	720.697	520.3006	2688.281	1408.507
Ltf	-3.24767	-1.69941	7.08E-09	77.11003	52.71527	289.3664	140.167
S100a9	-3.25683	-1.70347	4E-09	2607.264	1881.824	9987.688	4903.213
Itgb2l	-3.36598	-1.75103	0.000137	5.430969	2.360959	19.03058	7.780593
Camp	-3.5031	-1.80863	1.98E-10	190.5093	132.1865	788.0971	363.8535
Vcam1	-3.52524	-1.81772	0.000605	0.592729	0.511526	2.566018	1.417138
Hspa1b	-3.71873	-1.89481	0.002797	8.377991	8.363326	53.84236	9.760355
Hba-a1	-3.948	-1.98112	0.001542	233.9545	187.6547	1451.968	247.2298
Hba-a2	-4.1088	-2.03872	0.000312	304.7827	306.6775	2140.35	423.4718
Hbb-bs	-4.31971	-2.11094	0.000822	278.392	228.9297	1927.263	310.0142
Gm20075	-4.46956	-2.16013	0.004065	0	3.149403	8.58798	5.81676
Hbb-bt	-4.73043	-2.24197	2.62E-05	34.90044	40.33819	300.353	63.10778
Slc4a1	-5.46001	-2.4489	8.63E-05	4.514723	2.164566	31.42945	5.895952
Hspa1a	-5.67261	-2.50401	1.96E-06	2.835188	5.862066	39.77244	10.59152
Car2	-5.67485	-2.50458	3.98E-05	4.920316	2.653904	36.28854	7.7849
Elane	-6.22042	-2.63701	2.97E-08	9.973581	13.83305	117.0768	34.19033
Mpo	-6.37753	-2.673	1.44E-06	6.858501	8.282052	83.85907	14.79258

Supplementary table 28: Differentially expressed genes between male and female LPS stimulated monocytes.

Gene name	Fold change	Log fold change	FDR *p*-value	male LPS 1 - RPKM	male LPS 2 - RPKM	female LPS 1 - RPKM	female LPS 2 - RPKM
Jchain	3.575954	1.838328	3.32E-08	15.12274	11.71719	3.517664	4.564298
Gpr137b	3.466872	1.793635	3.73E-07	9.582678	5.956829	2.081928	2.742938
Gdf15	3.287951	1.717189	1.63E-05	14.47091	11.34017	5.432677	3.101603
Cd200r4	3.044346	1.606133	9.69E-05	12.5354	9.6144	3.542371	4.306956
Src	2.916144	1.544062	0.000402	4.887307	3.57808	1.565247	1.576985
Tnfsf15	2.847074	1.50948	0.004867	5.264962	2.760233	2.278816	0.788493
Lhfpl2	2.819148	1.495259	5.77E-07	5.446476	4.035732	1.817374	1.820295
Trim30c	2.568213	1.360765	3.32E-08	35.76247	27.86309	11.49195	15.17496
Rilpl1	2.502949	1.323629	0.00341	6.780969	5.805617	2.77779	2.643142
Abcg1	2.481132	1.310998	0.003231	2.235286	3.428838	1.323495	1.101923
Gpnmb	2.454288	1.295305	1.36E-06	18.30536	11.25017	5.745794	7.230915
Mx1	2.348531	1.231759	1.04E-08	192.7158	161.1497	68.47544	93.38384
Ifit2	2.334176	1.222914	1.42E-09	192.8685	148.7228	73.68564	83.86359
Ifit1bl1	2.32567	1.217646	1.21E-11	62.90141	60.1074	24.39647	32.3639
Fn1	2.280974	1.18965	2.73E-05	8.875039	5.162593	3.340857	3.310004
Plk2	2.266809	1.180663	3.09E-07	55.26441	42.98367	27.33201	19.52668
H2-Eb1	2.24861	1.169034	3.83E-09	47.55196	49.1904	22.15146	24.03253
C130026I21Rik	2.242309	1.164985	0.000567	8.322295	6.77224	3.470326	3.802428
Cxcl10	2.227607	1.155495	5.13E-12	287.3388	285.3339	124.5602	151.5114
Ddhd1	2.207337	1.142307	1.8E-07	5.601502	4.031691	2.63041	2.094823
Olfr56	2.204953	1.140748	3.32E-08	17.43065	17.12109	7.326616	9.484444
Pnp2	2.203404	1.139734	0.017601	11.25819	13.23378	8.114988	3.860815
H2-Aa	2.18644	1.128584	2.79E-09	31.49803	27.06049	14.72905	14.21674
Vat1	2.18559	1.128023	1.62E-06	22.60796	16.96289	10.18499	9.4144
Cd200r1	2.183583	1.126697	0.010957	6.960709	5.071787	3.125379	2.859502
Il15	2.182946	1.126277	0.008093	8.417502	9.288811	3.915949	4.742348
Mir155hg	2.178171	1.123117	1.04E-08	62.61141	74.52715	35.94832	31.53347
Plaat3	2.15183	1.105564	0.003231	3.765052	3.074022	1.635987	1.796175
AW011738	2.130588	1.091252	0.023458	4.116587	3.157338	2.290702	1.428056
Gbp3	2.122195	1.085557	1.25E-11	83.39164	81.97972	36.3625	47.26697
Gm15832	2.098521	1.069373	0.002943	11.23668	13.17137	7.029742	5.434803
Acp5	2.093575	1.065968	2.39E-08	52.61679	55.47117	23.79031	31.50332
Gm5431	2.023357	1.016751	4.34E-06	19.81261	14.81019	8.545086	9.915706
Ifit3	2.018743	1.013457	8.72E-06	426.9145	385.6491	181.5073	250.6147
Anpep	2.01297	1.009326	0.000422	48.84448	33.93259	17.81109	26.394
Slamf7	2.007857	1.005657	6.61E-06	212.3216	157.4767	96.45851	101.9903

Thap4	-2.00545	-1.00392	0.039811	1.42994	1.165281	3.025032	2.643428
Prkar2a	-2.00724	-1.00521	0.046511	0.974368	1.961717	3.407408	2.82195
Mras	-2.01263	-1.00908	0.047274	1.286118	1.392602	3.213978	2.610647
Ssh2	-2.03628	-1.02594	0.005642	0.566284	0.603233	1.238717	1.323422
Nbeal2	-2.04378	-1.03124	0.004147	1.626157	1.216049	3.538416	2.805748
Tuba4a	-2.04615	-1.03291	8.95E-07	11.54413	9.90051	26.96792	20.59064
Rab44	-2.08384	-1.05924	0.011688	3.297439	2.911369	9.217081	4.838786
Tpi1	-2.12062	-1.08449	9.74E-10	24.97208	30.02813	61.25234	63.56908
Tnfrsf21	-2.13611	-1.09498	0.016061	2.741256	2.827483	8.521145	4.380237
Cenpf	-2.14167	-1.09874	0.042357	0.679518	0.289543	1.303871	0.992534
Ets1	-2.1514	-1.10528	6.79E-05	2.566166	1.687026	5.460366	4.563167
Olfm4	-2.1721	-1.11909	0.01052	4.065036	3.620671	11.82086	6.335005
Slc2a3	-2.17256	-1.1194	0.024273	1.072209	0.925158	2.777451	1.955687
Pecam1	-2.21375	-1.14649	0.000687	3.242966	2.367708	5.298831	8.116359
Ptprs	-2.27129	-1.18351	0.011252	0.362756	0.626009	1.26186	1.124053
Stard9	-2.28902	-1.19473	0.045217	0.176125	0.283676	0.602228	0.520942
Chil1	-2.38957	-1.25675	0.004929	7.895589	4.78086	22.53391	10.51595
Kntc1	-2.3977	-1.26165	0.029266	0.535198	0.727679	1.714066	1.53504
Alox5	-2.43811	-1.28576	0.008093	1.513522	1.414775	4.312693	3.450791
Tbc1d8	-2.4482	-1.29172	0.004319	1.927581	1.194105	4.762754	3.654749
Traf3ip3	-2.45595	-1.29628	0.003231	1.214617	1.475012	3.915454	3.193422
Gys1	-2.47085	-1.30501	0.000189	2.108707	2.892542	5.96662	7.196703
Il16	-2.53824	-1.34383	0.002967	1.283992	1.136303	4.400627	2.288416
Megf9	-2.56305	-1.35786	0.000312	1.416512	1.140758	4.354278	2.793177
Panx1	-2.62657	-1.39318	0.005642	1.223838	0.963361	3.937763	2.349743
Slc16a3	-2.64773	-1.40476	2.22E-12	9.421696	12.94003	29.28718	33.98831
S100a8	-2.79796	-1.48437	9.09E-08	740.9966	530.5552	2545.194	1311.061
S100a9	-2.79897	-1.4849	4.1E-07	2227.763	1605.925	7901.026	3734.81
Ifitm6	-2.81314	-1.49218	0.000128	15.87965	12.34395	56.47679	30.04317
Thbs1	-2.81997	-1.49568	3.52E-15	56.15377	44.66303	152.2866	154.3633
Hba-a2	-2.82049	-1.49594	0.023645	98.41212	109.2005	541.8329	95.30554
Ctsg	-2.86409	-1.51808	0.001729	9.39999	7.786369	37.40122	16.31129
Marco	-2.89032	-1.53123	9.37E-18	286.5136	345.8743	980.5211	981.5317
Ngp	-2.92849	-1.55016	1.39E-06	553.3696	337.1495	1953.312	878.7042
Nedd4	-3.06763	-1.61713	0.001687	1.417883	0.390077	4.024208	2.066521
Syne1	-3.09251	-1.62878	0.000265	0.508399	0.198645	1.610169	0.784974
Elane	-3.10741	-1.63571	0.006389	6.710294	10.44469	44.58064	13.23182
Orm1	-3.12475	-1.64374	0.000149	9.021079	7.495567	31.15763	25.20022
Bnip3	-3.14492	-1.65302	9.4E-09	5.315954	8.483266	22.3881	23.66986
Acpp	-3.20767	-1.68153	0.000115	0.635865	1.158277	2.855053	3.239095
Mmp9	-3.25849	-1.70421	2.5E-05	5.487533	3.914208	23.88106	9.522216
Olfml2b	-3.26232	-1.7059	0.001756	1.631437	1.010649	5.071294	4.454283
Pglyrp1	-3.32433	-1.73307	0.002046	7.188818	2.675755	26.0707	10.00617
Ltf	-3.32738	-1.73439	6.97E-07	42.10563	25.2568	174.5128	69.26302
Hba-a1	-3.52037	-1.81573	0.00267	59.79181	63.28556	400.4702	71.2126
Septin5	-3.52466	-1.81748	0.000658	1.289731	1.369658	6.784643	3.423515
Hbb-bs	-3.56294	-1.83307	0.009158	66.25181	87.85744	525.075	72.30073
Itgb2l	-3.72515	-1.8973	0.001409	1.79652	0.930079	8.097453	3.09969
Camp	-3.73325	-1.90043	8.77E-11	149.1116	123.2083	773.049	329.8982
Mpo	-3.8918	-1.96044	5.55E-05	3.743414	3.654156	23.74283	7.605208
Pdk1	-4.81111	-2.26637	0.000239	0.149791	0.631876	1.707281	2.21526

Supplementary table 29: Expression levels of selected genes of interest in male and female EV stimulated monocytes (second sequencing run).

Gene name	male A1 EVs - RPKM	female A1 EVs - RPKM	male B2 EVs - RPKM	female B2 EVs - RPKM
Cd69	0.704507	1.926786	0.856788	2.083909
Cxcl10	5.746752	13.507854	5.306553	18.069491
Elane	1.656960	4.067673	1.889171	3.511202
Il1b	112.804046	204.012477	98.524482	198.488188
Ly6i	5.465388	3.000789	5.972882	2.988774
Mpo	2.113060	6.429395	1.822647	6.502834
Oasl2	4.796189	14.422052	2.874785	13.731919
Saa3	17.127218	9.932240	13.400461	10.115329
Vcam1	0.597402	2.135918	0.344304	2.063002

Marked in orange are genes for which the trend between male and female samples of the same stimulation condition does not correspond to previous findings.

References

1. Marshall, J. S., Warrington, R., Watson, W. & Kim, H. L. An introduction to immunology and immunopathology. *Allergy Asthma Clin. Immunol.* **14**, 49 (2018).
2. Turvey, S. E. & Broide, D. H. Chapter 2: Innate Immunity. *J. Allergy Clin. Immunol.* **125**, S24–S32 (2010).
3. Paludan, S. R., Pradeu, T., Masters, S. L. & Mogensen, T. H. Constitutive immune mechanisms: mediators of host defence and immune regulation. *Nat. Rev. Immunol.* **21**, 137–150 (2021).
4. Jakubzick, C. V., Randolph, G. J. & Henson, P. M. Monocyte differentiation and antigen-presenting functions. *Nat. Rev. Immunol.* **17**, 349–362 (2017).
5. Mildner, A., Marinkovic, G. & Jung, S. Murine Monocytes: Origins, Subsets, Fates, and Functions. *Microbiol. Spectr.* **4**, 4.5.01 (2016).
6. Zhu, Y. P., Thomas, G. D. & Hedrick, C. C. Transcriptional Control of Monocyte Development. *Arterioscler. Thromb. Vasc. Biol.* **36**, 1722–1733 (2016).
7. Auffray, C., Sieweke, M. H. & Geissmann, F. Blood Monocytes: Development, Heterogeneity, and Relationship with Dendritic Cells. *Annu. Rev. Immunol.* **27**, 669–692 (2009).
8. Swirski, F. K. *et al.* Identification of Splenic Reservoir Monocytes and Their Deployment to Inflammatory Sites. *Science* **325**, 612–616 (2009).
9. Zimmermann, H. W., Trautwein, C. & Tacke, F. Functional Role of Monocytes and Macrophages for the Inflammatory Response in Acute Liver Injury. *Front. Physiol.* **3**, (2012).
10. Wolf, A. A., Yáñez, A., Barman, P. K. & Goodridge, H. S. The Ontogeny of Monocyte Subsets. *Front. Immunol.* **10**, 1642 (2019).
11. Geissmann, F., Jung, S. & Littman, D. R. Blood Monocytes Consist of Two Principal Subsets with Distinct Migratory Properties. *Immunity* **19**, 71–82 (2003).
12. Serbina, N. V. & Pamer, E. G. Monocyte emigration from bone marrow during bacterial infection requires signals mediated by chemokine receptor CCR2. *Nat. Immunol.* **7**, 311–317 (2006).
13. Auffray, C. *et al.* Monitoring of Blood Vessels and Tissues by a Population of Monocytes with Patrolling Behavior. *Science* **317**, 666–670 (2007).
14. Menezes, S. *et al.* The Heterogeneity of Ly6Chi Monocytes Controls Their Differentiation into iNOS+ Macrophages or Monocyte-Derived Dendritic Cells. *Immunity* **45**, 1205–1218 (2016).
15. Villani, A.-C. *et al.* Single-cell RNA-seq reveals new types of human blood dendritic cells, monocytes and progenitors. *Science* **356**, eaah4573 (2017).
16. Yáñez, A. *et al.* Granulocyte-monocyte progenitors and monocyte-dendritic cell progenitors independently produce functionally distinct monocytes. *Immunity* **47**, 890-902.e4 (2017).
17. Zilionis, R. *et al.* Single-Cell Transcriptomics of Human and Mouse Lung Cancers Reveals Conserved Myeloid Populations across Individuals and Species. *Immunity* **50**, 1317-1334.e10 (2019).
18. Lee, K. Y. M1 and M2 polarization of macrophages: a mini-review. *Med. Biol. Sci. Eng.* **2**, 1–5 (2019).
19. Arango Duque, G. & Descoteaux, A. Macrophage Cytokines: Involvement in Immunity and Infectious Diseases. *Front. Immunol.* **5**, (2014).
20. Kratofil, R. M., Kubes, P. & Deniset, J. F. Monocyte Conversion During Inflammation and Injury. *Arterioscler. Thromb. Vasc. Biol.* **37**, 35–42 (2017).

21. Geissmann, F. *et al.* Development of monocytes, macrophages and dendritic cells. *Science* **327**, 656–661 (2010).
22. Mantovani, A. *et al.* The chemokine system in diverse forms of macrophage activation and polarization. *Trends Immunol.* **25**, 677–686 (2004).
23. Serbina, N. V., Salazar-Mather, T. P., Biron, C. A., Kuziel, W. A. & Pamer, E. G. TNF/iNOS-Producing Dendritic Cells Mediate Innate Immune Defense against Bacterial Infection. *Immunity* **19**, 59–70 (2003).
24. Lauvau, G., Chorro, L., Spaulding, E. & Soudja, S. M. Inflammatory monocyte effector mechanisms. *Cell. Immunol.* **291**, 32–40 (2014).
25. Nichols, B. A., Bainton, D. F. & Farquhar, M. G. DIFFERENTIATION OF MONOCYTES. *J. Cell Biol.* **50**, 498–515 (1971).
26. Ramos-Martínez, E. *et al.* Multiple Origins of Extracellular DNA Traps. *Front. Immunol.* **12**, 621311 (2021).
27. Granger, V. *et al.* Human blood monocytes are able to form extracellular traps. *J. Leukoc. Biol.* **102**, 775–781 (2017).
28. Amulic, B., Cazalet, C., Hayes, G. L., Metzler, K. D. & Zychlinsky, A. Neutrophil Function: From Mechanisms to Disease. *Annu. Rev. Immunol.* **30**, 459–489 (2012).
29. Jaillon, S. *et al.* Neutrophil diversity and plasticity in tumour progression and therapy. *Nat. Rev. Cancer* **20**, 485–503 (2020).
30. Mestas, J. & Hughes, C. C. W. Of Mice and Not Men: Differences between Mouse and Human Immunology. *J. Immunol.* **172**, 2731–2738 (2004).
31. Summers, C. *et al.* Neutrophil kinetics in health and disease. *Trends Immunol.* **31**, 318–324 (2010).
32. Rawat, K., Syeda, S. & Shrivastava, A. Neutrophil-derived granule cargoes: paving the way for tumor growth and progression. *Cancer Metastasis Rev.* **40**, 221–244 (2021).
33. Branzk, N. *et al.* Neutrophils sense microbial size and selectively release neutrophil extracellular traps in response to large pathogens. *Nat. Immunol.* **15**, 1017–1025 (2014).
34. Ohms, M., Möller, S. & Laskay, T. An Attempt to Polarize Human Neutrophils Toward N1 and N2 Phenotypes in vitro. *Front. Immunol.* **11**, 532 (2020).
35. Fridlender, Z. G. *et al.* Polarization of Tumor-Associated Neutrophil (TAN) Phenotype by TGF-β: "N1" versus "N2" TAN. *Cancer Cell* **16**, 183–194 (2009).
36. Tecchio, C., Micheletti, A. & Cassatella, M. A. Neutrophil-Derived Cytokines: Facts Beyond Expression. *Front. Immunol.* **5**, (2014).
37. Rose, S., Misharin, A. & Perlman, H. A novel Ly6C/Ly6G-based strategy to analyze the mouse splenic myeloid compartment. *Cytom. Part J. Int. Soc. Anal. Cytol.* **81**, 343–350 (2012).
38. Ribeiro-Gomes, F. L., Peters, N. C., Debrabant, A. & Sacks, D. L. Efficient Capture of Infected Neutrophils by Dendritic Cells in the Skin Inhibits the Early Anti-Leishmania Response. *PLOS Pathog.* **8**, e1002536 (2012).
39. Rosales, C. Neutrophil: A Cell with Many Roles in Inflammation or Several Cell Types? *Front. Physiol.* **9**, 113 (2018).
40. Stanley, S. L. Amoebiasis. *Lancet Lond. Engl.* **361**, 1025–1034 (2003).
41. Diamond, L. S. & Clark, C. G. A Redescription of Entamoeba Histolytica Schaudinn, 1903 (Emended Walker, 1911) Separating It From Entamoeba Dispar Brumpt, 1925. *J. Eukaryot. Microbiol.* **40**, 340–344 (1993).
42. Shirley, D.-A. T., Farr, L., Watanabe, K. & Moonah, S. A Review of the Global Burden, New Diagnostics, and Current Therapeutics for Amebiasis. *Open Forum Infect. Dis.* **5**, ofy161 (2018).

43. Salit, I. E., Khairnar, K., Gough, K. & Pillai, D. R. A Possible Cluster of Sexually Transmitted *Entamoeba histolytica:* Genetic Analysis of a Highly Virulent Strain. *Clin. Infect. Dis.* **49**, 346–353 (2009).
44. Hung, C.-C., Chang, S.-Y. & Ji, D.-D. Entamoeba histolytica infection in men who have sex with men. *Lancet Infect. Dis.* **12**, 729–736 (2012).
45. Haque, R., Huston, C. D., Hughes, M., Houpt, E. & Petri, W. A. Amebiasis. *N. Engl. J. Med.* **348**, 1565–1573 (2003).
46. Shirley, D.-A. & Moonah, S. Fulminant Amebic Colitis after Corticosteroid Therapy: A Systematic Review. *PLoS Negl. Trop. Dis.* **10**, e0004879 (2016).
47. Petri, W. A. & Haque, R. Entamoeba histolytica brain abscess. in *Handbook of Clinical Neurology* vol. 114 147–152 (Elsevier, 2013).
48. Maldonado-Barrera, C. A. *et al.* Clinical case of cerebral amebiasis caused by E. histolytica. *Parasitol. Res.* **110**, 1291–1296 (2012).
49. Juniper, K. *et al.* Serologic diagnosis of amebiasis. *Am. J. Trop. Med. Hyg.* **21**, 157–168 (1972).
50. Swaminathan, A. *et al.* A global study of pathogens and host risk factors associated with infectious gastrointestinal disease in returned international travellers. *J. Infect.* **59**, 19–27 (2009).
51. Liu, J. *et al.* Use of quantitative molecular diagnostic methods to identify causes of diarrhoea in children: a reanalysis of the GEMS case-control study. *The Lancet* **388**, 1291–1301 (2016).
52. Lozano, R. *et al.* Global and regional mortality from 235 causes of death for 20 age groups in 1990 and 2010: a systematic analysis for the Global Burden of Disease Study 2010. *The Lancet* **380**, 2095–2128 (2012).
53. Herricks, J. R. *et al.* The global burden of disease study 2013: What does it mean for the NTDs? *PLoS Negl. Trop. Dis.* **11**, e0005424 (2017).
54. Global, regional, and national age–sex specific all-cause and cause-specific mortality for 240 causes of death, 1990–2013: a systematic analysis for the Global Burden of Disease Study 2013. *The Lancet* **385**, 117–171 (2015).
55. Estimates of the global, regional, and national morbidity, mortality, and aetiologies of diarrhoea in 195 countries: a systematic analysis for the Global Burden of Disease Study 2016. *Lancet Infect. Dis.* **18**, 1211–1228 (2018).
56. Alvarado-Esquivel, C., Hernandez-Tinoco, J. & Sanchez-Anguiano, L. F. Seroepidemiology of Entamoeba histolytica Infection in General Population in Rural Durango, Mexico. *J. Clin. Med. Res.* **7**, 435–439 (2015).
57. Yanagawa, Y. *et al.* Seroprevalence of *Entamoeba histolytica* at a voluntary counselling and testing centre in Tokyo: a cross-sectional study. *BMJ Open* **10**, e031605 (2020).
58. Ito, D. *et al.* Amebiasis presenting as acute appendicitis: Report of a case and review of Japanese literature. *Int. J. Surg. Case Rep.* **5**, 1054–1057 (2014).
59. Shimokawa, C. *et al.* Entamoeba moshkovskii Is Associated With Diarrhea in Infants and Causes Diarrhea and Colitis in Mice. *J. Infect. Dis.* **206**, 744–751 (2012).
60. Kangussu-Marcolino, M. M. & Singh, U. Ponatinib, Lestaurtinib, and mTOR/PI3K Inhibitors Are Promising Repurposing Candidates against Entamoeba histolytica. *Antimicrob. Agents Chemother.* **66**, e01207-21 (2022).
61. Wuerz, T. *et al.* A review of amoebic liver abscess for clinicians in a nonendemic setting. *Can. J. Gastroenterol.* **26**, 729–733 (2012).
62. Mortimer, L. & Chadee, K. The immunopathogenesis of Entamoeba histolytica. *Exp. Parasitol.* **126**, 366–380 (2010).

63. Ngobeni, R. *et al.* Entamoeba Species in South Africa: Correlations With the Host Microbiome, Parasite Burdens, and First Description of Entamoeba bangladeshi Outside of Asia. *J. Infect. Dis.* **216**, 1592–1600 (2017).
64. Ali, I. K. M. *et al.* Evidence for a Link between Parasite Genotype and Outcome of Infection with Entamoeba histolytica. *J. Clin. Microbiol.* **45**, 285–289 (2007).
65. Lidell, M. E., Moncada, D. M., Chadee, K. & Hansson, G. C. Entamoeba histolytica cysteine proteases cleave the MUC2 mucin in its C-terminal domain and dissolve the protective colonic mucus gel. *Proc. Natl. Acad. Sci. U. S. A.* **103**, 9298–9303 (2006).
66. Petri, W. A., Haque, R. & Mann, B. J. The Bittersweet Interface of Parasite and Host: Lectin-Carbohydrate Interactions During Human Invasion by the Parasite Entamoeba histolytica. *Annu. Rev. Microbiol.* **56**, 39–64 (2002).
67. Carrero, J. C. *et al.* Intestinal amoebiasis: 160 years of its first detection and still remains as a health problem in developing countries. *Int. J. Med. Microbiol.* **310**, 151358 (2020).
68. Teixeira, J. E., Sateriale, A., Bessoff, K. E. & Huston, C. D. Control of Entamoeba histolytica Adherence Involves Metallosurface Protease 1, an M8 Family Surface Metalloprotease with Homology to Leishmanolysin. *Infect. Immun.* **80**, 2165–2176 (2012).
69. Leippe, M., Andrä, J., Nickel, R., Tannich, E. & Muller-Eberhard, H. J. Amoebapores, a family of membranolytic peptides from cytoplasmic granules of Entamoeba histolytica: isolation, primary structure, and pore bacterial cytoplasmic membranes. *Mol. Microbiol.* **14**, 895–904 (1994).
70. Yan, L. & Stanley, S. L. Blockade of Caspases Inhibits Amebic Liver Abscess Formation in a Mouse Model of Disease. *Infect. Immun.* **69**, 7911–7914 (2001).
71. Huston, C. D., Houpt, E. R., Mann, B. J., Hahn, C. S. & Petri Jr, W. A. Caspase 3-dependent killing of host cells by the parasite Entamoeba histolytica. *Cell. Microbiol.* **2**, 617–625 (2000).
72. Orozco, E., Guarneros, G., Martinez-Palomo, A. & Sánchez, T. Entamoeba histolytica. Phagocytosis as a virulence factor. *J. Exp. Med.* **158**, 1511–1521 (1983).
73. Ralston, K. S. *et al.* Trogocytosis by Entamoeba histolytica contributes to cell killing and tissue invasion. *Nature* **508**, 526–530 (2014).
74. Matthiesen, J. *et al.* Overexpression of Specific Cysteine Peptidases Confers Pathogenicity to a Nonpathogenic Entamoeba histolytica Clone. *mBio* **4**, e00072-13 (2013).
75. Dey, I. & Chadee, K. Prostaglandin E2 Produced by Entamoeba histolytica Binds to EP4 Receptors and Stimulates Interleukin-8 Production in Human Colonic Cells. *Infect. Immun.* **76**, 5158–5163 (2008).
76. Lejeune, M., Moreau, F. & Chadee, K. Prostaglandin E2 Produced by Entamoeba histolytica Signals via EP4 Receptor and Alters Claudin-4 to Increase Ion Permeability of Tight Junctions. *Am. J. Pathol.* **179**, 807–818 (2011).
77. Nakada-Tsukui, K. & Nozaki, T. Immune Response of Amebiasis and Immune Evasion by Entamoeba histolytica. *Front. Immunol.* **7**, (2016).
78. Marinets, A. *et al.* Protection against Invasive Amebiasis by a Single Monoclonal Antibody Directed against a Lipophosphoglycan Antigen Localized on the Surface of Entamoeba histolytica. *J. Exp. Med.* **186**, 1557–1565 (1997).
79. Ávila, E. E. *et al.* Entamoeba histolytica Trophozoites and Lipopeptidophosphoglycan Trigger Human Neutrophil Extracellular Traps. *PLOS ONE* **11**, e0158979 (2016).
80. Reed, S. L., Keene, W. E., McKerrow, J. H. & Gigli, I. Cleavage of C3 by a neutral cysteine proteinase of Entamoeba histolytica. *J. Immunol. Baltim. Md 1950* **143**, 189–195 (1989).
81. Kelsall, B. L. & Ravdin, J. I. Degradation of human IgA by Entamoeba histolytica. *J. Infect. Dis.* **168**, 1319–1322 (1993).

82. Weber, C. *et al.* Bioinformatics and Functional Analysis of an Entamoeba histolytica Mannosyltransferase Necessary for Parasite Complement Resistance and Hepatical Infection. *PLoS Negl. Trop. Dis.* **2**, e165 (2008).
83. Bhattacharya, A., Arya, R., Clark, C. G. & Ackers, J. P. Absence of lipophosphoglycan-like glycoconjugates in *Entamoeba dispar*. *Parasitology* **120**, 31–35 (2000).
84. Braga, L. L. *et al.* Inhibition of the complement membrane attack complex by the galactose-specific adhesion of Entamoeba histolytica. *J. Clin. Invest.* **90**, 1131–1137 (1992).
85. Calderón, J., de Lourdes Muñoz, M. & Acosta, H. M. Surface redistribution and release of antibody-induced caps in entamoebae. *J. Exp. Med.* **151**, 184–193 (1980).
86. Bruchhaus, I. & Tannich, E. Induction of the iron-containing superoxide dismutase in Entamoeba histolytica by a superoxide anion-generating system or by iron chelation. *Mol. Biochem. Parasitol.* **67**, 281–288 (1994).
87. Rastew, E., Vicente, J. B. & Singh, U. Oxidative stress resistance genes contribute to the pathogenic potential of the anaerobic protozoan parasite, Entamoeba histolytica. *Int. J. Parasitol.* **42**, 1007–1015 (2012).
88. Vicente, J. B., Ehrenkaufer, G. M., Saraiva, L. M., Teixeira, M. & Singh, U. Entamoeba histolytica modulates a complex repertoire of novel genes in response to oxidative and nitrosative stress: implications for amebic pathogenesis. *Cell. Microbiol.* **11**, 51–69 (2009).
89. Tillack, M. *et al.* Increased expression of the major cysteine proteinases by stable episomal transfection underlines the important role of EhCP5 for the pathogenicity of Entamoeba histolytica. *Mol. Biochem. Parasitol.* **149**, 58–64 (2006).
90. Noll, J. *et al.* IL-23 prevents IL-13-dependent tissue repair associated with Ly6C lo monocytes in Entamoeba histolytica -induced liver damage. *J. Hepatol.* **64**, 1147–1157 (2016).
91. Helk, E. *et al.* TNFα-Mediated Liver Destruction by Kupffer Cells and Ly6Chi Monocytes during Entamoeba histolytica Infection. *PLoS Pathog.* **9**, e1003096 (2013).
92. Rigothier, M.-C. *et al.* Fate of *Entamoeba histolytica* during Establishment of Amoebic Liver Abscess Analyzed by Quantitative Radioimaging and Histology. *Infect. Immun.* **70**, 3208–3215 (2002).
93. Lotter, H., Jacobs, T., Gaworski, I. & Tannich, E. Sexual Dimorphism in the Control of Amebic Liver Abscess in a Mouse Model of Disease. *Infect. Immun.* **74**, 118–124 (2006).
94. Lotter, H. *et al.* Natural Killer T Cells Activated by a Lipopeptidophosphoglycan from Entamoeba histolytica Are Critically Important To Control Amebic Liver Abscess. *PLoS Pathog.* **5**, e1000434 (2009).
95. Salata, R. A., Murray, H. W., Rubin, B. Y. & Ravdin, J. I. The role of gamma interferon in the generation of human macrophages cytotoxic for Entamoeba histolytica trophozoites. *Am. J. Trop. Med. Hyg.* **37**, 72–78 (1987).
96. Sellau, J., Groneberg, M., Hoenow, S. & Lotter, H. The underlying cellular immune pathology of Entamoeba histolytica-induced hepatic amoebiasis. *J. Hepatol.* **75**, 481–482 (2021).
97. Denis, M. & Chadee, K. Cytokine activation of murine macrophages for in vitro killing of Entamoeba histolytica trophozoites. *Infect. Immun.* **57**, 1750–1756 (1989).
98. Lin, J. Y. & Chadee, K. Macrophage cytotoxicity against Entamoeba histolytica trophozoites is mediated by nitric oxide from L-arginine. *J. Immunol. Baltim. Md 1950* **148**, 3999–4005 (1992).
99. Elnekave, K., Siman-Tov, R. & Ankri, S. Consumption of L-arginine mediated by Entamoeba histolytica L-arginase (EhArg) inhibits amoebicidal activity and nitric oxide production by activated macrophages. *Parasite Immunol.* **25**, 597–608 (2003).

100. Ziraldo, C. *et al.* Central Role for MCP-1/CCL2 in Injury-Induced Inflammation Revealed by In Vitro, In Silico, and Clinical Studies. *PLoS ONE* **8**, e79804 (2013).
101. Saiman, Y. & Friedman, S. L. The Role of Chemokines in Acute Liver Injury. *Front. Physiol.* **3**, 213 (2012).
102. Shahrara, S. *et al.* IL-17-mediated monocyte migration occurs partially through CCL2/MCP-1 induction. *J. Immunol. Baltim. Md 1950* **184**, 4479–4487 (2010).
103. Shi, C. & Pamer, E. G. Monocyte recruitment during infection and inflammation. *Nat. Rev. Immunol.* **11**, 762–774 (2011).
104. Stark, M. A. *et al.* Phagocytosis of Apoptotic Neutrophils Regulates Granulopoiesis via IL-23 and IL-17. *Immunity* **22**, 285–294 (2005).
105. Sellau, J. *et al.* Androgens predispose males to monocyte-mediated immunopathology by inducing the expression of leukocyte recruitment factor CXCL1. *Nat. Commun.* **11**, 3459 (2020).
106. Ritzman, A. M. *et al.* The Chemokine Receptor CXCR2 Ligand KC (CXCL1) Mediates Neutrophil Recruitment and Is Critical for Development of Experimental Lyme Arthritis and Carditis. *Infect. Immun.* **78**, 4593–4600 (2010).
107. Wang, L. *et al.* CXCL1–CXCR2 axis mediates angiotensin II-induced cardiac hypertrophy and remodelling through regulation of monocyte infiltration. *Eur. Heart J.* **39**, 1818–1831 (2018).
108. Das, P., Lahiri, A., Lahiri, A. & Chakravortty, D. Modulation of the Arginase Pathway in the Context of Microbial Pathogenesis: A Metabolic Enzyme Moonlighting as an Immune Modulator. *PLoS Pathog.* **6**, e1000899 (2010).
109. DeAngelis, R. A. *et al.* A Complement–IL-4 Regulatory Circuit Controls Liver Regeneration. *J. Immunol.* **188**, 641–648 (2012).
110. Campos-Rodríguez, R. *et al.* A review of the proposed role of neutrophils in rodent amebic liver abscess models. *Parasite* **23**, 6 (2016).
111. Blessmann, J. *et al.* Epidemiology of amebiasis in a region of high incidence of amebic liver abscess in central Vietnam. *Am. J. Trop. Med. Hyg.* **66**, 578–583 (2002).
112. Acuna-Soto, R. Gender Distribution in Asymptomatic and Invasive Amebiasis. **95**, (2000).
113. Klein, S. L. & Flanagan, K. L. Sex differences in immune responses. *Nat. Rev. Immunol.* **16**, 626–638 (2016).
114. Bernin, H. & Lotter, H. Sex Bias in the Outcome of Human Tropical Infectious Diseases: Influence of Steroid Hormones. *J. Infect. Dis.* **209**, S107–S113 (2014).
115. Marriott, I. & Huet-Hudson, Y. M. Sexual Dimorphism in Innate Immune Responses to Infectious Organisms. *Immunol. Res.* **34**, 177–192 (2006).
116. Klein, S. L. Hormonal and immunological mechanisms mediating sex differences in parasite infection. *Parasite Immunol.* **26**, 247–264 (2004).
117. Roberts, C. W., Walker, W. & Alexander, J. Sex-Associated Hormones and Immunity to Protozoan Parasites. *Clin. Microbiol. Rev.* **14**, 476–488 (2001).
118. Gourdy, P. *et al.* Relevance of sexual dimorphism to regulatory T cells: estradiol promotes IFN-γ production by invariant natural killer T cells. *Blood* **105**, 2415–2420 (2005).
119. Lotter, H. *et al.* Testosterone Increases Susceptibility to Amebic Liver Abscess in Mice and Mediates Inhibition of IFNγ Secretion in Natural Killer T Cells. *PLoS ONE* **8**, e55694 (2013).
120. Bernin, H. *et al.* Immune markers characteristic for asymptomatically infected and diseased Entamoeba histolytica individuals and their relation to sex. *BMC Infect. Dis.* **14**, 621 (2014).
121. Snow, M., Chen, M., Guo, J., Atkinson, J. & Stanley, S. L. Differences in complement-mediated killing of Entamoeba histolytica between men and women--an explanation for the increased susceptibility of men to invasive amebiasis? *Am. J. Trop. Med. Hyg.* **78**, 922–923 (2008).

122. Van Niel, G., D'Angelo, G. & Raposo, G. Shedding light on the cell biology of extracellular vesicles. *Nat. Rev. Mol. Cell Biol.* **19**, 213–228 (2018).
123. Carrera-Bravo, C., Koh, E. Y. & Tan, K. S. W. The roles of parasite-derived extracellular vesicles in disease and host-parasite communication. *Parasitol. Int.* **83**, 102373 (2021).
124. Johnstone, R. M., Adam, M., Hammond, J. R., Orr, L. & Turbide, C. Vesicle formation during reticulocyte maturation. Association of plasma membrane activities with released vesicles (exosomes). *J. Biol. Chem.* **262**, 9412–9420 (1987).
125. Colombo, M., Raposo, G. & Théry, C. Biogenesis, Secretion, and Intercellular Interactions of Exosomes and Other Extracellular Vesicles. *Annu. Rev. Cell Dev. Biol.* **30**, 255–289 (2014).
126. Théry, C. *et al.* Minimal information for studies of extracellular vesicles 2018 (MISEV2018): a position statement of the International Society for Extracellular Vesicles and update of the MISEV2014 guidelines. *J. Extracell. Vesicles* **7**, 1535750 (2018).
127. O'Grady, T. *et al.* Sorting and packaging of RNA into extracellular vesicles shape intracellular transcript levels. *BMC Biol.* **20**, 72 (2022).
128. Valadi, H. *et al.* Exosome-mediated transfer of mRNAs and microRNAs is a novel mechanism of genetic exchange between cells. *Nat. Cell Biol.* **9**, 654–659 (2007).
129. van der Koog, L., Gandek, T. B. & Nagelkerke, A. Liposomes and Extracellular Vesicles as Drug Delivery Systems: A Comparison of Composition, Pharmacokinetics, and Functionalization. *Adv. Healthc. Mater.* **11**, 2100639 (2022).
130. Antimisiaris, S. G., Mourtas, S. & Marazioti, A. Exosomes and Exosome-Inspired Vesicles for Targeted Drug Delivery. *Pharmaceutics* **10**, 218 (2018).
131. Sabanovic, B., Piva, F., Cecati, M. & Giulietti, M. Promising Extracellular Vesicle-Based Vaccines against Viruses, Including SARS-CoV-2. *Biology* **10**, 94 (2021).
132. Dang, X. T. T., Kavishka, J. M., Zhang, D. X., Pirisinu, M. & Le, M. T. N. Extracellular Vesicles as an Efficient and Versatile System for Drug Delivery. *Cells* **9**, 2191 (2020).
133. Ciferri, M. C., Quarto, R. & Tasso, R. Extracellular Vesicles as Biomarkers and Therapeutic Tools: From Pre-Clinical to Clinical Applications. *Biology* **10**, 359 (2021).
134. Fabbiano, F. *et al.* RNA packaging into extracellular vesicles: An orchestra of RNA-binding proteins? *J. Extracell. Vesicles* **10**, e12043 (2020).
135. Villarroya-Beltri, C. *et al.* Sumoylated hnRNPA2B1 controls the sorting of miRNAs into exosomes through binding to specific motifs. *Nat. Commun.* **4**, 2980 (2013).
136. Hanson, P. I. & Cashikar, A. Multivesicular Body Morphogenesis. *Annu. Rev. Cell Dev. Biol.* **28**, 337–362 (2012).
137. Cruz Camacho, A., Alfandari, D., Kozela, E. & Regev-Rudzki, N. Biogenesis of extracellular vesicles in protozoan parasites: The ESCRT complex in the trafficking fast lane? *PLOS Pathog.* **19**, e1011140 (2023).
138. Sahu, R. *et al.* MICROAUTOPHAGY OF CYTOSOLIC PROTEINS BY LATE ENDOSOMES. *Dev. Cell* **20**, 131–139 (2011).
139. Stuffers, S., Sem Wegner, C., Stenmark, H. & Brech, A. Multivesicular Endosome Biogenesis in the Absence of ESCRTs. *Traffic* **10**, 925–937 (2009).
140. van Niel, G. *et al.* The tetraspanin CD63 regulates ESCRT-independent and dependent endosomal sorting during melanogenesis. *Dev. Cell* **21**, 708–721 (2011).
141. Trajkovic, K. *et al.* Ceramide triggers budding of exosome vesicles into multivesicular endosomes. *Science* **319**, 1244–1247 (2008).
142. Goñi, F. M. & Alonso, A. Effects of ceramide and other simple sphingolipids on membrane lateral structure. *Biochim. Biophys. Acta BBA - Biomembr.* **1788**, 169–177 (2009).

143. Andreu, Z. & Yáñez-Mó, M. Tetraspanins in Extracellular Vesicle Formation and Function. *Front. Immunol.* **5**, (2014).
144. Sharma, M. *et al.* Characterization of Extracellular Vesicles from Entamoeba histolytica Identifies Roles in Intercellular Communication That Regulates Parasite Growth and Development. *Infect. Immun.* **88**, e00349-20 (2020).
145. Díaz-Godínez, C., Ríos-Valencia, D. G., García-Aguirre, S., Martínez-Calvillo, S. & Carrero, J. C. Immunomodulatory effect of extracellular vesicles from Entamoeba histolytica trophozoites: Regulation of NETs and respiratory burst during confrontation with human neutrophils. *Front. Cell. Infect. Microbiol.* **12**, 1018314 (2022).
146. Galindo, A. *et al.* EhVps23, an ESCRT-I Member, Is a Key Factor in Secretion, Motility, Phagocytosis and Tissue Invasion by Entamoeba histolytica. *Front. Cell. Infect. Microbiol.* **12**, 835654 (2022).
147. Sharma, M., Zhang, H., Ehrenkaufer, G. & Singh, U. Stress Response in Entamoeba histolytica Is Associated with Robust Processing of tRNA to tRNA Halves. *mBio* **14**, e03450-22 (2023).
148. Gavinho, B. *et al.* Peptidylarginine Deiminase Inhibition Abolishes the Production of Large Extracellular Vesicles From Giardia intestinalis, Affecting Host-Pathogen Interactions by Hindering Adhesion to Host Cells. *Front. Cell. Infect. Microbiol.* **10**, 417 (2020).
149. Evans-Osses, I. *et al.* Microvesicles released from Giardia intestinalis disturb host-pathogen response in vitro. *Eur. J. Cell Biol.* **96**, 131–142 (2017).
150. Siddiq, A., Allain, T., Dong, G., Olivier, M. & Buret, A. Giardia extracellular vesicles disrupt intestinal epithelial junctions and inhibit the growth of commensal bacteria while increasing their swimming motility. *FASEB J.* **34**, 1–1 (2020).
151. Zhao, P. *et al.* Extracellular vesicles secreted by Giardia duodenalis regulate host cell innate immunity via TLR2 and NLRP3 inflammasome signaling pathways. *PLoS Negl. Trop. Dis.* **15**, e0009304 (2021).
152. Ankarklev, J., Hjelmqvist, D. & Mantel, P.-Y. Uncovering the Role of Erythrocyte-Derived Extracellular Vesicles in Malaria: From Immune Regulation to Cell Communication. *J. Circ. Biomark.* **3**, (2014).
153. Mantel, P.-Y. *et al.* Malaria-Infected Erythrocyte-Derived Microvesicles Mediate Cellular Communication within the Parasite Population and with the Host Immune System. *Cell Host Microbe* **13**, 521–534 (2013).
154. Regev-Rudzki, N. *et al.* Cell-cell communication between malaria-infected red blood cells via exosome-like vesicles. *Cell* **153**, 1120–1133 (2013).
155. Mantel, P.-Y. & Marti, M. The role of extracellular vesicles in Plasmodium and other protozoan parasites. *Cell. Microbiol.* **16**, 344–354 (2014).
156. Mantel, P.-Y. *et al.* Infected erythrocyte-derived extracellular vesicles alter vascular function via regulatory Ago2-miRNA complexes in malaria. *Nat. Commun.* **7**, 12727 (2016).
157. Twu, O. *et al.* Trichomonas vaginalis Exosomes Deliver Cargo to Host Cells and Mediate Host∶Parasite Interactions. *PLoS Pathog.* **9**, e1003482 (2013).
158. Nievas, Y. R., Lizarraga, A., Salas, N., Cóceres, V. M. & Miguel, N. Extracellular vesicles released by anaerobic protozoan parasites: Current situation. *Cell. Microbiol.* **22**, (2020).
159. Atayde, V. D. *et al.* Leishmania exosomes and other virulence factors: Impact on innate immune response and macrophage functions. *Cell. Immunol.* **309**, 7–18 (2016).
160. Silverman, J. M. *et al.* An exosome-based secretion pathway is responsible for protein export from Leishmania and communication with macrophages. *J. Cell Sci.* **123**, 842–852 (2010).
161. Silverman, J. M. *et al.* Leishmania Exosomes Modulate Innate and Adaptive Immune Responses through Effects on Monocytes and Dendritic Cells. *J. Immunol.* **185**, 5011–5022 (2010).

162. Atayde, V. D. *et al.* Exosome Secretion by the Parasitic Protozoan Leishmania within the Sand Fly Midgut. *Cell Rep.* **13**, 957–967 (2015).
163. Beauvillain, C., Juste, M. O., Dion, S., Pierre, J. & Dimier-Poisson, I. Exosomes are an effective vaccine against congenital toxoplasmosis in mice. *Vaccine* **27**, 1750–1757 (2009).
164. Trocoli Torrecilhas, A. *et al.* Trypanosoma cruzi: parasite shed vesicles increase heart parasitism and generate an intense inflammatory response. *Microbes Infect.* **11**, 29–39 (2009).
165. Meyer, M. *et al.* Overexpression of Differentially Expressed Genes Identified in Non-pathogenic and Pathogenic Entamoeba histolytica Clones Allow Identification of New Pathogenicity Factors Involved in Amoebic Liver Abscess Formation. *PLOS Pathog.* **12**, e1005853 (2016).
166. Bärreiter, V. Immunomodulatory functions of Entamoeba histolytica-derived extracellular vesicles on primary neutrophils. (Ludwig Maximilian University of Munich, 2023).
167. Aurrecoechea, C. *et al.* AmoebaDB and MicrosporidiaDB: functional genomic resources for Amoebozoa and Microsporidia species. *Nucleic Acids Res.* **39**, D612–D619 (2011).
168. The Galaxy Community. The Galaxy platform for accessible, reproducible and collaborative biomedical analyses: 2022 update. *Nucleic Acids Res.* **50**, W345–W351 (2022).
169. Babicki, S. *et al.* Heatmapper: web-enabled heat mapping for all. *Nucleic Acids Res.* **44**, W147–W153 (2016).
170. Heberle, H., Meirelles, G. V., Da Silva, F. R., Telles, G. P. & Minghim, R. InteractiVenn: a web-based tool for the analysis of sets through Venn diagrams. *BMC Bioinformatics* **16**, 169 (2015).
171. Paysan-Lafosse, T. *et al.* InterPro in 2022. *Nucleic Acids Res.* **51**, D418–D427 (2023).
172. Sayers, E. W. *et al.* Database resources of the national center for biotechnology information. *Nucleic Acids Res.* **50**, D20–D26 (2022).
173. Thomas, P. D. *et al.* PANTHER: Making genome-scale phylogenetics accessible to all. *Protein Sci.* **31**, 8–22 (2022).
174. Ye, J. *et al.* Primer-BLAST: A tool to design target-specific primers for polymerase chain reaction. *BMC Bioinformatics* **13**, 134 (2012).
175. Untergasser, A. *et al.* Primer3—new capabilities and interfaces. *Nucleic Acids Res.* **40**, e115 (2012).
176. Supek, F., Bošnjak, M., Škunca, N. & Šmuc, T. REVIGO Summarizes and Visualizes Long Lists of Gene Ontology Terms. *PLoS ONE* **6**, e21800 (2011).
177. Ge, S. X., Jung, D. & Yao, R. ShinyGO: a graphical gene-set enrichment tool for animals and plants. *Bioinformatics* **36**, 2628–2629 (2020).
178. The UniProt Consortium *et al.* UniProt: the Universal Protein Knowledgebase in 2023. *Nucleic Acids Res.* **51**, D523–D531 (2023).
179. Kalra, H. *et al.* Vesiclepedia: A Compendium for Extracellular Vesicles with Continuous Community Annotation. *PLoS Biol.* **10**, e1001450 (2012).
180. Diamond, L. S., Harlow, D. R. & Cunnick, C. C. A new medium for the axenic cultivation of Entamoeba histolytica and other Entamoeba. *Trans. R. Soc. Trop. Med. Hyg.* **72**, 431–432 (1978).
181. Lötvall, J. *et al.* Minimal experimental requirements for definition of extracellular vesicles and their functions: a position statement from the International Society for Extracellular Vesicles. *J. Extracell. Vesicles* **3**, 26913 (2014).
182. Cheng, Y., Zeng, Q., Han, Q. & Xia, W. Effect of pH, temperature and freezing-thawing on quantity changes and cellular uptake of exosomes. *Protein Cell* **10**, 295–299 (2019).
183. Gardiner, C. *et al.* Measurement of refractive index by nanoparticle tracking analysis reveals heterogeneity in extracellular vesicles. *J. Extracell. Vesicles* **3**, 10.3402/jev.v3.25361 (2014).

184. Hughes, C. S. *et al.* Single-pot, solid-phase-enhanced sample preparation for proteomics experiments. *Nat. Protoc.* **14**, 68–85 (2019).
185. Rappsilber, J., Mann, M. & Ishihama, Y. Protocol for micro-purification, enrichment, pre-fractionation and storage of peptides for proteomics using StageTips. *Nat. Protoc.* **2**, 1896–1906 (2007).
186. Cox, J. & Mann, M. MaxQuant enables high peptide identification rates, individualized p.p.b.-range mass accuracies and proteome-wide protein quantification. *Nat. Biotechnol.* **26**, 1367–1372 (2008).
187. Benjamini, Y. & Hochberg, Y. Controlling the False Discovery Rate: A Practical and Powerful Approach to Multiple Testing. *J. R. Stat. Soc. Ser. B Methodol.* **57**, 289–300 (1995).
188. Cox, J. *et al.* Accurate proteome-wide label-free quantification by delayed normalization and maximal peptide ratio extraction, termed MaxLFQ. *Mol. Cell. Proteomics MCP* **13**, 2513–2526 (2014).
189. Tyanova, S. *et al.* The Perseus computational platform for comprehensive analysis of (prote)omics data. *Nat. Methods* **13**, 731–740 (2016).
190. Mi, H. *et al.* Protocol Update for large-scale genome and gene function analysis with the PANTHER classification system (v.14.0). *Nat. Protoc.* **14**, 703–721 (2019).
191. Zhang, X., Yang, Q., Lang, Y., Jiang, X. & Wu, P. Rationale of 3,3′,5,5′-Tetramethylbenzidine as the Chromogenic Substrate in Colorimetric Analysis. *Anal. Chem.* **92**, 12400–12406 (2020).
192. Mar-Aguilar, F. *et al.* Identification and Characterization of microRNAS from Entamoeba histolytica HM1-IMSS. *PLoS ONE* **8**, e68202 (2013).
193. Moraga, C. *et al.* BrumiR: A toolkit for *de novo* discovery of microRNAs from sRNA-seq data. *GigaScience* **11**, giac093 (2022).
194. Lorenzi, H. A. *et al.* New Assembly, Reannotation and Analysis of the Entamoeba histolytica Genome Reveal New Genomic Features and Protein Content Information. *PLoS Negl. Trop. Dis.* **4**, e716 (2010).
195. Schroeder, A. *et al.* The RIN: an RNA integrity number for assigning integrity values to RNA measurements. *BMC Mol. Biol.* **7**, 3 (2006).
196. Pfaffl, M. W. A new mathematical model for relative quantification in real-time RT-PCR. *Nucleic Acids Res.* **29**, 45e–445 (2001).
197. Bachurski, D. *et al.* Extracellular vesicle measurements with nanoparticle tracking analysis – An accuracy and repeatability comparison between NanoSight NS300 and ZetaView. *J. Extracell. Vesicles* **8**, 1596016 (2019).
198. Choi, D.-S., Kim, D.-K., Kim, Y.-K. & Gho, Y. S. Proteomics of extracellular vesicles: Exosomes and ectosomes: PROTEOMICS OF EXTRACELLULAR VESICLES. *Mass Spectrom. Rev.* **34**, 474–490 (2015).
199. Tomii, Santos, & Nozaki. Genome-Wide Analysis of Known and Potential Tetraspanins in Entamoeba histolytica. *Genes* **10**, 885 (2019).
200. López-Reyes, I. *et al.* Detection of the Endosomal Sorting Complex Required for Transport in Entamoeba histolytica and Characterization of the EhVps4 Protein. *J. Biomed. Biotechnol.* **2010**, 890674 (2010).
201. MacFarlane, L.-A. & Murphy, P. R. MicroRNA: Biogenesis, Function and Role in Cancer. *Curr. Genomics* **11**, 537–561 (2010).
202. Zhang, H., Ehrenkaufer, G. M., Pompey, J. M., Hackney, J. A. & Singh, U. Small RNAs with 5′-Polyphosphate Termini Associate with a Piwi-Related Protein and Regulate Gene Expression in the Single-Celled Eukaryote Entamoeba histolytica. *PLoS Pathog.* **4**, e1000219 (2008).

203. Zhang, H., Ehrenkaufer, G. M., Hall, N. & Singh, U. Small RNA pyrosequencing in the protozoan parasite Entamoeba histolytica reveals strain-specific small RNAs that target virulence genes. *BMC Genomics* **14**, 53 (2013).
204. Bofill-De Ros, X., Yang, A. & Gu, S. IsomiRs: Expanding the miRNA repression toolbox beyond the seed. *Biochim. Biophys. Acta BBA - Gene Regul. Mech.* **1863**, 194373 (2020).
205. Lewis, B. P., Shih, I., Jones-Rhoades, M. W., Bartel, D. P. & Burge, C. B. Prediction of Mammalian MicroRNA Targets. *Cell* **115**, 787–798 (2003).
206. Lassen, L. B. *et al.* Septin9 is involved in T-cell development and CD8+ T-cell homeostasis. *Cell Tissue Res.* **352**, 695–705 (2013).
207. Wu, X. *et al.* The Roles of CCR9/CCL25 in Inflammation and Inflammation-Associated Diseases. *Front. Cell Dev. Biol.* **9**, 686548 (2021).
208. Maldonado-Bernal, C. *et al.* The innate immune response to Entamoeba histolytica lipopeptidophosphoglycan is mediated by toll-like receptors 2 and 4. *Parasite Immunol.* **27**, 127–137 (2005).
209. Mortimer, L., Moreau, F., Cornick, S. & Chadee, K. Gal-lectin-dependent contact activates the inflammasome by invasive Entamoeba histolytica. *Mucosal Immunol.* **7**, 829–841 (2014).
210. Quach, J., Moreau, F., Sandall, C. & Chadee, K. Entamoeba histolytica-induced IL-1β secretion is dependent on caspase-4 and gasdermin D. *Mucosal Immunol.* **12**, 323–339 (2019).
211. Van Der Veen, B. S., De Winther, M. P. J. & Heeringa, P. Myeloperoxidase: Molecular Mechanisms of Action and Their Relevance to Human Health and Disease. *Antioxid. Redox Signal.* **11**, 2899–2937 (2009).
212. Amici, S. A. *et al.* CD38 Is Robustly Induced in Human Macrophages and Monocytes in Inflammatory Conditions. *Front. Immunol.* **9**, 1593 (2018).
213. De Maria, R. *et al.* Triggering of human monocyte activation through CD69, a member of the natural killer cell gene complex family of signal transducing receptors. *J. Exp. Med.* **180**, 1999–2004 (1994).
214. Hoenow, S. *et al.* The Properties of Proinflammatory Ly6Chi Monocytes Are Differentially Shaped by Parasitic and Bacterial Liver Infections. *Cells* **11**, 2539 (2022).
215. Ivetic, A., Hoskins Green, H. L. & Hart, S. J. L-selectin: A Major Regulator of Leukocyte Adhesion, Migration and Signaling. *Front. Immunol.* **10**, 1068 (2019).
216. Raudvere, U. *et al.* g:Profiler: a web server for functional enrichment analysis and conversions of gene lists (2019 update). *Nucleic Acids Res.* **47**, W191–W198 (2019).
217. Li, P., Kaslan, M., Lee, S. H., Yao, J. & Gao, Z. Progress in Exosome Isolation Techniques. *Theranostics* **7**, 789–804 (2017).
218. Patel, G. K. *et al.* Comparative analysis of exosome isolation methods using culture supernatant for optimum yield, purity and downstream applications. *Sci. Rep.* **9**, 5335 (2019).
219. Liangsupree, T., Multia, E. & Riekkola, M.-L. Modern isolation and separation techniques for extracellular vesicles. *J. Chromatogr. A* **1636**, 461773 (2021).
220. Gelibter, S. *et al.* The impact of storage on extracellular vesicles: A systematic study. *J. Extracell. Vesicles* **11**, e12162 (2022).
221. Rosa-Fernandes, L., Rocha, V. B., Carregari, V. C., Urbani, A. & Palmisano, G. A Perspective on Extracellular Vesicles Proteomics. *Front. Chem.* **5**, 102 (2017).
222. Ujang, J. A. *et al.* Proteome analysis of excretory-secretory proteins of Entamoeba histolytica HM1:IMSS via LC–ESI–MS/MS and LC–MALDI–TOF/TOF. *Clin. Proteomics* **13**, 33 (2016).
223. Espinosa, A. *et al.* The Bifunctional Entamoeba histolytica Alcohol Dehydrogenase 2 (EhADH2) Protein Is Necessary for Amebic Growth and Survival and Requires an Intact C-terminal Domain

for Both Alcohol Dehydrogenase and Acetaldehyde Dehydrogenase Activity*. *J. Biol. Chem.* **276**, 20136–20143 (2001).

224. Pineda, E. *et al.* The bifunctional aldehyde-alcohol dehydrogenase controls ethanol and acetate production in *Entamoeba histolytica* under aerobic conditions. *FEBS Lett.* **587**, 178–184 (2013).
225. Galindo, A. *et al.* EhVps23: A Component of ESCRT-I That Participates in Vesicular Trafficking and Phagocytosis of Entamoeba histolytica. *Front. Cell. Infect. Microbiol.* **11**, 770759 (2021).
226. König, C. *et al.* Taxon-Specific Proteins of the Pathogenic Entamoeba Species E. histolytica and E. nuttalli. *Front. Cell. Infect. Microbiol.* **11**, (2021).
227. König, C. Analyse des intestinalen Invasionsprozesses von Entamoeba histolytica (SCHAUDINN, 1903) unter Verwendung eines humanen 2D-Organoidmodells. (University of Hamburg, 2022).
228. Saito-Nakano, Y. *et al.* ArfX2 GTPase Regulates Trafficking From the Trans-Golgi to Lysosomes and Is Necessary for Liver Abscess Formation in the Protozoan Parasite Entamoeba histolytica. *Front. Cell. Infect. Microbiol.* **11**, 794152 (2021).
229. Schorey, J. S., Cheng, Y., Singh, P. P. & Smith, V. L. Exosomes and other extracellular vesicles in host–pathogen interactions. *EMBO Rep.* **16**, 24–43 (2015).
230. Marchat, L. A., Hernández-de La Cruz, O. N., Ramírez-Moreno, E., Silva-Cázares, M. B. & López-Camarillo, C. Proteomics approaches to understand cell biology and virulence of Entamoeba histolytica protozoan parasite. *J. Proteomics* **226**, 103897 (2020).
231. Luna-Nácar, M. *et al.* Proteomic Study of Entamoeba histolytica Trophozoites, Cysts, and Cyst-Like Structures. *PLOS ONE* **11**, e0156018 (2016).
232. Biller, L. *et al.* Comparison of two genetically related Entamoeba histolytica cell lines derived from the same isolate with different pathogenic properties. *PROTEOMICS* **9**, 4107–4120 (2009).
233. Buck, A. H. *et al.* Exosomes secreted by nematode parasites transfer small RNAs to mammalian cells and modulate innate immunity. *Nat. Commun.* **5**, 5488 (2014).
234. Zhang, H., Veira, J., Bauer, S. T., Yip, C. & Singh, U. RISC in Entamoeba histolytica: Identification of a Protein-Protein Interaction Network for the RNA Interference Pathway in a Deep-Branching Eukaryote. *mBio* **12**, e01540-21.
235. Maldonado, C. *et al.* Lipophosphopeptidoglycan of Entamoeba histolytica Induces an Antiinflammatory Innate Immune Response and Downregulation of Toll-Like Receptor 2 (TLR-2) Gene Expression in Human Monocytes. *Arch. Med. Res.* **31**, S71–S73 (2000).
236. Kammanadiminti, S. J., Mann, B. J., Dutil, L. & Chadee, K. Regulation of Toll-like receptor-2 expression by the Gal-lectin of Entamoeba histolytica. *FASEB J. Off. Publ. Fed. Am. Soc. Exp. Biol.* **18**, 155–157 (2004).
237. Séguin, R., Mann, B. J., Keller, K. & Chadee, K. The tumor necrosis factor alpha-stimulating region of galactose-inhibitable lectin of Entamoeba histolytica activates gamma interferon-primed macrophages for amebicidal activity mediated by nitric oxide. *Infect. Immun.* **65**, 2522–2527 (1997).
238. Wang, S., Moreau, F. & Chadee, K. The colonic pathogen Entamoeba histolytica activates caspase-4/1 that cleaves the pore-forming protein gasdermin D to regulate IL-1β secretion. *PLoS Pathog.* **18**, e1010415 (2022).
239. Ngobeni, R. *et al.* Entamoeba histolytica–Encoded Homolog of Macrophage Migration Inhibitory Factor Contributes to Mucosal Inflammation during Amebic Colitis. *J. Infect. Dis.* **215**, 1294–1302 (2017).
240. Li, X. *et al.* A Novel TLR4-Binding Domain of Peroxiredoxin From Entamoeba histolytica Triggers NLRP3 Inflammasome Activation in Macrophages. *Front. Immunol.* **12**, 758451 (2021).

241. Ghosh, S., Jiang, N., Farr, L., Ngobeni, R. & Moonah, S. Parasite-Produced MIF Cytokine: Role in Immune Evasion, Invasion, and Pathogenesis. *Front. Immunol.* **10**, 1995 (2019).
242. Moonah, S. N., Abhyankar, M. M., Haque, R. & Petri, W. A. The Macrophage Migration Inhibitory Factor Homolog of Entamoeba histolytica Binds to and Immunomodulates Host Macrophages. *Infect. Immun.* **82**, 3523–3530 (2014).
243. Pacheco-Yépez, J. *et al.* Myeloperoxidase binds to and kills Entamoeba histolytica trophozoites: Myeloperoxidase kills Entamoeba histolytica trophozoites. *Parasite Immunol.* **33**, 255–264 (2011).
244. Lefkowitz, D. L. *et al.* Regulation of macrophage function by human recombinant myeloperoxidase. *Immunol. Lett.* **36**, 43–49 (1993).
245. Cruz-Baquero, A. *et al.* Different behavior of myeloperoxidase in two rodent amoebic liver abscess models. *PLoS ONE* **12**, e0182480 (2017).
246. Díaz-Godínez, C. *et al.* Entamoeba histolytica Trophozoites Induce a Rapid Non-classical NETosis Mechanism Independent of NOX2-Derived Reactive Oxygen Species and PAD4 Activity. *Front. Cell. Infect. Microbiol.* **8**, 184 (2018).
247. Fonseca, Z., Uribe-Querol, E., Díaz-Godínez, C., Carrero, J. C. & Rosales, C. Pathogenic Entamoeba histolytica, but not Entamoeba dispar, induce neutrophil extracellular trap (NET) formation. *J. Leukoc. Biol.* **105**, 1167–1181 (2019).
248. Lande, R. *et al.* CD38 ligation plays a direct role in the induction of IL-1β, IL-6, and IL-10 secretion in resting human monocytes. *Cell. Immunol.* **220**, 30–38 (2002).
249. Linsley, P. S. *et al.* Human B7-1 (CD80) and B7-2 (CD86) bind with similar avidities but distinct kinetics to CD28 and CTLA-4 receptors. *Immunity* **1**, 793–801 (1994).
250. Radulovic, K. & Niess, J. H. CD69 Is the Crucial Regulator of Intestinal Inflammation: A New Target Molecule for IBD Treatment? *J. Immunol. Res.* **2015**, 497056 (2015).
251. Gren, S. T. *et al.* A Single-Cell Gene-Expression Profile Reveals Inter-Cellular Heterogeneity within Human Monocyte Subsets. *PLOS ONE* **10**, e0144351 (2015).
252. Meghraoui-Kheddar, A., Barthelemy, S., Boissonnas, A. & Combadière, C. Revising CX3CR1 Expression on Murine Classical and Non-classical Monocytes. *Front. Immunol.* **11**, 1117 (2020).
253. Pelosof, L. C., Davis, P. H., Zhang, Z., Zhang, X. & Stanley Jr, S. L. Co-ordinate but disproportionate activation of apoptotic, regenerative and inflammatory pathways characterizes the liver response to acute amebic infection. *Cell. Microbiol.* **8**, 508–522 (2006).
254. Suttles, J. *et al.* CD40 Signaling of Monocyte Inflammatory Cytokine Synthesis through an ERK1/2-dependent Pathway: A TARGET OF INTERLEUKIN (IL)-4 AND IL-10 ANTI-INFLAMMATORY ACTION *. *J. Biol. Chem.* **274**, 5835–5842 (1999).
255. Pearson, L. L., Castle, B. E. & Kehry, M. R. CD40-mediated signaling in monocytic cells: up-regulation of tumor necrosis factor receptor-associated factor mRNAs and activation of mitogen-activated protein kinase signaling pathways. *Int. Immunol.* **13**, 273–283 (2001).
256. Vivanco-Cid, H. *et al.* Lipopopeptidephosphoglycan from Entamoeba histolytica activates human macrophages and dendritic cells and reaches their late endosomes. *Parasite Immunol.* **29**, 467–474 (2007).
257. Patin, E. C., Orr, S. J. & Schaible, U. E. Macrophage Inducible C-Type Lectin As a Multifunctional Player in Immunity. *Front. Immunol.* **8**, 861 (2017).
258. Zhang, C., Ni, C. & Lu, H. Polo-Like Kinase 2: From Principle to Practice. *Front. Oncol.* **12**, (2022).
259. Lara, S. *et al.* The Human Monocyte—A Circulating Sensor of Infection and a Potent and Rapid Inducer of Inflammation. *Int. J. Mol. Sci.* **23**, 3890 (2022).

260. Wu, R., Chen, F., Wang, N., Tang, D. & Kang, R. ACOD1 in immunometabolism and disease. *Cell. Mol. Immunol.* **17**, 822–833 (2020).
261. Zhao, F., Zhou, J., Li, R., Dudley, E. A. & Ye, X. Novel function of LHFPL2 in female and male distal reproductive tract development. *Sci. Rep.* **6**, 23037 (2016).
262. Duo, M. *et al.* Integrative bioinformatics analysis to explore a robust diagnostic signature and landscape of immune cell infiltration in sarcoidosis. *Front. Med.* **9**, 942177 (2022).
263. Wang, Z., Meng, Z. & Chen, C. Screening of potential biomarkers in peripheral blood of patients with depression based on weighted gene co-expression network analysis and machine learning algorithms. *Front. Psychiatry* **13**, 1009911 (2022).
264. Hill-Burns, E. M. *et al.* Identification of genetic modifiers of age-at-onset for familial Parkinson's disease. *Hum. Mol. Genet.* **25**, 3849–3862 (2016).
265. Su, P., Peng, Z., Xu, B., Yang, B. & Jin, F. Establishment and validation of an individualized macrophage-related gene signature to predict overall survival in patients with triple negative breast cancer. *PeerJ* **9**, e12383 (2021).
266. Li, R., Zhao, W., Liang, R., Jin, C. & Xiong, H. Identification and Validation of a Novel Tumor Microenvironment-Related Prognostic Signature of Patients With Hepatocellular Carcinoma. *Front. Mol. Biosci.* **9**, 917839 (2022).
267. Hatfield, K. J., Reikvam, H. & Bruserud, Ø. Identification of a subset of patients with acute myeloid leukemia characterized by long-term in vitro proliferation and altered cell cycle regulation of the leukemic cells. *Expert Opin. Ther. Targets* **18**, 1237–1251 (2014).
268. Ishii, K. J., Koyama, S., Nakagawa, A., Coban, C. & Akira, S. Host Innate Immune Receptors and Beyond: Making Sense of Microbial Infections. *Cell Host Microbe* **3**, 352–363 (2008).
269. Shi, J. *et al.* Inflammatory caspases are innate immune receptors for intracellular LPS. *Nature* **514**, 187–192 (2014).
270. Wang, G., Shen, G., Jiang, X., Chen, Z. & Yin, T. Assessment of para-inflammation in a wound healing model. *Exp. Ther. Med.* **20**, 655–661 (2020).
271. Lee, J. J. *et al.* Hypoxia activates the cyclooxygenase-2–prostaglandin E synthase axis. *Carcinogenesis* **31**, 427–434 (2010).
272. Chen, X., Kang, R., Kroemer, G. & Tang, D. Ferroptosis in infection, inflammation, and immunity. *J. Exp. Med.* **218**, e20210518 (2021).
273. Akimov, S. S. & Belkin, A. M. Cell surface tissue transglutaminase is involved in adhesion and migration of monocytic cells on fibronectin. *Blood* **98**, 1567–1576 (2001).
274. Sun, H. & Kaartinen, M. T. Transglutaminases in Monocytes and Macrophages. *Med. Sci.* **6**, 115 (2018).
275. Martinez, F. O. *et al.* Genetic programs expressed in resting and IL-4 alternatively activated mouse and human macrophages: similarities and differences. *Blood* **121**, e57–e69 (2013).
276. Czopek, A. *et al.* A novel role for myeloid endothelin-B receptors in hypertension. *Eur. Heart J.* **40**, 768–784 (2019).
277. Helset, E., Sildnes, T., Seljelid, R. & Konopski, Z. S. Endothelin-1 stimulates human monocytes in vitro to release TNF-α , IL-1β and IL-6. *Mediators Inflamm.* **2**, 417–422 (1993).
278. Fehling, H. Analyse der Unterschiede pathogener und apathogener Entamoeba histolytica (SCHAUDINN, 1903) Klone in der Parasit-Wirt Interaktion. (University of Hamburg, 2017).
279. Jumeau, C. *et al.* Expression of SAA1, SAA2 and SAA4 genes in human primary monocytes and monocyte-derived macrophages. *PLOS ONE* **14**, e0217005 (2019).

280. Buck, M. *et al.* Structure and Expression of Different Serum Amyloid A (SAA) Variants and their Concentration-Dependent Functions During Host Insults. *Curr. Med. Chem.* **23**, 1725–1755 (2016).
281. Leão, F. B. *et al.* Toll-like Receptor (TLR)-induced Rasgef1b expression in macrophages is regulated by NF-κB through its proximal promoter. *Int. J. Biochem. Cell Biol.* **127**, 105840 (2020).
282. Ferreira, L. R. P. *et al.* Identification and characterization of a novel mouse gene encoding a Ras-associated guanine nucleotide exchange factor: expression in macrophages and myocarditis elicited by Trypanosoma cruzi parasites. *J. Leukoc. Biol.* **72**, 1215–1227 (2002).
283. Andrade, W. A. *et al.* Early endosome localization and activity of RasGEF1b, a toll-like receptor-inducible Ras guanine-nucleotide exchange factor. *Genes Immun.* **11**, 447–457 (2010).
284. Carvalho, B. C. *et al.* Both knock-down and overexpression of Rap2a small GTPase in macrophages result in impairment of NF-κB activity and inflammatory gene expression. *Mol. Immunol.* **109**, 27–37 (2019).
285. Tagliabracci, V. S. *et al.* A Single Kinase Generates the Majority of the Secreted Phosphoproteome. *Cell* **161**, 1619–1632 (2015).
286. Palma-Lara, I. *et al.* FAM20C Overview: Classic and Novel Targets, Pathogenic Variants and Raine Syndrome Phenotypes. *Int. J. Mol. Sci.* **22**, 8039 (2021).
287. Weinreb, C., Rodriguez-Fraticelli, A., Camargo, F. & Klein, A. M. Lineage tracing on transcriptional landscapes links state to fate during differentiation. *Science* **367**, eaaw3381 (2020).
288. Ikeda, N. *et al.* The early neutrophil-committed progenitors aberrantly differentiate into immunoregulatory monocytes during emergency myelopoiesis. *Cell Rep.* **42**, 112165 (2023).
289. Considerations for RNA Seq read length and coverage. https://knowledge.illumina.com/library-preparation/rna-library-prep/library-preparation-rna-library-prep-reference_material-list/000001243., last accessed on 09.07.2023.
290. Groneberg, M. *et al.* HIF-1α modulates sex-specific Th17/Treg responses during hepatic amoebiasis. *J. Hepatol.* **76**, 160–173 (2022).
291. DeMichele, E., Sosnowski, O., Buret, A. G. & Allain, T. Regulatory Functions of Hypoxia in Host–Parasite Interactions: A Focus on Enteric, Tissue, and Blood Protozoa. *Microorganisms* **11**, 1598 (2023).
292. Haralanova-Ilieva, B., Ramadori, G. & Armbrust, T. Expression of osteoactivin in rat and human liver and isolated rat liver cells. *J. Hepatol.* **42**, 565–572 (2005).
293. Sasaki, F. *et al.* Expression of glycoprotein nonmetastatic melanoma protein B in macrophages infiltrating injured mucosa is associated with the severity of experimental colitis in mice. *Mol. Med. Rep.* **12**, 7503–7511 (2015).
294. Saade, M., Araujo de Souza, G., Scavone, C. & Kinoshita, P. F. The Role of GPNMB in Inflammation. *Front. Immunol.* **12**, 674739 (2021).
295. Schulz, E., Karagianni, A., Koch, M. & Fuhrmann, G. Hot EVs – How temperature affects extracellular vesicles. *Eur. J. Pharm. Biopharm.* **146**, 55–63 (2020).
296. Chen, X. *et al.* Characterization of microRNAs in serum: a novel class of biomarkers for diagnosis of cancer and other diseases. *Cell Res.* **18**, 997–1006 (2008).
297. Bernardi, S. *et al.* Sex Differences in Proatherogenic Cytokine Levels. *Int. J. Mol. Sci.* **21**, 3861 (2020).
298. Chait, A. *et al.* Sexually Dimorphic Relationships Among Saa3 (Serum Amyloid A3), Inflammation, and Cholesterol Metabolism Modulate Atherosclerosis in Mice. *Arterioscler. Thromb. Vasc. Biol.* **41**, e299–e313 (2021).

299. Reardon, C. A. Saa3 Deficiency Identifies a Sexually Dimorphic Effect on Atherosclerosis That May Be Mediated In Part by Alterations in Trem2 Expression in Macrophages. *Arterioscler. Thromb. Vasc. Biol.* **41**, 1890–1892 (2021).
300. Hartigh, L. J. den *et al.* Deletion of Serum Amyloid A3 Improves High Fat High Sucrose Diet-Induced Adipose Tissue Inflammation and Hyperlipidemia in Female Mice. *PLOS ONE* **9**, e108564 (2014).
301. Blanter, M. *et al.* Method Matters: Effect of Purification Technology on Neutrophil Phenotype and Function. *Front. Immunol.* **13**, (2022).
302. Balbi, C. *et al.* Circulating extracellular vesicles are endowed with enhanced procoagulant activity in SARS-CoV-2 infection. *eBioMedicine* **67**, (2021).
303. Mu, Y., McManus, D. P., Gordon, C. A. & Cai, P. Parasitic Helminth-Derived microRNAs and Extracellular Vesicle Cargos as Biomarkers for Helminthic Infections. *Front. Cell. Infect. Microbiol.* **11**, (2021).
304. Couper, K. N. *et al.* Parasite-derived plasma microparticles contribute significantly to malaria infection-induced inflammation through potent macrophage stimulation. *PLoS Pathog.* **6**, e1000744 (2010).
305. Holthaus, D. *et al.* Dissection of Barrier Dysfunction in Organoid-Derived Human Intestinal Epithelia Induced by Giardia duodenalis. *Gastroenterology* **162**, 844–858 (2022).
306. Coakley, G. *et al.* Extracellular Vesicles from a Helminth Parasite Suppress Macrophage Activation and Constitute an Effective Vaccine for Protective Immunity. *Cell Rep.* **19**, 1545–1557 (2017).
307. Maia, M. M. *et al.* Immunization with extracellular vesicles excreted by Toxoplasma gondii confers protection in murine infection, activating cellular and humoral responses. *Int. J. Parasitol.* **51**, 559–569 (2021).
308. Quach, J., St-Pierre, J. & Chadee, K. The future for vaccine development against Entamoeba histolytica. *Hum. Vaccines Immunother.* **10**, 1514–1521 (2014).
309. Petri, W. A. & Ravdin, J. I. Protection of gerbils from amebic liver abscess by immunization with the galactose-specific adherence lectin of Entamoeba histolytica. *Infect. Immun.* **59**, 97–101 (1991).
310. Lotter, H., Zhang, T., Seydel, K. B., Stanley, S. L. & Tannich, E. Identification of an Epitope on the Entamoeba histolytica 170-kD Lectin Conferring Antibody-mediated Protection against Invasive Amebiasis. *J. Exp. Med.* **185**, 1793–1801 (1997).
311. Min, X. *et al.* Evaluation of the C-Terminal Fragment of Entamoeba histolytica Gal/GalNAc Lectin Intermediate Subunit as a Vaccine Candidate against Amebic Liver Abscess. *PLoS Negl. Trop. Dis.* **10**, e0004419 (2016).
312. Wong-Baeza, I. *et al.* The Role of Lipopeptidophosphoglycan in the Immune Response to *Entamoeba histolytica*. *J. Biomed. Biotechnol.* **2010**, 1–12 (2010).
313. Liu, S. *et al.* Extracellular vesicles: Emerging tools as therapeutic agent carriers. *Acta Pharm. Sin. B* **12**, 3822–3842 (2022).

Schematic figures were created with a licensed version of BioRender (https://www.biorender.com/).

Publications

Within the framework of this project, the author contributed to the following publications:

König, C., **Honecker, B.**, Wilson, I. W., Weedall, G. D., Hall, N., Roeder, T., Metwally, N. G., & Bruchhaus, I. (2021). Taxon-Specific Proteins of the Pathogenic Entamoeba Species E. histolytica and E. nuttalli. *Frontiers in cellular and infection microbiology*, 11, 641472.

Wu, Y., Leyk, S., Torabi, H., Höhn, K., **Honecker, B.**, Tauler, M. D. P. M., Cadar, D., Jacobs, T., Bruchhaus, I. & Metwally, N. G. (2023). Plasmodium falciparum infection reshapes the human microRNA profiles of red blood cells and their extracellular vesicles. *iScience*.

Anders, J., König, C., Lender, C., Hellhund, A., Nehls, S., Shalabi, I., **Honecker, B.**, Lorenzen, S., Meyer, M., Matthiesen, J., Cadar, D., Roeder, T., Metwally, N. G., Lotter, H. & Bruchhaus, I. (2023). Proteins differentially expressed between pathogenic and non-pathogenic Entamoeba histolytica clones influence pathogenicity by different mechanisms. *bioRxiv*, 2023.06.29.547007 (preprint).

Er-Lukowiak, M., Haenzelmann, S., Rothe, M., Moamenpour, D., Hausmann, F., Khatri, R., Boldt, J., Bärreiter, V., **Honecker, B.**, Groneberg, M., Hansen, C., Fehling, H., Marggraff, C., Cadar, D., Bonn, S., Sellau, J. & Lotter, H. (2023). Testosterone affects type I/type II interferon response of neutrophils during hepatic amebiasis. *Front. Immunol.* (accepted)

Acknowledgments

First, I would like to thank Prof. Dr. Hanna Lotter and Prof. Dr. Iris Bruchhaus for the supervision of this doctoral project and the scientific guidance throughout the last years. I consider myself lucky to have had two supervisors that were able to provide input from different perspectives, which helped shape this project. I have learned a lot in the last three years and am very grateful for the experience. Thanks also to Prof. Dr. Esther Schnettler for the examination of this thesis.

I would also like to thank Karel Harant for the fruitful collaboration on the mass spectrometry, Balázs Horváth for his work on the miRNA sequencing data and the BNITM NGS facility under the lead of Dr. Dániel Cadar, with special thanks to Heike Baum. Thanks to Dr. Katharina Höhn for all the work on the electron microscopy, for countless discussions and for your patience and persistence with protocol optimization whenever the EV samples proved difficult to work with. Thanks to the Institute of Neuropathology at the University Hospital Hamburg Eppendorf for letting me use their NanoSight for NTA, especially to Dr. Mohsin Shafiq and Dr. Andreu Matamoros Angles for instructions as well as assistance with issues and scientific exchange. Big thank you also to the staff of the BNITM animal facility for assistance with the mice.

Thank you to Dr. Tobias Spielmann and Dr. Anna Bachmann for taking over as co-supervisors of this project. Special thanks to Anna for all the bioinformatics-related discussions and help, which I also thank Yannick Höppner for.

Furthermore, I would like to thank all current and former members of both of my working groups for all the help and input I have received over the last years, for having each other's back during difficult times and brightening everyday lab life. Although I can not name you all, please know that I am grateful to everyone that has helped out in any way with this project!

Thanks to Valentin Bärreiter – you did a great job on the EV neutrophil project for your master thesis and thus also helped this project further along. Thank you also for offering a helping hand whenever you felt it may be needed. Special thanks go to Claudia 'Klossi' Marggraff. Not only do I have to thank you for all your help with the RT-qPCRs, but also for always being there to answer questions and being the good soul of lab 6. Thank you to Dr. Nahla Metwally, especially for your help with the miRNA sequencing analysis, and to Dr. Helena Fehling and Dr. Marco Er-Lukowiak for scientific exchange and support. Thanks to my amebae-teammate and lab 4 buddy Juliett Anders, to my EV partner in crime Pilar Martínez and to Annika Bea, Charlotte Hansen, Melanie Lütkemeyer and Stefanie Tewes for good times, laboratory and moral support.

I am very grateful for all the wonderful people I have met at BNITM in the last three years that I can not all name here. Thank you for all the lunchtime and in-between chats, fun times at regular's tables, summer schools, game nights or on the Hedi, and of course for all the moral support that helped ease a lot of the stress, especially in the last phase of this project! Special thanks to my Herzis, Lennart Heepmann, Johanna Steffen, Annika Bea, Cari Lehmann and András Bencsik. I am very glad to have been a part of our small graduate school, to have had a group of people going through everything at the exact same time. Thanks for all our good times we've had over wine and pizza or on our trip to Rügen and for sharing the pain with fun stuff like thirty or more ELISA plates in one run for our joint project. I am also very happy to have had the opportunity to shape PhD life at BNITM as part of two

PhD speaker teams, alongside Lennart and Johanna as well as Pilar and Yannick. Thanks to you four for sharing these experiences and helping each other out to advocate for all PhDs, especially to Johanna and Lennart for making things like preparing big PhD surveys after work fun. Thanks to Dr. Janne Grünebast not only for proofreading this thesis (I owe you one!), but also for your friendship and for fruitful PhD coordinator-PhD speaker collaborations.

Last but not least, I would like to thank my family and friends outside the BNITM for your support in the last years. Special thanks to Philipp for your moral support, understanding and countless motivational words especially during the writing phase. It would have been a lot harder to do this without you.